DEPARTAMENT DE FARMACOLOGIA

MITOCHONDRIAL ROLE OF APOPTOSIS-INDUCING FACTOR (AIF): OXIDATIVE PHOSPHORYLATION AND REACTIVE OXYGEN SPECIES

NADEZDA APOSTOLOVA

UNIVERSITAT DE VALÈNCIA
Servei de Publicacions
2008

Aquesta Tesi Doctoral va ser presentada a València el dia 12 de març de 2008 davant un tribunal format per:

- D. Salvador Aliño Pellicer
- D. Leonardus G.J. Nijtmans
- D. Nicholas A. Joza
- D. Jordi Muntané Relat
- Dª. Pilar D'Ocón Navaza

Va ser dirigida per:
D. Juan Vicente Esplugues Mota
D. Kenneth James McCreath
Dª. Ana María Cervera Zamora

UNIVERSITAT DE VALÈNCIA

FACULTAT DE MEDICINA I ODONTOLOGIA

DEPARTAMENT DE FARMACOLOGIA

"MITOCHONDRIAL ROLE OF APOPTOSIS-INDUCING FACTOR (AIF): OXIDATIVE PHOSPHORYLATION AND REACTIVE OXYGEN SPECIES"

TESIS DOCTORAL

NADEZDA APOSTOLOVA

Valencia, 2008

UNIVERSITAT DE VALÈNCIA

FACULTAT DE MEDICINA I ODONTOLOGIA

DEPARTAMENT DE FARMACOLOGIA

Dr. Juan Vicente Esplugues Mota, Catedrático del Departamento de Farmacología de la Universidad de Valencia,

Dr. Kenneth James McCreath, Investigador de la Fundación Centro Nacional de Investigaciones Cardiovasculares Carlos III (CNIC) y

Dra. Ana María Cervera Zamora, Investigadora de la Fundación Centro Nacional de Investigaciones Cardiovasculares Carlos III (CNIC)

hacen constar:

Que el trabajo titulado "Mitochondrial role of Apoptosis-inducing factor (AIF): oxidative phosphorylation and reactive oxygen species", presentado por la licenciada Nadezda Apostolova para obtener el grado de Doctora, ha sido realizado en la Unidad Mixta de Investigación CNIC-UVEG (Centro Nacional de Investigaciones Cardiovasculares-Universitat de València), bajo nuestra dirección.

Concluido el trabajo experimental y bibliográfico, autorizamos la presentación y la defensa de esta Tesis Doctoral.

en Valencia, a 20 de enero de 2008

Fdo. Dr. Juan V. Esplugues Mota

Fdo. Dr. Kenneth J. McCreath

Fdo. Dra. Ana M. Cervera Zamora

To my family

PREFACE

After finishing University and obtaining a Degree in Biology I had just a few clear ideas. Luckily, one of them was that I knew I wanted to do science, although I was not quite certain of what that actually meant. Even now, nearly 7 years later, after working in several laboratories and meeting many people, I still cannot define "doing science". It can definitely mean many quite different things, "research" being the most meaningful and worthy scientific activity.

Therefore, I am glad that I was able to do true research while working on my Doctoral Thesis, although it often meant wasting precious time, nerves and energy (and sometimes even more precious reagents!). When I started working on this project it felt like I was jumping into a big, blue ocean full of life, light and colourful shapes but I also expected that it would certainly be full of surprises and hide dark and dangerous places. Thus "taking the plunge" into this big ocean was thrilling but it took courage. Doing this Doctoral Thesis has been a challenge for me from the very first day until now, when I see it coming to an end.

I am glad to have learnt many things; not only theoretical scientific knowledge but also how to read articles (not surprisingly also called "papers"!) without getting frustrated, how to be persistent, how to think, how to plan and organize an experiment and later present the data (often the most tricky part of the whole procedure!), how to build a personal opinion, how to cope with technical and other difficulties. I have understood that there is no, nor should there be, such a thing as positive and negative data, it is all simply "data". Some of these abilities may eventually fade, vanish or become unnecessary for my future work, yet there are some skills that I hope never to forget. These include the special ability to be surprised (it somehow diminishes with age) and to feel excited and enthusiastic about little things even when they do not look promising at first glance.

ACKNOWLEDGEMENTS

ABBREVIATIONS

aa	Amino acids (amino acid residues)
ACTB	Beta-actin
ActD	Actinomycin D
AD	Alzheimer´s disease
ADP	Adenosine diphosphate
AIDS	Acquired immunodeficiency syndrome
AIF	Apoptosis-inducing factor
AIFL	AIF-like
ALDOA	Aldolase A
α-KGDH	Alpha-ketoglutarate dehydrogenase
ALS	Amyotrophic lateral sclerosis
ALT	Adult T-cell leukaemia
AMID	AIF-homologous mitochondrion-associated inducer of death
AMS	4-acetamido-4´-maleimidylstilbene-2,-2´-disulfonic acid
Apaf-1	Apoptotic peptidase activating factor 1
APS	Ammonium persulfate
ARE	Antioxidant response element
ASK-1	Apoptosis signaling kinase-1
Asp	Asparagine
ATP	Adenosine triphosphate
Atr	Atractyloside
Bak	Bcl-2 homologous antagonist/killer
Bax	Bcl-2 associated X protein
BCA	Bicinchoninic acid
Bcl-2	B-cell lymphoma 2
β-NF	Beta-naphtoflavone
BSA	Bovine serum albumin
CAD	Caspase-activated DN-ase
CAT	Catalase
cDNA	Complementary DNA
CI(39)	Complex I 39 kDa subunit
CI(20)	Complex I 20 kDa subunit
CMFDA	5-Chloromethylfluorescein diacetate
c-myb	v-myb myeloblastosis viral oncogene homologue
c-Myc	v-myc myelocytomatosis viral oncogene homologue
CNS	Central nervous system
COX1	Cytochrome c oxidase-subunit I
COX2	Cytochrome c oxidase-subunit II
CYCA	Rat Cyclophilin A
CYPA	Human Cyclophilin A
Cys	Cysteine
cyt c	Cytochrome c
DCFH	Dichlorofluorescin
ΔΨ$_m$	Mitochondrial transmembrane potential
DEPC	Diethylpyrocarbonate
Dld	Dihydrolipoyl dehydrogenase
DMEM	Dulbecco´s modified Eagle´s medium
DMSO	Dimethylsulfoxide
dNTPs	Deoxinucleoside triphosphates

dsRNA	Double-stranded RNA
DTT	Dithiothreitol
EB	Embryonic body
E. coli	*Escherichia coli*
EDTA	Ethylenediamine tetraacetic acid
ER	Endoplasmatic reticulum
ERK	Extracellular-regulated kinase
ES cells	Embryonic stem cells
ETC	Electron transport chain
EthBr	Ethidium bromide
F	Forward
FAD	Flavine adenine dinucleotide
FBS	Fetal bovine serum
FISH	Fluorescent *in situ* hybridization
GAPDH	Glyceraldehyde-3-phosphate dehydrogenase
GFP	Green fluorescent protein
GLUT1	Facilitated glucose transporter 1
Gpx	Glutathione peroxidase
GR	Glutathione reductase
GSH	Reduced glutathione
GSSG	Oxidized glutathione (Glutathione disulfide)
hAIF	Human AIF
HBSS	Hank's buffered salt solution
HCl	Hydrochloric acid
HD	Huntington´s disease
HE	Hydroethidine (Dihydroethidium)
HEPES	4-(2-hydroxyethyl)-1-piperazineethanesulfonic acid
HIF-1	Hypoxia-inducible factor-1
HIV	Human immunodeficiency virus
Hq	Harlequin
HRE	Hypoxia-response element
HRP	Horseradish peroxidase
Hsp70	Heat-shock protein 70
HTLV-I	Human T-cell leukaemia virus Type-I
H_2O_2	Hydrogen peroxide
IAP	Inhibitor of apoptosis protein
IF-γ	Interferon-gamma
IκB	Inhibitor of NF-κB
IL-1	Interleukin-1
IMM	Inner mitochondrial membrane
IMS	Intermembrane space
Kb	Kilobase
KD	Knock Down
KDa	Kilodalton
KEAP1	Kelch-like ECH-associated protein 1
KO	Knock Out
LB	Luria Bertani
LHON	Leber´s hereditary optic neuropathy
LIF	Leukaemia inhibitory factor
LPS	Lipopolysaccharides
Lys	Lysine
mAIF	Mouse AIF

MAO	Monoamine oxidase
MAPK	Mitogen-activated protein kinase
Me-Hg	Methylmercury
MEM	Minimal essential medium
MMP	Mitochondrial membrane permeabilization
MPP$^+$	N-methylpyridinium ion
MPTP	1-methyl-4-phenyl-1,2,3,6-tetrahydropyridine
mtDNA	Mitochondrial DNA
NAC	N-acetyl cysteine
NAD	Nicotinamide adenine dinucleotide
NADP	Nicotinamide adenine dinucleotide phosphate
NADPH	Reduced nicotinamide adenine dinucleotide phosphate
n.e.a.a.	Non-essential amino acids
NF-κB	Nuclear factor-kappa B
NLS	Nuclear localization sequence
NMDA	N-methyl-D-aspartate
NQO1	NAD(P)H quinone oxidoreductase
Nrf2	Nuclear factor (erythroid-derived 2)-like 2
O$_2$•$^-$	Superoxide
OH•	Hydroxyl radical
OMM	Outer mitochondrial membrane
o/n	Over night
Ox-LDL	Oxidized low density lipoprotein
OxPhos	Oxidative phosphorylation
PBS	Phosphate-buffered saline
PCD	Programmed cell death
pCMPS	*Para*-chloromercuryphenylsulphonic acid
PCR	Polymerase chain reaction
PD	Parkinson´s disease
PI	Propidium iodide
PI3K	Phosphoinositide 3-kinase
PNPP	*Para*-nitrophenylphosphate
Pol III	RNA polymerase III
PRG3	p53-responsive gene 3
Pro	Proline
Prx	Peroxiredoxin
PTP	Permeability transition pore
R	Reverse
RHD	Rel homology domain
RNAi	RNA interference
ROS	Reactive oxygen species
RT	Room temperature
RT-PCR	Reverse transcriptase polymerase chain reaction
SDS-PAGE	Sodium dodecyl sulphate-polyacrilamide gel electrophoresis
Ser	Serine
siRNA	Small interfering RNA
Smac/Diablo	Second mitochondria-derived activator of apoptosis/ Direct inhibitor-of-apoptosis-protein-binding protein with low pI
SOD	Superoxide dismutase
Sp-1	Specificity protein-1
STS	Staurosporine
T°	Temperature

t-BHQ	*Tert* -butylhydroquinone
TBS-T	Tris-buffered saline-Tween
TCA	Trichloroacetic acid
TEMED	N,N,N´,N´-tetramethylethylendiamine
Thr	Threonine
TMRM	Tetramethylrhodaminemethylester
TNF-α	Tumour necrosis factor alpha
Tris	Trishydroxymethylaminomethane
Trp	Tryptophane
Trx	Thioredoxin
TUBA	Alpha-Tubulin
Tyr	Tyrosine
VDAC	Voltage-dependent anion channel
WB	Western blot
WT	Wild type
Z-VAD.fmk	Carbobenzoyl-Val-Ala-Asp-fluoromethylketone

LIST OF FIGURES

LIST OF TABLES

ABSTRACT

The apoptotic function of Apoptosis-inducing factor (AIF) is well documented in the literature, but its physiological role in the mitochondrion is less certain. Using a small interfering RNA (siRNA) strategy, we studied whether modulation of AIF in cultured cells influenced the production of reactive oxygen species (ROS). We found that siAIF-transfected cells had reduced AIF protein levels and this was paralleled by a significant increase in ROS. We tested the generality of this response by using two different human cell lines, Hep3B and HeLa, and also by employing a mouse ES AIF-KO cell line. The increased ROS were mitochondrial in origin as a similar silencing strategy in cells devoid of a functioning electron transport chain (ETC) did not result in a ROS-increase. The augmented ROS levels were sufficient to activate Hypoxia-inducible factor 1α (HIF-1α), a ROS-sensitive transcription factor, and this effect could be reversed using antioxidants, both the broad-range antioxidant (N-acetyl cysteine) and a specific mitochondrial-targeted antioxidant (MitoQ), proving the implication of ROS in the HIF-1α stabilization.

Examination of oxygen consumption revealed that AIF-depleted cells had a major impairment of respiration, at Complex I in the ETC. Western blot analysis also showed a loss of Complex I 39 and 20 kDa subunits. Studies using the antioxidants mentioned above, revealed that the respiratory competence could be regained in *AIF*-silenced cells. However, neither of the antioxidant treatments we used could recover Complex I assembly. Studies of the energetic state of siAIF cells showed that despite a 30% decrease in the overall intact cell respiration, these cells maintain normal basal levels of ATP, due to a higher glycolytic capacity and a lower proliferation rate. Moreover, we analyzed the expression of thioredoxin by Western blot and found that the mitochondrial isoform, Trx2, was significantly decreased when *AIF* was silenced. Preliminary co-immunoprecipitation analyses and proteomic studies failed to show any direct correlation between AIF and Trx2 at the protein level.

Our results lead us to the conclusion that the defect in respiration in siAIF cells is downstream of Complex I protein loss and is presumably due to ROS-mediated damage to the ETC. This suggests an integral mitochondrial function of AIF, as a redox modifier and chaperone-like molecule, necessary for Complex I assembly. Additional studies are required to define the detailed mechanism of the AIF enzymatic activity in the mitochondrion and to establish its binding partners.

INDEX

I. INTRODUCTION

"We are made of dreams"

William Shakespeare (1564-1616)

I.1. Apoptosis - chronicle of a death foretold

Programmed cell death (PCD) is known to play a major role in the development and stress responses of all three metazoan kingdoms (Plantae, Animalia and Fungi). It is essential for organ development, tissue homeostasis, aging and removal of infected or damaged cells [Jacobson M.D. *et al.*, 1997]. Every year humans lose their body weight in cells through the process of PCD. Failure to invoke appropriate cell death can result in autoimmune disorders or cancer, whereas increased PCD leads to degenerative processes such as immunodeficiency and neurodegenerative diseases [Thompson C.B., 1995; Okouchi M. *et al.*, 2007]. The biochemical and ultrastructural features of PCD are highly conserved throughout the evolution of multicellular animals [Jacobson M.D. *et al.*, 1997].

Classical apoptosis, the best known phenotypic expression of PCD, consists of two phases, initiation and execution. The initiation phase can be triggered by extrinsic pathways - through activation of the death receptors, on the cell membrane, and intrinsic pathways - involving mitochondria and other organelles such as the endoplasmatic reticulum (ER) or lysosomes (Fig.I.1).

Generally, the apoptotic changes in a mammalian cell comprise shrinkage and loss of the cell volume, degradation of proteins, chromatin condensation and DNA loss, "blebbing" of the cell surface and exposure of specific phospholipids, namely phosphatidylserines, and breakdown in the mitochondrial integrity.

In contrast to a couple of decades ago, when it was believed that only or mainly nuclei undergo important structural and biochemical modifications in dying cells, it is now recognized that mitochondria are the central player in the majority of the PCD-events in mammalian cells [Green D.R. and Kroemer G., 1998; Kroemer G. and Reed J.C., 2000]. Mitochondrial damage can directly activate apoptosis or amplify receptor-mediated apoptotic pathways, as shown in Fig.I.1.

One of the decisive steps of the apoptotic cascade is the permeabilization of the outer mitochondrial membrane (OMM), culminating in the release of soluble intermembrane proteins from the mitochondrion to the cytosol [Zamzami N. *et al.*, 1996; Susin S.A. *et al.*, 1996]. Such proteins are: cytochrome *c* (cyt *c*), procaspase-2, -3 and –9 [Mancini M. *et al.*, 1998; Krajewski S. *et al.*, 1999], the inhibitor of apoptosis proteins (IAP),

Smac/Diablo [Du C. *et al.*, 2000], endonuclease G and AIF (Fig.I.1). The exact mechanisms of mitochondrial membrane permeabilization (MMP) are still a matter of debate. Physical disruption of OMM, due to swelling of the matrix has been suggested by several authors [Petit P.X. *et al.*, 1998]. Others postulate the existence of non-specific protein permeable pores in OMM [Desagher S. *et al.*, 1999; Shimizu S. *et al.*, 1999]. Irrespective of the exact mechanism(s) of MMP, it appears that anti-apoptotic members of the Bcl-2 family such as Bcl-2 or Bcl-xl stabilize the mitochondrial membrane whereas the pro-apoptotic Bcl-2 homologues such as Bax or Bak compromise the mitochondrial barrier function. The first apoptogenic intermembrane protein to be identified was cyt *c* [Liu X. *et al.*, 1996]. Soon, many investigators assumed that cyt *c* is the major rate-limiting factor of apoptotic cell death, a finding that was later found to be insubstantial.

Other important hallmarks of mitochondria in apoptotic cells are the disruption (decrease) of the mitochondrial transmembrane potential ($\Delta\psi_m$), present in most models of apoptosis [Hirsch T. *et al.*, 1997] and the increase in reactive oxygen species (ROS). These phenomena, which are very closely related, have been shown to be both a cause and a consequence of the apoptotic process in mitochondria.

Mammalian PCD, apoptosis, is mostly coupled to the activation of caspases. But, in contrast to a previous belief, inhibition of caspases *per se* does not prevent cell death in most mammalian models of apoptosis induction. Thus, when cell death is induced by Bax [Xiang J. *et al.*, 1996, Pastorino J.G. *et al.*, 1998; Marzo I. *et al.*, 1998], Bak [McCarthy N.J. *et al.*, 1997], c-Myc [McCarthy N.J. *et al.*, 1997], ligation of glucocorticoid receptors [Hirsch T. *et al.*, 1997; Brunet C.L. *et al.*, 1998], tumour necrosis factor (TNF-α), [Vercammen D. *et al.*, 1998], interferon-γ (IF–γ), [Quignon F. *et al.*, 1998], staurosporine (STS), [Deas O. *et al.*, 1998; Bossy-Wetsel E. *et al.*, 1998] and DNA-damage [Hirsch T. *et al.*, 1997; Sun X.M. *et al.*, 1999], cells normally die from full-blown apoptosis and manifest caspase activation. However, pancaspase inhibitors do not prevent cytolysis, nor do they prevent MMP, although they usually abolish oligonucleosomal DNA fragmentation. The morphology of cells dying in the presence of caspase inhibitors resembles that of unicellular eukaryotes (which lack caspases), induced to undergo PCD-like death. When caspase activation is inhibited indirectly, for instance by culturing cells in conditions in which both glycolytic and respiratory ATP generation are prevented, cells also die without oligonucleosomal DNA

fragmentation and without shell shrinkage [Leist M. *et al.*, 1997; Eguchi Y. *et al.*, 1997; Bradham C.A. *et al.*, 1998], yet manifest nuclear condensation and DNA cleavage into large 50-150 kb fragments, undistinguishable from that seen in the early stage of apoptosis [Dong Z. *et al.*, 1998]. Moreover, there are several well-studied models of apoptosis where no caspase activation is detected. For example, the neurotoxic agents hydrogen peroxide (H_2O_2) and methylmercury (Me-Hg), provoke apoptosis of cultured rat cerebellar granule cells without activation of the caspase-3 pathway [Fonfria E. *et al.*, 2002].

Altogether, there are different observations that underline the existence of controlled caspase-independent death mechanisms in the mammalian system.
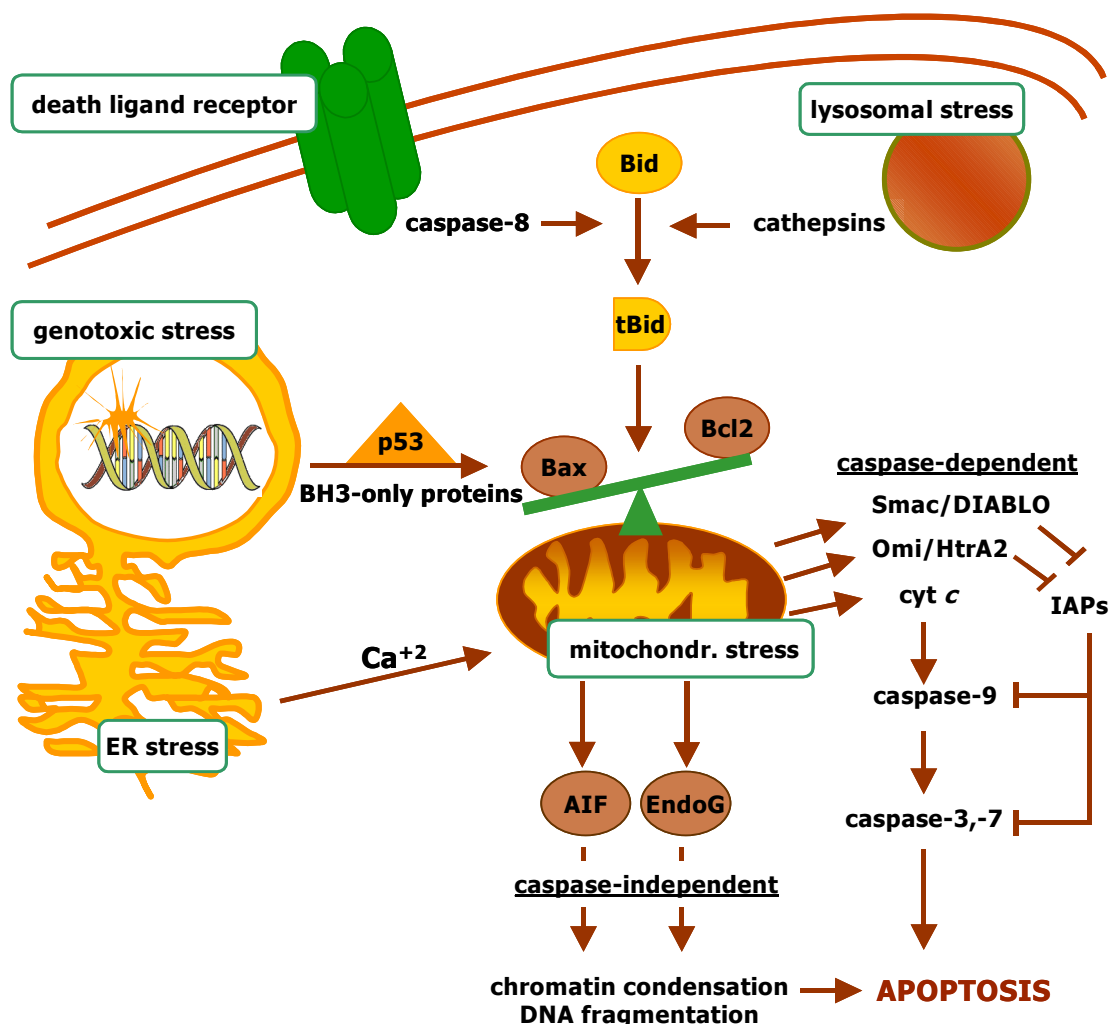
Figure I.1. Mitochondrial control of apoptosis. Many cellular death-promoting pathways converge at the mitochondrion. Furthermore, mitochondria participate in both caspase-dependent and -independent cell suicide [modified from Taha T.A. *et al.*, 2006].

I.2. Apoptosis-inducing factor (AIF) - balancing life and death

I.2.1. The discovery

In 1996, Santos A. Susin and co-workers found that the mitochondrial intermembrane protein fraction contains an activity which suffices to force isolated HeLa nuclei to adopt an apoptotic morphology and to lose part of their DNA content [Zamzami N. *et al.*, 1996; Susin S.A. *et al.*, 1996]. This activity was termed "apoptosis-inducing factor" (AIF). Based on a semi-automated cytofluorometric assay allowing measurement of the frequency of subdiploid nuclei exposed to mitochondrial proteins, Guido Kroemer and colleagues purified a protein that maintained its activity in the presence of the broad-range caspase inhibitor Z-VAD.fmk [Susin S.A. *et al.*, 1999 A]. AIF was found to be an ubiquitous FAD-binding flavoprotein [Susin S.A. *et al.*, 1999 B]. Cloning of the full-length cDNAs, corresponding to mouse AIF (mAIF), 612 amino acids (aa) and human AIF (hAIF), 613 aa, revealed that AIF is strongly conserved between these two mammalian species (92% aa identity in the whole protein) and bears a highly significant homology with oxidoreductases from all eukaryotic and prokaryotic kingdoms in its C-terminal portion (95% aa identity between aa 128-612 in mAIF and hAIF), [Susin S.A. *et al.*, 1999 B]. The aa sequence homology between hAIF and mAIF and their more distant relative from *Pseudomonas putida* can be appreciated in Fig.I.3.

I.2.2. Evolutionary origins and phylogeny of AIF

The evolutionary origins of AIF are worth studying. AIF possesses significant homology with NADH ferredoxin reductases, from both Eubacteria and Archaebacteria [Lorenzo H.K. *et al.*, 1999]. As represented in Fig.I.2, the strongest homology among eukaryotes, is seen with several plant ascorbate oxidoreductases, in particular with dehydroascorbate reductase from *Arabidopsis thaliana*, monodehydroascorbate reductase from *Cucumis sativus* and the ascorbate free radical reductase from *Lycopersicum esculentum* [Lorenzo H.K. *et al.*, 1999]. Several, among these plant genes, are induced by stress such as heat, cold, superoxide anion, fungal pathogens or wounding [Grantz A.A. *et al.*, 1995; Van Camp W. *et al.*, 1996; Vanacker H. *et al.*, 1998]. More studies are needed to be able to determine whether these plant proteins have a true apoptogenic function, yet it is very intriguing that dehydroascorbate reductase has been reported to redistribute from mitochondria to cytosol in the dark-

induced senescence of *Pisum sativum* leaves [Jimenez A. *et al.*, 1998].

Phylogenetic analyses reveal that AIF has a very significant homology with four putative oxidoreductases from vertebrate (*Xenopus laevis*), invertebrate animals (*Drosophila melanogaster, Caenorabditis elegans*), as well as *Saccharomyces pombae* [Lorenzo H.K. *et al.*, 1999]. In contrast, there is no AIF homologue in *S. cerevisiae*.

Most if not all amino acids supposed to interact with the prosthetic groups FAD and NAD are strongly conserved between AIF and two reductases, whose three-dimensional structure have been elucidated, namely dihydrolipoamide dehydrogenase from *Pseudomonas putida* and human glutathione reductase (GR). The core consensus of the typical motif GXGXXG/A of the Rossman fold [Rossmann M.G. *et al.*, 1975] is found at two distinct regions of the AIF sequence (aa 138-143 and aa 307-312 in human AIF), as displayed in Fig.I.3, the more N-terminal motif seems to be involved in the NAD(P)H binding, whereas the more C-terminal one binds to FAD. Moreover, AIF does not belong to the subfamily of disulfide reductases because it lacks two cysteines (Cys) essential to form the redox-active disulfide bond in the catalytic site and it does not belong to the superfamily of flavoprotein disulfide oxidoreductases, which include: mercuric reductase, alkylhydroperoxide reductase, glutathione reductase, dihydrolipoamide reductase and thioredoxin reductase [Lorenzo H.K. *et al.*, 1999]. However, the strong conservation of NAD/FAD binding motifs (Fig.1.4) strongly suggests that AIF possesses an oxidoreductase activity. The oxidoreductase and the apoptogenic activity of AIF can be separated because the entire AIF protein precursor (aa 1-612), which does not bind FAD, the group indispensable for the electron donor/acceptor function, becomes apoptogenic when refolded *in vitro* [Susin S.A *et al.*, 1999 B].

AIF is believed to be part of a particularly ancient PCD pathway, highly conserved through evolution. In this direction, it is very important to emphasize that AIF is strikingly ubiquitious, both at the phylogenetical and oncogenetical level. AIF homologues have been found in all metazoan phyla [Lorenzo H.K. *et al.*, 1999], including organisms that lack clear-cut homologues of caspases, such as plants and fungi, as shown in Fig.I.2. Interestingly, these AIF homologues show similar cellular behaviour to mammalian AIF. For example, the AIF homologue in the slime mold, *Dictyostelium discoideum*, normally localizes in mitochondria and is translocated to the nucleus during developmental cell death. Even more intriguingly, recombinant *D.*

discoideum AIF can induce chromatin condensation in purified HeLa nuclei [Arnoult D. *et al.*, 2001]. AIF mRNA and protein can be detected all throughout murine embryogenesis and in all developmental organs [Joza N. *et al.*, 2001].

All together, these observations point to a role of AIF in early stages of phylogeny, which makes it a very interesting subject of phylogenetic comparisons, undertaken to weigh the relative importance of death pathways (especially caspase-dependent versus caspase-independent death programs) and to apprehend the original death machinery.
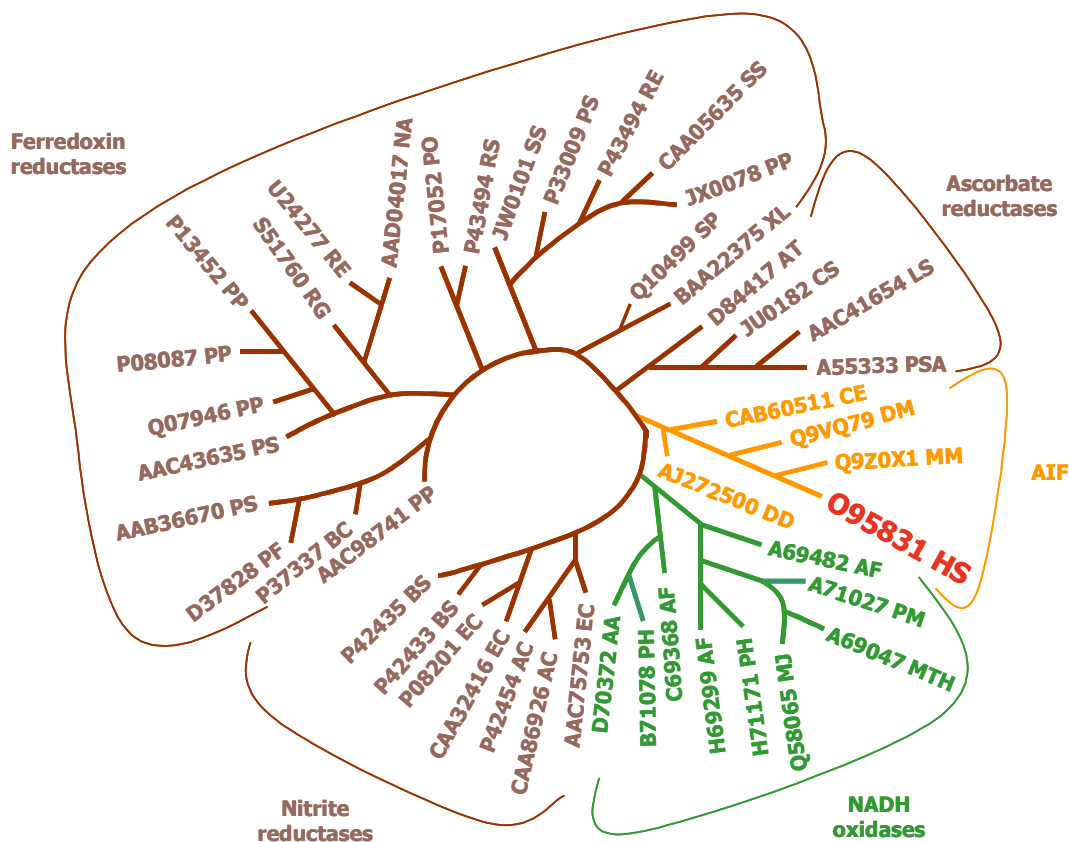
Figure I.2. Phylogenetic tree showing the relationship between AIF (human AIF in red) and other oxidoreductases from different species. The PIR accession numbers are enumerated following the abbreviation of the species: AA: Aquifex aeolicus; AC: Acinetobacter calcoaceticus; AF: Archaeoglobus fulgidus; AT: Arabidopsis thaliana; BC: Burkholderia cepacia; BS: Bacillus subtilis; CE: Caenorhabditis elegans; DD: Dictyostelium discoideum; DM: Drosophila melanogaster; EC: Escherichia coli; HS: Homo sapiens; LS: Lycopersicon esculentum; MJ: Methanocaldococcus jannaschii; MM: Mus musculus; MTH: Methanobacterium thermoautotrophicum; NA: Novosphingobium aromaticivorans; PF: Pseudomonas fluorescens; PH: Pyrococcus horikoshii; PO: Pseudomonas oleovorans; PP: Pseudomonas putida; PS: Pseudomonas sp.; PSA: Pisum sativum; RE: Rhodococcus erythropolis; RG: Rhodococcus globerulus; RS: Rhodococcus sp.; SP: Schizosaccharomyces pombae; SS: Sphingomonas sp.; XL: Xenopus laevis [modified from Lorenzo H.K. and Santos S.A., 2004].

AIF has also distantly-related homologues in humans, called AIF-homologous mitochondrion-associated inducer of death, also known as p53-responsive gene 3 (AMID-PRG3) and AIF-like (AIFL). It has been described that AMID-PRG3 also exerts a pro-apoptotic function, although there is conflicting evidence about its localization [Wu M. *et al.*, 2002; Ohiro Y. *et al.*, 2002]. AIFL is a mitochondria-confined ubiquitously expressed protein, able to provoke apoptosis through caspase-dependent pathway [Xie Q. *et al.*, 2005].

I.2.3. Morphology, structure and distribution of AIF

I.2.3.1. Biogenesis of AIF

The mouse AIF cDNA codes for a protein which is organized in three domains: an amino-terminal mitochondrial localization sequence (MLS) of 100 aa, a spacer region of 27 aa and a carboxyterminal of 485 aa oxidoreductase domain (Fig.I.5). Natural AIF purified from mouse liver mitochondria was found to be a FAD-binding protein and recombinant AIF can be refolded *in vitro*, in the presence of FAD, resulting in stable FAD binding [Daugas E. *et al.*, 2000 A]. A recombinant protein corresponding to the mAIF precursor does not bind FAD when purified from inclusion bodies of *E. coli*, whereas a shorter protein lacking the MLS (AIF Δ1-100) or lacking the MLS and part of the spacer region (Δ1-120) does [Susin S.A *et al.*, 1999 B]. Similarly, mature AIF protein from mitochondria (Δ1-101) is a flavoprotein.

These data suggest the following scenario for biogenesis of AIF. The AIF precursor, encoded by a nuclear gene, is synthetized in the cytosol and then imported into mitochondria through the general import pathway [Susin S.A *et al.*, 1999 B]. Once in the mitochondrial intermembrane space (IMS), the MLS of the AIF precursor is proteolytically removed as described for other mitochondrial flavoproteins [Robinson K.M. and Lemire B.D., 1996]. Next, the protein refolds, while non-covalently incorporating the FAD prosthetic group at a molar ratio 1:1.

Santos A. Susin and colleagues raised an antibody against aa 151-200 of AIF which recognized a single protein with a relative molecular mass of 57 kDa in mitochondria from many different tissues. In contrast, the primary transcription/translation product of AIF cDNA *in vitro* is 67 kDa [Susin S.A *et al.*, 1999 B].

When imported into mitochondria *in vitro*, this gives rise to a shorter protein corresponding to mature AIF whose first amino acid is at position 102 of the full-length precursor protein. There is no mitochondrial import if residues 1-120 of the protein are deleted, which proves the existence of a true MLS [Susin S.A *et al.*, 1999 B].

```
mAIF    1    MFRCGGL  AGAFKQKLVPLVRTVYVQRPKQRNRLPGNLFQQWRVPLELQM
hAIF    1    — — — — — — A — — — L — — — — — — — — — — — — — C — R S — R — — — — — — — — — — R — H — — — — — — —
BDSF    1    — 

mAIF   50    ARQMASSGSSGGKMDNSVLVLIVGLSTIGAGAYAYKTIKEDQKRYNERVM
hAIF   51    T — — — — — — — A — — — I — — — — — — — — — — — — — — — — — M — — — E — — — — — — I S

mAIF  100    GLGLSPEEKQRRAIASATEGGSVPQIRAPSHVPFLLIGGTAAFAAARSI
hAIF  101    — — — — T — — Q — — KK — AL — — S — — EE — — — DK — — — — — — — — — — — — — — — — — — — — —
BDSF    2    AN — — A    I — — N — V — G — TT — QAL

mAIF  150    RARDPGARVLIVSEDPELPYMRPPLSKELWFSDDPNVTKTLQFRQWNGKE
hAIF  151    — — — — — — — — — — — — — — — — — — — — — — — — — — — — — — — — — — — — — — R — K — — — — — —
BDSF   22    — — EGYEG — ISLIG — EQH — — — D — — S — — — AV        —        D — S

mAIF  200    RSIYFQPPSFYVSAQDLPNIENGGVAVLTGKKVHLDVRGNMVKLNDGSQ
hAIF  201    — — — — — — — — — — — — — — — — — — — — H — — — — — — Q — — — — D — — — — — — — — — —
BDSF   55        FE — — — R    LAEA — W    YSEASIEM — — SE — TD — TQKK — IS — — — — — T

mAIF  250    ITFEKCLIATGGTPRSLSAIDRAGAEVKSRTLFRKIGDFRALEKISREV
hAIF  251    — — Y — — — — — — — — — — — — — — — — — — — — — — — — — — — — — — — — — — — S — — — — — — —
BDSF   98    SADAIV — — — — SRA — M — — L        P — SQLPGVV — — TY — — VQL — RDSWTPN

mAIF  300    KSITVIGGFLGSELACALGRKSQASGIEVIQLFPEKGNMGKILPQYLSN
hAIF  301    — — — — — I — — — — — — — — — — — — — — ARAL — T — — — — — — — — — — — — — — — — E — — — —
BDSF  144    TRLLTV — — — LI — C — V — — TTA — —    L — LS — TI — EAGDELLVRV — GRRIGA

mAIF  350    WTMEKVKREGVKVMPNAIVQSVGVSGGRLLIKLKDGRKVETDHIVTAVGL
hAIF  351    — — — — — — — — — R — — — — — — — — — — — S — K — — — — — — — — — — — — A — — — —
BDSF  190    — LRGLLTEQ — — Q — ELKTG — SGFSGEGQLEKVMVN — — — SFIA — NALIQ — — A

mAIF  400    EPNVELAKTGGLEIDSDFGGFRVNAELQARSNIWVAGDAACFYDIKLGRR
hAIF  401    — — — — — — — — — — — — — — — — — — — — — — — — — — — — — — — — — — — — — — — — — — — —
BDSF  240    D — ADQ — — RQA — — — Q — R    — VVVDHRGATSAKG — FAV — — V — I WPLHSG — K —

mAIF  450    RVEHHDHAVVSGRLAGENMTGAAKPYWHQSMFWSDLGPDVGYEAIGLVDS
hAIF  451    — — — — — — — — — — — — — — — — — — — — — — — — — — — — — — — — — — — — — — — — —
BDSF  288    SL — TY    MNAQ        QA — AV — — AI            — — KE — S            AP

mAIF  500    SLPTVGVFAKATAQDNPKSATEQSGTGIRSESETESEASEITIPPSAPAV
hAIF  501    — — — — — — — — — — — — — — — — — — — — — — — — — — — — — — — — — — T — —
BDSF  315    Q — — — S    WTWIAGH    RMQM — GDIE — P — EYVLRG — LGIG — ALLFRLLDGRI

mAIF  550    PQVPVEGEDYGKGVIFYLRDKVVVGIVLWNVFNRMPIARKIIKDGEQHED
hAIF  551    — — A — — Q — — — — — — — — — — — — — — — — — I — — — — — — — — — — — — — — — —
BDSF  362    — AV — AVDA    PRD    — A — ANRL — EAQ —    II B        PE — L        ADVSNN

mAIF  600    LNEVAKLFNIHED
hAIF  601    — — — — — — — — — — — — —
BDSF  362    MRDIVRANEGNQK
```

Figure I.3. Sequence alignment of mouse and human AIF (GenBank accession numbers AIF100927 and AIF100928, respectively) with BDSF from *Pseudomonas putida* (benzene 1,2-dioxygenase ferredoxin NADH reductase), an AIF homologue showing 30% identity with AIF. Dashes indicate aa identity, lined boxes indicate aa similarity. Predicted MLS is shown in orange whereas the site of the MLS-domain cleavage upon mitochondrial import is marked with an arrow. NLS is shown in green and the conserved Rossmann fold motifs in grey [modified from Susin S.A. *et al.*, 1999 B].

However, a detailed study by Hidenori Otera and colleagues published in the EMBO J. [Otera H. *et al.*, 2005], suggested a different biogenesis process of AIF. According to this study, mature mitochondrial AIF is a 62 kDa protein and its apoptotic release from the mitochondria needs proteolytic processing from 62 kDa to the apoptotic form of 57 kDa.

AIFΔ1-120 does not contain significant amounts of metals, including Ca^{2+}, Co^{2+}, Cu^{2+}, Mg^{2+}, Fe^{2+}, Se^{2+} and Zn^{2+}, however it contains phospho-groups among Ser and Thr residues [Miramar M.D. *et al.*, 2001]. Moreover, it has 3 Cys in its sequence but none of them engages in a disulfide link [Miramar M.D. *et al.*, 2001]. Recombinant AIF has been shown to act as a monomer in solution and it is possible that AIF dimerizes upon interaction with putative protein or DNA partners or after post-translational modifications [Mate M.J. *et al.*, 2002].

I.2.3.2. Molecular structure of AIF

In 2002, María J. Maté and co-workers revealed the fine structure of mAIF at 2 Å. The overall structure of AIF displays a GR-like fold and includes one FAD molecule per monomer. Similarly to other enzymes of the GR family, AIF's oxidoreductase domain is organized in three subdomains: a FAD-binding region (aa 122-262 and 400-477), NADH-binding region (aa 263-399) and a C-terminal region (aa 478-610), which in GR constitutes most of its dimer interface. Both the FAD and the NADH-binding domain show a classical Rossmann fold, whereas the C-terminal domain is composed of five anti-parallel β-strands followed by two α-helices. A tridimensional model of AIF is shown in Fig.I.4.

It seems that structurally the most similar protein to AIF is BphA4, the ferredoxin reductase part of biphenyl dioxygenase from *Pseudomonas sp*. The structural comparison of AIF, BphA4 and GR from *E.coli* highlights their overall similarity, however with the presence of several important differences. The most remarkable difference is a long C-terminal insertion region present only in AIF (aa 509-559), (Fig.I.4). The N-terminal part of this insertion displays a defined secondary structure: two short helices that fold back onto the FAD-binding domain. Following the short helices is a Pro-rich loop, creating an open conformation, stabilized by crystal contacts with a neighbouring monomer.

It has been suggested that this C-terminal insertion is related to the pro-apoptotic function of AIF but the fact that some AIF homologues from non-mammalian species such as *D. discoideum* lack this region and still display a pro-apoptotic role, clearly denies this hypothesis.

FAD-binding domain

NADH-binding domain
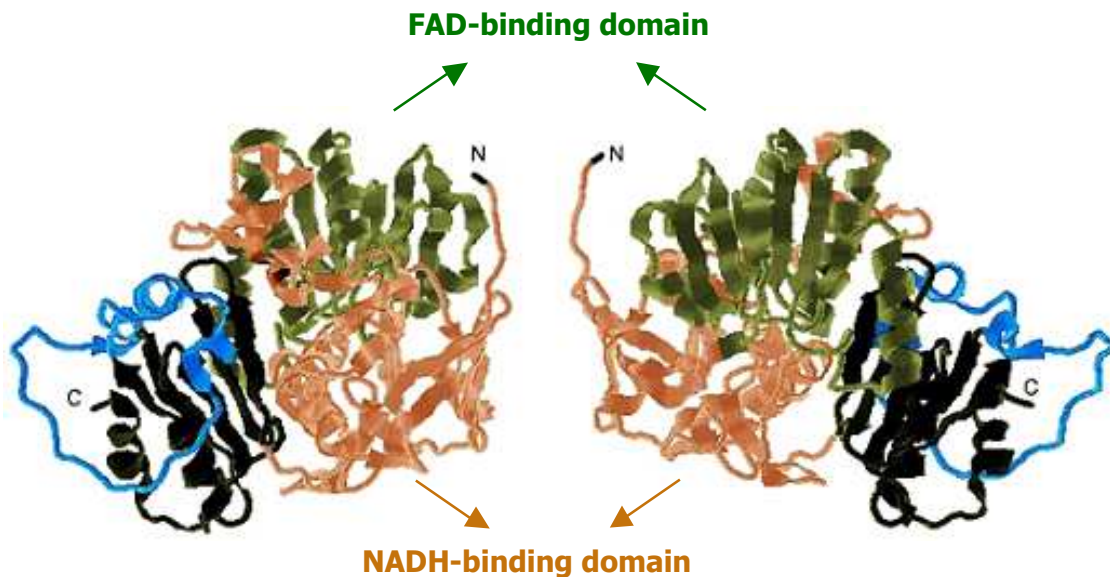
Figure I.4. AIF-tridimensional model. The C-terminal region is represented in black. In blue, the AIF-specific insertion (Lys 509-Tyr 559).

However, the Pro-rich loop includes a PEST sequence [Rogers S. *et al.*, 1986], which is characteristic of proteins with a rapid intracellular turn-over and is also involved in protein-protein interactions [Ernst M.K. *et al.*, 1995]. Moreover, the insertion contains a Pro-rich motif (PPSAPAVPQVP) which displays an extended, left-handed oriented helical conformation, termed the polyproline-2-helix (PPII). This structural motif suggests a presence of interaction with proteins containing modules such as SH3 or WW, involved in a variety of cellular processes. Also, the open structure of the insertion could indicate putative binding for different proteins such as chaperones. Actually, to date, one chaperone, Heat shock protein-70 (Hsp70) has already been shown to interact with AIF [Ravagnan L. *et al.*, 2001].

The second important structural difference corresponds to the presence of two long α-helices in GR from *E.coli*. This region is essential for catalysis and dimerization and includes 64 aa residues in GR. The equivalent regions in AIF and BphA4 are shorter (47 and 25 aa residues respectively), so that they adopt a more extended conformation without the formation of the α-helices.

The same authors describe the non-covalent interaction between AIF and NAD and it seems quite similar to the described interaction in other flavoproteins.

Unlike the FAD binding domain, the NADH binding domain of AIF is quite specific and shows some differences in comparison with BpHA4 of GR from *E. coli*. GR-like proteins possess a conserved disulfide bridge which acts as an electron acceptor to oxidize the isoalloxazine ring of the nucleotide. This centre is missing in AIF and BphA4 and instead, there is a specific stretch of three aa, namely Trp-Ser-Asp. Moreover, the Trp residue of this sequence is largely exposed to the solvent and probably is involved in electron transport in BphA4 whereas in AIF this Trp (Trp482) is occluded from the bulk solvent because the helical region of the C-terminal insertion folds back onto the FAD-binding domain of the protein. The NADH-binding pocket of AIF is comparatively larger and contains fewer specific contact spots for NADH than the same structure in similar proteins. This might suggest a weaker NADH binding. The presence of a bigger NADH-binding pocket may also be an indication of the presence of a binding site for some unknown substrate that could be reduced by $FADH_2$.

In this publication, María J. Maté and colleagues claimed that they had not found any obvious DNA-binding structural motifs in mAIF. However, the C-terminus of the *D. discoideum* AIF homologue has been proposed to include a helix-turn-helix motif [Arnoult D. *et al*., 2001]. Moreover, there have been several publications proving that AIF does actually bind to DNA and RNA [Vahsen N. *et al*., 2006]. The crystal structure of AIF revealed the presence of a strong positive electrostatic potential at its surface, despite the calculated neutral isoelectrical point, hence AIF could be binding DNA through electrostatic interactions [Ye H. *et al*., 2002]. The interaction of AIF with DNA is in line with one hypothesis in which AIF might induce chromatin condensation and DNA fragmentation not directly but by increasing the susceptibility of DNA to latent nucleases.

I.2.3.3. The *AIF* gene and transcript variants

Eric Daugas and co-workers, using the Fluorescent *in situ* hybridization technique (FISH), revealed that only one single mouse chromosome hybridizes with the Aif cDNA [Daugas E. *et al*., 2000 A]. So, the *Aif* gene is localized within the mouse X chromosome region A6 which is syntenic to the human X chromosome region Xq25-26.
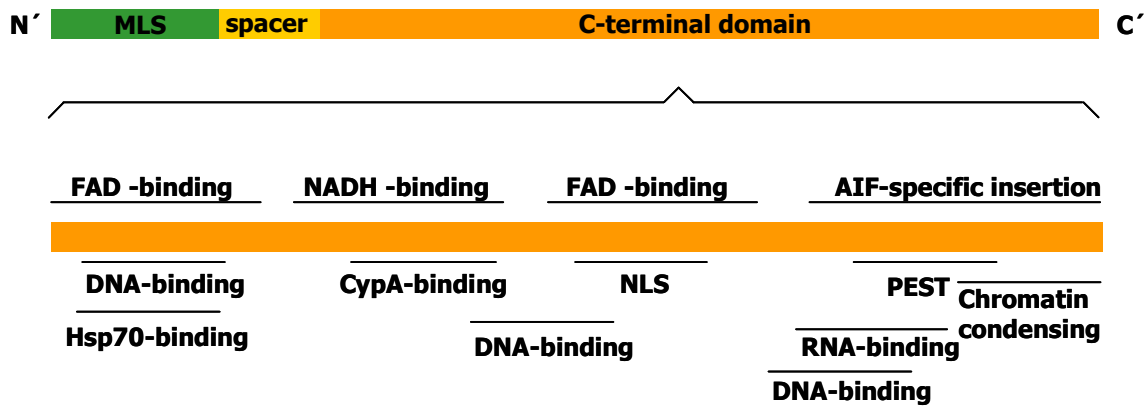
Figure I.5. Schematic representation of the molecular structure of AIF. The location of the structural domains of AIF is schematically shown but not on scale.

FISH analyses confirmed that human cells only contain one *AIF* on Xq. Based on Northern blot analysis using full-length AIF cDNA as a probe, only one single 2.4 kb AIF mRNA species could be found and it is expressed ubiquitously in human tissues [Daugas E. *et al.*, 2000 A]. This finding was corroborated at the protein level for mouse tissues using an antibody raised against aa 151-200 of AIF which recognizes a single protein band of about 57 kDa. Thus, in spite of the several cDNA variants listed in the GenBank data base (AF100928, AL049703 and AL049704) suggesting alternative splicing of the primary AIF transcript, these authors could only discern one dominant AIF mRNA and protein species, by standard Northern and Western blot techniques [Daugas E. *et al.*, 2000 A].

One year later, Markus Loeffler and colleagues reported the existence of a second splice form of AIF mRNA, corresponding to the cDNA with accession number AL049703. The *AIF* gene is composed of a total of 16 exons. RT-PCR cloning using primers for the extreme 5' and 3' termini of the *AIF* coding sequence yielded an AIF cDNA species (AIF-exB), [Loeffler M. *et al.*, 2001], that differed from the original AIF sequence [Susin S. *et al.*, 1999 B]. These results, originally obtained with the murine *Aif* gene, were then confirmed for the human *AIF*, yielding two very similar sequence variants [Loeffler M. *et al.*, 2001]. Alternative exon usage was shown to affect part of the 100-aa N-terminal MLS. Both exons possess significant homology in the C-terminal moiety. When green fluorescent protein (GFP) was fused to the C-terminus of AIF (AIF-GFP) or AIF-exB (AIF-exB-GFP) to generate chimeric proteins, transient transfection of COS cells revealed that the GFP-dependent fluorescence was targeted to mitochondria [Loeffler M. *et al.*, 2001]. These observations indicate that the

alternative exon 2 usage does not affect the mitochondrial import of AIF. It may be expected, then, that the mature AIF arising from canonical AIF cDNA of AIF-exB would be the same protein. The AIF transcript variant corresponding to the accession number AL049704 lacks several in-frame exons in the 5´-coding region, resulting in a significantly shorter protein, however the presence of this form has not been described in cell lines or tissues so far.

More recently, two new isoforms of AIF were described, named AIFsh (AIFshort) and AIFsh2, restricted to cytoplasm and mitochondria respectively [Delettre C. *et al.*, 2006 A; Delettre C. *et al.*, 2006 B]. AIFsh is a 35 kDa cytosolic protein, resulting from transcription of exons 10-16 of the *AIF* gene using an alternate transcriptional site located at intron 9. AIFsh2 contains the MLS and the oxidoreductase domain but lacks the C-terminal part due to the transcription of additional exon 9b which contains a transcription stop-code. Whilst AIFsh is translocated to the nucleus upon induction of cell death, AIFsh2 is released from mitochondria but cannot be translocated to the nucleus, in accord with the absence of NLS.

I.2.3.4. Cellular and sub-cellular localization of AIF

AIF has so far been detected in numerous human tissues and human cancer cell lines (more than 65 lines tested so far). It is ubiquitously expressed all throughout embryonic development as well as in adults [Daugas E. *et al.*, 2000 A]. Some of the AIF splicing variants, however, are not ubiquitously expressed [Delettre C. *et al.*, 2006 B].

In normal, non-apoptotic cells, the sub-cellular localization of AIF is the mitochondria. This has been proved many times. *In vitro* assays performed with the primary transcription/translation product of full-length AIF cDNA revealed that AIF is imported into mitochondria and that this import is dependent on the presence of the N-terminal MLS [Susin S.A. *et al.*, 1999 B]. Transient transfection of COS cells with GFP fused to the C-terminus of AIF to generate a chimeric AIF-GFP protein, targets this GFP to mitochondria [Vieira H.L. and Kroemer G., 1999]. In contrast, a truncated AIF-GFP fusion protein in which the N-terminal MLS was removed (AIF-GFP-Δ1-100), exhibits a diffused cytoplasmic localization of AIF, compared to the staining pattern obtained with GFP alone [Vieira H. and Kromer G., 1999]. Immunofluorescence staining of

untransfected cells with an AIF-specific antiserum, raised against aa 151-200, revealed that endogenous AIF is exclusively found in the mitochondria. [Susin S.A. *et al.*, 1999, B]. Detailed sub-cellular and sub-mitochondrial fractionation experiments showed that in healthy, non-apoptotic cells, AIF is confined to the mitochondrial IMS [Susin S.A. *et al.*, 1999 B]. However, Xiaopeng Zhang and co-workers in 2002, working on brain traumatic injury in rats and using immunoelectronmicroscopy, detected AIF in the hippocampus as a mitochondrial protein within the cristae and the inner membrane (IMM), [Zhang X. *et al.*, 2002]. Similar results were obtained by Hidenori Otera and colleagues, in 2005, who showed that AIF is a type-I inner membrane protein with its N-termuinus in the matrix and the bulk of the C-terminal portion in IMS [Otera H. *et al.*, 2005].

I.2.4. AIF and apoptosis

I.2.4.1. Translocation of AIF

Sub-cellular fractionation, immunoelectronmicroscopy as well as immunofluorescence experiments have established that AIF in normal, healthy cells is confined to mitochondria [Daugas E. *et al.*, 2000 B]. Nevertheless, AIF undergoes mitochondrio-nuclear translocation upon apoptosis induction, provoked by a plethora of pro-apoptotic stimuli such as the second messengers ceramide and ganglioside GD3, the protein kinase inhibitor STS, ROS and reactive nitrogen species (RNS) such as H_2O_2 and peroxinytrite, adriamycin, glucocorticoids, arsenite, the chemotherapeutic, genotoxic agents etoposide, doxorubicin and cisplatin, the alkylating agents, melphalan and chlorambucil, neurotoxic agents, such as the environmental pollutant Me-Hg and the microtubule-disrupting agent colchicine, Complex II inhibitor 3-nitropropionic acid (3-NP), the permeability-transition-pore (PTP) opening agents atractyloside, Ca^{2+}, *tert*-butylhydroperoxide or serum withdrawal [Susin S.A *et al.*, 1999 B; Daugas E. *et al.*, 2000 A; Daugas E. *et al.*, 2000 B; Susin S.A *et al.*, 2000; Loeffler M. *et al.*, 2001; Zhang X. *et al.*, 2002; Fonfria E. *et al.*, 2002; Almeida S. *et al.*, 2006]. AIF translocation has also been shown in several specific models of apoptosis such as T-cell hybridoma cells treated with dexamethasone [Susin S.A. *et al.*, 1999 B] or human glioma cell lines subjected to hyperthermia [Fukami T. *et al.*, 2004].

AIF translocation has been observed in a variety of cell lines induced to undergo

apoptosis, including peripheral T-lymphocytes, CEM and Jurkat lymphoma cells, COS renal cells, fibroblats, Rat-1, HeLa cervix carcinoma cells, primary rat neurons, SHEP neuroblastoma cells [Susin S.A. *et al.*, 1999 B; Daugas E. *et al.*, 2000 B; Vieira H.L. and Kroemer G., 1999; Loeffler M. and Kroemer G., 2000; Jacotot E. *et al.*, 2000; Dumont C. *et al.*, 2000; Ferri K.F. *et al.*, 2000 C; Braun J.S. *et al.*, 2002; Zhang X. *et al.*, 2002]. The translocation of AIF has also been reported for cell death occurring *in vivo*, in models of retinal degeneration [Hisatomi T. *et al.*, 2001], in the ipsilateral cortex and hippocampus after traumatic brain damage in rats [Zhang X. *et al.*, 2002], as well as brain damage induced by hypoglycaemia or ischaemia, or in myocardial infarction. The mitochondrial release of AIF is inhibited by cyclosporin A, a specific inhibitor of PTP [Miramar M.D. *et al.*, 2001]. It is also important to mention that the translocation of AIF can occur both in apoptosis and necrosis and thus can participate in the common death pathways [Daugas E. *et al.*, 2000 B], in line with the belief that early phases of apoptosis and of some types of necrosis may involve common mitochondrial events. Also, AIF translocation is a rapid event occurring in an all-or-nothing fashion [Loeffler M. *et al.*, 2001]. Taken together, it seems completely certain that AIF translocation invariantly accompanies apoptosis**.**

In contrast to cyt *c* which remains cytosolic after its translocation from the mitochondrion, AIF moves to the nucleus [Susin S.A *et al.*, 1999 B; Daugas E. *et al.*, 2000 B; Ferri K.M *et al.*, 2000 A], concomitant to the initial phase of chromatin condensation. In a model of traumatic brain injury in rats, translocated neuronal AIF was found to accumulate in the euchromatin regions and euchromatin-heterochromatin boundries of the nucleus [Zhang X. *et al.*, 2002]. The nuclear translocation of AIF is compatible with the presence of several putative NLS present within the oxidoreductase domain of AIF [Susin S.A *et al.*, 1999 B]. AIF translocation, in the model of photoreceptor apoptosis induced by retinal detachment, is inhibited by injection of nerve cell growth factor [Hisatomi T. *et al.*, 2002]. AIF translocation in general, seems to be inhibited by Bcl-2 as shown by the transfection-enforced overexpression of Bcl-2 [Daugas E. *et al.*, 2000 A; Loeffler M. *et al.*, 2001]. In clear contrast, different studies have showed that none of the apoptogenic effects of ectopic (extramitochondrial) AIF are prevented by overexpression of Bcl-2 [Loeffler M. *et al.*, 2001; Susin S.A. *et al.*, 1996; Susin S.A. *et al.*, 1999 B]. Transfection with AIF Δ1-100 or AIF Δ1-100-GFP causes accelerated cell death, as compared to full-lenth AIF cDNA or AIF-GFP overexpression which does not (Loeffler M. and Kroemer G., 2000; Loeffler

M. *et al.*, 2001; Ravagnan L. *et al.*, 2001].

So, all together, there is a widely accepted belief that only ectopic (extramitochondrial) AIF fulfils an apoptogenic function, while eutopic (mitochondrial) AIF is innocuous.

The true mechanism for translocation of AIF is still a subject of debate and whether the mitochondrio-cytosolic-nuclear translocation of AIF is dependent on caspase activation remains unclear. Several publications suggest that AIF translocation is caspase-independent, as it is not prevented by pharmacological inhibition using Z-VAD.fmk [Daugas E. *et al.*, 2000 B]. Similarly, the translocation of AIF can be observed *in vitro* in cells where there is no caspase activation, owing to knock out (KO) of Apaf-1, caspase-9 or caspase-3 [Susin S.A. *et al.*, 2000]. However, there is also strong evidence that in some death programs AIF is released secondary to caspase activation. For example, when caspase activation occurs early during apoptosis, as in CD95-triggered cell death *via* caspase-8 [Susin S.A. *et al.*, 1997] or during etoposide-induced apoptosis where the activation of caspase-2 occurs upstream of MMP [Lassus P. *et al.*, 2002]. Moreover, it is quite clear that caspases and caspase-activated proteins can trigger the release of AIF, as shown in purified mitochondria [Zamzami N. *et al.*, 2000]. All these observations then suggest that there are crosstalk pathways between AIF and caspases probably at several levels. Yet, the most acceptable idea, at the moment, is that AIF translocation and whether it is dependent on caspases or not is governed by the apoptotical "context" such as the cell type and pro-apoptotic stimulus used.

In several models of apoptosis induction, the release of AIF from mitochondria precedes that of cyt *c*, although how AIF can be released before cyt *c* is not clear. AIF is translocated prior to cyt *c* in STS-induced apoptosis [Susin S.A *et al.*, 1999 B; Daugas E. *et al.*, 2000 B], apoptosis induced by HIV-1 infection [Ferri K.M *et al.*, 2000 A; Genini D. *et al.*, 2001] or apoptosis triggered by fusion of cells expressing the HIV-1 envelope (Env) glycoprotein complex with cells expressing CD4 [Ferri K.M *et al.*, 2000 A; Ferri K.M. *et al.*, 2000 B]. In some of these paradigms of cell death, neutralization of AIF prevents mitochondrial release of cyt *c*, underscoring the possibility of AIF being required for cyt *c*-dependent caspase activation in some models. However, in other examples of cell death, mitochondria release AIF well after cyt *c* [Cregan S.P. *et al.*, 2002], which underlines the idea that several MMP mechanisms can cooperate in apoptosis.

Also of interest is the relation between the translocation of AIF and the dissipation of $\Delta\psi_m$ which is also a subject of an ongoing debate. In some models, the translocation of AIF and/or cyt c is strongly associated with $\Delta\psi_m$ reduction [Susin S.A *et al.*, 1999 B; Daugas E. *et al.*, 2000 B], whereas in others it appears to be accompanied by a transient increase in $\Delta\psi_m$, [Vander Heiden M.G. and Thompson C.B., 1999] or no change in $\Delta\psi_m$ [Goldstein J.C. *et al.*, 2000].

The exact rules governing the AIF import to the nucleus are also yet to be fully described. Nuclear apoptosis induced by microinjected AIF is inhibited by co-microinjection of the lectin wheat-germ agglutinin which acts as an active nuclear transport inhibitor. Blockade of the lectin moiety by N-acetylglucosamine abolished the wheat-germ agglutinin mediated inhibition of AIF-induced nuclear apoptosis. This observation suggests that AIF would be imported into the nucleus through an active and energy-consuming process. However, AIF has been shown to translocate to the nucleus in conditions of ATP-depletion [Daugas E. *et al.*, 2000 B] and is expected to interact with DNA in a non-specific fashion as a result of its basic pI [Miramar M.D. *et al.*, 2001].

As mentioned previously, Santos A. Susin and co-workers in 1999 suggested that AIF is synthetized in the cytosol as a 67 kDa precursor, further it gets cleaved after mitochondrial import by mitochondrial proteases giving rise to a 57 kDa mature form which translocates to the nucleus after a pro-apoptotic stimulus. Yet, there are several publications where the size of AIF in the nucleus and/or mitochondria are shown to be different than the suggested by Santos A. Susin. In 2002, Xiaopeng Zhang and colleagues reported the AIF species in the nucleus of cultured primary rat neurons treated with peroxynitrite, was of 67 kDa. The same authors performed an *in vivo* traumatic brain injury experiment in rats and found that the predominant AIF species in the neuronal mitochondria was 67 kDa and this band size was also predominant in the ipsilateral hippocampus after the brain injury. However, a 57 kDa AIF band was predominantly detected in the nuclei of ipsilateral cortex cells in the same experiment [Zhang X. *et al.*, 2002].

I.2.4.2. The apoptotic role of AIF

The apoptotic role of AIF after its translocation from the mitochondrion has been

studied extensively.

In cell-free systems, when added to purified nuclei from HeLa cells, recombinant AIF induces DNA loss [Loeffler M. *et al.*, 2001], peripheral chromatin condensation and large-scale DNA fragmentation, into 50 kb fragments, but no oligonucleosomal fragmentation or generation of nuclear bodies [Susin S.A *et al.*, 1999 B]. This pattern of chromatin modification is clearly distinct from that induced by CAD or Acinus [Samejima K. *et al.*, 1998; Sahara S. *et al.*, 1999]. The large-scale DNA fragmentation can be inhibited by EDTA or by the thiol-reactive compound *p*-chloromercuryphenylsulphonic acid (pCMPS) but not by Z-VAD.fmk [Susin S.A *et al.*, 1999 B]. This type of DNA fragmentation precedes oligonucleosolmal DNA degradation in several cellular models of apoptosis [Lagarkova M.A. *et al.*, 1995] and can be caspase-independent [Trbovich A.M. *et al.*, 1998; Susin S.A. *et al.*, 1999 B]. The nuclear effects of AIF are observed in the absence of cytosolic extracts. However, AIF has no effect on pre-heated nuclei (56 °C, 30 min) or naked DNA. Moreover, AIF has no intrinsic DNAse activity. All these data suggest that the effects of AIF on purified nuclei depend on the functional and/or physical interaction with some nuclear protein, likely a sessile nuclear DNase.

In addition to its nuclear effects, recombinant AIF also acts on isolated mitochondria. In strict contrast to isolated nuclei, AIF has no direct effect on purified mitochondria *in vitro*. Only in the presence of a thermo-labile cytosolic co-factor (abolished by mild heat treatment of the cytosolic extract at 70 °C, for 30 min), AIF causes purified mitochondria to dissipate the $\Delta\psi_m$ and also to release pro-apoptotic proteins such as cyt c and procaspase-9 [Susin S.A. *et al.*, 1999 B]. Again, this effect of AIF occurs in the presence of Z-VAD.fmk which means it is caspase-independent.

Microinjection of recombinant AIF into the cytoplasm of live cells induces several hallmarks of "typical" apoptosis such as: dissipation of $\Delta\psi_m$, nuclear chromatin condensation and DNA loss and exposure of phosphatidylserine on the outer leaflet of the plasma membrane [Susin S.A. *et al.*, 1999 B; Loeffler M. *et al.*, 2001]. None of these effects either on intact cells or isolated organelles can be prevented by overexpression of Bcl-2 nor by addition of Z-VAD.fmk, indicating that they are caspase-independent [Susin S.A *et al.*, 1999 B]. Similar *in vivo* effects have been seen by transfection-enforced overexpression of mAIF cDNA in Jurkat cells [Susin S.A. *et al.*,

1999 B] or overexpression of a truncated AIF-GFP construct lacking the N-terminal MLS (AIF-GFP-Δ1-100), [Vieira H.L. and Kroemer G., 1999]. COS cells transfected with AIF-GFP, AIF-exB-GFP and AIF-Δ1-100 constructs undergo nuclear apoptosis, both stage 1 and 2, in such a way that stage 1 is not, whereas progression to stage 2 is inhibited by Z-VAD.fmk preincubation [Loeffler M. *et al.*, 2001]. In the same study, it is shown that when cells are transfected with suitable AIF-GFP or cyt *c*-GFP fusion constructs targeted to mitochondria, microinjection of recombinant AIF rapidly triggers the release of either AIF-GFP or cyt *c*-GFP, suggesting that AIF, once present in the cytosol, can trigger the release of further AIF from mitochondria and thus engages in a positive feedback amplification loop [Loeffler M. *et al.*, 2001]. Such a feed-forward system would accelerate the process of AIF release upon apoptotic induction. This action of AIF was found to be independent of caspases [Loeffler M. *et al.*, 2001]. It is also important to mention that AIF microinjection has similar consequences in wild-type mouse embryonic fibroblasts (MEF) and MEF lacking the caspase activator Apaf-1 or caspase-3, which underscores, once again, the fact that AIF can act in a caspase-independent way [Susin S.A. *et al.*, 2000].

Taken together, extramitochondrial AIF is a well-accepted candidate for a caspase-independent cell death effector. Nevertheless, how AIF mediates its apoptogenic role still remains elusive. Neither the AIF-interacting protein(s) in the cytosol nor its target(s) in the nucleus have so far been fully identified.

Full-length AIF precursor protein (without FAD), AIF Δ1-100 and AIF Δ1-120 (both with FAD) all induce nuclear apoptosis when added to purified HeLa nuclei [Daugas E. *et al.*, 2000 A]. This indicates that the oxidoreductase activity (which depends on the presence of the prosthetic group) is not relevant to the apoptogenic effects of AIF. However, deletions affecting parts of the oxidoreductase domain (Δ1-351, Δ155-612, Δ538-612) abolish the apoptotic potential of AIF, both on isolated nuclei or mitochondria and in live cells, indicating that at least some of the structural features of the oxidoreductase domain are necessary for the apoptotic effects of AIF [Susin S.A *et al.*, 1999 B]. Yet, recombinant AIF precursor protein becomes apoptogenic after refolding on a nickel-affinity matrix even in the absence of FAD. This function seems to be conformation-dependent as it can be readily destroyed by trichloric acid treatment, exposure to mild heat (65 °C) or precipitation with ammonium sulphate [Susin S.A *et al.*, 1999 B].

AIF has also been implicated in several disease models. Illustratively, syncytia arising from the fusion of cells expressing the HIV type-1 envelope glycoprotein complex and cells expressing the CD4/CXC chemokine receptor 4 complex undergo AIF-dependent apoptotic cell death [Ferri K.F. *et al.*, 2000 A], indicating that AIF may be involved in the pathogenesis of HIV infections. Another case is the microglial and neuronal apoptosis in the hippocampus caused by *Pneumococcus* infections where caspase-independent, AIF-dependent apoptosis is thought to play a role [Braun J.S. *et al.*, 2001], indicating the AIF may be involved in meningitis pathogenesis.

But, is AIF required for apoptosis to occur?

This question has been addressed in various studies and currently there is not an established consensus yet. Although, AIF can clearly induce certain aspects of cell death in cultured cells and cell models, the question as to whether it is really essential for PCD *in vivo* remains unresolved [Joza N. *et al.*, 2001]. It seems that the real role of AIF in the cell death initiation and/or executing is strongly dependent on the cell type and the cell death context. Also, AIF may be an important executioner of apoptosis in scenarios where the role of caspases is not prominent [Braun J.S. *et al.*, 2001].

Still, at least in some pathways of apoptosis induction, AIF is both sufficient and required to induce apoptosis. For example, microinjection of a specific antiserum into the cytoplasm of Rat-1 cells treated with STS prevents nuclear apoptosis. Control experiments involving a pre-immune antiserum or an anti-AIF antibody blocked by pre-incubation with the AIF-derived immunogenic peptides, yielded no inhibition of STS-stimulated apoptosis [Susin S.A. *et al.*, 1999 B]. Taking into account the fact that in several models of apoptosis, AIF translocation precedes that of cyt *c*, one may postulate a slightly different hypothesis for the importance of AIF in the early stages of cell death initiation rather than in the final execution. In that direction, microinjection of the AIF-specific antiserum abolishes morphological signs of atractyloside (Atr)-induced nuclear apoptosis, although it does not impede the Atr-induced $\Delta\psi_m$ dissipation and later cell death [Susin S.A. *et al.*, 1999 B].

There are several studies which link AIF to PCD at the genetic level.

The KO of the AIF gene, in embryonic stem (ES) cells, using homologous

recombination technology, refined the knowledge on the contribution of AIF to apoptosis [Joza N. *et al.*, 2001]. It was performed in male ES cells, leading to an $Aif^{-/y}$ genotype. Unlike cyt $c^{-/-}$, Apaf1$^{-/-}$ and caspase-9$^{-/-}$ ES cells [Yoshida H. *et al.*, 1998; Hakem R. *et al.*, 1998; Li K. *et al.*, 2000], $Aif^{-/y}$ ES cells display normal susceptibility to death induced by STS, etoposide, anisomycin, UV-radiation, azide or *tert*-butylhydroperoxide. This normal susceptibility to apoptosis was observed both in the absence and the presence of Z-VAD.fmk. Nevertheless, the $Aif^{-/y}$ ES cells were resistant to cell death following serum withdrawal [Joza N. *et al.*, 2001]. Moreover, in the presence (but not in its absence) of Z-VAD.fmk, $Aif^{-/y}$ ES cell lines failed to die in response to vitamine K3 (menadione) as pro-apototic treatment [Joza N. *et al.*, 2001]. Thus, AIF seems rate-limiting for some pathways of cell death induction.

As to the role of AIF in embryogenesis, the same authors showed that AIF-deficient ES cells can differentiate into cells from all three germ layers, suggesting that it is not generally required for proliferation and differentiation. However, they found that AIF is essential for cavitation, a phenomenon which comes as a result of the first wave of apoptotic cell death during embryogenesis and is essential for the initiation of gastrulation [Coucouvanis E. and Martin G.R., 1995]. This early developmental process can be mimicked *in vitro* by culturing aggregates of ES cells in the absence of leukaemia inhibitory factor (LIF) and/or feeder cells which results in formation of embryonic bodies (EBs). The inner cells of these structures later undergo PCD to form cystic EBs, which mimics the cavitation process in the embryo. The role of AIF in cavitation was thus tested in the process of EBs formation using $Aif^{+/y}$ and $Aif^{-/y}$ ES cells. Both cell lines were able to form simple and complex EBs with comparable kinetics. However, whereas a significant proportion of $Aif^{+/y}$ EBs underwent cavitation, EBs from differentiated $Aif^{-/y}$ ES cells exhibited complete inhibition of the cavitation process [Joza N. *et al.*, 2001]. Cavitation was shown to be normal in $Aif^{+/y}$ EBs in the presence of Z-VAD.fmk. Further analysis in the same publication, showed that the impaired cavitation in $Aif^{-/y}$ EBs is not caused by enhanced proliferation but is due to a failure of the inner cells to undergo apoptosis which underlines the important role of AIF in the embryonic apoptosis program. Considering that cavitation is essential for embryogenesis, these results are in line with the fact that no viable mouse embryos can be generated from $Aif^{-/y}$ ES cells [Joza N. *et al.*, 2001], whereas Apaf1$^{-/-}$ and caspase-9$^{-/-}$ mice are viable until birth, although affected by severe developmental defects, particularly in the central nervous system (CNS), [Yoshida H. *et al.*, 1998;

Hakem R. *et al.*, 1998; Cecconi F. *et al.*, 1998]. Cyt *c* was found to be released from mitochondria of WT, Apaf1$^{-/-}$ and caspase-9$^{-/-}$ inner mass cells undergoing cavitation-associated apoptosis. Still, there was no cyt *c* translocation from mitochondria to the cytosol in inner mass cells of *Aif*$^{-/y}$ EBs, indicating that the OMM failed to permeabilize. So, during cavitation in EBs, AIF seems to act upstream of cyt *c* and independently of the cyt *c*/Apaf1-triggered caspase activation cascade, making this another case of AIF-dependent but caspase-independent PCD pathway. Moreover, the AIF-regulated pathway of PCD required for embryonic cavitation exhibits classical ultrastructural features of apoptosis with the exception of caspase-dependent advanced chromatin condensation [Joza N. *et al.*, 2001].

Another genetic model to address the importance of AIF in embryogenesis was the study of Apaf-1 KO mice, which fail to activate caspases [Cecconi F. *et al.*, 1998; Yoshida H. *et al.*, 1998]. In such mice, the interdigital web persists transiently during embryonic development, although interdigital cells eventually die without caspase activation, which allows generation of correctly formed toes [Cecconi F. *et al.*, 1998; Yoshida H. *et al.*, 1998]. Moreover, addition of a chemical caspase inhibitor to explanted embryonic limbs fails to inhibit cell death *in vitro* which proves the caspase independency of interdigital cell death. Importantly, it appears that in dying Apaf-1$^{-/-}$ cells, AIF is overexpressed and translocated to the nucleus.

Of note, a recent publication by Doris Brown and colleagues analyzed the consequences of inactivating *Aif* function in the early mouse embryo [Brown D. *et al.*, 2006]. Unexpectedly and in contrast to pervious reports, these authors found that *Aif* function was not required for apoptotic cell death in the embryo. Moreover, by embryonic day 9, loss of *Aif* function caused abnormal cell death, leading to death of *Aif* null embryos at embryonic day 12.

So, it seems quite clear that AIF is involved in early stages of ontogeny, however this finding awaits future detailed research.

I.2.5. The oxidoreductase function of AIF

In accordance with its flavoprotein structure, AIF has an oxidoreductase function. This electron transport function of AIF *in vitro* was thoroughly analyzed by María Dolores

Miramar and collaborators in 2001. They found that the absorption spectrum of AIF shows the typical features of an oxidized FAD flavoprotein, with the visible maximum at 378 nm and 450 nm and a shoulder at 467 nm [Miramar M.D. *et al.*, 2001]. AIF has a redox potential strongly influenced by pH. Assuming a two-electron reduction step, the midpoint redox potential is −308±15 mV at pH 7.5, whereas it reaches −373±15 mV at pH 9.0. In the same publication, these authors also showed that natural AIF purified from mitochondria and recombinant AIF purified from bacteria (AIFΔ1-120) exhibit NADH oxidase activity and can generate superoxide anion ($O_2 \cdot^{-}$) upon addition of NADH or NADPH. The K_m for NADH was calculated as 99.4±10 μM with a turnover number of 2.09 min^{-1}, whereas if NADPH is used as an electron donor, the K_m value is 52.9±12 μM and the turnover number 2.8 min^{-1}. These kinetics parameters are very similar to values described for other NADH oxidases forming $O_2 \cdot^{-}$. Addition of exogenous FAD does not stimulate the NADH oxidase activity of AIFΔ1-120, in contrast to NADH oxidases from bacteria. It also catalyzes cyt *c* reduction in the presence of NADH, with a K_m of 0.46 mM and a k_{cat} of 21.76 min^{-1}. In addition, AIF exhibits monodehydroascorbate reductase activity with a specific activity of 8.8 units/mg and a k_{cat} of 0.505 min^{-1}, a feature common to several AIF homologues described in plants [Lorenzo H.K. *et al.*, 1999]. Both the cyt *c* reductase and the monodehydroascorbate reductase activity of AIF can be inhibited by the enzyme superoxide dismutase (SOD), indicating that the reaction occurs *via* $O_2 \cdot^{-}$ formation. In addition, the same authors show that AIF does not exhibit peroxidase activity.

Altogether, the results from this work show that AIF has a marked NADH oxidase activity, thus according to the classification by Vincent Massey [Massey V., 1994], it may belong to the electron-transferase class of NADH reductases, as it can rapidly react with oxygen, forming $O_2 \cdot^{-}$ and flavoprotein neutral radical as products. Several NADH oxidases from bacterial sources have been isolated and characterized [Arcari P. *et al.*, 2000], their putative role is expected to be in the maintenance of the cellular redox balance under aerobic conditions, by converting NADH to NAD$^+$ [Toomey D. and Mayhew S.G., 1998]. However, AIF is not similar to any of the previously described NADH oxidases. First, it is monomeric, whereas bacterial NADH oxidases are usually dimeric or tetrameric [Jarasch E.D. *et al.*, 1981]. Second, AIF transfers electrons without the involvement of cysteinyl groups, whereas other NADH oxidases rely on a redox-active disulfide center formed by two vicinal cysteine residues [Toomey D. and Mayhew S.G., 1998; Arcari P. *et al.*, 2000]. Third, AIF oxidizes NADH *via* a mechanism

that does not require the addition of exogenous FAD, whereas several NADH oxidases from bacteria do require FAD [Toomey D. and Mayhew S.G., 1998; Arcari P. *et al.*, 2000]. Fourth, in contrast to several NADH oxidases [Toomey D. and Mayhew S.G., 1998], AIF does not function as a H_2O_2 scavenger.

Very importantly, AIF has an oxidoreductase function which can be dissociated from its apoptogenic activity, both in cell-free systems and in intact cells [Miramar M.D. et al., 2001]. First, addition of NADH or NADPH fails to enhance the apoptogenic activity of AIFΔ1-120 and second, inhibition of the oxidoreductase activity by removal of FAD or external addition of SOD or diphenyleneiodonium (DPI, an inhibitor of flavonoid-containing enzymes) fails to modify the apoptogenic activity of AIF [Loeffler M. *et al.*, 2001; Miramar M.D. *et al.*, 2001]. In contrast, pCMPS abolishes the pro-apoptotic function of AIF without affecting its oxidoreductase activity [Miramar M.D. *et al.*, 2001]. Moreover, recombinant AIF-precursor protein becomes apoptogenic after refolding on a nickel-affinity matrix even in the absence of FAD, indicating that the oxidoreducatse activity is unnecessary for its apoptogenic function [Susin S.A. *et al.*, 1999 B].

I.2.6. Second role of AIF

There is not a single cell line or primary tumour analyzed in which AIF expression is not present. Taking into account this highly ubiquitous distribution, it is possible to suggest that, in addition to its apoptogenic function, AIF also exerts a yet-to-be-defined vital function, perhaps related to its oxidoreductase activity [Daugas E. *et al.*, 2000 A].

Like cyt *c*, AIF is likely to be a phylogenetically old, bifunctional protein with an electron donor/acceptor function and a second, independent apoptogenic function. Yet, AIF has no shown homology with any of the members of the mitochondrial electron transport chain (ETC), [Susin S.A. *et al.*, 1999 B]. It is tempting to speculate that AIF may act as a vital oxidoreductase catalyzing electron transfer between cyt *c* and NAD [Loeffler M. *et al.*, 2001]. Little attention has been given to the physiological role of AIF within the mitochondria [Mate M.J. *et al.*, 2002].

A very important break-through in the search for the second role of AIF was the work of Jeffrey A. Klein and colleagues published in Nature, 2002. They studied the

Harlequin (Hq) mutant mice model which harbours a murine ecotropic pro-viral insertion in intron 1 of the *Aif* gene. As a consequence of this mutation, the *Aif* transcript and protein levels in homozygous Hq mice are reduced by 80% relative to wild-type levels in the cerebellum, as well as in other organs such as brain, kidney, muscle, heart, eyes and liver. Hq mice are a late-onset neurodegenerative mouse model which can be phenotypically identified by the complete loss of hair in hemizygous males (Hq/Y) and homozygous females (Hq/Hq), ataxia and blindness, due to loss of cerebellar and retinal neurons, progressive with age [Barber B.R., 1971; Bronson R.T. *et al.*, 1990]. Moreover, loss of AIF was shown to lead to oxidative stress as catalase activity and glutathione levels are increased in the cerebella of Hq mice compared to wild-type controls [Klein J.A. *et al.*, 2002]. Interestingly, neither of these effects was seen in the other parts of the brain and there were no detected changes in the expression of SOD1 and SOD2. Moreover, lipid peroxides were increased in Hq cerebella, as well as the remainder of the brain and in the heart and oxidatively damaged DNA was detected both in cerebellum and retina of Hq mice. In addition, down-regulation of AIF was shown to confer sensitivity to both exogenous and endogenous peroxides in cultured granule cerebellar cells measured by cell viability assays. This is very specific for granule cerebellar cells as other types of neurons such as cortical neurons, are more resistant to oxidative stress-induced cell death. Also, cultured mutant cerebellar granule cells showed increased sensitivity to non-oxidative stress-mediated cell death such as serum withdrawal. However, no differences in cell death were observed between Hq mutant and wild-type granule cells subjected to either etoposide or STS. This last result is in line with the result obtained using ES cells lacking AIF [Joza N. *et al.*, 2001]. Further studies on the Hq mouse model showed an important antioxidant role of AIF in the myocardium [van Empel V.P. *et al.*, 2005]. Namely, Hq mouse cardiomyocytes demonstrated increased sensitivity to H_2O_2-induced cell death and Hq hearts subjected to ischemia/reperfusion revealed more cardiac damage compared to wild-type counterparts.

Taken together, the results obtained with the Hq mouse model suggested, for the first time, that AIF has an antioxidant activity, particularly as a peroxide scavenger, in line with its structure similar to glutathione peroxidase, a potent scavenger of peroxides in mammalian cells [Klein J.A. *et al.*, 2002].

In their paper detailing protein structure of mAIF, María J. Maté and co-workers [Mate

M.J. *et al.*, 2002] suggested that the analysis of the structure of AIF as well as the function of the non-apoptogenic homologues of AIF should offer an essential framework to study the mitochondrial, physiological and non-cytocidal role of AIF. In that direction, these authors compared AIF with its most similar homologue, the bacterial protein BphA4. This enzyme reduces the ferredoxin component (BphA3) of the biphenyl dioxygenase complex. Interestingly, BphA3 is similar to the ferredoxin from the mitochondrial cytochrome bc1 complex which is the complex that catalyzes the electron transfer from ubiquinone to cyt *c* in the mitochondrial ETC. Indeed, the globular domain of this iron-sulphur protein is exposed to the IMS, which is where AIF is believed to be located. These comparative structural analyses suggest a possible role of AIF in the electron transfer in the mitochondrial ETC.

When this work was initiated, the idea about the second role of AIF was still vague and elusive. However, the fact that AIF holds a mitochondrial role, different from its role in apoptosis, is nowadays widely accepted. Several publications showed that AIF-depleted cells have compromised oxidative phosporylation (OxPhos). Very recently, Eric C.C. Cheung and colleagues managed to dissociate this dual AIF function and showed a novel role of AIF, in controlling mitochondrial morphology and cristae structure [Cheung E.C. *et al.*, 2006].

I.2.7. AIF and the electron transport chain (ETC)

In the course of this thesis, several publications appeared reporting a connection between AIF and Complex I of the ETC. Nicola Vahsen and co-workers found that reduced OxPhos in retina and some brain regions of Hq mice correlates with decreased expression of nuclear-encoded respiratory Complex I subunits [Vahsen N. *et al.*, 2004]. This group also reported that inhibition of AIF expression in both mouse and human cells by either homologous recombination or siRNA results in severe reduction of Complex I expression and activity. Moreover, mice in which *Aif* has been inactivated specifically in cardiac and skeletal muscle exhibit impaired activity and protein expression of respiratory Complex I, leading to development of severe skeletal muscle atrophy and heart failure [Joza N. *et al.*, 2005]. In this work, loss of AIF was shown to result in increased levels of some markers of oxidative stress, such as lipid peroxidation products and catalase activity. However, the authors postulate a primary role of AIF in regulating Complex I integrity rather than primarily acting as a ROS scavenger.

27

Likewise, neurons from forebrain-specific AIF null mice have decreased Complex I expression and defective mitochondrial respiration, leading to defects in the cortical development and reduced neuronal survival [Cheung E.C. *et al.*, 2006]. Also, *Aif* null embryos display diminished Complex I protein expression and impaired Complex I activity [Brown D. *et al.*, 2006]. Since AIF is not an integral part of Complex I, it was assumed to play a role in the organizing and/or maintenance of the integrity of this complex. Importantly, AIF does not directly bind to Complex I, nor does its loss affect transcription of Complex I subunits [Vahsen N. *et al.*, 2004]. Despite the remarkable progress in this research, what is the exact mechanism by which AIF interacts with Complex I, remains unclear and needs future investigation.

Interestingly, it has been reported that cells deficient in Complex I display a lower efficiency in H_2O_2 detoxification [Zoccarato F. *et al.*, 2004]. On the other hand, however, it was also shown that KO or silencing of AIF in various cancer cell lines reduces ROS levels, possibly correlated with Complex I decreased activity [Urbano A. *et al.*, 2005]. This can be reversed by over-expressing AIF with intact NADH-binding capacity, thus demonstrating that the oxidoreductase activity of AIF is required for Complex I function [Urbano A. *et al.*, 2005]. Recent studies have revealed possible links between Complex I deficiency and AIF translocation in certain models of neurodegeneration. 1-methyl-4-phenyl-1,2,3,6-tetrahydropyrimidine (MPTP) is a cytotoxic compound which causes AIF translocation from the mitochondria to the nucleus in both neuron-differentiated PC-12 cells [Liou A.K. *et al.*, 2005] and a mouse mesencephalic dopaminergic cell line [Chee J.L. *et al.*, 2005]. It has been postulated that N-methylpyridinium (MPP$^+$) blocks Complex I and consequently inhibits OxPhos which triggers cell death. In light of these data, one could speculate that inhibition of Complex I by MPP$^+$ could perturb the Complex I-associated oxido-reductase activity of AIF.

Noteworthy, Complex I deficiency has been shown to be the main cause of several mitochondrial diseases such as Leber´s hereditary optic neuropathy (LHON), mitochondrial encephalomyopathy with lactic acidosis and stroke-like episodes (MELAS) etc. Moreover, a 30-40% decrease in Complex I activity has been reported in the substantia nigra of idiopathic patients with Parkinson´s disease (PD), [Jellinger K.A., 1999] and Complex I was shown to be misassembled and oxidatively damaged in neocortical samples of PD patients obtained post-mortem [Keeney P.M. *et al.*, 2006].

I.2.8. AIF and neurodegenerative disorders

Alterations in the function of mitochondrial proteins, both mitochondrial- and nuclear encoded, can result in abnormal energy production and/or generation of ROS. Either effect can progress into PCD. Mitochondrial dysfunction and PCD, resulting in selective neuron loss, have been implicated in numerous neurodegenerative diseases including PD, Alzheimer's disease (AD), amyotrophic lateral sclerosis (ALS), Huntington´s disease (HD), diabetic encephalopathy and retinal degeneration [Cassarino D.S. and Bennet J.P. Jr., 1999; Almeida S. *et al.*, 2006; Krantic S. *et al.*, 2007].

Oxidative stress has been observed in neurons of patients with several neurodegenerative diseases, yet the means by which such stress is generated and how it leads to cell death, is not fully understood. Moreover, in several models, such as cerebral ischaemia, AD, Pick's disease and intractable temporal lobe epilepsy, oxidative stress-induced neuronal apoptosis has been correlated with abortive cell cycle re-entry [Klein J.A. *et al.*, 2002; Klein J.A. and Ackerman S.L., 2003]. The oxidative stress manifested as presence of ROS-induced damage in proteins, lipids and nucleic acids in dying neurons is age-related and consistent with the disease severity.

Growing biochemical and pharmacological evidence suggests that AIF is involved in many neuropathies, both chronic and acute. The best studied model for the importance of AIF in such diseases is the Hq mouse mutant [Klein J.A. *et al.*, 2002]. In this model, the expression pattern of AIF is much wider then the tissues phenotipically affected by its down-regulation, similar to many gene products involved in neurodegenerative disorders. In the brain, AIF is expressed in cerebellar neurons, hippocampus, dentate gyrus, olfactory bulb, brainstem nuclei and cerebral cortex. In the Hq mouse model of neurodegeneration, neuronal loss is not observed in non-cerebellar brain structures.

Another approach to address the role of AIF in neurodegenerative disorders is to first study its involvement in acute neuronal apoptosis. The translocation of AIF has been observed in several paradigms of post-mitotic-neuronal apoptosis, including death of photoreceptors induced by retinal detachment [Hisatomi T. *et al.*, 2001], neuronal cell death induced by brain traumatic injury *in vivo* [Zhang X. *et al.*, 2002] and cerebral ischaemia [Zhu C. *et al.*, 2003]. As to the pro-apoptotic agents which trigger neuronal

AIF translocation, there have been several reported: H_2O_2, peroxynitrite, the topoisomerase I inhibitor camptothecin, 3-NP, the excitotoxin N-methyl-D-aspartate (NMDA), Aβ peptides, MPTP etc. Moreover, several of these apoptotic programs appear to be caspase-independent. On the other hand, certain contexts of neurodegeneration involve increased AIF protein expression in the mitochondria without major AIF nuclear translocation, as suggested by the data obtained from surgical resections of the temporal lobe from patients suffering medically intractable epilepsy [Schindler C.K. *et al.*, 2006].

It is interesting to mention also the fact that AIF expression is age-related in normal neuronal tissues, such as the human cerebral cortex where it increases with age, however this increase does not occur in AD patients [Reix S. *et al.*, 2007]. Herein, this increase of AIF has been attributed a protective role, presumably as a defense mechanism aimed at maintaining the integrity and function of the respiratory chain against age-related changes in the brain, such as increase in the ROS production. In addition, AIF expression patterns regarding its different isoforms have also been shown to vary with the age, from the neonatal stage throughout the adulthood, as it is the case with the total protein extracts of rat parietal cortex [Zhang X. *et al.*, 2002; Zhu C. *et al.*, 2003].

In all, the role of AIF in neurodegeneration remains very intriguing. The same way its physiological role is clearly dual, its involvement in neurodegenerative pathologies may be dual. It could be based on its direct apoptotic function outside the mitochondria as well as its vital function in the mitochondria, in maintenance of OxPhos and the ROS status, which may be an indirect apoptotic regulator.

I.2.9. Clinical aspects

It has been shown that AIF is required for experimental apoptosis induction in several human cancers such as T-cell lymphoma, lung or cervix carcinoma. Thus, it is tempting to speculate that the identification of AIF targets and AIF inhibitors (both endogenous and exogenous) may lead to the generation of a new class of cytotoxic or cytoprotective drugs which can be used for the gene therapy of cancer [Daugas E. *et al.*, 2000 A]. Generating a dominant apoptosis inducer (AIF-Δ1-100) that overcomes Bcl-2 mediated apoptosis inhibition can be a useful tool in a gene therapy-induced

ablation of cancer cells, naturally over-expressing caspase inhibitor proteins and/or anti-apoptotic Bcl-2-like proteins [Loeffler M. *et al.*, 2001].

As there is growing evidence for involvement of AIF in neurodegenerative disorders, through AIF-depending and AIF-related cell death programs, another possible neuroprotective strategy could be based on blocking mitochondrial release and/or its take-up by the nucleus [Krantic S. *et al.*, 2007].

It is evident that clinical aspects of AIF remain elusive and future detailed studies are necessary.

I.3. Mitochondria- more than just "power houses of the cell"

Virtually all eukaryotic cells contain mitochondria. These cytoplasmic organelles, 0.5-1 μm in size, were once free-living bacteria which adapted to life inside larger cells some 2 billion years ago. On average, there are 300-400 mitochondria in every cell, giving rise to 10 million billion in the entire human body, which is about 10% of our body weight. Metabolically active cells, such as brain, muscle or kidney cells, can have thousands of mitochondria in a single cell, making up some 40-50% of the cytoplasm. Every mitochondrion contains 5-10 copies of its genome, in a circular, bacterial-like chromosome, which means that there are hundreds or thousands of copies of the mitochondrial genome in a single cell. Human mtDNA is a 16 569 bp, double-stranded DNA molecule containing 37 genes which encode only 13 proteins. The rest of the mitochondrial proteins, some 1000, are encoded by nuclear genes. This is due to the fact that modern mitochondria have lost the bulk of their genes through the course of evolution, as most were transferred across to the nucleus.

Mitochondria have versatile functions in the cell. Although an extensive review of the complex mitochondrial role is beyond the scope of this thesis, some mention of the importance of mitochondria is warranted.

Energy generation

Mitochondria generate almost all our energy, in form of ATP, in the OxPhos process [Tyler D.D., 1992]. In this process, electrons liberated from reducing substrates,

produced in the Krebs cycle and β-oxidation, are delivered to O_2 *via* a chain of multimeric protein complexes (complexes I-IV of the ETC), embedded in the IMM (for detailed composition of the complexes, see Tab.I.1). Some of the respiratory complexes function as proton (H^+) pumps, pumping H^+ form the negative matrix to the positive IMS, establishing a H^+ gradient across the IMM, as initially suggested by Peter Mitchell [Mitchell P. and Moyle J., 1965]. This provides electrochemical energy to drive ATP synthesis at complex V (ATP synthase), (Fig.I.6).

There are tens of thousands of complete respiratory chains in a single eukaryotic cell, enabling the mitochondria to produce approximately 15 times more ATP than the glycolytic pathway, a condition which has given the mitochondria their traditional moniker of "power houses of the cell".

The function of the OxPhos system began to be revealed with the discovery of ATP and its role in energy metabolism in the 1930s. Three-dimensional structures at atomic resolution are now available, giving a complete picture of the arrangement of the ETC. However, despite these advances in understanding the molecular structures of the complexes, the overall respiratory chain synthesis, organization and regulation remain largely unknown.

Complex	Name	Nº of proteins	Prosthetic groups
I	NADH Dehydrogenase	46	FMN, 8 Fe-S centers
II	Succinate-CoQ reductase	5	FAD, cyt b_{560}, 3 Fe-S centers
III	CoQ-cyt *c* Reductase	11	cyt b_H, cyt b_L, cyt c_1, Fe-S_{rieske}
IV	Cytochrome *c* Oxidase	13	cyt a, cyt a_3, Cu_A, Cu_B

Table I.1. Composition of the mitochondrial ETC.

More than 80 different proteins take part in the assembly of the ETC complexes, 13 of which are encoded by mtDNA. The mtDNA-encoded proteins are all essential for OxPhos and include seven subunits of Complex I, one subunit of Complex III, three subunits of Complex IV and two subunits of Complex V. The rest are nuclear encoded and can be divided into two groups: structural components of ETC and proteins which control the formation, assembly and turnover of the respiratory complexes.

Mammalian ETC consists of five macromolecular complexes, as depicted in Fig.I.6. Complex I (NADH-ubiquinone oxidoreductase; EC 1.6.5.3), one of the most

complicated enzymes of the eukaryotic cell, is the point of entry for the major fraction of electrons that traverse the respiratory chain. Although four decades have passed since the first isolation of Complex I from bovine heart mitochondria by Joe Hatefi and co-workers, information on its structure and mechanism of action is still limited. This enzymatic complex is the largest (and least understood) of the respiratory complexes, consisting of 46 subunits and with a total relative molecular mass of 980 kDa [Hirst J. *et al.*, 2003]. It is L-shaped and composed of 14 central or "core" subunits and 32 accessory subunits organized in two major domains or "arms" separated by a thin collar, the membrane-embedded arm and the peripheral arm protruding into the mitochondrial matrix (Fig.I.7). The peripheral arm contains a non-covalently-bound FMN prosthetic group and eight Fe-S clusters (two binuclear and six tetranuclear), [Grigorieff N., 1998]. The enzyme oxidizes NADH, transfers the electrons through FMN and eight Fe-S centres and finally reduces ubiquinone (coenzyme Q10 or just Q) using the energy released in this process to pump H^+ across the IMM (Fig.I.7). The exergonic transfer of two electrons from NADH to Q is coupled to translocation of four H^+. What is the exact pathway of the electron transfer through the subunits of Complex I and how is this transfer linked to the proton translocation is still a matter of debate as several models for the energy transduction have been proposed. Moreover, as Complex I is a large, multiunit enzyme, under bigenomic control, its biogenesis and assembly are very complicated and still poorly understood. Recent investigation has shown that assembled Complex I associates with Complex III and Complex IV into supercomplexes or "respirasomes" which may have a role in complex stability and/or substrate channelling [Schägger H., 2002; Schägger H. *et al.*, 2004].

Research on Complex I has recently taken on greater significance since the finding that many human mitochondrial diseases (even 50% of the reported cases) involve structural and functional defects at the level of this enzyme complex and it is involved in a growing list of human pathological conditions such as neurodegenerative disorders or diabetes. Complex I is the target of many environmental toxins and molecules such as pesticides and insecticides. There is also a long list of natural inhibitors of Complex I, derived from microorganisms and plants.

Complex II (succinate-ubiquinone reductase) participates in the citric acid cycle (Krebs cycle) by oxidizing succinate to fumarate, thus transferring electrons to the ubiquinone pool but without translocating protons (schematically shown in Fig.I.6).
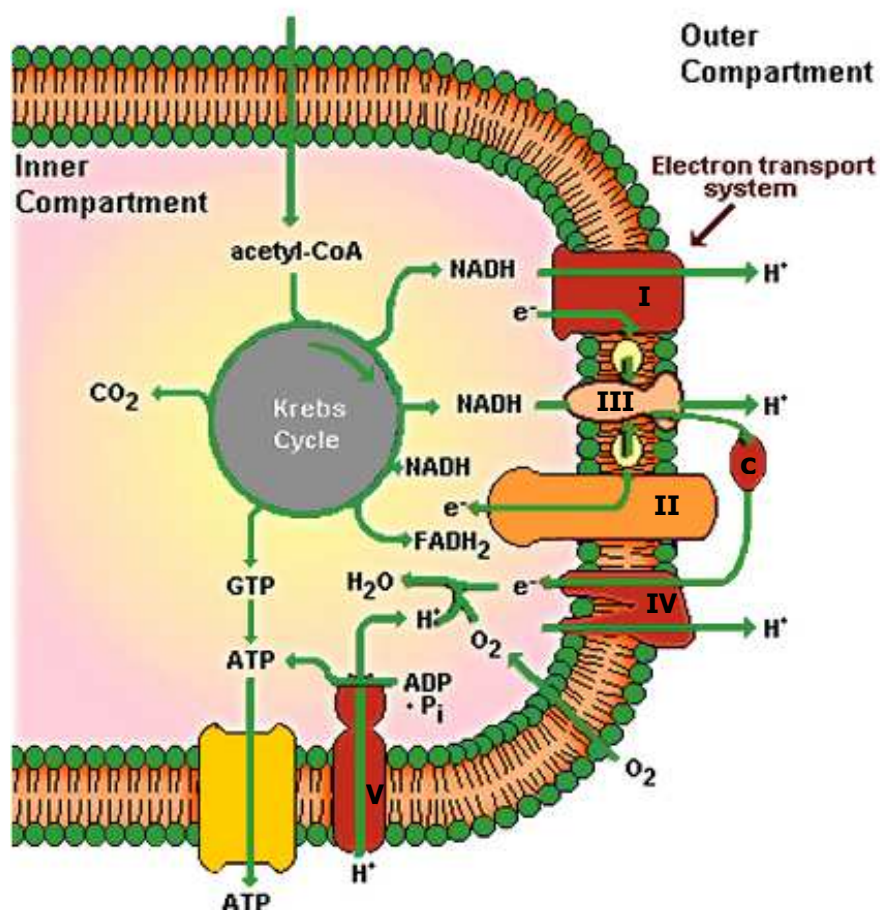
Figure I.6. Mitochondrial physiology, molecular connections between ETC and the Krebs cycle. Abbreviations: I-V (ETC complexes I-V), c (cytochrome *c*).

Complex III (cytochrome bc_1, or ubiquinol/cyt *c* oxidoreductase) delivers electrons from ubiquinol (QH_2) to cyt *c* and pumps protons across the IMM. The electron flow from cyt *c* continues to the binuclear copper centre CuA and to the heme a_2-CuB in Complex IV (cyt *c* oxidase). This is where electrons are donated to molecular oxygen, reducing it to water. Complex V (ATP synthase) utilizes the electrochemical gradient generated by Complexes I, III and IV to generate ATP, from ADP and P_i (Fig.I.6).

ROS generation

Mitochondria are a significant and in most cells, major source of ROS. This production is both a physiological and a pathological phenomenon. High, non-physiological levels of ROS have been correlated with aging and an increasing number of diseases (cancer, diabetes, neurodegenerative diseases, inflammation, heart failure). Yet, mitochondrial ROS are not just damaging by-products of respiration, but important players in cell signalling [Brookes P.S. *et al.*, 2002], (the involvement of mitochondrial ROS in human

disease is schematically shown in Fig.I.9)
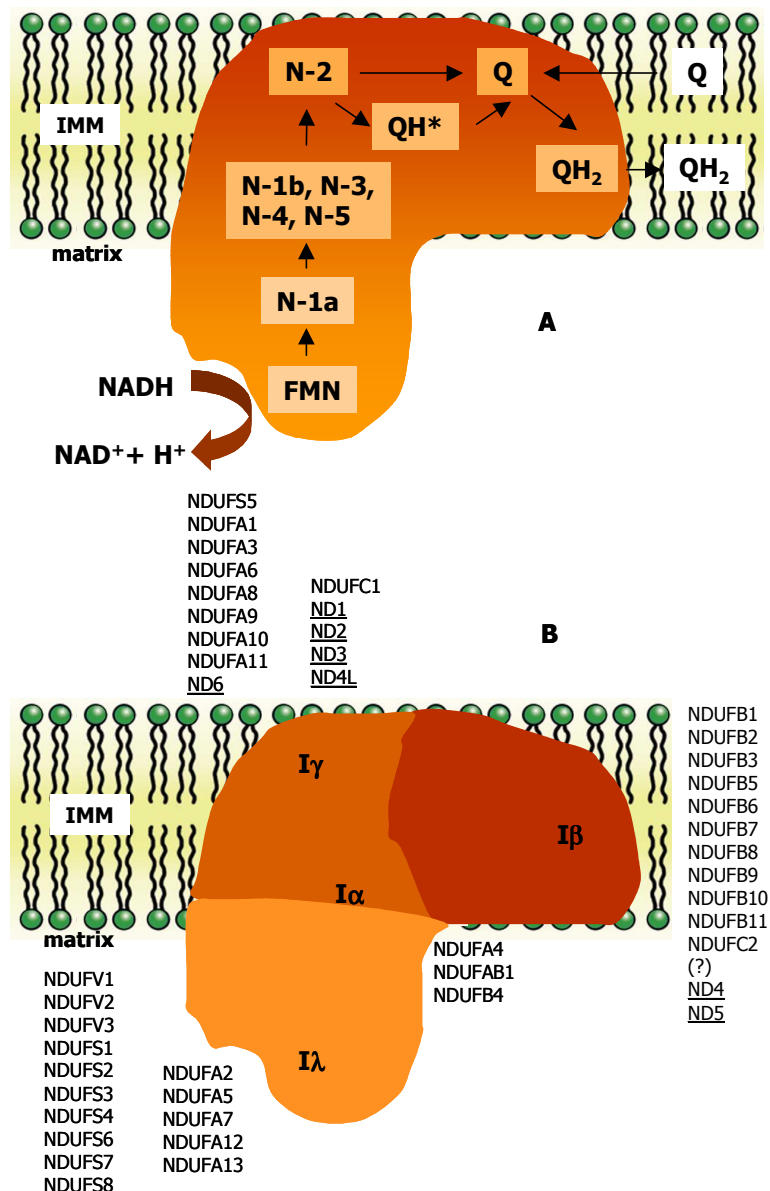
Figure I.7. Complex I structure. A. Diagram showing the electron flow through Complex I. B. Schematic representation of human Complex I and the topology of its subunits; mtDNA-encoded subunits are underlined.

PCD

As mentioned in the chapter "I.1. Apoptosis-chronicle of a death foretold", it is now well known that mitochondria play a major role in regulating cell death. Regarding this, mitochondria can both initiate the death signalling by changes in ATP, NAD(P)H and Ca^{2+} concentration, ROS generation, $\Delta\psi_m$ disruption or respond to external stimuli and thus amplify the cellular death signal. Mitochondria contain many proteins involved in

the apoptotic process such as: procaspases -2,-3 and -9, Smac/Diablo, AIF, cyt c, Endo G, Omi/HtrA2.

Ca^{2+} homeostasis

Mitochondria also play a very important role in regulating spatiotemporal Ca^{2+} homeostasis in the cell, thus participating in different physiological and pathological paradigms [Babcock D.F. *et al.*, 1997]. This control occurs at two levels: by maintenance of the intracellular energetic levels (if mitochondria become dysfunctional and ATP synthesis is impaired, cellular Ca^{2+} homeostasis is rapidly affected) and secondly, by active accumulation of high concentrations of Ca^{2+} (1 μM in the mitochondrial matrix), mainly by the activity of a selective uniporter.

Metabolic pathways

Mitochondria are the site of important metabolic reactions such as the urea cycle, the carnitine cycle, the Krebs cycle, β-oxidation, steroid and porphyrin synthesis, inter-conversion of amino acids and xenobiotic metabolism [Lehninger A.L., 1964]. Of note, mitochondria are active regulators of the cytosolic concentrations of many molecules such as inorganic ions and NAD$^+$.

Thermogenesis

Heat generation (thermogenesis) is achieved when the chemical energy contained in reduced substrates is released, but not used for ATP synthesis i.e. the OxPhos process is uncoupled. This is essential in cold-adapted, hibernating and newborn mammals, where the body temperature is maintained in a manner independent of shivering and is due to the presence of mitochondrial uncoupling proteins [Nicholls D.G. and Locke R.M., 1984].

Mitochondrial pathologies

Since the 1960s, over 120 human mitochondrial diseases have been discovered. Many of them have been associated with specific, inherited mtDNA mutations producing ETC deficiencies. Mitochondrial diseases are surprisingly common (it is believed that 1 in

5000 newborns carries some kind of a mitochondrial disorder) and bizarre (some do not follow Mendel´s laws of inheritance due to the astonishing fact that mtDNA is almost exclusively maternally inherited). Mitochondrial diseases typically affect metabolically active tissues such as the brain and muscle, producing movement disorders and neuronal diseases, known alltogether as mitochondrial encephalomyopathies. The most common ones are: LHON, MELAS, MERRF (myoclonus epilepsy with ragged red fibers) and the Leigh syndrome.

I.4. Reactive oxygen species (ROS)

ROS are generated by all aerobic cells as by-products of a number of metabolic reactions and in response of various stimuli [Fridovich I., 1978]. The term ROS is often replaced by the term "free oxygen radical" though they are not synonymous. Some of the ROS are indeed free radicals as defined by the chemical definition of a free radical being the atom or molecule that contains one or more unpaired electrons (Tab.I.2). Yet, as some ROS are not free radicals, it is more appropriate to speak of ROS when referring to this complex group of molecules. Intracellular generation of ROS occurs in many different cellular compartments and situations. The endogenous ROS sources include the mitochondrial ETC, NADPH oxidase, peroxisomes, cytochrome p450, glucose oxidase, xanthine oxidase, cyclooxygenase, lipooxygenase and γ-glutamyl transpeptidase as well as several non-enzymatic autooxidation processes [Sauer H. *et al.*, 2001]. The number of enzymes which can directly generate ROS or indirectly contribute to ROS synthesis, under certain physiological and pathological circumstances, is growing rapidly. In addition to endogenous sources, many exogenous agents such as hyperoxia, anoxia/reoxygenation, mineral dusts, smoke, toxins and ionising radiation are capable of inducing ROS formation at the cellular level. ROS can cause cell injury by reacting with proteins, lipids and nucleic acids but they are also an essential part of normal physiology, such as signal transduction and the killing of micro-organisms by phagocytic cells.

I.4.1. Mitochondrial ROS

In most cell types, mitochondria are considered a predominant source of ROS, which mainly include $O_2\cdot^-$, H_2O_2, and the hydroxyl free radical (OH·), [Loschen G. *et al.*, 1971; Chance B. *et al.*, 1979].

Since mitochondria consume about 85-90% of the oxygen used by the cell, the mitochondrial ETC generates a substantial amount of intracellular ROS [Shigenaga M.K. *et al*., 1994]. During mitochondrial respiration under normal conditions, 1-5% of the electron flow is reported to result in the formation of H_2O_2 [Chance B. *et al*., 1979]. Yet, given that these initial estimates were made on isolated mitochondria in the presence of high, non-physiological concentrations of O_2, the *in vivo* rate of mitochondrial ROS production is, most likely, considerably less. Several studies have proven that mitochondria produce low levels of ROS that can be effectively scavenged by the cellular antioxidant defences at resting conditions. The steady state intracellular concentration of $O_2\cdot^-$ and H_2O_2 have been estimated as $\sim 10^{-11}$ and 10^{-9} M respectively [Boveris A. and Cadenas E., 1997; Forman H.J. and Boveris A., 1982]. These low basal level of ROS produced by mitochondria at rest, makes mitochondrial ROS ideal signalling molecules providing a physiologically safe window for redox signalling, which allows the cell to regulate mild to moderate oxidative changes and critically respond to them by activating cellular processes such as proliferation and differentiation. Mitochondrial ROS also fulfil other pre-requisites of a second messenger since they are short-lived (rapidly generated and degraded), produced in response to a stimulus, specific in action, enzyme-regulated, highly diffusible and ubiquitously present in most cell types.

Reactive oxygen species	
Radicals	**Non-radicals**
Superoxide ($O_2\cdot^-$)	**Hydrogen peroxide (H_2O_2)**
Hydroxyl (OH·)	**Ozone (O_3)**
Peroxyl ($RO_2\cdot$)	**Singlet oxygen ($^1\Delta gO_2$)**
Alkoxyl (RO·)	
Hydroperoxyl ($HO_2\cdot$)	

Table I.2. Reactive oxygen species generated in a mammalian cell.

Mitochondrial ROS are mainly generated at the ETC. As electrons pass through the mitochondrial ETC, some electrons leak out to molecular oxygen (O_2) to form $O_2\cdot^-$. It has been shown that the ETC can produce $O_2\cdot^-$ at Complex I and Complex III (Fig.I.8). Whereas some studies claim that the later accounts for 80% of the total generation under normal conditions, others suggest Complex I to be a more relevant location for

ROS formation [Brand M.D. et $al.$, 2004; Adam-Vizi V. and Chinopoulos C., 2006]. The molecular source of $O_2 \cdot^-$ at Complex III is believed to be the ubisemiquinone radical intermediate (QH·), formed during the Q cycle at the Q_o site of Complex III [Muller F.L. et $al.$, 2003]. In the case of Complex I, several domains have been suggested to be the site of ROS generation, including some of the Fe-S centers, the flavin moiety and the enzyme-bound NADH [Krishnamoorthy G. and Hinkle P.C., 1988; Genova M.L. et $al.$, 2001; Kudin A.P. et $al.$, 2004]. It is likely that Complex I and III actually generate two different pools of superoxide, Complex I releases it in the matrix, while Complex III in the IMS [Jezek P. and Hlavata L., 2005].

Generated $O_2 \cdot^-$ has a short life and under normal conditions is rapidly dismutated by manganese superoxide dismutase (MnSOD) to form H_2O_2 [Loschen G. et $al.$, 1971; Boveris A. and Cadenas E., 1975]. A reductive transition metal-dependent homolytic cleavage of H_2O_2 produces the highly oxidative and cytotoxic hydroxyl radical (OH·). This (Fenton) reaction, is balanced by the metal chaperone proteins present in the mitochondrial matrix. OH· is also produced when H_2O_2 reacts with $O_2 \cdot^-$ in a reaction that also generates a molecule of water and molecular oxygen. While $O_2 \cdot^-$ and H_2O_2 are not extremely toxic, OH· has strong cytotoxic affects. Furthermore, $O_2 \cdot^-$ can also react with nitric oxide (NO) and thus generate the harmful radical peroxynitrite ($ONOO \cdot^-$). Both H_2O_2 and $O_2 \cdot^-$ can enter the cytosol and further participate in redox signaling. H_2O_2 produced within the mitochondria is highly diffusible in contrast to $O_2 \cdot^-$, which cannot diffuse through membranes, making it easily compartmentalized. Thus, mitochondrial generated $O_2 \cdot^-$ may be kept separated from the cytosol until an appropriate stimulus releases it through VDAC [Han D. et $al.$, 2003]. Another route for $O_2 \cdot^-$ release may be through PTP, as low molecular weight compounds up to molecular weight 1500, can be exchanged between the mitochondrial matrix and the cytosol via this pore [Szewczyk A. and Wojtczak L., 2002]. Since PTP is reported to reversibly open/close naturally in intact cells without resulting in apoptosis, mitochondrial signaling molecules could be exchanged with the cytosol by the transient "flickering" (open/closing) of the PTP in response to certain stimuli [Minamikawa T. et $al.$, 1999]. In regard to turning the mitochondria ROS signal off, cellular antioxidant defenses such as SOD, catalase, and glutathione peroxidase easily degrade ROS, which terminates the signal.

Mitochondria are highly dynamic structures capable of changing their shape (by

elongation, branching, swelling) and their location inside a living cell [Bereiter-Hahn J. and Voth M., 1994]. These dynamic changes can create sub-compartments or "microzones" within the cytoplasm and this is very important for signal transduction as it depends on the close proximity of substrates and effector molecules. Compartmentalization has already been reported to play a key role in redox signaling and this attribute should be considered when describing the mitochondria as a signal transducer [Pani G. *et al.*, 2001]. In adult cells, mitochondrial clustering functions to create steep gradients of low molecular weight species such as O_2, ATP, and pH resulting in specialized microzones that may facilitate signal specificity [Aw T.Y., 2000].
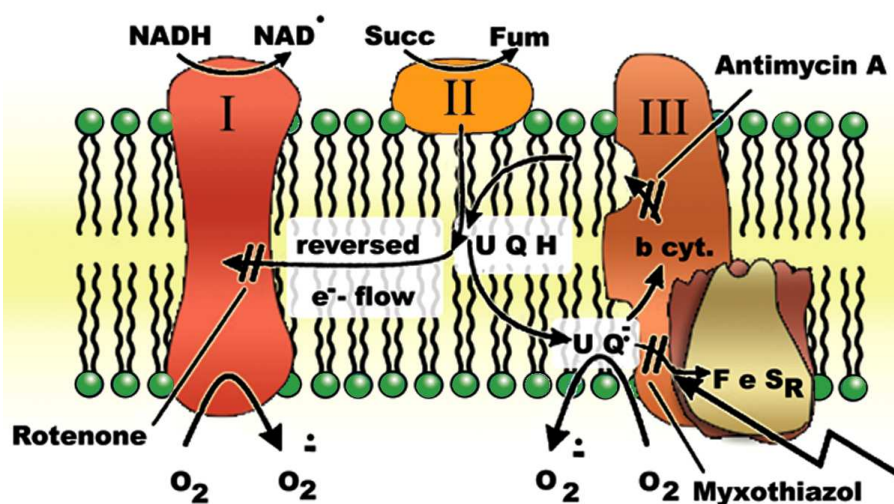
Figure I.8. Schematic representation of part of the mitochondrial ETC, showing ROS generation. $O_2\cdot^-$ is generated at Complex I and Complex III. (Succ: succinate; Fum: fumarate; UQ: ubiquinone; UQ$\cdot^-$: ubisemiquinone), [modified from Nohl H. *et al.*, 2005].

Many, versatile endogenous and exogenous stimuli have been described to induce incremented ROS production in the mitochondria. They include: disruption of the ETC, changes in the O_2 concentration (ischaemia-reperfusion), changes in $\Delta\psi_m$ (particularly increase but decrease has also been shown), lack of ADP, increment in the NADH/NAD$^+$ ratio, decompartmentalization of Ca^{2+}, endogenous molecules such as ceramide, TNF-α as well as a long list of drugs (for eg. ETC inhibitors such as rotenone, MPP$^+$ ion, 3-NP, piericidin, antimycin A, azide, cyanide; uncoupling agents), [Adams J.D. Jr *et al.*, 1993; Quillet-Mary A. *et al.*, 1997; Rosenstock T.R. *et al.*, 2004]. Nevertheless, a number of signalling pathways involved in triggering mitochondrial ROS production remain largely unknown.

The pathologically increased mitochondrial ROS can lead to oxidative stress, a condition characterized by damage of proteins, lipids and nucleic acids which culminates in cell death by apoptosis or necrosis.

Mitochondria-derived pathological ROS have been implicated in numerous diseases and in the aging process [Harman D., 1956; Balaban R.S. *et al.*, 2005], as schematically depicted in Fig.I.9. The human CNS is relatively deficient in oxidative defences [Marttila R.J. *et al.*, 1988], rendering it more susceptible to ROS-induced damage. Oxidative damage has been implicated in the major neurodegenerative disorders such as AD, PD, ALS and Friedreich´s ataxia [Beal M.F., 1995; Swerdlow R.H. *et al.*, 1996].
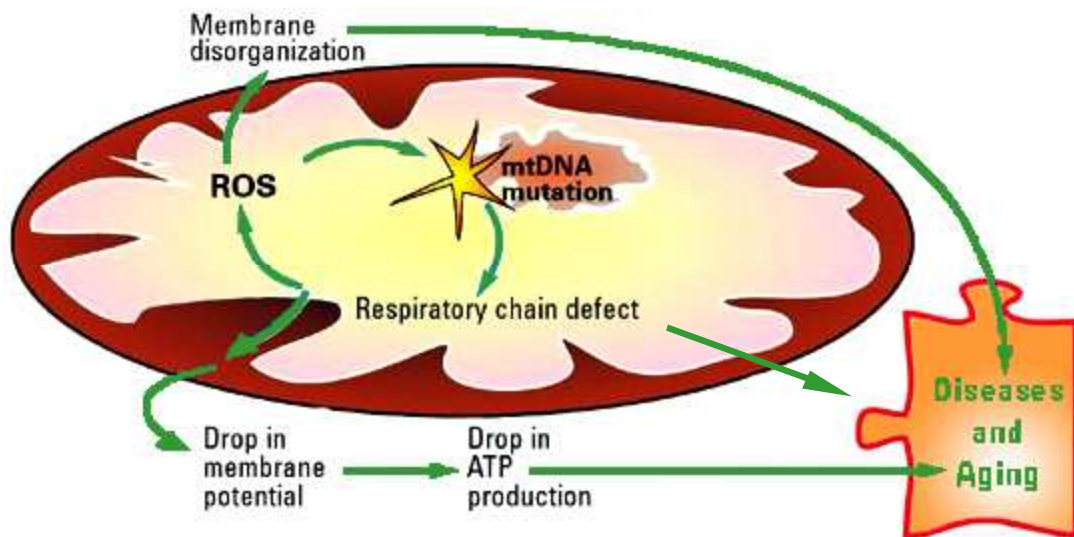
Figure I.9. Mechanism of mitochondrial dysfunction; mtDNA mutations, ETC defects and increased ROS production are closely related. The respiratory chain defect generates ROS which can produce mtDNA mutations and lead to drop in the mitochondrial membrane potential and further damage of ETC. This can result in drop in the ATP production. Consequently, these effects can provoke diseases and aging [modified from Rustin P. *et al.*, 2000].

In addition to the respiratory chain, a significant amount of ROS in mitochondria can be produced by the TCA cycle enzyme α-ketoglutarate dehydrogenase (α-KGDH), located in the mitochondrial matrix [Starkov A.A. *et al.*, 2004; Tretter L. and Adam-Vizi V., 2004] and the monoamine oxidase (MAO) in the OMM [Andreyev A.Y. *et al.*, 2005].

I.4.2. Detoxification of ROS

Detoxification of ROS is one of the pre-requisites for all aerobic life forms, thus multiple

enzymatic and non-enzymatic defence systems have evolved forming the oxidant defence network. An imbalance between these defence mechanisms and ROS generation leads to a state termed "oxidative stress". Both acute and chronic oxidative stress can have deleterious effects, as alterations in the cellular redox state clearly reflect in alterations of many cellular functions such as proliferation and differentiation. Antioxidants are molecules that combat oxidative stress by direct scavenging of ROS, act to prevent ROS formation or can repair cellular and tissue damage caused by this stress.

The non-enzymatic antioxidant defences comprise versatile low molecular weight molecules such as vitamins (vitamin A, C and E), coenzyme Q, cyt c, glutathione (GSH), NADPH, melatonin, uric acid, α-keto acids, bilirubin, carotenoids as well as metal-binding proteins (transferrin, ferritin, albumin).

The antioxidant-reacting enzymes mainly include: superoxide dismutase (SOD), catalase (CAT) and the thiol-reducing system members: glutathione peroxidases (Gpx) and peroxiredoxins (Prx). The main enzymatic ROS-detoxifying system is schematically shown in Fig.I.10.

SOD is a metalloprotein that can very efficiently dismutate superoxide to H_2O_2 and molecular oxygen, as shown in the chemical reaction represented in Fig.I.11. Although dismutation of superoxide occurs rapidly without catalysis, SOD accelerates this reaction by 10^4 fold. Two types of SOD are found inside eukaryotic cells: Cu/ZnSOD (SOD1) and MnSOD (SOD2), interestingly showing no significant sequence homology. SOD1 is a homodimeric enzyme composed of subunits of molecular weight of 15.6 kDa, predominantly located in cytosolic fractions, but also found in peroxisomes and nuclei and even the mitochondrial IMS. Interestingly, it has also been shown to generate toxic OH· from H_2O_2, under certain circumstances [Yim M.B. *et al.*, 1990]. SOD2 is a homotetrameric enzyme whose subunits have molecular weight of 23 kDa. It is located in the mitochondrial matrix and encoded by a nuclear gene. There is a relationship between the metabolic activity and MnSOD levels. Tissues with high metabolic activity and correspondingly increased ROS production, such as liver, kidney, heart and brain, possess higher levels of MnSOD [Marklund S.L. *et al.*, 1982].

Unlike SOD1, SOD2 is strongly induced by a wide variety of factors such as hyperoxia,

irradiation, TNF-α, lipopolysaccharides (LPS), interleukin-1 (IL-1), oxidized low density lipoprotein (ox-LDL) and IF-γ.

Interestingly, SOD2 expression was reported to decrease during hypoxia. The crucial importance of this enzyme has been shown with KO studies, i.e. mutant mice lacking MnSOD die within 10-21 days of life from severe cardiomyopathy, neurodegeneration and metabolic acidosis [Lebovitz R.M. *et al*., 1996]. In contrast, the phenotype of SOD1 KO mice is less dramatic, as they are fairly normal but more susceptible to neuronal injury [Reaume A.G. *et al*., 1996].
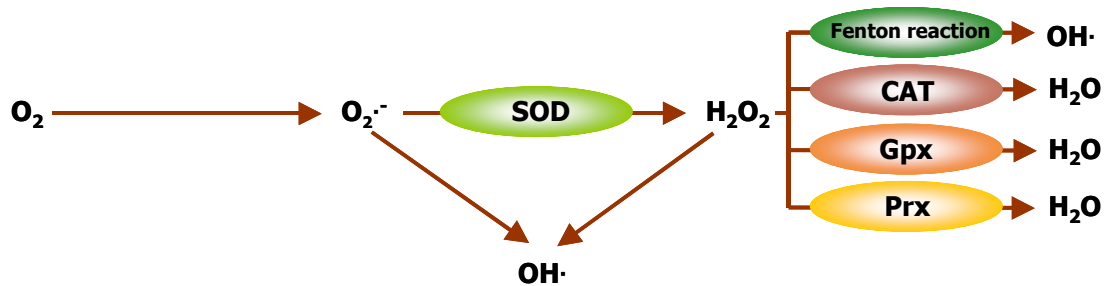
Figure I.10. Simplified schematic representation of the fate of mitochondrial ROS.

CAT is a homotetrameric ferriheme protein that removes H_2O_2 by the reaction represented in Fig.I.11 CAT is one of the most efficient enzymes known with a turnover of 300 000 sec^{-1}. In most cells, CAT is confined to peroxisomes, where it detoxifies the H_2O_2 generated in the process of lipid oxidation. Interestingly, it has also been found in the IMM. In humans, most tissues possess only low levels of CAT.
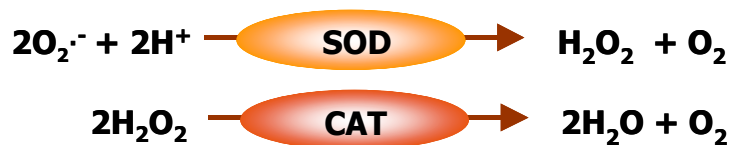
Figure I.11. Enzymatic reactions catalyzed by SOD and CAT.

I.4.2.1. Thiol-reducing systems: the thioredoxin and the glutathione systems

Proteins in the extracellular environment or on the cell surface are rich in disulfides. In contrast, the inside of the cell is kept reduced and proteins contain free sulfhydryl groups rather than disulfides. There are several systems which are in charge of

maintaining proteins in their reduced state. In some cases, thiol-disulfide reactions overlap with ROS-detoxifying reactions.

The glutathione system

Reduced glutathione (GSH) is recognized as one of the most important intracellular and extracellular non-enzymatic antioxidants. It is a cysteine-containing tripeptide (γ-glutamyl-cysteinyl-glycine) which exists in very large (mM) levels inside cells where it acts by quenching free radicals, detoxifies peroxides and participates in maintaining other important redox molecules in their reduced state (α-tocopherol, ascorbic acid) [Tarpey M.M. *et al*., 2004]. GSH is continuously regenerated from its oxidized form GSSG by the action of NADPH-dependent glutathione disulfide reductase (GR or GSSG-R), as depicted in Fig.I.12. The balance of GSH and GSSG concentrations (GSH/GSSG ratio) is a dynamic indicator of oxidative stress. GSH is a substrate for the glutathione peroxidases (Gpx), a family of Se-requiring proteins which reduce H_2O_2 or alkylhydroperoxides, such as those generated by the oxidation of polyunsaturated lipids. Gpx is localized both in the cytoplasm and the mitochondrion.

The thioredoxin system

Thioredoxins are small, ubiquitously expressed, multifunctional proteins whose main function is to reduce disulfide bonds formed between Cys residues in a target protein. These disulfide bonds formed between Cys residues can occur as a part of a catalytic cycle or are often produced by ROS damage [Ritz D. and Beckwith J., 2001]. The active centre of the thioredoxins is characterized by the presence of two redox-active cysteine residues, as a part of a conserved amino acid sequence: -Cys-Gly-Pro-Cys-, thus they participate in redox reactions through the reversible oxidation of their active centre dithiol to a disulfide. Trx acts as a protein disulfide reductant for ribonucleotide reductase and several transcription factors including NF-κB, and AP-1, p53 and the glucocorticoid receptor [Ueno M. *et al*., 1999; Nordberg J. and Arnér E.S., 2001].

Oxidized Trx are reduced to the dithiol form by the selenocysteine-containing flavoenzyme Trx reductase (TrxR), with the use of electrons from NADPH [Powis G. and Montfort W.R., 2001], as shown in Fig.I.12. Several studies have shown that TrxR and Trx have considerably different expression patterns in different mammalian tissues

[Rozell B. *et al.*, 1985, Spyrou G. *et al.*, 1997]. It is also suggested that TrxR of higher organisms can reduce many other substrates, in addition to reducing Trx-S2 (Arner E.S. *et al.*, 1999). Thus, it is perfectly established that both Trx and TrxR can modulate signal transduction properties of ROS by the reduction of intracellular disulfides.

It is also important to say that Trx exerts part of its antioxidant properties through Trx peroxidases (also called peroxiredoxins, Prx). This is a family of non-Se peroxidases expressed in several subcellular compartments including mitochondria, which use –SH groups, obtained from Trx or GSH as reducing equivalents. Trx reduces the oxidized form of Trx peroxidase and the reduced Trx peroxidase scavenges ROS, such as H_2O_2 [Kang S.W. *et al.*, 1998], (Fig.I.12).
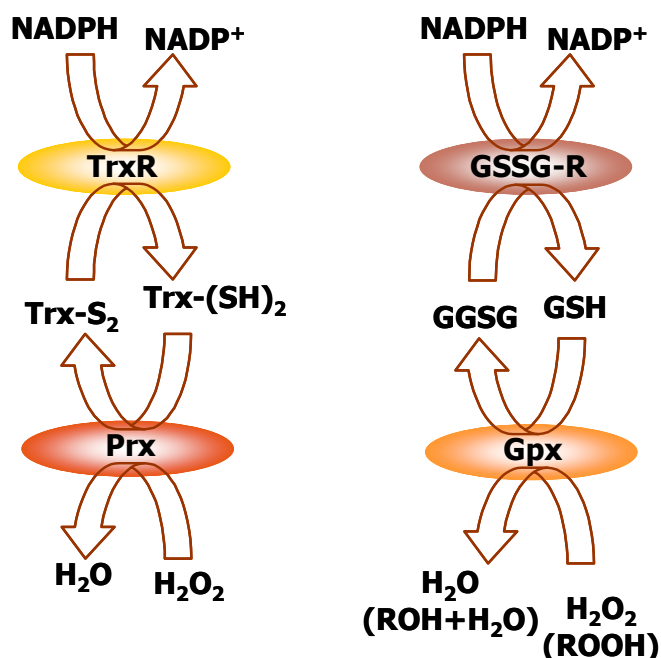
Figure I.12. The GSH and Trx system. The regeneration of both systems is possible in the presence of NADPH equivalents.

The human Trx system has been related to several pathological conditions since its discovery. Such cases are the adult T-cell leukaemia (ALT), caused by human T-cell leukaemia virus Type-I (HTLV-I) infection and the acquired immunodeficiency syndrome (AIDS), caused by human immunodeficiency virus (HIV), [Masutani H. *et al.*, 2005]. In the case of ALT, Trx expression has been shown to be augmented in HTLV-I-transformed T-cell lines which may result in stimulated growth and inhibited apoptosis of these cells leading to cellular transformation and leukemogenesis. HIV-infected T-

cells, on the contrary, display downregulation of the Trx system which accounts for the increased apoptosis in these cells, a well-known hallmark of AIDS. However, the plasma levels of Trx in HIV-infected individuals have been shown to be elevated reflecting the presence of chronic oxidative stress in AIDS patients.

There are two mammalian forms of Trx, the cytosolic, Trx1 and the mitochondrial, Trx2. Trx1, lack of which is embryonic lethal [Matsui M. *et al.*, 1996], is the major dithiol reductant in the cytosol. It has numerous functions such as defence against oxidative stress, control of growth and apoptosis and is also secreted with co-cytokine and chemokine activities [Arner E.S. and Holmgren A., 2000]. These multiple roles of Trx1 have been also observed in transgenic mice, as constitutively overexpressing Trx1 confers elongated lifespan and protection against acute lung failure, ischemic injury or diabetes mellitus [Hotta M. *et al.*, 1998; Takagi Y. *et al.*, 1999; Mitsui A. *et al.*, 2002; Hoshino T. *et al.*, 2003]. Most of these functions, but probably not all of them, depend on the disulfide reductase activity of Trx1.

Human Trx2 was cloned in 1997 [Spyrou G. *et al.*, 1997]. It possesses a Cys-rich active site common for Trx but lacks the structural cysteines present in Trx1. Trx2 has a MLS at the N-terminus and after the cleavage by a mitochondrial peptidase, the mature protein has a relative molecular weight of 12.2 kDa. Its presence in mitochondria is accompanied by the presence of a mitochondrial isoform of TrxR. Specific sub-mitochondrial localization to the IMM and high resistance to oxidation suggest that Trx2 provides a primary line of defence against oxidative stress, caused by ROS generated at the ETC [Spyrou G. *et al.*, 1997; Masutani H. *et al.*, 2005].

Trx2 also displays a documented anti-apoptotic role, based on the inhibition of apoptosis signal-regulating kinase 1 (ASK1), [Zhang R. *et al.*, 2004] and prevention of cyt *c* release from the mitochondrion [Chen Y. *et al.*, 2002], a critical hallmark of mitochondria apoptosis-signalling pathway. Also, overexpression of Trx2 confers an increase in $\Delta\psi_m$ and resistance to etoposide-induced cell death [Damdimopoulos A.E. *et al.*, 2002], whereas suppression of Trx2 expression in a conditional Trx2-defficient chicken B cell line, DT-40, causes accumulation of ROS and induced cyt *c* release and apoptosis [Tanaka T. *et al.*, 2002]. The KO of the *Trx2* gene in mice is embryonic lethal, indicating that Trx2 is indispensable for cell survival and that Trx1 and Trx2 cannot compensate for each other [Nonn L. *et al.*, 2003].

The mitochondrial Trx system has been demonstrated to play a role in cell survival and cell cycle progression. A biological role for TrxR2 in cell growth was demonstrated in HeLa cells using a dominant negative form of TrxR2 (TrxR2DN), [Kim MR *et al.*, 2003]. An increase of G_1 to S phase transition, cell growth, and transcription of cell cycle genes was induced by TrxR2DN expression. TrxR2DN expression was suggested to increase intracellular H_2O_2, which in turn signalled cell proliferation. Alterations in cellular redox status by increased expression of TrxR2 have been suggested to play a role in the growth of hepatocellular carcinomas [Choi J.H. *et al.*, 2002]. In addition, it has been reported that mice lacking TrxR2 die in the embryonic stage because of reduced myocardial function and perturbed hematopoiesis [Conrad M. *et al.*, 2004].

In summary, the known physiological roles of the Trx system are many and have grown in a remarkable way over the last few decades. Interestingly, one could speculate that the pro-apoptotic function of AIF might be regulated by Trx1 and/or Trx2 in some way [Masutani H. *et al.*, 2005].

In addition, it is important to stress that the thiol-reducing and related systems are clearly coupled to NADPH oxidation. Thus, the cellular levels of NADPH play a very important role in the thiol and antioxidant reactions. In this respect, it is worth noting that the cellular NADPH pool is normally maintained in an equilibrium between the NADPH-generating processes which include the pentose phosphate pathway above all and the NADPH-consuming processes such as lipogenesis, monooxygenations and urogenesis. The major metabolic impact of perturbing the redox state NADP/NADPH is not completely elucidated.

I.5. Redox-dependent transcription factors

Several mammalian transcription factors have been shown to be redox-regulated, in a direct or indirect way. They include Hypoxia-inducible factor 1 (HIF-1), Nuclear factor E2-related factor 2 (Nrf2), Nuclear factor–kappa B (NF-κB), p21ras, Activator protein 1 and 2, p53, c-Myb, Sp-1 and others.

I.5.1. Hypoxia-inducible factor 1 (HIF-1)

HIF-1 is a heterodimer consisting of a HIF-1α subunit and a HIF-1β subunit (also

known as ARNT), [Wang G.L. and Semenza G.L., 1995]. HIF-1 was first described as a hypoxia-inducible DNA-binding factor that mediates transcriptional activation of the human erythropoietin gene enhancer [Semenza G.L. and Wang G.L., 1992]. The HIF heterodimer recognizes a conserved DNA consensus sequence, known as the hypoxia-response element (HRE), located usually in the promoters of target genes (Fig.I.13). At least 70 genes have been identified so far as targets of HIF, comprising of genes encoding for proteins involved in different cellular metabolic functions such as cell proliferation, cell survival, glucose metabolism, oxygen transport and apoptosis, as indicated in Tab.I.3. For full transcriptional activity, HIF-1 recruits the transcriptional coactivator p300/CREB-binding protein (CBP), [Arany Z. *et al.*, 1996].

Both HIF-1 subunits are constitutively expressed in cells at mRNA level. However, in normoxia (normal oxygen concentrations), HIF-1α protein is rapidly degraded by the proteasome after the hydroxylation of two Pro residues and subsequent ubiquitination (Fig.I.13). Apart from this oxygen-depending regulation, HIF-1α can also be regulated by oxygen-independent mechanisms. Several oncogenes, growth factors, hormones and inflammation mediators have been shown to activate HIF-1α [Bardos J.I. and Ashcroft M., 2004]. The majority of these factors converge on two common cellular kinase pathways: the mitogen-activated protein kinase (MAPK) and the phosphoinositide 3-kinase (PI3K)/ Akt pathways.

An important non-hypoxic stimulus that induces HIF-1 activation is oxidative stress. Different mediators such as growth factors, thrombin or insulin have been shown to promote the HIF-1 response following stimulation of cellular ROS generation [BelAiba R.S. *et al.*, 2004; Leek R.D. *et al.*, 2005]. This response can be inhibited by antioxidants or overexpression of redox-modifying enzymes.

I.5.2. Nuclear factor E2-related factor 2 (Nrf2)

Nrf2 was identified in 1994 as a factor that binds to the NF-E2 repeat of the β-globin gene promoter [Moi P. *et al.*, 1994]. It is a member of the Cap´n´Collar family of basic region-leucine zipper (bZIP) transcription factors and acts as a central regulator of both constitutive and inducible antioxidant-related gene expression [Nguyen T. *et al.*, 2003]. Nrf2-deficient mice although viable (and not showing a very strong phenotype) display an altered antioxidant genetic program and a higher susceptibility to oxidative damage

and chemical toxicity [Ramos-Gomez M. *et al.*, 2001; Chan K. *et al.*, 2001]. Of note, Nrf2 is ubiquitously expressed in a wide range of tissues and cell lines.

However, under normal conditions, Nrf2 is bound to the cytoskeleton-associated Kelch-like ECH-associated protein 1 (Keap1), [Jaiswal A.K., 2000], which targets it for ubiquitin-dependent degradation, as represented in Fig.I.13. Many pro-oxidant and/or toxic molecules such as tBHQ, sodium *m*-arsenite, sulforaphane and β-naphtoflavone (β-NF) have been shown to provoke Nrf2 stabilization and translocation to the nucleus. Once in the nucleus, Nrf2 recruits other leucine zipper proteins, such as small Maf, which are necessary for its transactivation activity (Fig.I.13).

Together with these interaction partners Nrf2 binds to *cis*-acting elements, called antioxidant response element (ARE), located in the promoters of target genes [Rushmore T.H. *et al.*, 1991] which are involved in different cellular functions such as maintenance of the cellular redox homeostasis, cell growth and apoptosis, inflammatory response and the ubiquitin-mediated degradation pathway. Some of the best studied Nrf2-regulated genes are shown in Tab.I.3.

Cis-acting sequence	Target gene function	Target gene
ARE	Antioxidant and phase II detoxifying enzymes	NAD(P)H:quinone reductase (NQO1)
		γ-glutamylcysteine synthetase heavy subunit (γ-GCS$_h$)
		γ-glutamylcysteine synthetase light subunit (γ-GCS$_l$)
		Heme oxygenase 1 (HO-1)
HRE	Angiogenesis	Vascular endothelial growth factor (VEGF)
	Vascular tone	Endothelin 1 (ET1)
		Heme oxygenase (HO-1)
	Erythropoiesis	Erythropoietin (EPO)
	Fe metabolism	Ceruloplasmin
		Transferrin
	Glucose metabolism	Glucose transporter 1 (GLUT-1)
		Aldolase A (AldoA)
		Lactate dehydrogenase A
		Gliceraldehyde-3-phosphate dehydrogenase (GADPH)
	Proliferation	Insulin-like growth factor 2 (IGF2)
		Cyclin G2

Table I.3. Some of the genes known as down-stream transcriptional targets of HIF-1 and Nrf2.
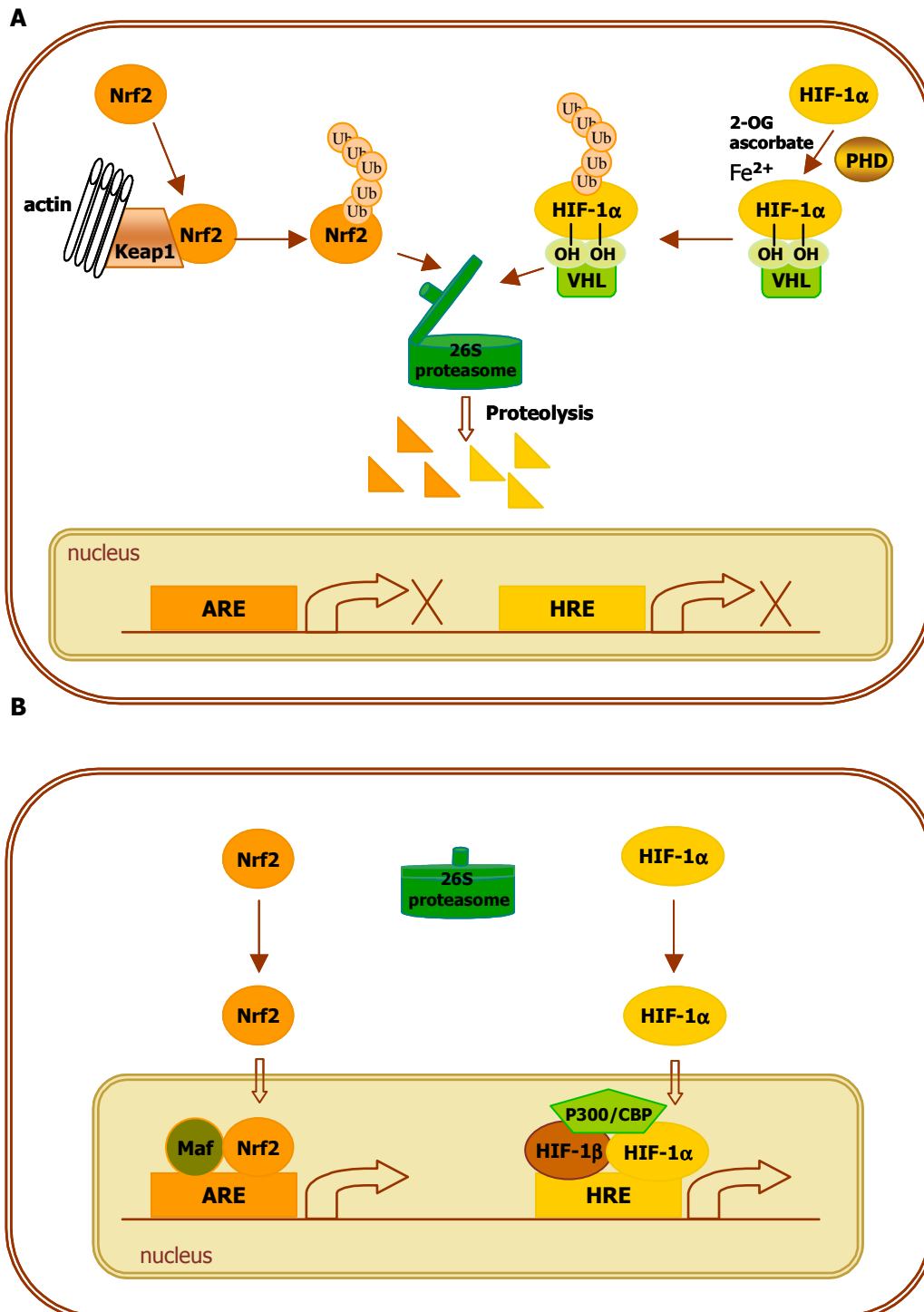
Figure I.13. Parallelism between HIF-1 and Nrf2 regulation. Under basal conditions (A), HIF-1α is hydroxylated by proline hydroxylases (PHD) in the presence of O$_2$, Fe^{2+}, 2-oxoglutarate (2-OG) and ascorbate, tagged for ubiquitination and subsequently proteolytically degraded. Nrf2 binds to Keap1 and is also ubiquinated and proteolytically degraded by the 26S proteasome. In response to different stimuli (B), proline hydroxylation is inhibited, HIF-1α is not targeted for degradation and is thus stabilized. Nrf2 dissociates from Keap1 and is thus stabilized in the cytosol. After migration to the nucleus HIF-1α dimerizes with HIF-1β, binds to transcriptional co-activators and transactivates HRE-containing target genes. As to Nrf2, it translocates to the nucleus and transactivates ARE-containing genes.

This Nrf2-mediated defence response has been suggested to play a protective role in many human pathological conditions such as cardiovascular diseases, cancer, chronic inflammation diseases (ex. lupus-like autoimmune nephritis) and neurodegenerative disorders (for ex. PD), [Zhang D.D., 2006].

A large body of evidence demonstrates that Nrf2 activity is regulated by phosphorylation and several upstream kinases have been reported to be involved in this regulation, namely the MAPK pathway, PI3K and extracellular-regulated kinase (ERK). Apart from this, post-transcriptional regulation, certain endogenous and exogenous stimuli, such as inorganic arsenic, keratocyte growth factor and the pyrethroid pesticide, deltamethrin have been reported to increase Nrf2 expression at the transcriptional level [Braun S. *et al.*, 2002; Pi J. *et al.*, 2003; Li H-Y. *et al.*, 2007].

I.5.3. Nuclear factor–kappa B (NF-κB)

Since its discovery in 1986, NF-κB has been widely studied and it is now known to play a central role in the regulation of the expression of many genes involved in cellular defense mechanisms.

The NF-κB family (also known as the Rel/NF-kB family) of transcription factors consists of five members: p50, p52, RelA (or p65), RelB and c-Rel [Baeuerle P.A., 1991; Grilli M. *et al.*, 1993]. All carry a Rel homology domain (RHD), which contains a NLS and is involved in homomeric and heteromeric dimer formation among the members. Dimerized NF-κB family members translocate to the nucleus, bind to DNA in a sequence-specific manner and thus *trans*-activate target genes. The proteins encoded by these NF-κB-responsive genes play important roles in inflammation as well as innate and acquired immunity (comprise cytokines, cytokine receptors, cell adhesion molecules and hematopietic growth factors). Importantly, NF-κB proteins interact with members of the IκB family (in the cytoplasm or the nucleus), which renders them transcriptionally inactive. NF-κB appears to be present in most cell types of higher vertebrates, sequestered in the cytoplasm by IκB proteins.

Binding of cytokines, growth factors and other inflammatory stimuli, such as TNF-α, IL-1, phorbol esthers or LPS, to specific sub-cellular receptors, as well as traumatic insults, ionizing radiation or UV-C, lead to activation of the NF-κB pathway.

Many of these mediators use ROS as second messengers and an increase of the ROS level has been shown to activate NF-κB in several cellular physiological and pathological paradigms [Piette J. *et al.*, 1997]. In addition, a large number of studies have demonstrated that the majority of the stimuli known to activate NF-κB, can be blocked using antioxidants, such as NAC, vitamin E and thiols.

Mitochondria (acrylic on canvas in wood, 12"x 18")

Scientific artists are the visual storytellers of science. They need a strong scientific focus but also a keen imagination as they often illustrate what cannot be seen. These days scientific art is everywhere, on the internet, in magazines and posters. Now more than ever are artists demanded because they can thus bring complicated research closer to the general public.

II. OBJECTIVES

"Science may set limits to knowledge, but should never set limits to imagination"

Bertrand Russell (1872-1970)

The aim of this study was to analyze the role of AIF in the mitochondria. To achieve this goal, we set up several objectives:

1. Design efficient siRNA cassettes to abolish the expression of the *AIF* gene.

2. Generate stable AIF KD cell lines in a appropriate cellular background.

3. Characterize these cell lines, using biochemical and molecular approaches.

4. Establish a correlation between the observed phenotype in the *AIF*-silenced cells and the physiological role of AIF in order to elaborate a theoretical model of the mitochondrial role of AIF.

III. MATERIALS AND METHODS

"Life is like riding a bicycle, one can only fall if one stops pedalling"

Frederic Bonomelli (1959-)

III.1. Reagents

All reagents used in this study were of analytical grade.

Unless otherwise stated, most of the general chemical reagents were purchased from Sigma-Aldrich. These include: sodium chloride (NaCl), magnesium chloride (MgCl$_2$), potassium chloride (KCl), sodium acetate (CH$_3$COONa), sodium metavanadate (NaVO$_3$), sodium molybdate (Na$_2$MoO$_4$), sodium fluoride (NaF), sodium dodecyl sulphate (SDS), Tween-20, β-mercaptoethanol, dithiothreitol (DTT), bromophenol blue, sodium cyanide (NaCN), potassium cyanide (KCN), ethidium bromide (EthBr), uridine, dimethylsulfoxide (DMSO), glucose, glycerol, bovine serum albumin (BSA), Hank's buffered salt solution (HBSS), mannitol, potassium hydrogen phosphate (K$_2$HPO$_4$), β-glycerolphosphate, *p*-nitrophenylphosphate (PNPP), adenosine diphosphate (ADP), adenosine triphosphate (ATP), nicotinamide adenine dinucleotide phosphate (NADP), hexokinase, glucose-6-phosphate dehydrogenase, galactose, malic acid, succinic acid, glutamic acid, actinomycin D, rotenone, hydrogen peroxide (H$_2$O$_2$), N-acetyl cysteine (NAC) and Luria Bertani (LB) broth for bacterial culture.

NP-40 was from Pierce Biotechnology, Inc. Tris-base, glycine and agarose were from Roche Diagnostics. Methanol, ethanol and iso-propanol were from Merck. Magnesium sulphate 7-hydrate (MgSO$_4$·7H$_2$O), sucrose and ethylenediamine tetraacetic acid (EDTA) were from Panreac Quimica S.A. HEPES and phosphate-buffered saline (PBS) were from Gibco. Acetic acid, ammonium bicarbonate (NH$_4$HCO$_3$) and acetonitrile were from Fluka.

The mitochondria-targeted antioxidant MitoQ was a kind gift of Dr. Michael P. Murphy (Wellcome Trust MRC-Dunn Human Nutrition Unit, Cambridge, UK).

III.2. Cell culture

The cell lines used in this study were: the human hepatoblastoma cell line Hep3B (ATCC HB-8064), the human cervical carcinoma cell line HeLa (ATCC CCL-2) and two sublines of the mouse embryonic stem cell (ES) line E14K.

Hep3B cells were cultured in minimal essential medium (MEM), supplemented with 10% heat-inactivated fetal bovine serum (FBS), 2 mM L-glutamine, 1 mM non-essential

amino acids (n.e.a.a) and 1 mM sodium pyruvate.

HeLa cells were routinely cultured in Dulbecco´s modified Eagle´s medium (DMEM) with high glucose concentration (4.5 g/L) and supplemented with 10% heat-inactivated FBS, 2 mM L-glutamine, 1 mM sodium pyruvate and 1 mM n.e.a.a.

Mouse ES cell lines were maintained in DMEM-GlutaMax^{TM} with high glucose concentration (4.5 g/L) and supplemented with 10% heat-inactivated FBS, 2 mM L-glutamine, 1 mM n.e.a.a, 0.8% (v/v) β-mercaptoethanol and 1000 U/mL LIF (Chemicon, UK), [Smith A.G., 1991]. These cell lines were a generous gift from Dr. Josef Penninger (Institute of Molecular Biotechnology of the Austrian Academy of Sciences, Vienna, Austria).

All cell culture media were supplemented with antibiotics, penicillin (50 units/mL) and streptomycin (50 μg/mL). These and all the other reagents used for cell culture, indicated above, were purchased form GIBCO, Invitrogen. Cell cultures were maintained in a cell culture incubator (IGO 150, Jouan) at 37 ºC, with a humidified atmosphere of 5% CO_2/ 95% air (AirLiquide). All cell lines were subcultured once they reached 90-95% confluence, using Trypsin-EDTA (GIBCO, Invitrogen) to detach them and re-fed with fresh medium every 2-3 days. For all experiments, we used sub-confluent cell cultures of passage nº lower than 25.

III.2.1. Generation and maintenance of rho^{o} cells

In order to generate rho^{o} cell lines, routinely cultured Hep3B and HeLa cells were treated with the mutagenic chemical ethidium bromide (EthBr), 100 ng/mL, to deplete mtDNA and the medium was supplemented with uridine at 50 μg/mL [Mansfield K.D. *et al.*, 2005]. The treatment was continued over 6 weeks, changing the culture medium every 2 days.

III.2.2. Hypoxia experiments

For hypoxia experiments, cells were seeded the day before the experiment at cell density of approximately 70% and re-fed with fresh medium immediately before the experiment. Cellular hypoxia was achieved placing the cells in a hypoxic incubator (IG

650/750, Jouan), maintaining a humidified environment at 37 ºC and the following gas mixture: 92% N_2/ 3% O_2/ 5% CO_2 (AirLiquide). Hypoxic treatment was routinely performed over 4 h.

III.2.3. Transfection experiments

For transfection experiments, we used LipofectAMINE™ 2000 (Invitrogen Life Technologies) and followed the protocol supplied by the manufacturer. Cells were seeded the day before the experiment, at cell density of approximately 90-95%. DNA/Lipofectamine complexes were formed in the serum-free OptiMEM (GIBCO, Invitrogen), usually 10 µg of plasmid DNA was used per 25 cm^2 tissue culture flask. Transfections were performed in complete cell culture medium without antibiotics, over 5 h and then cells were re-fed with fresh complete medium containing antibiotics.

III.3. Plasmid construction

III.3.1. Silencing of *AIF* and *TRX2* by RNA interference

In order to silence *AIF* and *TRX2* in our model cells, we used RNA interference (RNAi), a potent and highly specific posttranscriptional gene silencing process mediated by double-stranded RNA (dsRNA), [Fire A. *et al.*, 1998]. More specifically, we used the DNA vector-based RNAi technology and silencing cassettes were generated following a hairpin small interfering RNA (siRNA) strategy, as this strategy was proved to be very efficient [Yu J.Y. *et al.*, 2002]. In addition, RNA polymerase III (Pol III) promoter was used to direct *in vivo* synthesis of functional siRNA.

The murine Pol III U6 promoter was amplified from genomic DNA using the primer pair: U6 Forward (F) (5´-GCGGATCCGACGCCGCCATCTCTA-3´) and U6 Reverse (R)(5´-CGAATTCGAAGACCACAAACAAGGCTTTTCTCCAA-3´). Engineered restriction sites were added at both ends to facilitate future clonings. The amplified PCR product was then cloned into pBlueScript vector (Stratagene) opened at *Bam*HI and *Eco*RI. This new vector, named pBS U6/Pol III, was used for cloning and expressing the siRNA cassette. To target different regions of the *AIF* transcript, three siRNA cassettes were designed, termed siAIF1, siAIF2 and siAIF3 as represented in the Fig.III.1. The targeted sites from the gene, accession number NM_004208, are schematically shown in Fig.III.1.B. These

sites comprise (sense strand): GTACTGATTGTATCTGAAGAT (for siAIF1), GTAGTACAGCTGGATGTGAGA (for siAIF2), and GACCACATAGTGGCAGCTGTG (for siAIF3). Each siRNA cassette is composed of two complementary oligonucleotides and a short loop in between (TTCAAGAGA). These siRNA cassettes were verified by sequence analysis and cloned into pBS U6/PolIII vector opened at *Bbs*I-*Hind*III in a 5´-3´orientation. The vector obtained was termed pBS U6/PolIII/siRNA (Fig.III.1.A).

TRX2 was silenced in a very similar way. Two different silencing cassettes were designed and named siTrx2-A and siTrx2-B. The targeted sites from this gene, accession number NM_012473, were (sense strand): GACTTCTTCTGAGGAGGTTCC (for siTrx2-A) and GACAATATACACCACGAGGAT (for Trx2-B).

For transient silencing of *AIF*, Hep3B and HeLa cells were transfected with pBS U6/PolIII/siRNA, twice, at 24 h intervals and processed for analysis 48 h after the second transfection. For transient silencing of *TRX2*, Hep3B cells were transfected with pBS U6/PolIII/siRNA and processed for analysis at 72 h after the transfection. In both cases, we also used a control siRNA directed to the GFP transcript as described [Sui, G *et al.*, 2002], which we named pU6 GFP.
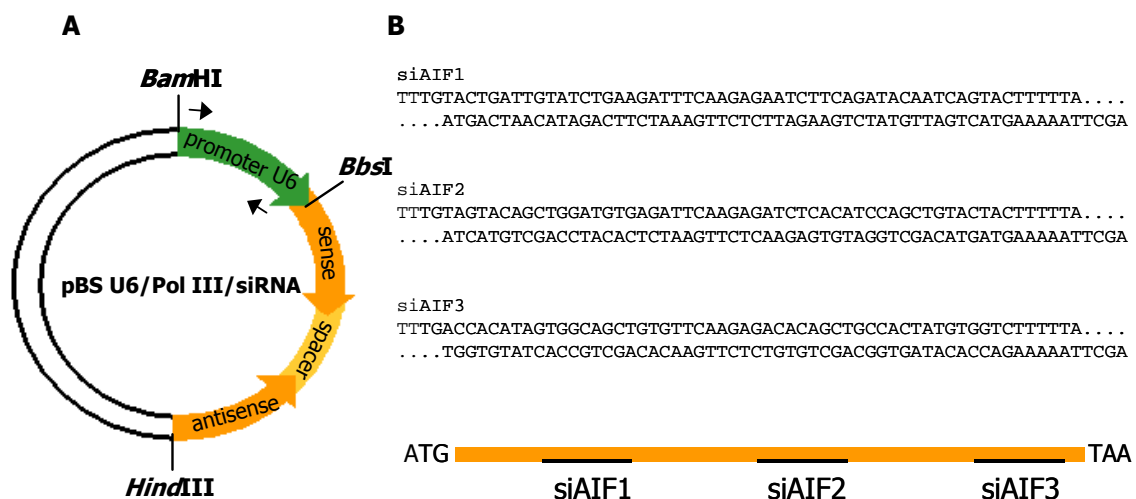
Figure III.1. *AIF*-silencing vector and cassettes. A. pBS U6/PolIII/siRNA vector. Black arrows indicate the position of the pair of primers used for screening for positive clones by genomic PCR. B. The three siRNA cassettes (siAIF1, siAIF2 and siAIF3) and their corresponding targeting regions in AIF mRNA.

For establishment of stable lines with silenced *AIF*, we co-transfected the Hep3B cells with the pBS U6/PolIII/siRNA and the pcDNA3 vector, at a ratio of 10:1. Then, 48 h

after the transfection, we selected for resistant clones in growth medium containing 200 μg/ml geneticin (G-418 sulphate), (GIBCO, Invitrogen). Cells were maintained under selection until colonies were visible (about 14 days); individual clones were then isolated with cloning cylinders and amplified under selection in complete growth medium.

As an additional control, in some experiments we used a stable Hep3B cell line, in which the *SURF1* gene had been silenced by the same methodologies.

III.3.2. Protein overexpression plasmids

To construct Trx1 and Trx2 expression vectors, the respective full length cDNA were amplified by standard PCR from a sample of Hep3B RNA after single-strand complementary DNA was synthesized using RT-PCR. The following primers were used: Trx1-5 CAG GGA TCC AAG ATG GTG AAG CAG ATC GAG AGC AAG and Trx1-3 CGG AAT TCT TAG ACT AAT CA TTA ATG GTG GC amplified the Trx1 cDNA (accession number NM_003329), including *Bam*HI and *Hin*dIII sites underlined respectively); Trx2-5 CGC AAG CTT AAG ATG GCT CAG CGA CTT CTT CTG AGG and Trx2-3 CGG AAT TCT CAG CCA ATC AGC TTC TTC AGG AAG GC amplified the Trx2 cDNA (accession number NM_012473), including *Hin*dIII and *Eco*RI sites underlined respectively). The PCR products were gel purified and cloned into the "pGEM-T Easy vector" (Promega), using a T-A cloning strategy. Nucleotide sequence analysis of various clones confirmed the correct structure of the Trx1 and Trx2 genes.

A Trx2 construct with a deletion of the mitochondrial targeting sequence (aa1-60), [Zhang R. *et al.*, 2004], named Trx2Δ, was also prepared by using the primer Trx2-5Δ CGC AAG CTT AAG ATG ACA ACC TTT AAT ATC CAG GAT GG ACC T in conjunction with Trx2-3. Both the Trx2 full length cDNA and also Trx2Δ were also epitope-tagged using the FLAG peptide. This was done using a two-step PCR extension strategy using the primers FLAG1, GTC TTT GTA GTC GCC AAT CAG CTT CTT CAG GAA GGC, and FLAG2, TTA CTT ATC GTC ATC GTC TTT GTA GTC GCC AAT CAG.

All the cloning procedures in this thesis, namely digestions, ligations and transformations, were performed using standard molecular biology procedures. The *E. coli* strain used was DH5α. Bacterial cells were cultured in Innova 4200 Incubator Shaker, New Brunswick Scientific (Edison, NJ, USA) and for centrifugation we used SORVALL RC5Cplus centrifuge, Kendro® Laboratory Products (Philadelphia, PA, USA).

The restriction enzymes and buffers used in the cloning procedures, were from New England Biolabs Inc., whereas "Rapid DNA ligation kit" was from Roche Diagnostics. Ampicillin was purchased from Sigma. The DNA molecular weight markers used were "Ready-Load^{TM} 100bp DNA ladder" and "TrackIt^{TM} 1 Kb DNA Ladder", both purchased from Invitrogen.

III.4. Cell proliferation assay

Cell proliferation was detected by two methods. The first method consists of counting the cells using a hemacytometer (Bright Line Counting Improved Neubauer Chamber, Hausser Scientific). It contains an etched glass chamber and a cover glass. The hemacytometer is filled with the cell suspension by capillary action. For this, the attached cells were washed with PBS and trypsinized. Consecutively, they were resuspended in complete culture medium and mixed thoroughly in order to homogenize the suspension. A portion of it was taken to the hemacytometer and the cells were counted. We also performed selective staining of cells which not only facilitates visualization and counting but also discriminates the live from the dead cells. Here, the cell suspension was mixed with an equal volume of trypan blue solution (0.4 % (w/v) trypan blue (Sigma) in PBS) and incubated for 2-3 min at RT. The dead cells are stained blue.

The second method is using the MTT assay. Yellow MTT (3-(4,5-Dimethylthiazol-2-yl)-2,5-diphenyltetrazolium bromide, a tetrazole) is reduced to purple formazan in the mitochondria of living cells [Mosmann T., 1983]. This reduction takes place only when mitochondrial reductase enzymes are active and therefore the conversion is directly related to the number of viable cells. A solubilization solution, usually either DMSO or a solution of the detergent SDS in dilute hydrochloric acid (HCl), is added to dissolve the insoluble purple formazan product into a colored solution. The absorbance of this solution is quantified by measuring at a 500-600 nm wavelength by a spectrophotometer.

In our experiments, cells were seeded the day before the experiment using 96-well cell culture plates, 100 μL/well. In order to assess the cell proliferation, MTT reagent (Roche) was added (20 μL/well) and cells were incubated for 4 h in the cell culture incubator. Then, medium was discarded and DMSO was added, to solubilize the cells,

at 100 μL/well. The plate was incubated for 5 min, at 37 ºC, in the dark and immediately after this, absorbance was measured at 570 nm and 690 nm using a "Multiscan" plate-reader spectrophotometer (Thermo Labsystems). Results were obtained subtracting the absorbance value recorded at 690 nm (background absorbance) from the 570 nm absorbance value, as indicated in the instructions provided with the kit.

III.5. Measurement of lactate concentration

Lactate concentration in the cell culture medium was measured spectrophotometrically. The measurement is based on two consecutive reactions. First, lactic acid is converted to pyruvate and H_2O_2 by lactate oxidase. Then, in the presence of the formed H_2O_2, horseradish peroxidase (HRP) catalyzes the oxidative condensation of a chromogen precursor to produce a colored dye with an absorption maximum at 540 nm [Barhan D. and Trinder P., 1972]. The increase in absorbance is directly proportional to the lactate concentration in the sample. In our experiment, we used a lactate reagent (Sigma) which contains all the necessary compounds for the chemical reaction. Lactate standard solution (Sigma) was used to generate a standard curve (range: 12.5-400 μg/mL).

The experiment was carried out by the following protocol. Cells were seeded and allowed to grow in complete growth medium for the indicated period of time. Later, the culture medium was collected, filtered using 0.2 μm syringe filters (Millipore) and stored at −20 ºC until the measurement. Cells were also collected by trypsinization and counted using a hemacytometer, in order to normalize the results. The measurement was performed in a 96-well plate, in triplicate, adding 2-10 μL of the standard serial dilutions or the culture medium and 100 μL of the lactate reagent. Complete culture medium without cells was used to assess background absorbance. The plate was incubated at 37 ºC, for 10 min, in the dark. Absorbance was measured at 570 nm, using a "Multiscan" plate-reader spectrophotometer (Thermo Labsystems).

III.6. Measurement of ATP concentration

Intracellular ATP concentration was assessed in a bioluminescent assay based on the luciferase oxidation of luciferin to oxyluciferin, as described in Fig.III.2. For this, we used the "ATP Bioluminescence kit" (Roche) and the assay was performed according to

the manufacturer´s protocol. Briefly, cells were detached by trypsinization and counted using a hemacytometer.

luciferin + ATP ⟶ **luciferyl adenylate + Ppi**

luciferyl adenylate + O$_2$ ⟶ **oxyluciferin + AMP + light**
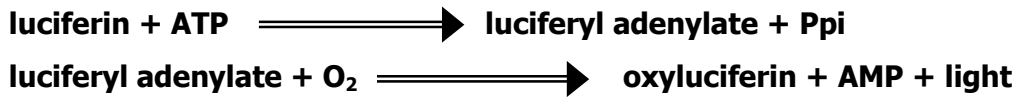
Figure III.2. Luciferase-mediated oxidation of luciferin to oxyluciferin is a double-step reaction.

Then, 1 million cells were resuspended in 1 mL dilution buffer. ATP standard curve was prepared (10^{-10}-10^{-3} M) using ATP stock solution (10 mg/mL) provided by the kit in dilution buffer in order to minimize the background luminescence. Moreover, 25 μL of the sample or the standard solution were applied per well in a 96-well plate, in triplicate. Then, 25 μL of cell lysis buffer were added to all wells and the plate was incubated for 5 min, at RT. It was then taken to the Luminoscan (Thermo Labsystems) and luminescence was detected immediately after injecting 50 μL/well of the luciferase reagent by the luminoscan dispenser.

In order to normalize the ATP concentration values with the protein amount, after the cell lysis had been performed 10 μL/well of the cell lysate solution were removed and total protein concentration determined using the "BCA Protein Assay Kit" (Pierce), (see section: "III.13.2. Protein quantification").

III.7. Glucose-uptake detection

In this spectrophotometric assay, we detected the concentration of glucose in the culture medium as an indicator of the cellular glucose uptake. The mechanism of the reaction is shown in Fig.III.3.

glucose ⟶ **glucose-6-phosphate**
    hexokinase
ATP   ADP

glucose-6-phosphate ⟶ **6-phospho-gluconate**
    glucose-6-phosphate-dehydrogenase
NADP   NADPH
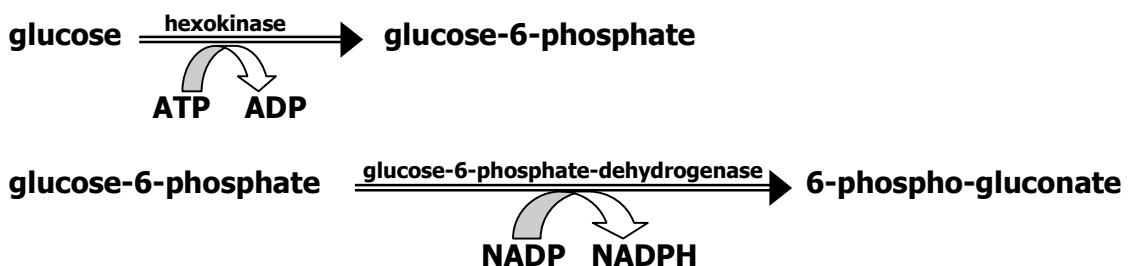
Figure III.3. Glucose conversion to 6-phospho-gluconate.

The detection was carried out by measuring NADPH maximal absorbance at 340 nm, which is equivalent to the glucose concentration in the sample. Linear range glucose standard curve (0.016-1 g/L) was prepared, using the culture medium (1 g/L glucose) as a standard stock solution of glucose. The reaction was performed in a 96-well plate, adding 20 μL of the standard or the sample and 200 μL of the reaction mixture and incubated at RT, for 5 min. The reaction mixture was prepared fresh, composition: 0.3 M Tris-HCl pH 7.5, 10 mM $MgSO_4 \cdot 7H_2O$, 10 mM ATP, 0.8 mM NADP, 4.5 U/mL hexokinase and 5 U/L glucose-6-phosphate dehydrogenase. Absorbance was recorded using a "Multiscan" plate-reader spectrophotometer (Thermo Labsystems). In parallel, the cell number was also assessed, using a hemacytometer, in order to normalize the results.

III.8. Detection of ROS using the "Amplex Red Kit"

To evaluate ROS production, particularly H_2O_2, in cultured cells, we employed the "Amplex Red Hydrogen Peroxide/Peroxidase Assay Kit" (Molecular Probes, A22188). This kit uses the Amplex Red Reagent (10-acetyl-3,7-dihydroxyphenoxazine) to detect H_2O_2 released from cells [Mohanty J.G. *et al.*, 1997]. In the presence of HRP, Amplex Red reacts with H_2O_2 in a 1:1 stoichiometric ratio and turns into red-fluorescent oxidation product, resorufin, which can be detected both fluorometrically (emission at 587 nm) and spectrophotometrically (absorbance at 563 nm). In our case, we used a "Multiscan" plate-reader spectrophotometer (Thermo Labsystems) and absorbance was quantified at 570 nm.

In order to detect H_2O_2 production, cells were seeded the day before the experiment. The following day, they were washed using PBS, detached by trypsinization and resuspended in HBSS. H_2O_2 was detected in the cell suspension and quantified using H_2O_2 standard curve ranging 0-40 μM and prepared in HBSS with serial dilutions using 3% H_2O_2 stock, provided by the kit. The assay was performed in a 96-well plate by applying, per well, 20 μL of blank (HBSS), standard (H_2O_2 solution) or sample (5×10^4-10×10^4 cells) and further adding 100 μL of the reaction mixture, containing 0.1 U/mL HRP and 50 μM Amplex Red in HBSS. Results were normalized with the cell number, having counted the cells in the suspension with a standard hemacytometer (see chapter "III.4. Cell proliferation assay"), and expressed as concentration of H_2O_2 ($nmol/5 \times 10^4$ cells).

III.9. Confocal microscopy

The aim of the confocal microscopy experiments was to study the intracellular ROS levels, the redox status (assessed as glutathione concentration) and the $\Delta\psi_m$ status in our model cells. For this purpose, we used the following suitable fluorochromes: hydroethidine (Dihydroethidium, HE), 2'7'-dichlorofluorescin diacetate (DCFH-DA), tetramethylrhodaminemethylester (TMRM) and 5-chloromethylfluorescein diacetate (CMFDA). In the presence of superoxide, HE is oxidized to become ethidium which emits red fluorescence [Rothe G. and Valet G., 1990]. DCFH-DA is hydrolysed by cellular esterases to dichlorofluorescin (DCFH) and is then oxidized to a green fluorescent product dichlorofluorescein (DCF) primarily by H_2O_2 [Rothe G. and Valet G., 1990; Carter W.O. *et al.*, 1994]. TMRM which fluoresces in red, is a fluorochrome used to detect mitochondrial inner membrane potential [Nieminen A.L. *et al.*, 1997], whereas CMFDA (green fluorescence) detects glutathione (GSH).

For these measurements, cells were seeded one day before the experiment in complete culture medium. Prior to the staining, the medium was removed and cells were re-fed with MEM supplemented with 2% FBS. Cells were stained with Hoechst 33342 (blue fluorescence) at 10 μg/mL to stain the nuclei. TMRM was added at 0.05 μM, CMFDA at 0.5 μM, HE at 10 μM and DCFH-DA at 0.4 μM. Incubation was carried out in the dark, at 37 ºC, for 30 min. Cell viability was assessed with the fluorochrome propidium iodide (PI), at 0.001%, which fluoresces in red and this incubation was performed for 3 min. All fluorochromes were purchased from Molecular Probes.

Cellular fluorescence intensity was visualized using a Radiance 2100 Confocal microscope (BioRad, Hampstead, England). Digital image analysis from cellular fluorescence was carried out with Laserpix Software (BioRad). In all the experiments, the mean fluorescence intensity was captured per image (404 μm^2) corresponding to 25-35 cells. At least three images were captured per experiment and these experiments were repeated three times.

III.10. Glutathione (GSH) concentration measurement by fluorimetry

GSH was also detected by a fluorometric method, using the fluorochrome monochlorobimane [Rice G. *et al.*, 1986; Sebastiá J. *et al.*, 2003]. This is a common

technique to measure GSH in cultured cells as monochlorobimane can readily pass the plasma membrane and form an intracellular fluorescent GSH-monochlorobimane adduct in a reaction catalyzed by glutathione S-transferase.

For the measurement, cells were seeded in standard culture medium in a 96-well plate, 5×10^4/well, and left to attach for 6 h. Then, the culture medium was discarded and 95 μL/well of HBSS were added. A standard curve, using GSH (Sigma) was prepared in HBSS, to minimize the background fluorescence, in the range of 10^{-8}–10^{-3} M GSH. After this, 5 μL/well of monochlorobimane (Molecular Probes), final concentration of 0.04 mM, was added both to standards and to samples, all measured in triplicate. Then, the plate was incubated at 37 ºC, for 30 min, in the dark. Fluorescence was detected using a Fluoroscan (Thermo Labsystems), at λ_{exc} of 355 nm and λ_{emis} of 460 nm and the results obtained were expressed as concentration of GSH (nmol/5×10^4 cells).

III.11. Gene reporter assay

The gene reporter assay was used to study the transcriptional activity of HIF-1. As a reporter gene we used the firefly (*Photinus pyralis*) luciferase, coupled to several minimal hypoxia responsive elements (HRE), a normal regulatory sequence present in the promoter and enhancers of HIF-target genes.

The experimental reporter gene construct used in this experiment, pHRE-1, was kindly gifted by Dr. Kaye Williams (University of Manchester, UK). It contains 3 copies of a synthetic oligonucleotide of the minimal phosphoglucose kinase (PGK-1) HRE, cloned upstream of a simian virus SV40 minimal promoter in the pGL3 vector (Promega).

The control reporter gene construct used in our experiments was pHTK-RL; contains a thymidine kinase promoter cloned upstream of the *Renilla* luciferase gene. Its activity serves as a background control and is used to correct the obtained result for the transfection efficiency. The experiment was performed using the "STOP and GLOW reporter assay system" (Promega). Following the manufacturer´s suggestions and after transfecting with both vectors, Dual-Glo™ Luciferase reagent-lysed cells were transferred to a 96-well plate and luminescence was detected using a luminometer (Thermo Labsystems), obtaining a ratio between the Firefly and the *Renilla* luciferase activity.

III.12. PCR analyses

III.12.1. Genomic PCR

Genomic DNA from mammalian cells was obtained by resuspending cellular pellets in 50 μL lysis buffer containing 10 mM Tris-HCl pH 8.0, 50 mM KCl, 1.5 mM MgCl$_2$, 0.5% NP-40, 0.5% Tween and 100 μg/mL Recombinant Proteinase K (Roche Diagnostics). Samples were incubated at 65 ºC, for 40 min followed by heat-inactivation of proteinase K at 95 ºC, for 10 min. Normally, 10 μL of lysate were used as a template for genomic DNA.

The genomic PCR was used to detect the presence of the integrated siRNA cassettes in the stable clones of silenced *AIF*. The product obtained by the PCR amplification corresponds with part of the murine PolIII U6 promoter (Fig.III.1.A). The details of this PCR are summarized in Tab.III.1.

PCR conditions			Primer sequences
95 ºC	4 min		F: 5´-GACGCCGCCATCTCTAGG-3´
95 ºC	30 sec		R: 5´ACAAGGCTTTTCTCCAAG-3´
57.5 ºC	30 sec	30 or 35 cycles	
72 ºC	30 sec		
72 ºC	2 min		

Table III.1. PCR conditions and primer sequences for genomic PCR.

III.12.2. RT-PCR

Total RNA from mammalian cells was isolated using the "RNeasy Mini Kit" (Qiagen) according to manufacturer´s instructions. In brief, cellular pellets were resuspended in 350 μL lysis buffer and lysed by passage through a 20-Gauge needle. Then, 350 μL of 70% ethanol was added and the samples were applied to a column which retains RNA. After the column had been washed appropriately, RNA was eluted in 40-50 μL diethyl pyrocarbonate (DEPC), (Sigma)-treated H$_2$O (0.1% v/v). The concentration of the total RNA obtained was determined spectrophotometrically, using "GeneQuant pro" spectrophotometer (Amersham) and considering that one absorbance unit at 260 nm

wavelength correlates with about 40 μg/mL of RNA in the solution. RNA amount and integrity were also checked by standard electrophoresis (agarose gels containing EthBr and buffer TAE 1x).

Complementary DNA (cDNA) was synthetized using 1 or 2 μg of total RNA. For this, we used Superscript[TM] RNase H-Reverse Transcriptase (Invitrogen). The reaction was performed as suggested in the manufacturer´s protocol, in 20 or 40 μL final volume and the presence of buffer (50 mM Tris-HCl pH 8.3, 75 mM KCl, 3 mM $MgCl_2$), 10 mM DTT, 40 or 80 U RNAseOut Recombinant Ribonuclease Inhibitor (Invitrogen), oligo-dT primer (Invitrogen) and 0.5 mM mixture of deoxinucleoside triphosphates (dATP, dCTP, dGTP and dTTP, 0.5 mM each), (dNTPs), (Roche Diagnostics).

Reverse transcriptase PCR (RT-PCR) was performed using 2 μL cDNA, in a final volume of 20 μL. For this, we used "FastStart Taq Polymerase" (Roche Diagnostics). The reactions were performed in PCR buffer supplied by the manufacturer (50 mM Tris-HCl, 2 mM $MgCl_2$, 10 mM KCl and 5 mM $(NH_4)_2SO_4$; pH 8.3), 200 μM dNTPs (Roche Diagnostics), 2 μM F primer, 2 μM R primer and 1 U Taq DNA polymerase. The RT-PCRs were carried out using a PTC-200 DNA Engine Thermal Cycler (MJ Research) and RT-PCR products visualized by standard electrophoresis on 1-2% agarose gels containing EthBr and using buffer TAE 1x (20 mM Tris, pH 7.8, 10 mM sodium acetate and 0.5 mM EDTA). All RT-PCRs were performed in duplicate and together with a negative control (H_2O instead of cDNA).

The primer pairs were synthetized by Oswell DNA Service, UK, except for the oligonucleotide pair for GA3PDH which was purchased from BD Clontech (Control Amplimer set #5406-1). The optimal RT-PCR conditions for each pair of primers were established in pilot experiments, such that linear reaction rates were obtained and all PCR products were sequenced for verification. The primer sequences and PCR conditions are specified in Tab.III.2.

RT-PCR using commercial human cDNA panels

In order to analyze the expression of several potential AIF transcript variants in human tissues, we used Multiple Tissue cDNA (MTC[TM]) Panels, namely Human Tumor MTC[TM] Panel and the Human MTC[TM] Panels I and II (all from Clontech, BD Biosciences).

| Gene (mRNA, GenBank) | PCR conditions | | Primer sequences |
	T° annealing	N° cycles	
ACTB (NM_001101)	58 ºC	25/30	F: 5´-TGGCACCACACCTTCTACAATGAGC-3´ R: 5´-GCACAGCTTCTCCTTAATGTCACGC-3´
AIF (NM_004208)	66.8 ºC	35	F: 5´-GGCTCACGGTGTTTGACCCGT-3´ R: 5´-CTCGGGGAAGAGTTGAATCAC -3´
mAIF (NM_012019)	63.9 ºC	32	F: 5´-AAGACTGGCGGACTGGAAATAGAT -3´ R: 5´-AGGGGCGCTGGGAGGAA -3´
ALDOA (NM_000034)	67 ºC	35	F: 5´-CACTGGGATCACCTTCCTGT-3´ R: 5´-ACGACACCACACACCACTG-3´
CAT (NM_001752)	66.1 ºC	35	F: 5´-CAGATGGACATCGCCACATG-3´ R: 5´-AAGACCAGTTTACCAACTGGG-3´
CYPA (NM_021130)	56 ºC	20	F: 5´-CGTCTCCTTTGAGCTGTTTG-3´ R: 5´-GGTGATCTTCTTGCTGGTCT -3´
CYCA (NM_017101)	60 ºC	30	F: 5´-CGTCTGCTTCGAGCTGTTTG-3´ R: 5´-GTAAAATGCCCGCAAGTCAA -3´
GAPDH (NM_002046)	66 ºC	28	F: 5´-TGAAGGTCGGAGTCAACGGATTTGGT -3´ R: 5´-CATGTGGGCCATGAGGTCCACCAC -3´
GLUT1 (NM-006516)	67 ºC	30	F: 5´-ATGAAGGAAGAGAGTCGGCA-3´ R: 5´-TGAAGAGTTCAGCCACGATG-3´
HIF-1α (NM_001530)	55 ºC	40	F: 5'-CACAGCCTGGATATGAA-3' R: 5'-GAATTCTTGGTGTTATATATATATG -3'
KEAP1 (NM_203500)	63.9 ºC	35	F: 5´-CAGAGGTGGTGGTGTTGCTTAT -3´ R: 5´-AGCTCGTTCATGATGCCAAAG -3´
NQO1 (NM_000903)	66.1 ºC	35	F: 5´-GCCTAGCACAAGTACCACTCTTGGTC-3´ R: 5´-CTGAGGCAGGAGAATTGCTGGAACC-3´
NRF2 (NM_006164)	63.9 ºC	35	F: 5´-AGATTCACAGGCCTTTCTCG-3´ R: 5´-CAGCTCTCCCTACCGTTGAG-3´
SOD1 (NM_000454)	66.1 ºC	35	F: 5´-GCGACGAAGGCCGTGTGCGTGC-3´ R: 5´-ACTTTCTTCATTTCCACCTTTGCC-3´
SOD2 (NM_000636)	66.1 ºC	35	F: 5´-CTTCAGCCTGCACTGAAGTTCAAT-3´ R: 5´-CTGAAGGTAGTAAGCGTGCTCCC -3´

all RT-PCRs were performed:

	95 ºC	5 min	
	95 ºC	30 sec	
	T°$_{ann}$	30 sec	nº cycles
	72 ºC	30/60 sec	
	72 ºC	5 min	

Table III.2. RT-PCR: Primer pairs and PCR conditions used.

Using the primers for AIF (Tab.III.2), we were aiming to amplify three different cDNA variants of human AIF, listed in the GenBank namely AF100928, AL049703 and AL049704 [Daugas E. *et al.*, 2000 A]. The RT-PCRs were performed using 5 μL of the panel cDNA, in a total reaction volume of 20 μL and as described above. Negative control (water instead of DNA) was included. Also, for all the reactions we used human cDNA positive control, following the instructions provided with the cDNA panels.

Real time quantitative RT-PCR

Total RNA from mammalian cells was isolated and cDNA synthetized as indicated above. Quantitative real time RT-PCR was carried out in a LightCycler instrument with the use of LightCycler-FastStart DNA Master SYBR Green I kit, both from Roche Diagnostics. Samples containing 1 μL of cDNA were PCR-amplified in a final volume of 10 μL, in the presence of 0.5 μM primers F and R, 2 mM $MgCl_2$, 5% DMSO and 1 μL of the FastStart Reagent supplied by the kit, which contains the necessary buffer, the SYBR Green-marked nucleotides and the DNA polymerase. All reactions were performed in duplicate and a negative control, water instead of cDNA, was included in each run. Specificity was confirmed by melting curve analysis and agarose gel electrophoresis. In order to quantify the result as number of amplified copies in each reaction, we generated standard curves by PCR-amplifying serial dilutions of a previously purified PCR product for each primer pair, SOD1, SOD2 and Cyclophilin A (CYPA), (the primer sequences are shown in Tab.III.2). The later, was used as a housekeeping gene and results were normalized taking into consideration its expression.

III.13. Protein analyses

III.13.1. Protein extracts

Whole-cell extracts

Cells were collected on ice by the following procedure: the medium was removed, then the cells were washed with a suitable volume of ice-cold phosphate-buffered saline (PBS) and immediately after, scraped using plastic lifters (Corning Inc.), again in a suitable volume of ice-cold PBS (for ex. 1.5 mL of PBS for a t-25 flask). Immediately,

this cell suspension was centrifuged in a microcentrifuge (5415-R, Eppendorf) at 4 ºC, for 5 min, at 500 g. Supernatant was discarded and cell pellets were resuspended in 50-100 μL complete lysis buffer (depending on the size of the cell pellet, for example a pellet obtained from a confluent t-25 flask was normally lysed in 100 μL). The composition of the complete lysis buffer was: 20 mM HEPES pH 7.4, 400 mM NaCl, 20% (v/v) glycerol, 0.1 mM EDTA, 10 μM Na_2MoO_4. Immediately prior to use, 1 mM DTT, protease inhibitors ("Complete Mini" protease inhibitor cocktail, and "Pefabloc", both purchased from Roche Diagnostics), and phosphatase inhibitors mixture: 10 μM NaF, 10 mM $NaVO_3$, 10 mM p-nitrophenylphosphate (PNPP) and 10 mM β-glycerolphosphate were added. Then, samples were vortexed at maximum speed, for 15 sec, incubated on ice, for 15 min, vortexed again at maximum speed, for 30 sec and subsequently centrifuged in a microcentrifuge at 4 ºC, for 15 min, at 16100 g. Supernatants (whole-cell protein extracts) were collected and stored at −20 ºC until future use.

Mitochondria-enriched extracts

For these experiments, we routinely used confluent cell cultures plated in t-25 flasks. After washing with 5 mL ice-cold PBS, cells were scrapped in 1.5 mL ice-cold PBS and collected in a 1.5 mL ice-chilled eppendorf tubes. Immediately after, the suspension was centrifuged in a 4 ºC-chilled microcentrifuge (5415-R, Eppendorf), at 500 g, for 5 min. The supernatant was discarded and the cell pellet was resuspended in 0.5 mL fractionation buffer (10 mM Tris-HCl pH 7.5, 0.25 M sucrose and 1 mM EDTA) and immediately after lysed on ice by a passage through a 23-gauge needle in a 1 mL plastic syringe. Unbroken cells were pelleted by centrifugation in a microcentrifuge at 4 ºC, for 10 min, at 500 g. The supernatant was collected, transferred to a new eppendorf tube and centrifuged at 4 ºC, for 30 min, at 16100 g. The supernatant resulting from this centrifugation was collected representing the cytosolic fraction, whereas the pelleted mitochondrial fraction was washed by adding 1 mL fractionation buffer. Subsequently, another centrifugation step was performed, in a chilled microcentrifuge at 11000 g, for 10 min and the pellet obtained was resuspended in 50 μL mitochondrial buffer (10 mM Tris-acetate pH 8.0, 0.5% NP-40, 5 mM $CaCl_2$, 1 mM DTT and protease inhibitor cocktail, (Roche)), thus giving rise to a mitochondria-enriched cellular fraction. Next, the protein extracts obtained this way were stored at −20 ºC for further use.

Nuclear and cytoplasmic extracts

In order to obtain nuclear and cytoplasmic extracts, we used confluent cell cultures plated in t-25 flasks. After washing with 5 mL ice-cold PBS, cells were scrapped in 1.5 mL ice-cold PBS and further collected in a 1.5 mL ice-chilled eppendorf tubes. An immediate centrifugation step followed in a 4 ºC-chilled microcentrifuge (5415-R, Eppendorf), at 500 g, for 5 min. The supernatant was discarded and the cell pellet was resuspended in 100 μL Dig A Buffer which contains 10 mM HEPES pH 7.4, 1.5 mM $MgCl_2$, 10 mM KCl and 0.2% NP-40. Prior to use, this solution was supplemented with 1 mM DTT, protease inhibitors ("Complete Mini" protease inhibitor cocktail, and 0.1 mM "Pefabloc", both from Roche Diagnostics), and phosphatase inhibitors mixture: 10 μM NaF, 10 mM $NaVO_3$, 10 mM PNPP and 10 mM β-glycerolphosphate. Samples were vortexed at maximum speed, for 10 sec, then incubated on ice for 10 min, vortexed again at maximum speed, for 10 sec and centrifuged in a microcentrifuge at 4 ºC, for 1 min, at 13000 g. Supernatants (cytoplasmic fraction) were collected and immediately after stored at –20 ºC until future use. Next, the pellets were resuspended in 30 μL of Dig C Buffer, whose composition is: 20 mM HEPES, 1.5 mM $MgCl_2$, 400 mM KCl, 25% glycerol and 0.2 mM EDTA. In a similar fashion as Dig A Buffer, Dig C Buffer was also supplemented prior to use, with 1 mM DTT and protease inhibitors ("Complete Mini" protease inhibitor cocktail, and 0.1 mM "Pefabloc", both purchased from Roche Diagnostics). Then, the samples were vortexed at maximum speed, for 10 sec, followed by a 15 min-incubation on ice, and vortexed again at maximum speed, for 10 sec. This was followed by 1 min-centrifugation, at 16000 g, in a 4 ºC-chilled microcentrifuge. The supernatant (nuclear fraction) was collected and maintained at –20 ºC until use.

III.13.2. Protein quantification

In order to quantify the protein content in the whole-cell and mitochondria-enriched cellular extracts, we used the Bicinchoninic acid (BCA) assay. This method combines the well-known Biuret reaction (reduction of Cu^{2+} to Cu^{1+} by protein in an alkaline medium) with a colorimetric detection of the Cu^{1+}, based on its chelation with two molecules of BCA. The purple-colored reaction product exhibits a strong absorbance at 562 nm which is nearly linear with increasing protein concentrations over a broad working range.

To perform the assay we used "BCA Protein Assay Kit" (Pierce). A standard curve was prepared using BSA, serial dilutions (1-0.0156 mg/mL) were prepared in the same buffer as the samples to minimize the background absorbance. Both the samples and the standard dilutions were assayed in triplicate. Then, 20 μL of standard or sample were applied per well in a 96-well plate and 200 μL/well of working reagent was added. This reagent was always prepared fresh, mixing 50 parts of the BCA reagent A with 1 part of BCA reagent B, as indicated in the manufacturer´s protocol. The plate was then incubated at 37 ºC, for 30 min, with gentle shaking and protected from light. The absorbance was measured at 570 nm using a "Multiscan" plate reader spectrophotometer (Thermo Labsystems).

III.13.3. Sodium dodecyl sulphate-polyacrylamide gel electrophoresis (SDS-PAGE) and Western blot (WB)

SDS-PAGE and WB were performed using standard methods. SDS-PAGE was performed using "Mini-PROTEAN 3 Cell" System (BioRad). Polyacrylamide gels were prepared using mixture of acrylamide/bisacrylamide solution, ratio 37.5:1, (Sigma), resolving gels with different % of polyacrylamide were prepared in 0.375 M Tris-HCl pH 8.8 and 0.1% SDS, whereas stacking gels containing 3.75% polyacrylamide were prepared in 0.125 M Tris-HCl pH 6.8 and 0.1% SDS. To catalyze the reaction of polymerization we used ammonium persulfate (APS), (Biorad) and N,N,N´,N´-tetramethylethylendiamine (TEMED), (Fluka). Protein extracts, containing equal total protein amounts, were prepared before loading by adding Laemmli loading buffer (0.5 mM Tris-HCl pH 6.8, 25% glycerol v/v, 10% SDS, 0.5% v/v β-mercaptoethanol and 0.5% bromophenol blue) and boiled at 100 ºC for 5 min to enable protein denaturation [Laemmli U.K., 1970]. Commercial molecular weight marker was loaded in parallel to determine the molecular weight of the polypeptides on the gel ("Precision Plus Protein Standard-Kaleidoscope" from BioRad, or "Full Range Rainbow Molecular Weight Marker" from Amersham Biosciences). Electrophoresis was performed in running buffer (25 mM Tris pH 8.3, 192 mM glycine and 0.1% SDS), at constant voltage of 100-120 volts.

Then, resolved proteins were transferred from the polyacrylamide gel to a 0.2 μm Hybond ECL nitrocellulose membrane (Amersham), using "Mini Trans-Blot Electrophoretic Transfer Cell" (BioRad). The transfer was performed during 1 h, at 4 ºC and constant electric current of 0.35 amperes, in transfer buffer (25 mM Tris pH 8.3, 192 mM glycine and 20% methanol).

Primary antibodies		
Protein	**Antibody**	**Work.solution**
ACTB	rabbit polyclonal (Sigma)	1:500 / 1:1000
AIF	rabbit polyclonal (ψProSci)	1:500
CI(39)	mouse monoclonal (Molecular Probes)	1:1000
CI(20)	mouse monoclonal (Molecular Probes)	1:1000
COXI	mouse monoclonal (Molecular Probes)	1:250
COXII	mouse monoclonal (Molecular Probes)	1:250
Flag epitope	rabbit polyclonal (Sigma)	1:500
HIF-1α	mouse monoclonal (BD Transduct. Lab.)	1:250
Nrf2 (C-20)	rabbit plyclonal (Santa Cruz Biotech. Inc.)	1:200
Nrf2 (H-300)	rabbit plyclonal (Santa Cruz Biotech. Inc.)	1:200
Porin	mouse monoclonal (Molecular Probes)	1:500
SDHB	mouse monoclonal (Molecular Probes)	1:800
SOD2	sheep polyclonal (Abcam)	1:200
SURF1	mouse monoclonal (Molecular Probes)	1:500
Survivin	rabbit polyclonal (Abcam)	1:1000
Trx1	rabbit polyclonal (Abcam)	1:1000
Trx2	rabbit polyclonal (Abcam)	1:1000
TUBA	mouse monoclonal (Sigma)	1:8000
Secondary antibodies		
Antibody		**Work. solution**
Peroxidase-labeled goat anti-rabbit IgG (Vector laboratories)		1:5000
Peroxidase-labeled goat anti-mouse IgG (Dako)		1:2000
Peroxidase-labeled anti-goat IgG (Santa Cruz Biotechnology Inc.)		1:3000

Table III.3. WB: Primary and secondary antibodies used.

After the transfer, the nitrocellulose membrane was incubated in fresh-made blocking solution (5% fat-free milk powder, in TBS-T buffer), with continuous gentle shaking, for 1 h, at RT or o/n, at 4 ºC. The composition of Tris-buffered saline-Tween (TBS-T) was: 20 mM Tris-HCl pH 7.2, 150 mM NaCl and 0.1% v/v Tween-20. The membrane was then incubated with the primary antibody, prepared in blocking solution containing 0.02% sodium azide (NaN_3), (Merck), for 3 h, at RT or o/n, at 4 ºC. After a washing step, the membrane was incubated with the secondary antibody, prepared fresh in blocking solution, for 1 h, at RT. Another washing step followed. Both washing steps

were performed in TBS-T, 4x10 min, at RT, with vigorous shaking. Details about the antibodies used are summarized in Tab.III.3.

Immunolabeling was detected by enhanced chemiluminescent reagent (ECL), (Amersham) or SuperSignal WestFemto (Pierce) and visualized with a digital luminescent image analyzer (FUJIFILM LAS 3000). Densitometric analyses were performed using ImageQuant software.

Stripping

The stripping process removes bound antibodies from the nitrocellulose membrane which enables to probe the same membrane with other antibodies. For this, after the completed immunoblot and visualization of the proteins, the membrane was washed in TBS-T for 15 min, at RT. Then, the membrane was incubated for 30 min, at 56 ºC and vigorous shaking in stripping buffer (62.5 mM Tris-HCl pH 6.7, 100 mM β-mercaptoethanol and 2% SDS). Subsequently, the membrane was washed 3x5 min in TBS-T, at RT. After this, the Western blotting continued as in the standard protocol, starting with blocking the membrane with fresh-made blocking solution, with continuous gentle shaking for 1 h, at RT or o/n, at 4 ºC, followed by primary and secondary antibody incubation, as described above.

III.13.4. Immunoprecipitation and co-immunoprecipiration

Immunoprecipitation of AIF and co-immunoprecipitation of Trx2 were performed by standard procedures. For the immunoprecipitation experiments, we cultured approximately 15 t-75 flasks of pU6-2 and AIF1-10 cells in complete MEM following the standard routine. Once the cultures reached confluence, the cells were trypsinized and cellular pellets collected. Whole-cell extracts were obtained and total protein amount in them determined, as described in chapter "III.13.1. Protein extracts". Then, whole-cell extracts containing 5 mg of total protein were diluted to 1 mL with complete lysis buffer and incubated with 60 μL (30 μg Ig) of agarose coupled to mouse monoclonal antibody against AIF (AIF (E-1): sc-13116, Santa Cruz Biotechnology, Inc.), for 1 h, at 4 ºC , with gentle shaking. Further, the samples were centrifuged in a microcentrifuge at 400 g, for 3 min, at 4 ºC and supernatant discarded. The agarose-conjugate pellet was then washed 3-5 times with 1 mL lysis buffer, in the absence of phosphatases and

proteases inhibitors (the composition of lysis buffer is described in chapter "III.13.1. Protein extracts"). Lastly, the agarose-conjugate pellet was resuspended in 60 μL Laemmli loading buffer 2X and boiled at 100 ºC, for 5 min. After another centrifugation step (microcentrifuge 400 g, 3 min, 4 ºC), the supernatant was collected and loaded on a polyacrylamide gel. Next, a standard procedure for SDS-PAGE followed (see chapter "III.13.3. Sodium dodecyl sulphate-polyacrylamide gel electrophoresis (SDS-PAGE) and Western blot (WB)"). Immunoprecipitated AIF was detected with the corresponding antibodies indicated in Tab.III.3. As a control, we used whole-cell extracts without immunoprecipitation.

For co-immunoprecipitation, the extract obtained from the immumoprecipitation was divided into two portions, one to detect the immunoprecipitated AIF and the other for Trx2, the protein assayed for co-immunoprecipitation. Standard SDS-PAGE and WB were performed employing the same primary and secondary antibodies as those used in the ordinary WB experiments (Tab.III.3).

III.13.5. Proteomic studies

For this approach, we cultured 20 t-150 flasks of pU6-2 and AIF1-10 cells in complete MEM following the standard routine and once the cultures reached confluence, the cells were detached by trypsinization and cellular pellets collected. Next, whole-cell extracts were obtained and total protein amount in them determined, following the protocol described in chapter "III.13.1. Protein extracts".

Immunoprecipitation

Whole-cell extracts containing 75 mg of total protein were diluted to 15 mL with complete lysis buffer and incubated with 500 μL (about 250 μg Ig) of agarose coupled to mouse monoclonal antibody against AIF (AIF (E-1): sc-13116, Santa Cruz Biotechnology, Inc.), in an orbital shaker, at 4 ºC, o/n. The samples were further centrifuged in a microcentrifuge at 400 g, for 3 min, at 4 ºC and the supernatant discarded. The immune matrices generated this way were further washed with basic lysis buffer, not containing detergent (composition: 20 mM HEPES pH 7.4, 400 mM NaCl, 0.1 mM EDTA). Three washing steps were carried out, the first one was with 15 mL of the basic lysis buffer, whereas the other two with 1 mL. Final equilibration in 50

mM ammonium bicarbonate was required for a further trypsin digestion process and mass spectrometric analysis. This was done by washing the immune matrices 5 times with 1 mL of fresh prepared 50 mM ammonium bicarbonate.

Also, 1/10 of the bound material was eluted by boiling in Laemmli loading buffer and processed for Western blot in order to corroborate specific AIF immunoprecipitation. A standard procedure for SDS-PAGE and WB followed (see chapter III.13.3), using the anti-AIF antibody indicated in Tab.III.3.

On-bead digestion for LC-MS/MS analysis

Resin-bound immunoprecipitated proteins were washed with 50 mM ammonium bicarbonate. After removing the liquid carefully, a volume equivalent to that of the resin of digestion buffer (20% v/v acetonitrile in 50 mM ammonium bicarbonate) was added to the beads. Samples were digested with 1 µg of modified porcine trypsin (Sequence grade, Promega), for 1 h, at 37 ºC under shaking conditions (1300 rpm). The reaction was quenched by adding a few microliters of glacial acetic acid and the digested material was loaded onto Handee spin columns (Pierce) and centrifuged (500 rpm) to collect the supernatant. The resulting solution was dried down on a speed-vacuum centrifuge at room temperature and finally re-dissolved in 5% acetonitrile with 0.5% acetic acid. A small aliquot of this material was analyzed by MALDI-TOF to check the tryptic digestion performance as well as to assess the complexity of the sample.

Nano-liquid chromatography and Ion-trap tandem mass spectrometric analysis of tryptic peptides

The resulting tryptic peptides were on line injected onto a C-18 reversed-phase self-packing nano-column (Discovery® BIO Wide pore, Supelco, Bellafonte, PA) and analyzed in a continuous acetonitrile gradient consisting of 0-50% buffer B for 50 min, 50-90% buffer B for 1 min, (buffer B contains acetonitrile 95% and acetic acid 0.5%). A flow rate of approximately 250 nL/min was used to elute peptides from the reversed-phase nano-column to a PicoTip™ emitter nano-spray needle (New Objective, Woburn, MA) for real-time ionization and peptide fragmentation on an Esquire HCT Ultra ion-trap (Bruker-Daltoniks, Bremen, Germany) mass spectrometer. Every 1 s, the instrument cycled through acquisition of a full-scan mass spectrum and two MS/MS spectra. A 3 Da window (precursor m/z±1.5), an MS/MS fragmentation amplitude of

0.90 V and a dynamic exclusion time of 0.20 min were used for peptide fragmentation. Nano-liquid chromatography was automatically performed on an advanced nano-gradient generator (Ultimate nano-HPLC, LC Packings, Amsterdam, The Netherlands) coupled to an autosampler (Famos, LC Packings). The software Hystar 3.4 was used to control the whole analytical process.

Database analysis

MS/MS spectra were batch-processed by using DataAnalysis 3.4 and BioTools 3.0 software packages and searched against the NCBI protein database using Mascot software (Matrix Science, London, UK).

III.13.6. Analysis of the redox state of Trx2

The aim of this experiment was to analyze the *in vivo* redox status of Trx2 in our model cells. For this we used 4-acetamido-4´-maleimidylstilbene-2,2´-disulfonic acid (AMS), a thiol-reactive probe which reacts with thiol groups in proteins and hence modifies their molecular weight by ca. 500 Da per free thiol. This enables the oxidized and the reduced form of the protein to be visualised as two different bands on a standard Western blot [Kobayashi T. *et al.*, 1997]. A protocol modified from Patrick J. Halvey and co-workers was used [Halvey P.J. *et al.*, 2005]. Confluent t-25 flasks were washed with ice-cold PBS and cells collected by scrapping. Pellets were obtained by centrifugation in a microcentrifuge (5415-R, Eppendorf) at 4 ºC, for 5 min, at 500 *g*. Supernatant was discarded and the cell pellet resuspended in 100 μL ice-cold 10% trichloroacetic acid (TCA), (Fluka) and incubated on ice, for 30 min, with gentle flicking of the tubes every 5 min. The suspension was then centrifuged in a microcentrifuge at 12000 *g*, for 10 min, at 4 ºC. The pellet was resuspended in 100 μL 100% acetone (Aldrich) and incubated on ice, for 30 min, with gentle flicking every 5 min. A centrifugation step followed, in a microcentrifuge at 12000 *g*, for 10 min, at 4 ºC. The supernatant was discarded and the pellet resuspended in 50 μL Tris-HCl 20 mM, pH 8.0. Then, the samples were incubated with 15 mM AMS (Invitrogen), for 3 h, at RT, protected from the light and with gentle shaking. Subsequently, Laemmli loading buffer without any reducing agent was added (0.5 mM Tris-HCl pH 6.8, 25% glycerol v/v, 10% SDS, and 0.5% bromophenol blue) and samples were boiled at 100 ºC, for 5 min. As a control, the same samples were used but without incubation with AMS. These

controls were boiled with Laemmli loading buffer containing the reducing agent DTT, the usual buffer for standard SDS-PAGE. All samples were then used for a standard SDS-PAGE and WB (see "III. Material and Methods", section III.13.3).

III.13.7. Confocal immunofluorescence microscopy

This technique was employed in order to monitor the location of Trx2 after its transient transfection in cells. First, HeLa cells were transfected with Trx2 (the vector construction was described in chapter "III.3.2. Protein overexpression plasmids") tagged with a Flag sequence. This enabled us to distinguish between the endogenous and the overexpressed Trx2, as the latter can be probed with anti-Flag antibody.

For the transfection, 2×10^5 cells/well were plated in 24-well plate, where the wells had previously been covered with UV-sterilized coverslips. The transfection was performed using LipofectAMINE^{TM} 2000 (Invitrogen Life Technologies), as described in chapter "III.2.3. Transfection experiments". Next, at 27 h after the transfection, the culture medium was removed and prewarmed growth medium containing 500 nM Mitotracker Red 580 (Molecular Probes) added. Then, the cells were incubated at 37 ºC, for 45 min. After this, the cells were PBS-washed and fixed using 2% p-formaldehyde (Sigma) PBS solution. The fixation was performed at RT, for 10 min, after which the plates were rinsed with TBS to eliminate the formaldehyde. Next, the cells were permeabilized by incubation in ice-cold acetone (Aldrich) for 30 sec and rinsed with TBS, 3 times.

For the immunofluoresce, we blocked with 30 μL of blocking solution (1% BSA in TBS), at RT, for 30 min, followed by 1 h incubation at RT with 30 μL of the primary antibody. We used rabbit polyclonal anti-Flag antibody (Sigma), at 8 μg/mL in TBS. Subsequently, we washed 3x5 min in TBS, at RT. After this, the coverslips were incubated with 30 μL of the secondary antibody solution (1% BSA in TBS), at RT, for 30 min. As a secondary Ab, we used anti-rabbit Ig FITC-conjugated (DAKO). Another washing step followed, 3x5 min in TBS, at RT. Finally, the coverslips were rinsed with distilled water and mounted on a slide glass with the aqueous mounting medium, Mowiol (Fluka). Then, the slides with the coverslips were taken to the confocal microscope (Leica TCS-SP confocal microscope, Heidelberg, Germany) and Mitotracker Red 580 fluorescence (in red) and Flag immunofluoresence (in green) visualized.

III.14. Oxygen consumption

The cellular oxygen (O_2) consumption was measured using a Clark-type electrode (Rank Brothers, Bottisham, UK). The Clark electrode [Clark L.C. *et al.*, 1953; Severinghaus J.W. and Astrup P.B., 1986] measures oxygen on a catalytic platinum surface using the reaction represented in Fig.III.4.

$$O_2 + 2e^- + 2H_2O \rightarrow H_2O_2 + 2OH^-$$

Figure III.4. Oxidation of atmospheric oxygen is the principle of the chemical reaction taking place in the Clark-type oxygen electrode.

The electrode compartment is isolated from the reaction chamber by a thin teflon membrane; the membrane is permeable to molecular oxygen and allows this gas to reach the cathode, where it is electrolytically reduced. This reduction allows a current to flow which creates a potential difference recorded on a flatbed chart recorder. The trace is thus a measure of the oxygen activity of the reaction mixture, where the current flowing is proportional to the activity of oxygen.

Before performing the measurement, the electrode was calibrated in air-saturated respiration buffer, considering the atmospheric O_2 concentration as maximal: 200 μM O_2. Electrode zero setting was performed by adding excess of sodium dithionite ($Na_2S_2O_4$), (Panreac), to the chamber. O_2 consumption was usually detected over a period of 30-40 min and mitochondrial respiration specificity was confirmed by adding 1mM KCN to the chamber.

The data from the electrode were obtained using the "DUO.18 programme" (World Precision Instrument, Sarasota, FL, USA) and analyzed with the "Tarragona programme" (Custom Written Software, University College London).

Oxygen consumption in intact cells

For these experiments, cells were detached immediately before the measurement and counted using hemacytometer. Then, 2-3 million cells were resuspended in HBSS as respiration buffer and taken to the respiration chamber, where the suspension is constantly stirred and maintained at 37 ºC.

Oxygen consumption in permeabilized cells

Eukaryotic cell membranes are selectively permeabilized with the non-ionic detergent digitonin to render a system in which mitochondrial respiration, dependent on exogenous substrates, can be measured rapidly and with considerable sensitivity [Hofhaus G. *et al*., 1996]. At moderate concentrations of digitonin the plasma membrane is permeabilized while mitochondria remain intact.

The aim of this experiment was to study the mitochondrial O_2-consumption on individual mitochondrial complexes by addition of exogenous substrates to the respiration chamber. For this, the cell culture was performed as usual, but cells were permeabilized immediately prior to the O_2 consumption measurement, basically following the protocol described by Antoni Barientos [Barrientos A., 2002]. Generally, 2-3 million cells were trypsinized and resuspended in 1 mL respiration buffer (10 mM K_2HPO_4, 10 mM KCl, 5 mM $MgCl_2$ and 0.3 M mannitol, pH adjusted to 7.4). 100 μg/mL of digitonin (GIBCO) was added and the suspension was incubated for 2 min, at RT, with gentle shaking. Then, the permeabilization was stopped by adding 5 volumes (5 mL) of respiration buffer containing 1 mg/mL BSA and the suspension was centrifuged at RT, for 5 min, at 300 *g*. Permeabilized cells were resuspended in 0.5 mL respiration buffer with 1 mg/mL BSA and 0.5 mM ADP and taken to the respiration chamber where the electrode had been previously calibrated with the same buffer. The respiration without any substrates added, corresponds with the basal level of O_2 consumption. After this consumption had been recorded, the following compounds were added using a Hamilton syringe: 30 mM glutamic acid, 0.4 mM malic acid, 6 μM rotenone, 10 mM succinic acid and 0.2 mM ATP. All respiration substrates had previously been adjusted to pH 7.

III.15. Statistical analyses

Statistical analyses were performed using the "Student´s t-test" provided by the GraphPad software programme. Unless indicated differently, we applied unpaired, two-tailed t-test, with confidence interval of 95%. Values were considered significantly different if $p < 0.05$.

The *Harlequin* mouse
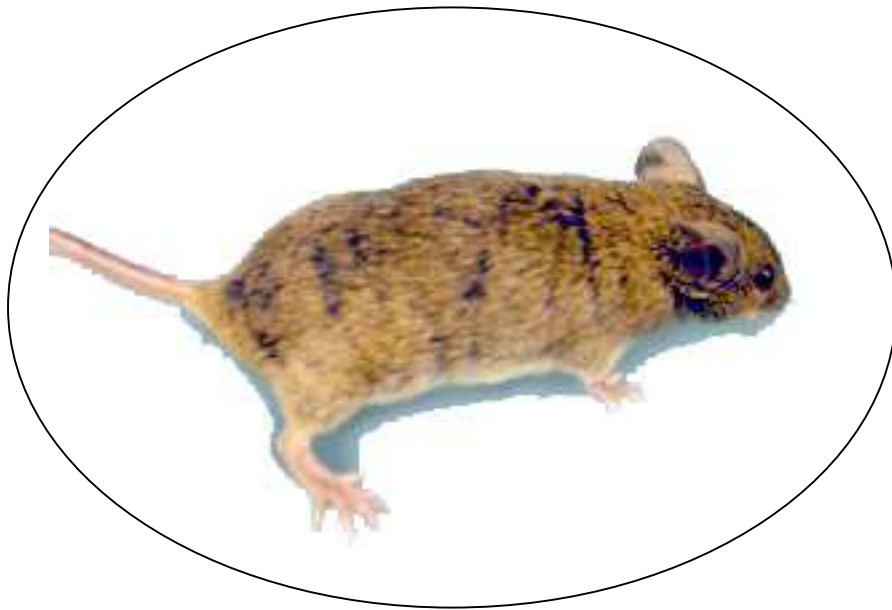
In 2002, Dr. Susan Ackerman´s group at Jackson laboratory, USA, reported the identification of a mouse gene implicated in oxidative stress and neurodegeneration. This gene was *Aif* and thus a new and promising field was opened for the AIF research. *Hq* mouse became the first mouse model for studying the role of oxidative stress on aberrant cell cycle re-entry and subsequent neuronal death - a hallmark of many human neurodegenerative disorders.

IV. RESULTS

"There are no such things as applied sciences, only applications of science"

Louis Pasteur (1822-1895)

IV.1. Analysis of the splicing variants of AIF

We were interested in studying the expression pattern of *AIF* in different human tissues and to analyze the presence of the three transcript variants, described in the literature, at that time, listed in the GenBank as AF100928, AL049703 and AL049704 [Daugas E. *et al.*, 2000 A]. This was important for us because we wanted to design *AIF* silencing vectors which would be general for all potential splicing variants. For this, we performed RT-PCR with primers to amplify specific *AIF* species and employed commercially available human cDNA panels. The primers we first used were designed in such a way, that they could amplify all three splicing variants. Variant 2 (accession number AL049703) differs from variant 1 as it contains an alternative exon II, called exon IIB, but the overall protein length is the same (Fig.IV.1.A). Variant 3 (accession number AL049704) has a large central deletion and is shorter in length (Fig.IV.1.A). Performing RT-PCR in the human normal tissue cDNA we obtained a single band, of 1080 bp corresponding to the amplified fragment of *AIF* variant 1 and 2, but not variant 3 which was expected to give rise to a smaller (221 bp) product (Fig.IV.1.B).

1: heart
2: brain
3: placenta
4: lung
5: liver
6: skeletal muscle
7: kidney
8: pancreas
9: spleen
10: thymus
11: prostate
12: testis
13: ovary
14: small intestine
15: colon
16: leukocyte
17, 27: negative control
18, 28: positive control
19: breast carcinoma GI-101
20: lung carcinoma LX-1
21: colon adenocarcinoma CX-1
22: lung carcinoma GI-117
23: prostatic adenocarcinoma PC3
24: colon adenocarcinoma GI-112
25: ovarian carcinoma GI-102
26: pancreatic adenocarcinoma GI-103

Figure IV.1. RT-PCR analysis of *AIF* expression in human normal and tumour tissues. A. Schematic representation of *AIF* transcript variants 1, 2 and 3. Note that *AIF* variants 1 and 2 are similar in length unlike variant 3 which is shorter. B. RT-PCR reveals that variant 3 is absent both in normal and tumour human tissues.

Interestingly, some tissues display higher expression levels of *AIF*, namely pancreas, thymus, testis, whereas the brain, lung and skeletal muscle express less *AIF*, as shown in Fig.IV.1.B.

A similar result was obtained when using the human tumour cDNA panel. In this case, only a single 1080 bp band was visible in all tissues with significant differences in the strength, pointing to higher expression of *AIF* in breast carcinoma, colon adenocarcinoma CX-1 and prostatic adenocarcinoma, and lower expression in pancreatic and colon adenocarcinoma GI-112 (Fig.IV.1.B).

Next, we aimed to find out whether the amplified 1080 bp fragment corresponded to splicing variant 1 or with variant 2, as the designed pair of primers could amplify both *AIF* species. For this, we exploited the fact that *AIF* splicing variant 1 has a single *Bam*HI restriction site, whereas splicing variant 2 has two. After RT-PCR was performed, the amplified DNA fragment was ethanol-precipitated and the pellet suspended in water. Next, *Bam*HI digestion was performed by a standard procedure. Then, the digested products were run on an agarose gel (containing EthBr and using buffer TAE 1x) and the fragments were visualized. If only variant 1 was present, we expected to see a duplet band of approximately 500 bp, whilst, on the contrary, *Bam*HI digestion of *AIF* splicing variant 2 should release a doublet fragment, at 300 and 200 bp, and a single fragment at 500 bp.

1: spleen
2: thymus
3: prostate
4: testis
5: ovary
6: small intestine
7: colon
8: leukocyte
9,18: negative control
10: breast carcinoma GI-101
11: lung carcinoma LX-1
12: colon adenocarcinoma CX-1
13: lung carcinoma GI-117
14: prostatic adenocarcinoma PC3
15: colon adenocarcinoma GI-112
16: ovarian carcinoma GI-102
17: pancreatic adenocarcinoma GI-103
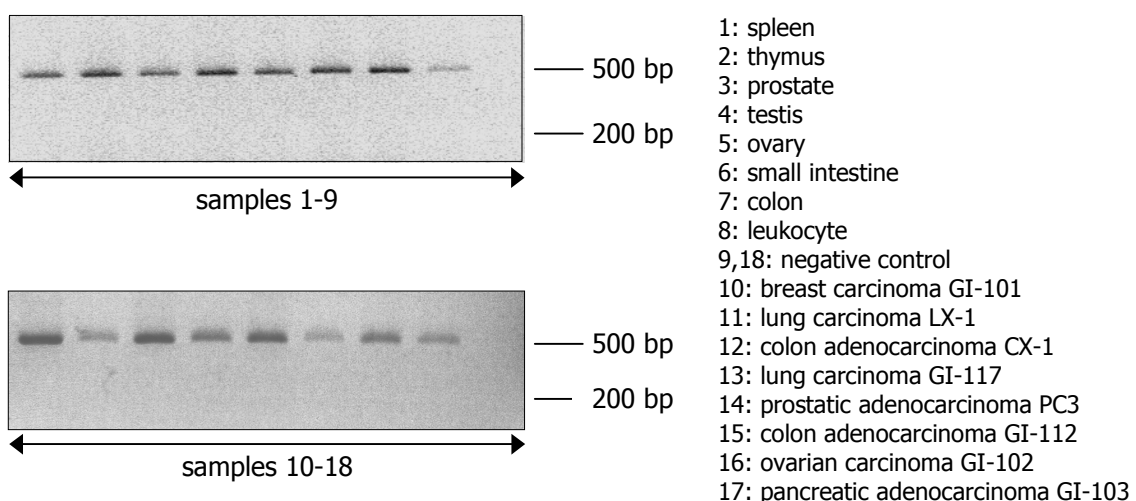
**Figure IV.2. RT-PCR results of AIF expression in human control and tumour cDNA, after *Bam*HI digestion. The presence of a single band ≈ 500 bp in size suggests the presence of only AIF spicing variant 1 in all the samples.**

As shown in Fig.IV.2, both normal and tumour cDNA panels displayed only one DNA fragment, at 500 bp, after *Bam*HI restriction, suggesting that splicing variant 2 was not present in any tissue, at least to the limits of detection of our experimental approach. Water instead of cDNA was employed as a negative control. This experiment was repeated with Hep3B mRNA, with similar results (not shown).

IV.2. Transient *AIF* silencing and ROS levels

As there was evidence for a connection between AIF and the cellular ROS status, we first decided to assess the basal cellular ROS levels in *AIF*-silenced cells. In order to avoid cell type specific phenotypes, we performed this experiment in two different cell lines, the human hepatoma cell line Hep3B and the human cervical carcinoma cell line HeLa. In both cases, sub-confluent cell cultures growing in t-25 flasks, were transiently transfected with pBS U6/PolIII empty vector, the pBS U6/PolIII vector containing the control silencing cassette siGFP and two *AIF*-silencing vectors: pBS U6/PolIII/siAIF1 and pBS U6/PolIII/siAIF2. Test transfections with pU6 GFP (siGFP) resulted in a robust knockdown of a co-transfected GFP expression vector (results not shown).
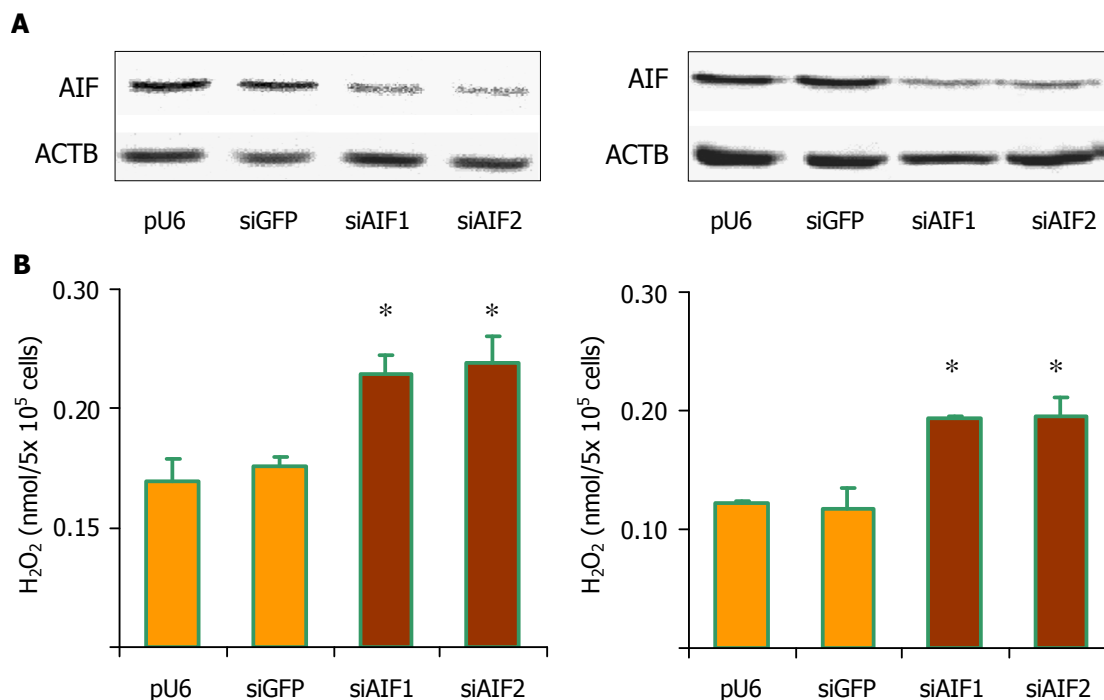

Figure IV.3. Transient *AIF* silencing is accompanied by an increase in ROS levels. A. WB showing AIF expression in transiently transfected Hep3B cells (left panel) and HeLa cells (right panel). B. H_2O_2 concentration in transiently transfected Hep3B cells (left panel) and HeLa cells (right panel). Results are represented as mv±SEM, n=2, *p<0.05.

At 72 h after the transfection, cells were collected and split in two halves, one half of the cells was immediately processed for H_2O_2 detection, using the "Amplex red kit", the other half was used to obtain whole-cell protein extracts. This experiment was performed twice, with similar results. As shown in Fig.IV.3, transient *AIF* silencing is followed by significant increase in ROS levels, determined as extracellular H_2O_2 concentration. In Hep3B cells, the H_2O_2 levels recorded were 0.23 ± 0.016 nmolH_2O_2/5x10^{5}cells in the case of siAIF1-transfected cells and 0.24 ± 0.022 nmolH_2O_2/5x10^{5}cells in the case of siAIF2-transfected cells, both values significantly higher in comparison with the control value of 0.14 ± 0.019 nmolH_2O_2/5x10^{5}cells, recorded in cells transfected with the empty pU6 vector. In HeLa cells, siAIF1-transfected cells show H_2O_2 level of 0.19 ± 0.001 nmolH_2O_2/5x10^{5}cells, an equal level was recorded in siAIF2-transfected cells, 0.19 ± 0.017 nmolH_2O_2/5x10^{5}cells, both significantly higher as compared to the control pU6-transfected cells with 0.12 ± 0.002 nmolH_2O_2/5x10^{5}cells.

Of note, this occurs both in Hep3B and HeLa cells and using both *AIF*-silencing vectors. It is not an artifact produced by intracellular RNA interference processes, as transfection with the control siGFP vector does not modify the basal ROS level in Hep3B nor in HeLa cells.

IV.3. H_2O_2 concentration measurement in Hep3B rho⁰ cells

We were interested in studying the origin of the observed increased ROS levels following silencing of *AIF*. As the mitochondrial ETC is a major source of intracellular ROS in most cell types, we decided to generate rho⁰ (ρ^0) cells and assess their ROS levels after transient *AIF* silencing in this cellular model. To this end, ρ^0 cells were generated in the Hep3B background by a prolonged treatment with EthBr as described in chapter "III. Materials and methods". EthBr is a known genotoxic compound which, used at an appropriate concentration, associates with mtDNA and disrupts mtDNA transcription. As a consequence, there is a lack of the mtDNA-encoded proteins and thus an inhibition of the OxPhos process, leading to the characteristic ρ^0 phenotype: slower cellular proliferation, inhibited cellular respiration, and a reduced capacity to grow on non-fermentable sugars (eg. galactose).

We verified the ρ^0 status of these cells by assessing the cellular proliferation in

glucose- and galactose-containing medium, using a hemacytometer to count the cells in culture; performed WB to analyze the expression of mtDNA-encoded ETC proteins, such as cytochrome c oxidase subunit II (COX2) and finally determined the respiration of intact cells by measuring O_2 consumption using a Clark-type electrode.

All of these parameters verified the ρ^o status of our cells (Fig.IV.4). The generated Hep3B ρ^o cells displayed significantly lower basal rate of proliferation (at day 4, ρ^o cells only proliferated 28% of the control Hep3B ρ^+ cells) and they were virtually unable to grow on galactose instead of glucose (Fig.IV.4.C). COX2 expression was also completely abolished (Fig.IV.4.B) and as expected, there was a dramatic decrease in the cellular respiration (remaining 15% of the WT O_2 consumption levels), as depicted in Fig.IV.4.A.
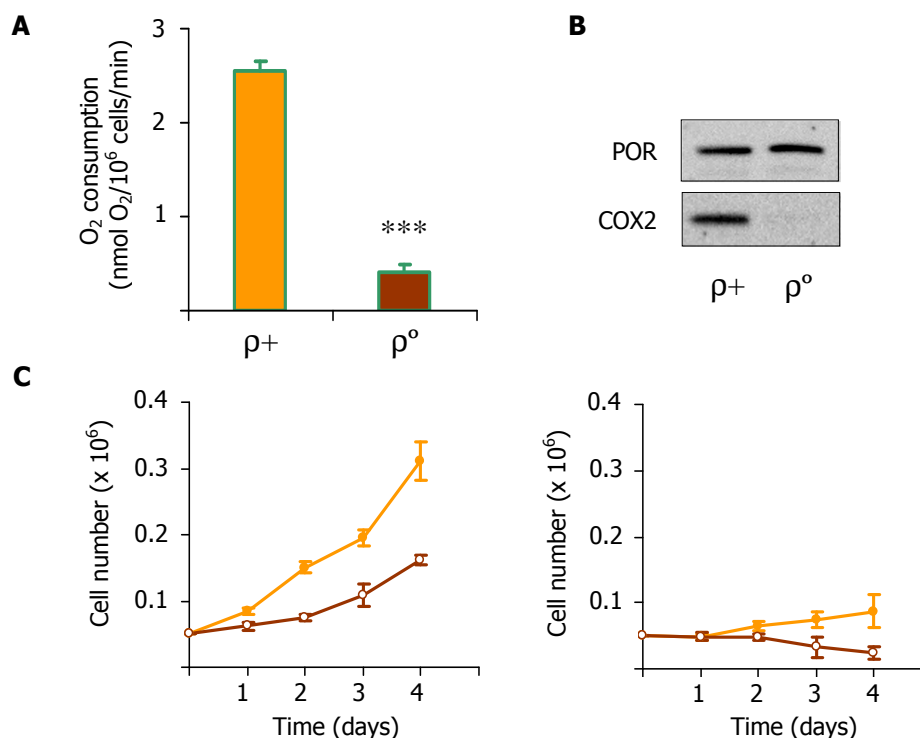
Figure IV.4. Analysis of the ρ^o phenotype. A. O_2 consumption in intact Hep3B ρ^+ and ρ^o cells, results represented as mv±SEM, n=4, ***p<0.001. B. Representative WB showing COX2 expression in mitochondria-enriched protein extracts of Hep3B ρ^+ and ρ^o cells. C. Cell proliferation of Hep3B ρ^+ (left panel) and ρ^o cells (right panel), in glucose- (orange) and galactose-containing (brown) growth medium, results are represented as mv±SD, n=3, p<0.05.

After confirming the ρ^o status, we next aimed to transiently silence *AIF* in these cells and determine the ROS levels. For this, both Hep3B WT (ρ^+) and Hep3B ρ^o cells were transiently transfected with pBS U6/PolIII/siAIF1 and pBS U6/PolIII/siGFP, as a control.

As shown in Fig.IV.5, *AIF* was successfully silenced in both cell lines and interestingly, while this silencing was correlated with higher H_2O_2 concentration in Hep3B WT cells (0.32 ± 0.013 nmolH_2O_2/5x10^5cells in *AIF*-silenced cells as opposed to 0.20 ± 0.006 nmolH_2O_2/5x10^5cells in control cells), there was no significant increase of H_2O_2 levels in Hep3B ρ^o cells (0.10 ± 0.009 nmolH_2O_2/5x10^5cells in *AIF*-silenced Hep3B ρ^o cells versus 0.09 ± 0.034 nmolH_2O_2/5x10^5cells in control Hep3B ρ^o cells). In addition, we found that the basal ROS levels of ρ^o cells were significantly lower compared to the WT background (Fig.IV.5.B). This experiment was performed three times, with similar results. Also, we repeated this approach in HeLa cells and obtained a similar result (not shown).

In summary, our finding points to the need of a functional mitochondrial ETC for the increase in ROS levels observed upon *AIF* silencing in our cellular model.
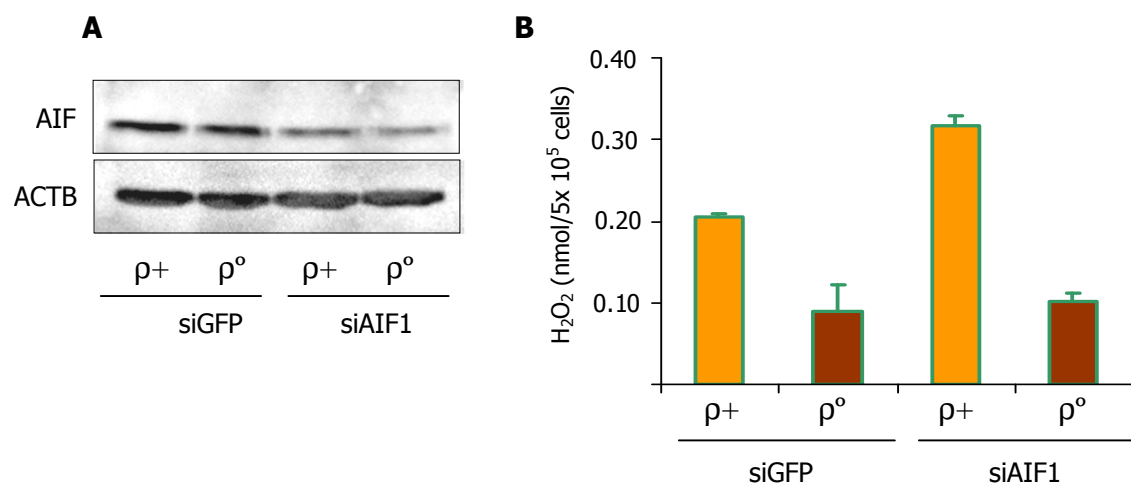
Figure IV.5. Transient *AIF* silencing in Hep3B ρ^o cells is not followed by an increase in the ROS levels. A. WB showing AIF expression in whole cell extracts obtained of transiently transfected Hep3B $\rho+$ and ρ^o cells B. H_2O_2 concentration in transiently transfected Hep3B$\rho+$ and ρ^o cells. Results are represented as mv±SEM, n=3.

IV.4. Generation of stable siAIF cell lines

Having shown that *AIF* silencing corresponds with ROS increase in two different cell lines and that this increase requires a functional mitochondrial ETC, we next decided to generate stable siAIF cell lines, in order to study this phenomenon in detail. As described in the "III. Materials and Methods" chapter, t-25 flasks of Hep3B cells were co-transfected with pBS U6/PolIII/siRNA and the pcDNA3 vector containing a Neomycin-resistance gene, in a 10:1 mass ratio.
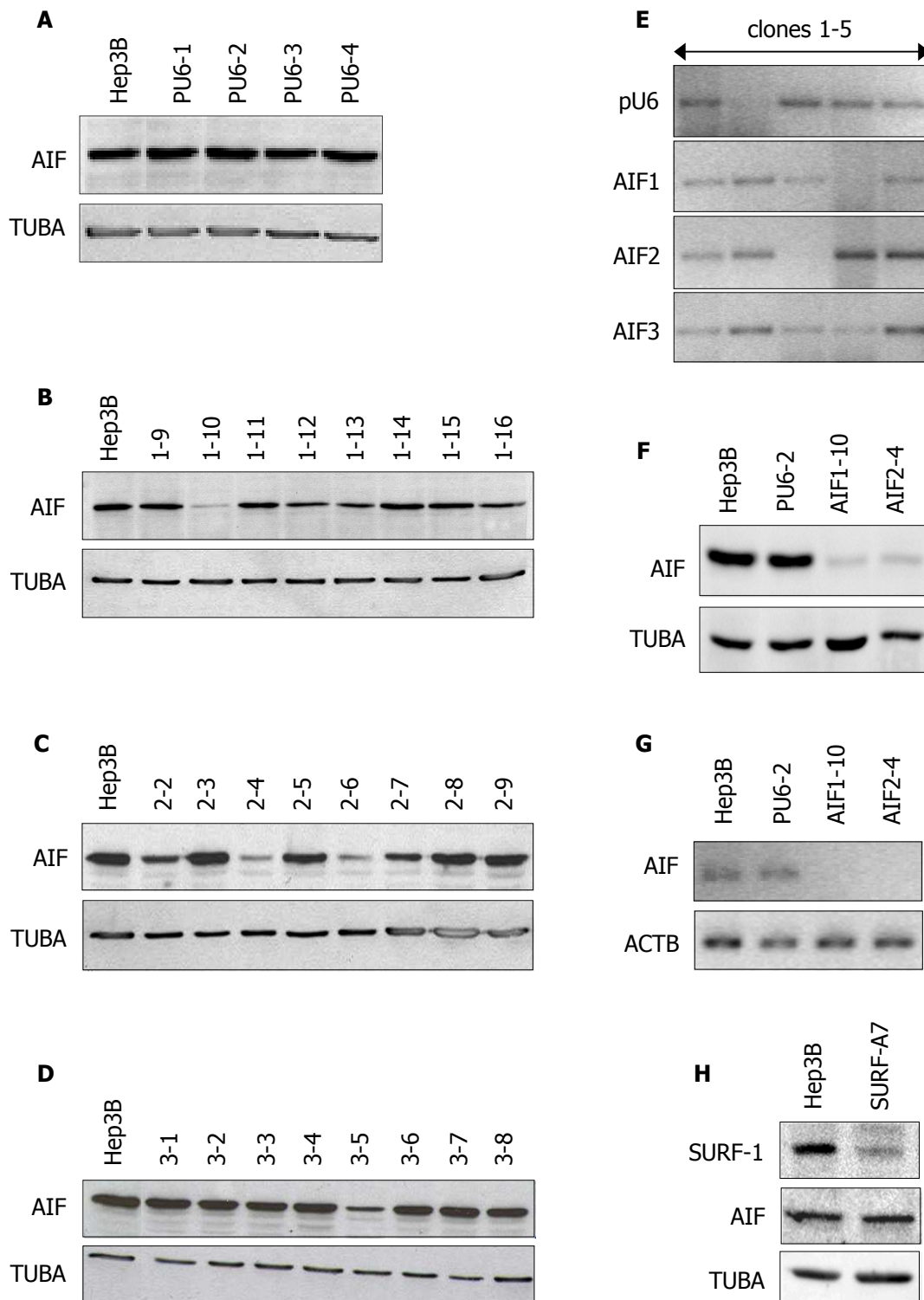
Figure IV.6. Generation of stable siAIF cell lines. AIF expression at the protein level was analyzed by WB in the clones obtained after transfection with the empty silencing vector pBS U6/PolIII/ (A), vector pBS U6/PolIII/AIF1 (B), vector pBS U6/PolIII/AIF2 (C) and vector pBS U6/PolIII/AIF3 (D). Genomic PCR was used to look for the presence of integrated pU6 vector (E). Clones AIF1-10 and AIF2-4 maintain low AIF levels after prolonged time in culture, detected by WB (F) and semi-quantitative RT-PCR (G). The control cell line SURF-A7 displays lower SURF1 expression without changes in AIF, as shown by WB (H).

94

This was performed in order to ensure that the cells which had integrated the *Neo* gene also possessed the RNAi cassette. Then, 24 h after the co-transfection, the cells were transferred to plates (Ø 90 mm) where selection was performed with 200 μg/mL geneticin (G418-sulphate), until individual colonies were visible (about 14 days). These were then isolated and sub-cultured separately in compete growth medium containing the same concentration of geneticin. When the subcultures (clones) reached a constant cellular proliferation and enough cells could be harvested, we collected cells of each one for analyses.

A total of 53 clones were obtained, 46 of which were generated by transfection with siAIF cassettes (16 with the cassette siAIF1, 14 with the cassette siAIF2 and 16 with the cassette siAIF3) and the other 7 clones, were control clones obtained by transfection with the pBS pU6/PolIII/ empty vector.

The screening of the clones included performing WB analyses, using whole-cell protein extracts, to assess the AIF expression and genomic PCR analyses to locate the integrated pU6 vector (see "III. Materials and methods", chapters III.3.1 and III.12.1). Fig.IV.6 (A, B, C and D) shows representative WB analysis in some of the clones of all three silencing cassettes and the control pU6 clones, whereas representative genomic PCR results are shown in Fig.IV.6.E.

	AIF1	AIF2	AIF3	pU6
nº of isolated cell lines	16	14	16	7
pU6 positive cell lines (PCR)	8 (50%)	13 (92.8%)	14 (87.5%)	6 (85.7%)
AIF-silenced cell lines (WB)	4 (25%)	6 (42.9%)	3 (18.8%)	/

Table IV.1. Screening for stable *AIF*-silenced cell lines. Genomic PCR analysis revealed the presence of the integrated pU6 vector, whereas WB was used to assess the AIF expression.

The overall screening results are summarized in Tab.IV.1. To our surprise, the generation of siAIF cell lines by stable transfection was not very efficient. Out of 46 putative siAIF clones, 35 had integrated the pU6 plasmid and only 13 of these displayed a significant decrease in *AIF* expression. The cassette siAIF2 seemed to be

the more successful as to the number of generated siAIF clones.

Next, we chose two clones, one of cassette siAIF1, named AIF1-10 and one of the cassette siAIF2, AIF2-4, for characterization. As the level of *AIF* silencing was not satisfactory in any of the siAIF3 clones, none of the latter was chosen. The selected clones were maintained in culture for longer periods, in the presence of 200 μg/mL geneticin and AIF expression was verified. Importantly, AIF expression was constant after prolonged passaging of the cells, even over several months (up to passage nº 20). This was verified by both WB and RT-PCR analysis, as shown in Fig.IV.6.F and Fig.IV.6.G respectively.

In some experiments, as an additional control for the stable siAIF lines, we used the SURF-A7 a cell line, where the SURF1 protein, a chaperone of the mitochondrial ETC Complex IV, was stably silenced by the same methodology and in the same cellular background as the *AIF* silencing. The expression of AIF and SURF1 at the protein level in this cell line are represented in Fig.IV.6.H.

IV.5. Analysis of the redox status in stable *AIF*-silenced cell lines

IV.5.1. H_2O_2 measurement using the Amplex red kit

As transient *AIF* silencing was shown to be followed by a significant increase in ROS levels, we next wanted to examine whether this increase is present in the stable siAIF cell lines. For this purpose, we measured H_2O_2 concentration by the same protocol, using the "Amplex red kit" as indicated in "III. Materials and methods", chapter III.8. As represented in Fig.IV.7, both siAIF cell lines, showed significantly incremented levels of ROS (0.12 ± 0.011 nmolH_2O_2/5x10^5cells in AIF1-10 cells and a very similar level of 0.12 ± 0.010 nmolH_2O_2/5x10^5cells in AIF2-4 cells), compared to the detected in the control cell lines, Hep3B and SURF-A7 (0.08 ± 0.006 nmolH_2O_2/5x10^5cells and 0.07 ± 0.010 nmolH_2O_2/5x10^5cells, respectively). Also, WT Hep3B cells have similar H_2O_2 level as pU6-2 cells (result not shown). These H_2O_2 measurements were performed many (at least six) times, using cells of different passage numbers. Fig.IV.7 comprises the data obtained in two separate experiments, using cells of passage nº 5-10.

Of note, prolonged maintenance of these siAIF lines in cell culture does not lead to

normalizing of the H_2O_2 levels as high passage number cells of AIF1-10 and AIF2-4 have very similar, increased H_2O_2 levels as low passage number cells (data not shown).
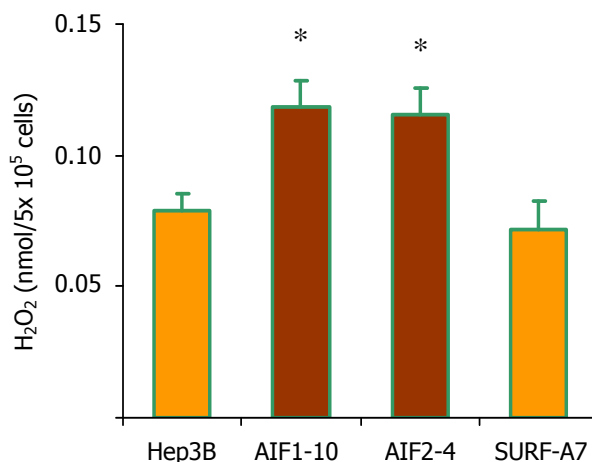
Figure IV.7. H_2O_2 concentration in stable siAIF cell lines compared to wild type Hep3B cells and control stable silenced cell line, SURF-A7. Results are represented as mv±SEM, n=6, *p<0.05.

IV.5.2. ROS level quantification by confocal microscopy

In order to obtain a more accurate quantification of the intracellular ROS production, we next conducted confocal microscopy experiments of the stable siAIF and control cells. This technique also enabled us to distinguish among different reactive oxygen species, which was achieved by using different redox-sensitive fluorochromes. We used HE to detect superoxide and DCFH-DA to determine H_2O_2 and hydroxyl radical concentration. As shown in Fig.IV.8, both HE (red) and DCFH-DA (green) fluorescence in AIF1-10 cells are increased in comparison with the control cell line, pU6-2, indicating higher intracellular levels of ROS. When quantified, the data of three independent experiments revealed that HE fluorescence in AIF1-10 was increased almost twice, compared to pU6-2 value, whereas in the case of DCFH-DA, the increase is even 2.5 fold, as depicted in the bar charts in Fig.IV.8.

IV.5.3. Analysis of the mitochondrial transmembrane potential (Δψ$_m$)

After having shown that *AIF* silencing is accompanied by increase in the intracellular levels of ROS, we assessed the mitochondrial transmembrane potential (Δψ$_m$), which is a ROS-related parameter. The latter assay was performed by confocal microscopy using the fluorochrome TMRM. Interestingly, compared to the control pU6-2 cell line,

AIF-10 cells display significantly lower $\Delta\psi_m$, visualized as a decreased TMRM fluorescence (in red), as shown in Fig.IV.9.A. The quantification, comprising data of three separate experiments, represented as a bar chart in Fig.IV.9.A, revealed that the reduction of the TMRM fluorescence in AIF1-10 was about 50% compared to pU6-2 (value normalized to 100%).
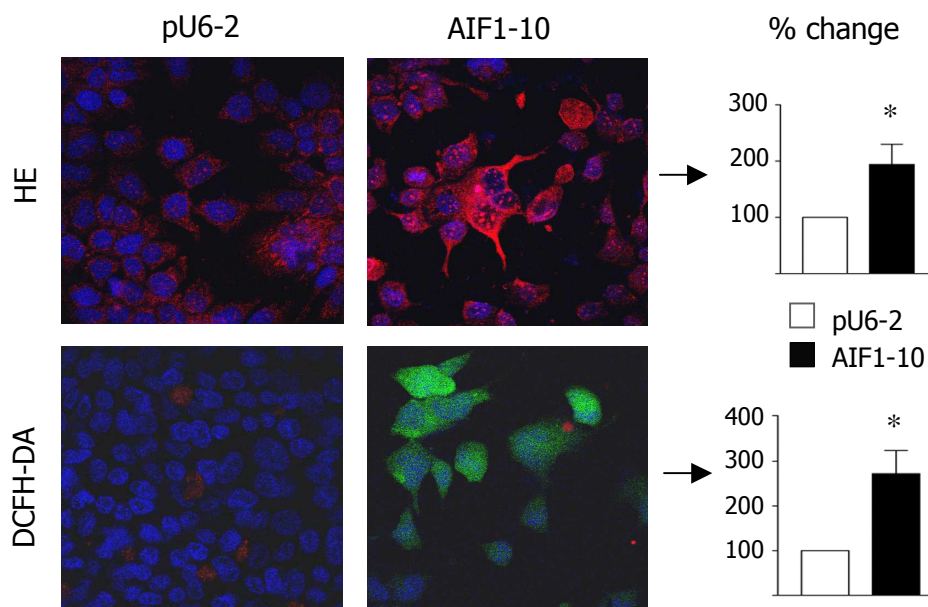
Figure IV.8. Analysis of the ROS levels in AIF1-10 cells versus control pU6-2 cell line. Representative confocal images of pU6-2 and AIF1-10 cells and corresponding data quantification are shown. Cells were stained with HE (red), DCFH-DA (green), and Hoechst 33342 (blue). Graphs indicate mean fluorescence intensity of three separate experiments, mv±SEM, n=3, *p<0.05.

IV.5.4. Quantification of intracellular glutathione (GSH) levels

The intracellular concentration of reduced (non-oxidized) glutathione (GSH) is an accurate and thus, often-used indicator of the intracellular redox status. We therefore, aimed to analyze the GSH levels in siAIF cells compared to control cell lines. Confocal images obtained by staining the cells with the thiol-sensitive probe CMFDA (green fluorescence) did not reveal any significant differences in the fluorescence intensity between AIF1-10 and pU6-2 cells (Fig.IV.9.A). Nevertheless, a fluorimetric assay performed on two siAIF cell lines, AIF1-10 and AIF2-4, and two control lines, the Hep3B WT cells and pU6-2 cell line, showed a visible (though non-significant) tendency of AIF1-10 to display lower levels of GSH (Fig.IV.9.B). More in a detail, AIF1-10 cells had 1.02 ± 0.226 nmol GSH/5×10^4 cells, compared to the 1.46 ± 0.318 nmol GSH/5×10^4 cells displayed by pU6-2 cells.

Thus in summary, silencing of *AIF* in our cell model, only leads to a slight, but non-significant, decrease of the GSH levels.
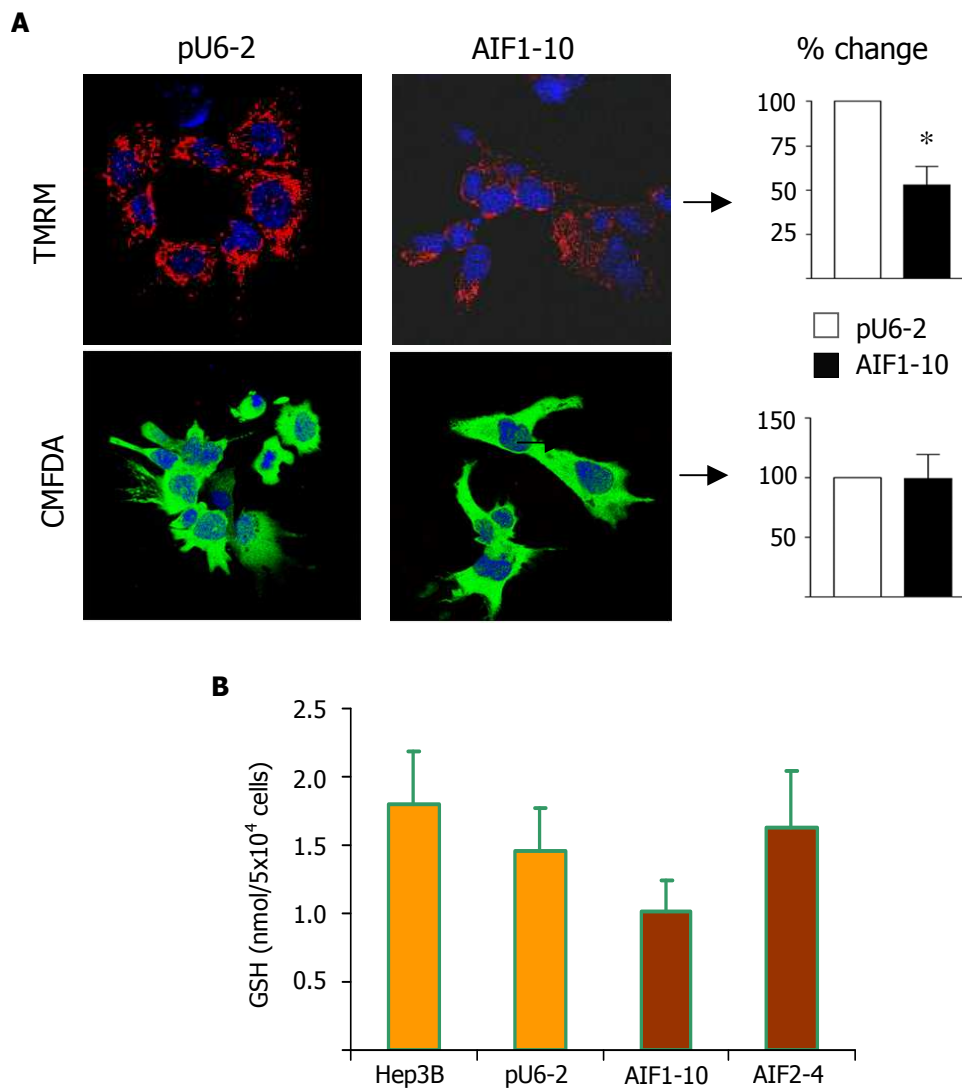
Figure IV.9. Analysis of the redox status of siAIF cells versus controls. A. Representative confocal images of pU6-2 and AIF1-10 cells and corresponding data quantification. Cells were stained with TMRM (red), CMFDA (green) and Hoechst 33342 (blue). Graphs indicate mean fluorescence intensity of three individual experiments, mv±SEM, n=3, *p<0.05. B. Graph showing intracellular GSH levels in two independent siAIF cell lines (AIF1-10 and AIF2-4) versus control cell lines (Hep3B and pU6-2), mv±SEM, n=3, p>0.05.

IV.6. HIF-1α expression in stable *AIF*-silenced cell lines

There is solid experimental evidence supporting the relationship between intracellular ROS levels and HIF-1α stabilization, under both normoxic and hypoxic conditions. This made HIF-1α an interesting candidate transcription factor to be studied in our model *AIF*-silenced cells. Prior to the analysis of HIF-1α expression in *AIF*-silenced cells, we

aimed to assess HIF1-α expression in the control pU6-2 line and test its stabilization under hypoxic conditions. For this, we exposed pU6-2 cells to 3% O_2 atmospheric environment, as described in the chapter "III.2. Cell culture", for 4 h. Next, whole-cell extracts were obtained and WB analysis was performed to observe HIF1-α expression. As shown in Fig.IV.10.A, basal normoxic (21% O_2) levels of HIF1-α in pU6-2 cells are very low or virtually non-existent and a similar result was obtained using another control cell line, SURF-A7. However, as expected, subjecting pU6-2 cells to 3% O_2, stabilizes HIF-1α (Fig.IV.10.A). As a control, house-keeping, gene we used β-actin expression. This experiment was performed a minimum of six times, with a very similar result.

As a further control, we treated pU6-2 cells with H_2O_2 and analyzed whether direct and short-term H_2O_2 treatment could stabilize HIF-1α, a phenomenon described in the literature. For this, sub-confluent cell cultures growing in t-25 flasks were treated with H_2O_2 for 30 min, after the standard growth medium had been replaced by HBSS. We did not maintain the cells in the standard growth medium MEM in order to avoid any influences of the presence of serum and other components of the MEM, as H_2O_2 is quite an unstable substance. This experiment was performed four times with similar results. Fig.IV.10.B shows a representative WB of HIF-1α expression and the control expression levels of the house-keeping protein ACTB. H_2O_2 treatment (both 50 and 100 μM) stabilized HIF-1α and these levels are in a similar range to HIF1-α stabilization under 4 h hypoxic treatment (3% O_2).

Next, we aimed to study the steady-state, normoxic expression of HIF-1α in our siAIF cells and found that it was significantly increased compared to control cell lines (Fig.IV.10.C). This observation raised a question about whether HIF-1α stabilization in *AIF*-silenced cells is a direct consequence of the increased ROS levels. To address this question, we decided to treat the cells with antioxidants. Thus, siAIF and control cell lines were cultured for 3 h in the presence of the broad-range antioxidant N-acetyl cysteine (NAC, 5 mM) and we then performed WB analysis on whole-cell extracts using an antibody directed to HIF-1α. These results, shown in Fig.IV.10.C, reveal that whereas the control cell lines Hep3B (WT) and pU6-2 express only basal levels of HIF-1α, both AIF1-10 and AIF2-4 express augmented levels of HIF-1α and these could be reduced by prior incubation with the antioxidant NAC. Hypoxic (3% O_2) Hep3B protein sample was used as a control. This experiment was performed three times and the

obtained results had a similar trend. Another antioxidant, the mitochondria-targeted Mitoquinone (MitoQ) showed a similar effect (data not shown).

Interestingly, semi-quantitative RT-PCR analyses revealed that HIF1-α mRNA was unchanged in siAIF cell lines (data not shown), indicating that a post-transcriptional mechanism is responsible for HIF-1α up-regulation in our model cells.

Extending these findings, we used an HIF-1α luciferase reporter construct and showed that HIF1-α protein in siAIF cell lines, AIF1-10 and AIF2-4, is not only stabilized but fully transcriptionally active. The reporter levels in both *AIF*-silenced cell lines were >2-fold higher compared to the pU6-2 control cell line, as shown in Fig.IV.10.E. As a control condition for the HIF-1α lucifearse reporter construct we used hypoxia-treated (4 h, 3% O_2) pU6-2 cells (Fig.IV.10.D). Both experiments were performed three times and similar results were obtained.

Finally, we also studied the hypoxic stabilization of HIF-1α and found that there were no visible differences in the HIF-1α stabilization in the *AIF*-KD cells compared to controls, at least under the hypoxic conditions routinely used (4 h, 3% O_2), (result not shown).

Overall, these data suggest that the increased level of HIF-1α protein in *AIF*-silenced cells was a direct consequence of the increased levels of ROS.

IV.7. AIF expression analysis after H_2O_2 treatment

The fact that lack of AIF in our cellular model leads to increase of ROS levels, points to a role of AIF the maintenance of the cellular redox balance. To further investigate this hypothesis, we wanted to analyze the expression of AIF after H_2O_2 treatment of the control pU6-2 cells. Short-term (up to 45 min), direct addition of H_2O_2 (concentration range 1 μM-1 mM) to cells in a suitable volume of HBSS did not lead to visible alterations in AIF expression, neither when mitochondria-enriched nor when whole-cell extracts were used for WB (data not shown).

However, prolonged (4 h) treatment of pU6-2 cells with H_2O_2 up-regulated the expression of AIF.
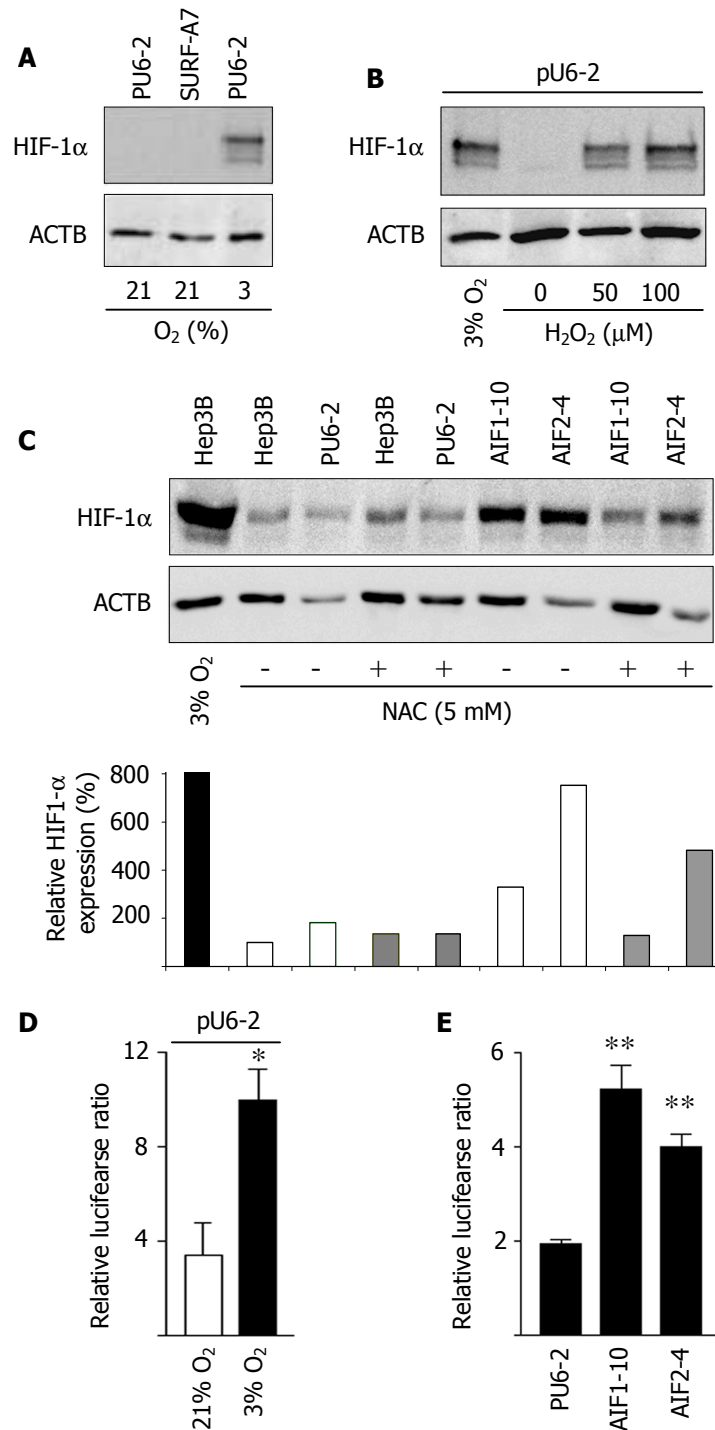
Figure IV.10. HIF-1α expression in stable *AIF*-silenced cell lines. A. Representative WB showing HIF-1α stabilization in pU6-2 under hypoxia (3% O$_2$, 4 h). B. Representative WB of HIF-1α after H$_2$O$_2$ treatment of pU6-2 cells, hypoxia (3% O$_2$, 4 h) was used as a control condition. C. Upper panel: Representative WB of HIF-1α in siAIF and control cell lines with and without NAC treatment, hypoxia (3% O$_2$, 4 h) was used as a control condition; lower panel: densitometry of the previous WB, HIF-1α expression levels normalized to ACTB expression and considering Hep3B control (without NAC) as 100% expression of HIF-1α. D. HRE-luciferase reporter assay to analyze hypoxic HIF-1 transcriptional activity. E. HRE-luciferase reporter assay to analyze steady-state HIF-1 transcriptional activity in our cell lines. For both gene reporter assays, data are represented as relative luciferase ratio (Firefly luciferase activity/ Renilla lucifearse activity), mv±SEM, n=3, *p<0.05, **p<0.005.

This experiment was performed in t-25 flasks containing sub-confluent cultures of pU6-2 cells, in HBSS. We did not use the standard culture medium MEM because some of its components would otherwise rapidly degrade any added peroxide. H_2O_2 was added in boluses every 15 min [Chandel N.S. *et al.*, 2000], to a final concentration of 250 or 500 μM. This protocol enabled us to have a prolonged and relatively stable treatment with H_2O_2. After the treatment, cells were harvested, whole-cell extracts were obtained and WB performed following a standard procedure (see "III. Materials and Methods", chapters III.13.1, III.13.2 and III.13.3). As shown in Fig.IV.11.A, exogenous H_2O_2 addition up-regulates the expression of AIF. As anticipated, HIF-1α expression was also increased, more significantly upon treatment with 250 μM H_2O_2.
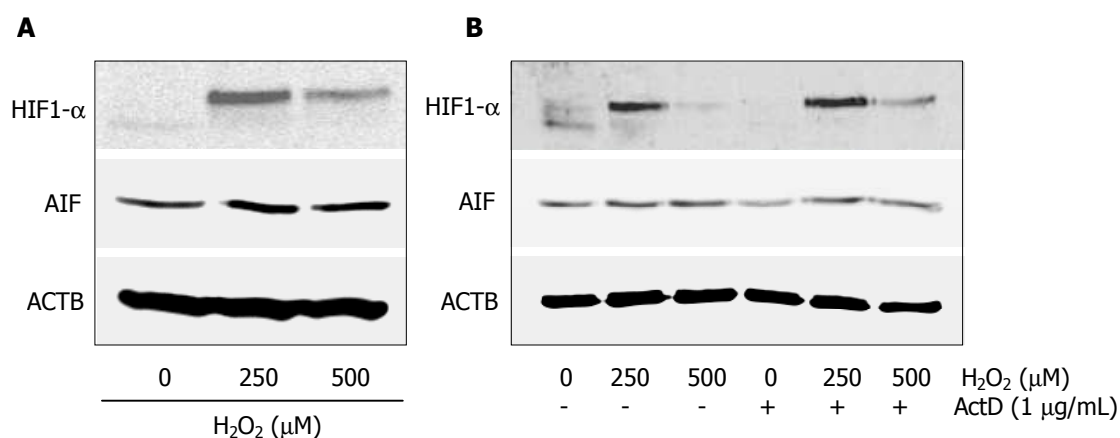
Figure IV.11. AIF expression is increased upon prolonged H_2O_2 treatment. A. Representative WB showing HIF-1α and AIF expression after H_2O_2 treatment (250 and 500 μM in boluses over 4 h). B. Representative WB of HIF-1α and AIF expression after H_2O_2 treatment (250 and 500 μM in boluses over 4 h), with and without ActD pre-treatment (1 μg/mL, 15 min).

Next, we aimed to see whether the observed AIF up-regulation is due to increase in the expression of the *AIF* gene. For this, we pretreated the cells with Actinomycin D (Act D), a general inhibitor of transcription. To this end, we added 1 μg/mL of ActD wad added to the cells 15 min prior to the addition of the first H_2O_2 bolus. As represented in Fig.IV.11.B, ActD-pretreatment of the cells did not impede AIF up-regulation induced by H_2O_2, pointing to a post-transcriptional mechanism responsible of the up-regulation of AIF. Both experiments were performed twice, with a very similar result. It would be interesting to pursue this avenue of research further.

Taken together, these data strongly confirm that AIF is involved in the ROS metabolism of our model cells.

IV.8. NF-κB and Nrf2 expression in stable *AIF*-silenced cell lines

As described in previous chapters, detailed studies showed that the transcription factor HIF-1 is up-regulated in the siAIF cell lines. Next, we assessed two other redox-sensitive transcription factors, namely NF-κB and Nrf2, to determine whether this was a general consequence. Western blot analysis using a specific antibody directed to the p65 subunit of NF-κB, both in whole-cell (Fig.IV.12.A) and nuclear protein extracts (Fig.IV.12.B) of siAIF cell lines, AIF1-10 and AIF2-4, did not reveal any significant differences in the expression levels, compared to the control pU6-2 cells.

However, WB analysis of Nrf2 showed higher levels of this transcription factor in AIF1-10 cells compared to control pU6-2, both in whole-cell extracts (Fig.IV.12.A) and nuclear protein extracts (Fig.IV.12.B). These experiments were performed several times (minimum 4) and similar results were obtained. Moreover, analysis of Nrf2 expression in cytoplasmic versus nuclear extracts revealed that a portion of Nrf2 in AIF1-10 cells was translocated into the nucleus (Fig.IV.12.B).

As a control condition for the Nrf2 expression we used pU6-2 cells treated with H_2O_2 over a prolonged period of time (4 h). The experiment was carried out in an identical manner to the one described in the section IV.7. Briefly, sub-confluent cell cultures of pU6-2 cells were treated with H_2O_2 boluses (250 and 500 μM final concentrations) every 15 min. Then, the cells were collected, whole-cell protein extracts obtained and WB performed. As represented in Fig.IV.12.C, Nrf2 expression in pU6-2 cells is induced by H_2O_2 treatment. This experiment was performed three times with very similar results.

Next, we examined whether the increase of Nrf2 expression in our siAIF cells was due to modifications in the transcription of *NRF2* or its inhibiting binding partner *KEAP1*. Semi-quantitative RT-PCR using RNA obtained of AIF1-10 and AIF2-4 cells and the control cell lines, Hep3B and pU6-2, showed that there were no significant changes in the basal transcription levels of neither *NRF2* nor *KEAP1* (data not shown).

Taken together these data suggest that Nrf2 but not NF-κB is up-regulated in stable siAIF cells and that this increase occurs at the protein level and does not result from augmented *NRF2* transcription.
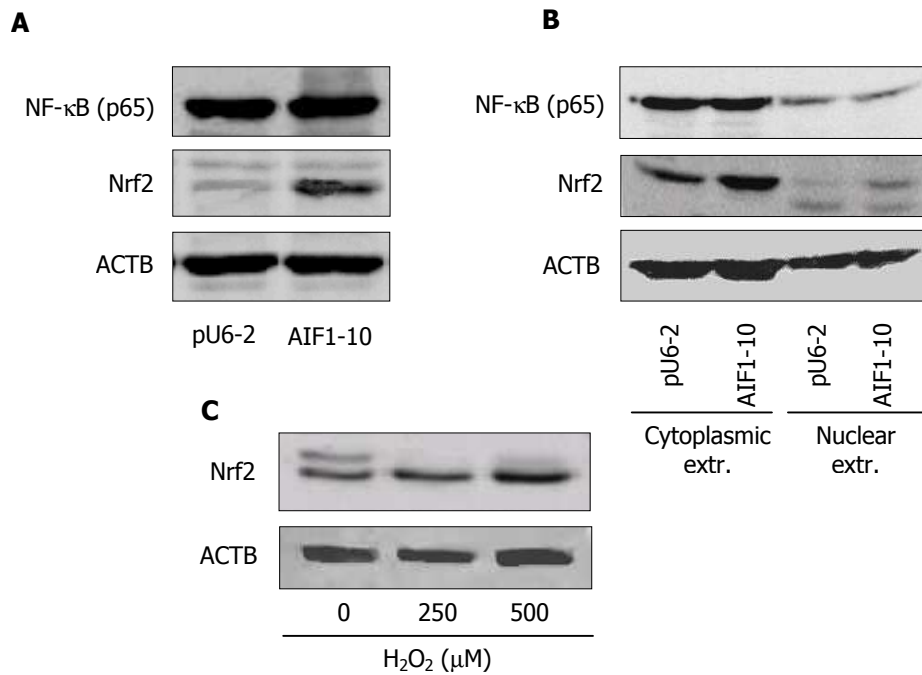
Figure IV.12. WB analysis of NF-κB and Nrf2 expression in pU6-2 and AIF1-10 cells. A. Representative WB showing the basal expression of NF-κB (p65 subunit) and Nrf2 in whole cell extracts of pU6-2 and AIF1-10 cells. B. Representative WB showing the basal expression of NF-κB (p65 subunit) and Nrf2 in nuclear and cytoplasmic extracts of pU6-2 and AIF1-10 cells. C. Representative WB showing Nrf2 expression in whole cell extracts of H_2O_2-treated pU6-2 cells.

IV.9. Analysis of the expression of redox-active enzymes: SOD1, SOD2, CAT and NQO1.

Next, we addressed the question about whether our siAIF cell lines displayed alterations in the expression of redox-related enzymes, such as cytosolic superoxide dismutase (SOD1), mitochondrial superoxide dismutase (SOD2), catalase (CAT) and NAD(P)H: quinone reductase (NQO1). As addressed in the Introduction chapter "I.5.2. Nuclear factor E2-related factor 2 (Nrf2)", *NQO1* is a well-known target gene for the Nrf2 transcription factor. The other enzymes are direct players in the cellular redox-defense machinery, thus they all promised to be interesting subjects to study. Semi-quantitative RT-PCR of *SOD1*, *CAT* and *NQO1*, performed on AIF1-10 and pU6-2 RNA revealed that there were no significant changes in the expression of any of these genes, though there was a slight tendency towards a decrease of *SOD2* expression in AIF1-10, yet without statistical significance. Fig.IV.13.A shows an image of a representative RT-PCR of *SOD1*, *SOD2*, *CAT* and *NQO1* in pU6-2 and AIF1-10 cells where cyclophilin A (*CYPA*) was used as a house-keeping control. The bar chart in Fig. IV.13.B depicts the levels of expression of the genes of interest, represented as a ratio

between the expression in pU6-2 and AIF1-10 cells, previously normalized with the *CYPA* expression (normalized value of 1).

As a complementary approach, and in particular as *SOD2* expression showed to be slightly diminished in AIF1-10 cells, we performed real-time quantitative RT-PCR analysis of *SOD1* and *SOD2* expression in pU6-2 and AIF1-10 cells. The bar chart depicted in Fig.IV.13.C summarizes the data obtained in 4 independent experiments, represented as a relative ratio of the expression (nº of RT-PCR-amplified units) in pU6-2 and AIF1-10. Both *SOD1* and *SOD2* results were previously normalized with the cyclophilin A expression value in each cell line. Again, the pU6-2/AIF1-10 expression ratio seemed to be slightly higher for *SOD2* indicating a lower, though without statistical significance, expression of this gene in AIF1-10 cells.
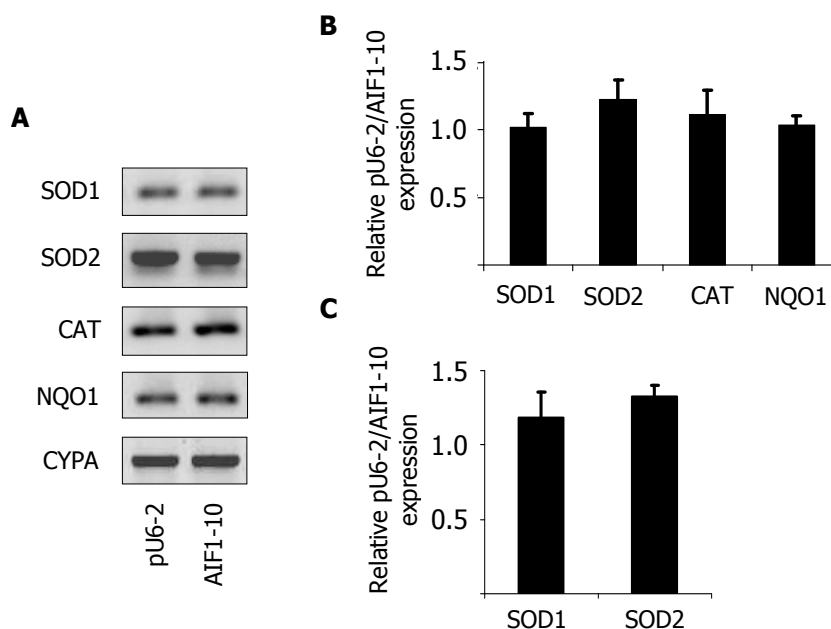
Figure IV.13. RT-PCR analyses of redox-sensitive genes A. Representative result of semi-quantitative RT-PCR for *SOD1*, *SOD2*, *CAT*, *NQO1* in pU6-2 and AIF1-10 mRNA, using cyclophilin A (*CYPA*) as a house-keeping gene. B. Bar chart representing relative pU6-2/AIF1-10 expression in semi-quantitative RT-PCR of *SOD1* (n=8), *SOD2* (n=8), *CAT* (n=6) and *NQO1* (n=7), previously normalized to *CYPA* expression, data represented as mv±SEM, p>0.05. C. Bar chart representing relative pU6-2/AIF1-10 expression in real-time RT-PCR of *SOD1* (n=4) and *SOD2* (n=4), previously normalized to *CYPA* expression, data represented as mv±SEM, p>0.05.

To support the result obtained by RT-PCR studies, we performed WB analysis of the basal SOD2 expression, in whole-cell and mitochondria-enriched extracts. However, we could not detect any changes in the expression of SOD2 in siAIF compared to control cell lines (data not shown), probably due to the technical sensitivity limits.

IV.10. O_2 consumption measurement in intact cells

Next, we addressed the question as to whether the increased ROS levels in siAIF cell lines could participate in causing respiratory dysfunction, a well-known outcome of ETC damage. For this, we measured the steady-state cellular respiration in intact cells by monitoring the O_2 consumption using a Clark-type O_2 electrode. A representative graph of basal O_2 consumption in intact cells of pU6-2, AIF-10 and AIF2-4 is shown in Fig.IV.14.A. These experiments revealed that siAIF cell lines, AIF1-10 and AIF2-4, (1.38 ± 0.030 nmolO_2/min/10^6cells, n=11, P<0.001 and 1.59 ± 0.050, n=6, P<0.05, respectively) had an approximately 35% decrease in the basal O_2 consumption rate, compared to pU6-2 and SURF-A7 control cells (2.2 ± 0.080 nmolO_2/min/10^6cells, n=12 and 2.04 ± 0.060, n=4), as represented in Fig.IV.14.B. We also confirmed that the respiration we were monitoring was mitochondrial by adding a specific inhibitor of OxPhos, 1 mM KCN, directly to the respiration chamber and recording the O_2 consumption subsequently (result not shown).

In order to investigate the implication of the increased ROS output in this respiration defect, we attempted to rescue this phenotype by performing antioxidant pretreatment of the cells in culture. For this, t-75 subconfluent cultures of siAIF cells and control pU6-2 cell lines, maintained in the normal growth medium, were treated with 5 mM NAC or 0.5 μM MitoQ, for 16 h. Then, the cells were detached and counted, using a hemacytometer. We could not detect any visible alterations in the cellular proliferation after the antioxidant treatment (result not shown), neither in the control cell lines, pU6-2 and SURF-A7, nor in the siAIF cell lines. Immediately, 2-3 million cells, suspended in HBSS, were added to the oxygen chamber and the cellular respiration monitored. Interestingly, preculturing with either NAC or MitoQ could reverse the respiratory defect in siAIF cells (Fig.IV.14.C). AIF1-10 steady-state O_2 consumption was recorded as 1.38 ± 0.030 nmolO_2/min/10^6cells, compared to the NAC-pretreated which was 1.98 ± 0.100 and MitoQ-pretreated 2.1 ± 0.110 nmolO_2/min/10^6cells. In the case of AIF2-4 the mean values were as follows: 1.59 ± 0.050 nmolO_2/min/10^6cells for the basal respiration, 2.45 ± 0.050 in NAC-pretreated cells and 1.87 ± 0.700 in MitoQ-pretreated cells. Importantly, neither of these antioxidants had any effect on the basal respiration in pU6-2 cells (basal respiration of 2.2 ± 0.080 nmolO_2/min/10^6cells versus NAC-pretreated respiration of 2.33 ± 0.127 nmolO_2/min/10^6cells and MitoQ-pretreated of 2.26 ± 0.134 (Fig.IV.14.C) or SURF-A7 cells (data not shown).
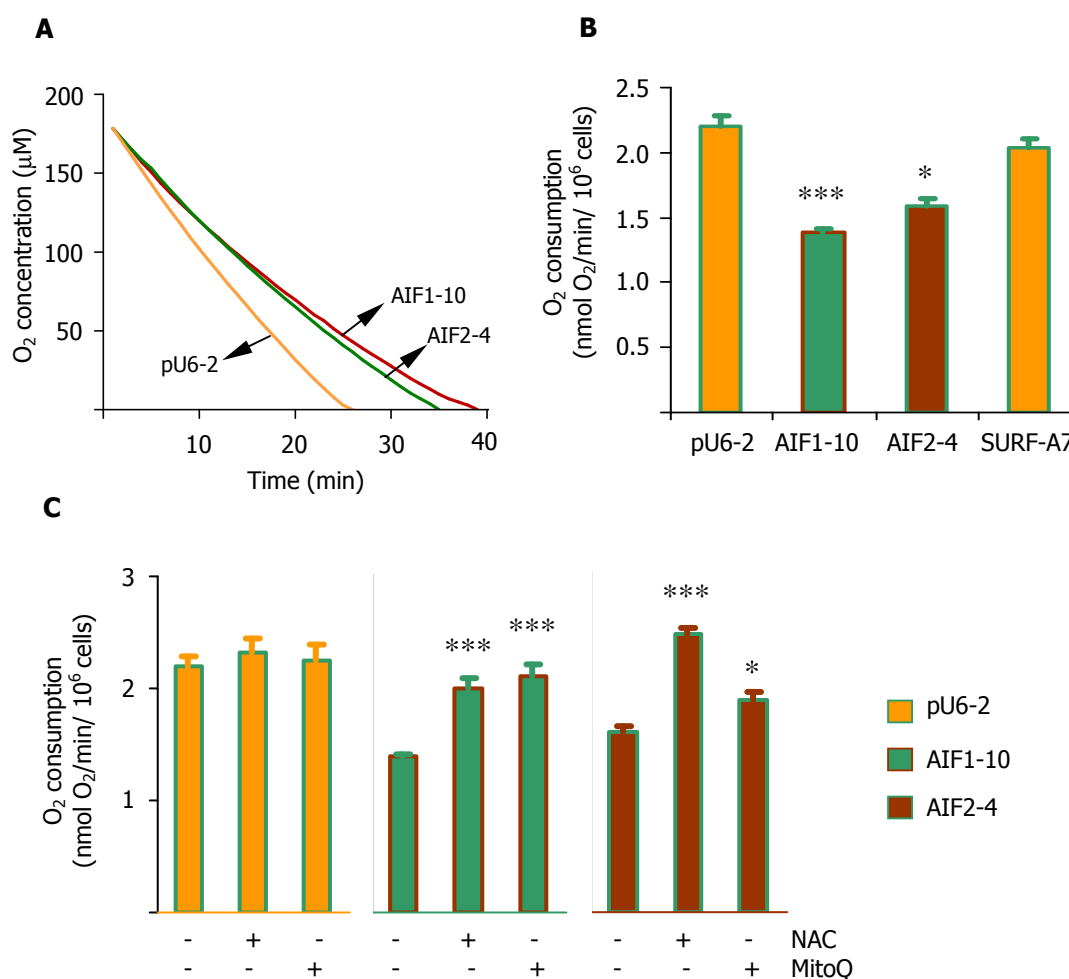
Figure IV.14. Analysis of the O₂ consumption in intact cells. A. Representative graph showing basal O₂ consumption in siAIF cells and control cell lines. B. Bar chart summarizing the results of basal O₂ consumption in pU6-2 (n=12), SURF-A7 (n=4), AIF1-10 (n=11) and AIF2-4 (n=6), data shown as mv±SEM, *p< 0.05, ***p <0.001. C. Bar chart summarizing the results of basal O₂ consumption and O₂ consumption after pretreatment with antioxidants in pU6-2 (n=7), AIF1-10 (n=5) and AIF2-4 (n=2), data shown as mv±SEM, *p< 0.05, ***p <0.001.

IV.11. O₂ consumption measurement in permeabilized cells

As described in the previous chapter, measurement of the cellular O₂ consumption using a Clark-type oxygen electrode revealed a significant decrease in the basal cellular respiration rate in siAIF cells, compared to control cell lines. For a more detailed study of this defect, at the sub-mitochondrial level, we analyzed the O₂-consumption dependent on the ETC complexes individually. This was approached by measuring the cellular respiration in digitonin-permeabilized cells. By addition of specific respiratory substrates, this method allowed us to study the respiration dependent on individual ETC complexes separately. As Complex I is very susceptible to ROS damage, we

hypothesized that this was the most likely candidate for the basal respiration defect in siAIF cells. To assess the respiration dependent on Complex I, Complex I-specific respiratory substrates, malate (0.4 mM) and glutamate (30 mM), were added to the digitonin-permeabilized cell suspension in the calibrated respiration chamber, where basal O_2 consumption had been previously recorded. Next, Complex I-dependent respiration was inhibited by the Complex I-specific inhibitor rotenone (6 μM) and further, the Complex II specific electron donor, succinate (10 mM), was added to the respiration chamber in order to assess Complex II-dependent O_2 consumption. As shown in Fig.V.15.A, both siAIF lines respired poorly on malate and glutamate (about 30% reduction compared to pU6-2). Furthermore, unlike the control (pU6-2) O_2 consumption, which could be inhibited by 90% with addition of rotenone, Complex I-dependent O_2 consumption in siAIF cells was almost insensitive to rotenone. When succinate was added in order to bypass Complex I-dependent respiration, both siAIF lines displayed respiration rates identical to the control cell line (Fig.V.15.A). This finding suggested that only Complex I and not Complex II is affected by *AIF* silencing. The experiment was performed several times and 3-5 determinations of each condition were obtained. Together with succinate, ATP (0.2 mM) was routinely added to the respiration chamber, as this stops the reaction of the competitive inhibitor oxaloacetate on the succinate dehydrogenase.

In addition, we aimed to study whether a pretreatment of siAIF cells with antioxidants could restore their respiration defect at Complex I. For this, the cells were pretreated in the same fashion as described in chapter "IV.10. O_2 consumption measurement in intact cells". We cultured subconfluent t-75 cultures of siAIF cells and the control cell line pU6-2, with 0.5 μM MitoQ for 16 h, maintaining the cells in the normal growth medium. Then we permeabilized the cells and proceeded with the measurement of O_2 consumption as described previously. Of note, the antioxidant pretreatment of siAIF cells could reverse their phenotype of diminished Complex I-dependent respiration without affecting significantly the other respiration parameters (Fig.IV.15.B). In the case of AIF1-10 cells, the mean steady-state value of Complex I-dependent O_2 consumption was 0.59 ± 0.043 nmolO_2/min/10^6 cells and after the antioxidant recovery it reached 2.15 ± 0.191, whereas the same values for AIF2-4 were 0.55 ± 0.040 nmolO_2/min/10^6 cells and 2.05 ± 0.011, respectively. Also, the O_2-consumption of pU6-2 cells was not altered significantly by the antioxidant pretreatment (1.9 ± 0.105 nmolO_2/min/10^6 cells in the control cells versus 2.27 ± 0.090 nmolO_2/min/10^6 in the

MitoQ-pretreated cells). This experiment was repeated three times.
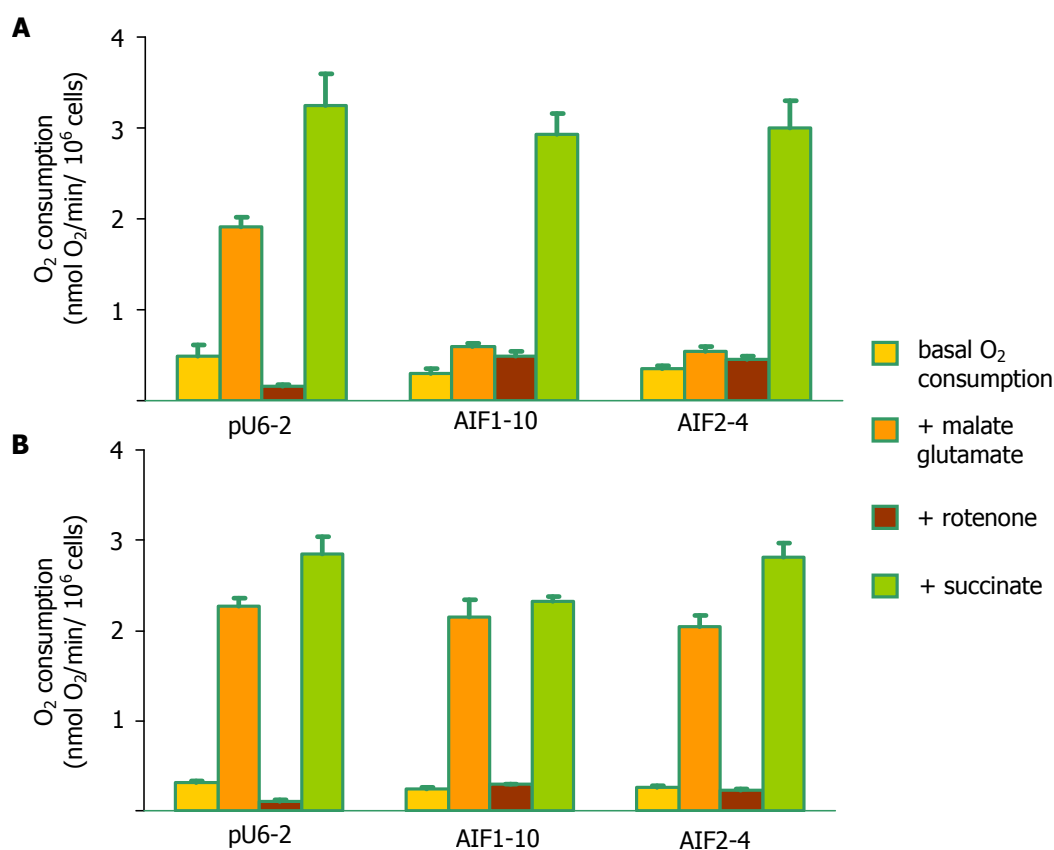
Figure IV.15. Analysis of O$_2$ consumption measurement in digitonin-permeabilized cells. The basal respiration and the respiration rates after addition of malate + glutamate, rotenone and succinate, for the three cell lines: pU6-2, AIF1-10 and AIF2-4 are shown. A. O$_2$ consumption of cells without previous antioxidant treatment, data represented as mv±SEM, n=3-5. B. O$_2$ consumption of cells after previous MitoQ treatment, data represented as mv±SEM, n=3.

IV.12. Analysis of the glycolytic capacity of siAIF cell lines

Having shown that siAIF cells display a significant decrease in the O$_2$ consumption and have a compromised OxPhos, the next parameter we considered to study was the glycolytic capacity of these cells.

The ATP concentration was determined using a bioluminescent assay and the values obtained where normalized to the protein amount in the cell lysates. The measurement of the basal ATP levels in Hep3B, pU6-2 and AIF1-10 cells was repeated five times and no significant differences were registered (Fig.IV.16.A, left panel).

To further investigate the ATP production, we cultured pU6-2 and AIF1-10 cells in

glucose-free MEM for 6 h. Briefly, the cells were counted and seeded in t-25 flasks and allowed to attach. The following day, the culture medium was replaced with either complete MEM or MEM without glucose. After 6 h, the cells were collected and the ATP measurement was performed as described in the chapter "III.6. Measurement of ATP concentration". The experiment was performed twice, with three flasks per cell line analyzed each time. Interestingly, whilst in the control pU6-2 cells, glucose withdrawal from the culture medium provokes a significant increase in the ATP production, there is just a slight increase in AIF1-10 cells, as shown in Fig.IV.16.A, right panel. This result points to the possibility that siAIF cells rely on glycolysis for ATP production and have a decreased capability of ATP production by the OxPhos process, when other substrates, rather then glucose, are used.

Next, we aimed to study the lactate production in siAIF cells versus the control cell line, pU6-2, by employing a spectrophotometric assay which determines the lactate concentration in the extracellular culture medium (i.e. detection of the lactate extrusion). First, we monitored the lactate production in pU6-2 and siAIF cell cultures, maintained under basal conditions. For this, 2×10^4 cells/well were seeded in 6-well plates, in triplicate, in three sets of wells, one set of wells was left in cell culture for 2 days, the second one for 4 days and the last one for 8 days without refreshing the culture medium, in order to allow lactate accumulation in the extracellular medium. Then, lactate concentration was determined and normalized to the number of cells which had proliferated in each well and represented as lactate amount (ng) per 5×10^4 cells. The results obtained in this experiment, repeated 4 times, revealed that there was no significant difference between siAIF cell lines, AIF1-10 and AIF2-4, and the control cell line, pU6-2, in the lactate production over a period of 2 days in culture. However, siAIF cells had released more lactate in the medium in comparison with the control, in prolonged, 4 and 8 days, periods in culture, as shown in Fig.IV.16.B, left panel.

A complementary approach to the lactate release measurement under standard culture conditions (glucose-containing MEM), was the detection of lactate production when cells were cultured in the absence of glucose or in a culture medium where the glucose had been replaced by the same concentration of the non-fermentable sugar, galactose (5.56 mM). The remainder of the components of the culture medium (Complete MEM, see chapter "III.2. Cell culture") were the same.

Here, we seeded pU6-2 and siAIF cells in 6-well plates, at 2×10^4 cells/well, per triplicate and cultured them for 4 days without refreshing the medium, under the conditions indicated above. This experiment was repeated twice and the mean values are represented in Fig.IV.16.B, right panel. While there were no significant differences in the lactate production among the cell lines when the cells were cultured in glucose-containing medium, siAIF cells produced significantly lower amounts of lactate compared to pU6-2 cells, when maintained in glucose-free MEM. Moreover, all cell lines showed a major decrease in lactate production when cultured in the absence of glucose. A similar decrease occurred when cells were cultured in galactose-instead-of-glucose containing MEM, however without significant differences among cell lines (Fig.IV.16.B, right panel).

Next, we studied the glucose up-take rate, knowing that the standard MEM we employed to routinely culture siAIF cells and the control cell lines contain 1 g/L (5.56 mM) glucose. In order to analyze the glucose up-take by the cells in culture, we monitored the decrease of the glucose concentration in the medium, when the cells were cultured. For this, we seeded 4 sets of 1×10^5 cells/well in a 6-well plate, in triplicate and allowed the cells to proliferate freely. Each set of wells was examined at the determined period of time, from day 1 to day 4. The culture medium was collected and glucose concentration was determined. Also, the cells in each well were detached and counted using a hemacytometer. Fig.IV.16.C summarizes the data of 4 individual experiments. The left panel in Fig.IV.16.C describes the mean values of the cellular proliferation rate of pU6-2 and AIF1-10 cells, over a period of 4 days. This cellular proliferation was followed by glucose concentration decrease in the culture medium, which can be seen in Fig.IV.16.C, right panel. Notably, AIF1-10 cells have a significantly lower proliferation rate compared to pU6-2 cells and thus the decrease of the glucose concentration in the culture medium is lower. However, when these data are normalized to the number of cells present in culture, it appears that the average glucose consumption in 4-days culture period is higher in AIF1-10 cell compared to pU6-2.

To complement this study, we performed RT-PCR analysis using mRNA of siAIF and control cell lines, directed to examine the basal expression of glycolytic genes, such as aldolase A (*ALDOA*), facilitated glucose transporter 1 (*GLUT1*) and glyceraldehyde-3-phosphate dehydrogenase (*GAPDH*).
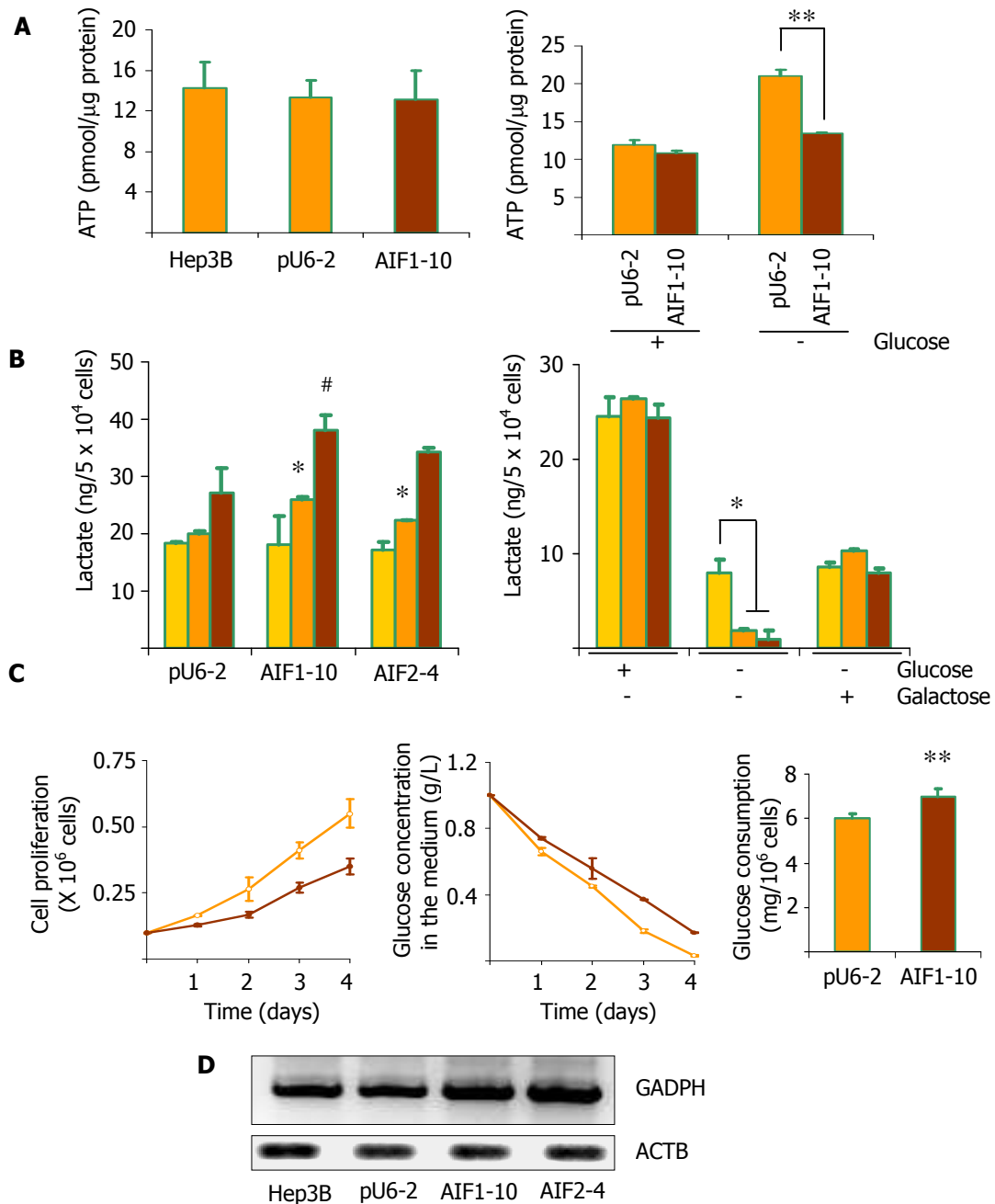
Figure IV.16. Analysis of the glycolytic capacity of siAIF cells versus controls. A. Basal levels of ATP concentration, data represented as mv±SD, n=5, p>0.05 (left panel), ATP concentration in pU6-2 and AIF1-10 cells, growing in medium with and without glucose, data represented as mv±SEM, n=2, **p<0.005 (right panel). B. Left panel: Lactate production in siAIF cell lines compared to control cell line pU6-2, over 2 (yellow bars), 4 (orange bars) and 8 days (brown bars), data represented as mv±SEM, n=4, *p<0.05, #p<0.05 in one-tailed t-test; right panel: lactate production in pU6-2 (yellow bars), AIF1-10 (orange bars) and AIF2-4 cells (brown bars) over 4 days culture in glucose-containing, glucose-free and galactose instead of glucose containing medium, data shown as mv±SEM, n=2, *p<0.05. C. Glucose uptake assay. Left graph: Cell proliferation, right graph: Parallel glucose concentration in the cell culture medium, data represented as mv±SEM, n=4. Bar chart: Average glucose consumption over 4 days in culture, data represented as mv±SEM, n=4, **p<0.005. D. Representative RT-PCR result for *GAPDH* expression in siAIF and control cell lines where β-actin was used as a house-keeping gene.

Whilst there were no significant differences in the expression of the first two genes (result not shown), *GAPDH* expression was significantly increased in AIF-10 and AIF2-4 cells (Fig.IV.16.D). This experiment was performed three times, with similar results.

In summary, all these data suggest that siAIF cells possess a higher glycolytic activity, compared to their control counterparts.

IV.13. Morphology and cell proliferation

As mentioned in previous chapters, we routinely cultured stable siAIF cell lines together with control cell lines, in parallel, over prolonged periods of time (even up to several months). Passaging of the cells was generally carried out once a week, whereas medium was refreshed every 2-3 days. Observation of siAIF cells in comparison with control cell lines, using a standard inverted light microscope, at several cell densities and passage nº, revealed that all cell lines displayed a similar morphology. No significant differences could be appreciated in neither the cell shape or the cell size (Fig.IV.17.C). Nevertheless, siAIF cells clearly proliferated more slowly and displayed a different distribution in the cellular monolayer as a siAIF cell culture of a similar visual cell density as a control one, was very likely to contain a lower number of cells, compared to the control cell line. Unfortunately, we were not able to approach this observation in any experimental way.

Assessment of the cell proliferation of siAIF cells and controls was performed many times and using two different techniques: by direct counting of the cells using a hemacytometer and using the MTT spectrophotometric assay. All these measurements showed that siAIF cells proliferate about 30-40% slower than control cell lines (Fig.IV.17.A and B).

Apart from assessing the cellular proliferation under basal conditions, i.e. the standard conditions of cell culture (Complete MEM which contains 5.56 mM glucose), we also wanted to address the question concerning the cellular proliferation in a medium containing a non-fermentable sugar, such as galactose, instead of glucose. For this purpose, we cultured the cells in complete MEM containing galactose, at 5.56 mM, the same concentration at which glucose is normally present in the standard MEM medium. To this end, siAIF and control cells were seeded in t-25 flasks at a cell density of 0.5

million of cells per flask and allowed to proliferate for 4 days. The culture medium was refreshed at day 2. This experiment was performed several times, the results shown in Fig.IV.17.A comprise the data of two independent experiments. As depicted in Fig.IV.17.A left panel, AIF1-10 and AIF2-4 cells, cultured in glucose-containing medium proliferate slower than their control counterparts (Hep3B and pU6-2). More specifically, at day 4, siAIF cell number was about 65% of the control cell number mean value, with AIF1-10 displaying a larger reduction of the proliferation (57% of the control cell lines mean value), in comparison with AIF2-4 (72% of the control cell lines mean value).
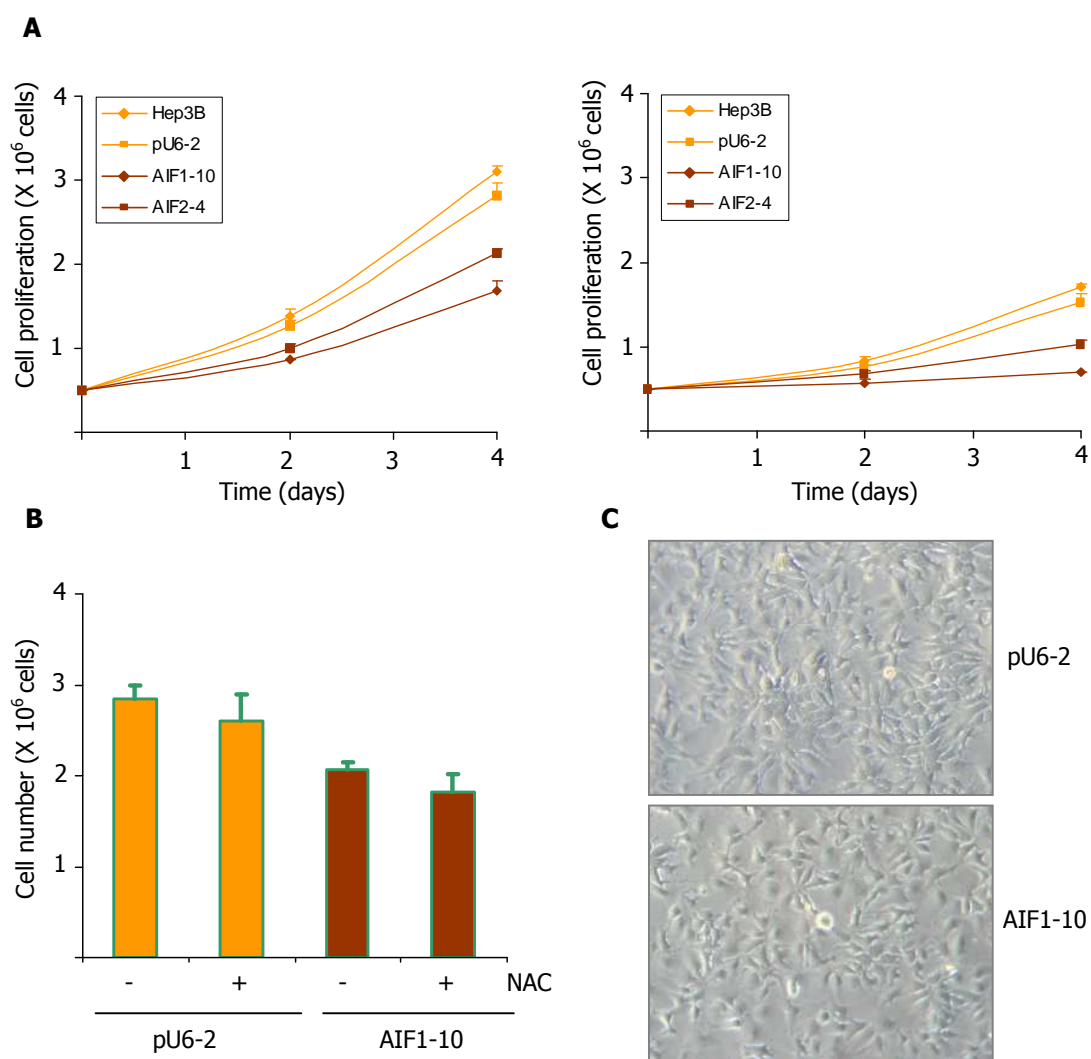
Figure. IV.17. Cell proliferation in siAIF and control cell lines. Control cell lines are depicted in orange, siAIF cell lines in brown. A. Cell proliferation over 4 days in medium containing 5.56 mM glucose (left panel) and 5.56 mM galactose, instead of glucose (right panel), the graphs represent the mean values of two independent experiments, *p<0.05. B. Bar chart representing the cell number after 4 days in culture, with and without 1 mM NAC, data represented as mv±SEM, n=2. C. Representative images of sub-confluent cultures of pU6-2 and AIF1-10.

As to the cell proliferation in galactose-containing culture medium (Fig.IV.17.A, right panel), we observed a significant decrease in the cell number, both at day 2 and at day 4, compared to the culture in glucose-containing medium, for all 4 cell lines tested. However, siAIF cell lines displayed a more severe reduction of the cellular proliferation. Under the presence of galactose as opposed to glucose in the culture medium, AIF1-10 cell number at day 4 was 43% of the control cell lines mean value, whereas, as expected, AIF2-4 showed a lower reduction of 64% of the control cell lines under the same conditions.

In summary, siAIF cells not only proliferate at a lower rate, compared to control cell lines, but they are also more susceptible to replacing the culture medium glucose with galactose. This result is in line with the observation that siAIF cells possess increased glycolytic capacity, shown in chapter IV.12.

Furthermore, we aimed to investigate whether the reduction of the cellular proliferation rate of siAIF cell lines under basal conditions, was a consequence of the incremented ROS levels. For this, we attempted to reverse the siAIF cell proliferation phenotype by culturing the cells in the presence of antioxidants. Both the general antioxidant NAC and the mitochondria-specific antioxidant MitoQ were used, at several concentrations, over a period of one week in culture. To our surprise, neither of the treatments could restore the cellular proliferation rate in siAIF cells. The bar chart in Fig.IV.17.B shows the data of two separate experiments, where 0.5 million cells of pU6-2 and AIF1-10 had been initially seeded in t-25 flasks. The result is represented as the number of cells after 4 days in culture.

IV.14. Analysis of Complex I expression

To further understand the respiration defect of Complex I in siAIF cells, we decided to investigate the expression of its subunits. During this time, a publication in the EMBO J. [Vahsen N. *et al.*, 2004] suggested that two Complex I subunits, CI(39) and CI(20) had a diminished expression when *AIF* was silenced. We thus studied these two subunits by WB in whole-cell and mitochondria-enriched extracts, using specific antibodies and found that the steady-state levels of both these subunits were also reduced in siAIF cells (Fig.IV.18). These experiments were performed several times (at least 3), using cells with different passage numbers.

Next, we attempted to reverse the Complex I expression defect by antioxidant treatment. For this, pU6-2 and AIF1-10 cells were treated with 5 mM NAC or 0.5 μM MitoQ for 16 h prior to cell harvesting and protein extraction. These were the same conditions, as those successfully used to reverse the respiration defect in siAIF cells (see chapter "IV.10. O_2 consumption measurement in intact cells"). Also, whole-cell extracts were obtained and WB performed following the standard protocol. As, demonstrated in Fig.IV.19, neither MitoQ nor NAC treatment could reverse the Complex I expression phenotype. This experiment was repeated, using higher concentrations of the antioxidants, and longer time of exposure (24 h), but none of the attempts resulted in recovery of Complex I subunits expression (data not shown).
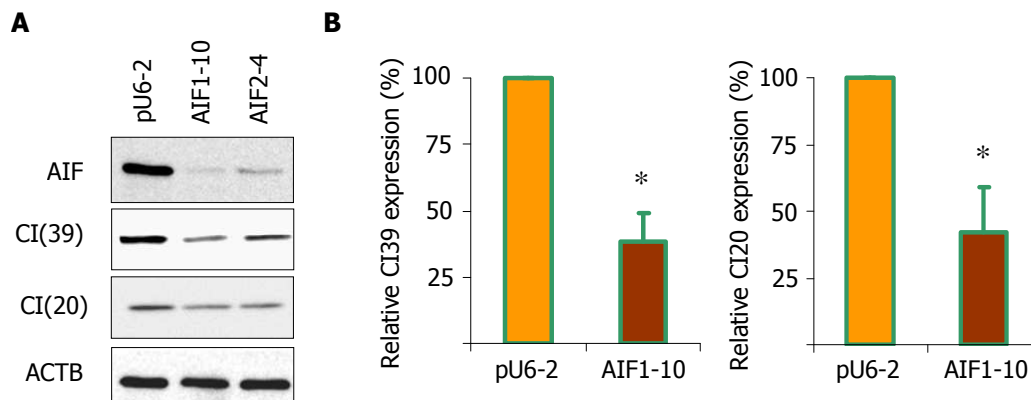
Figure IV.18. WB analysis of Complex I 39 and 20 kDa subunits. A. Representative WB using whole-cell extracts of pU6-2 and two siAIF cell lines, AIF1-10 and AIF2-4, showing AIF, CI(39), CI(20) and ACTB expression. B. A summary of WB data, expressed as relative CI(39), left graph, and CI(20) expression, right graph, in AIF1-10 cells compared to pU6-2 (pU6-2 expression was normalized to 100% in each experiment), results shown as mv±SEM, n=5, for CI(39), and n=3, for CI(20), *p<0.05.
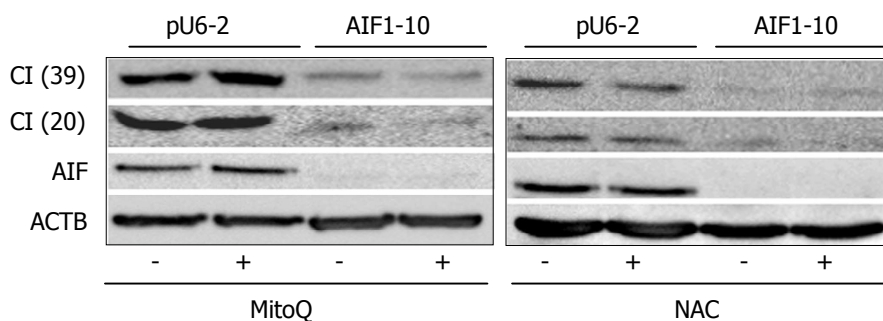
Figure IV.19. Analysis of Complex I 39 and 20 kDa subunits expression after an antioxidant treatment. Representative WB using whole-cell extracts of pU6-2 and AIF1-10, showing AIF, CI(39), CI(20) and ACTB.

Having shown that *AIF* silencing compromises Complex I protein expression and thus alters the mitochondrial respiration, we wanted to broaden this finding by analysis of

the expression levels of other proteins, also members of the mitochondrial ETC. Using whole-cell and mitochondria-enriched protein extracts to perform WB analysis, we assessed the expression of Complex II subunit B (SDHB), Complex IV subunits 1 and 2 (COXI and COXII) and none of these proteins showed any differences in the expression levels (results not shown).

Moreover, we analyzed by WB the basal expression levels of other mitochondrial proteins, not involved in the ETC, such as survivin and could not detect any significant differences between siAIF and control cells either (result not shown).

IV.15. Analysis of the siAIF phenotype in mouse ES cell lines

As a further support for our studies, we wished to assess the siAIF phenotype in a different cell type model and see if we could verify the results obtained in our hepatoma cell line. We, thus used two mouse ES lines: AIF-KO line and the control WT line, derived from the parental mouse ES line E14K by homologous recombination technology in the laboratory of Dr. Josef Penninger. The AIF KO cell line was generated using a targeting vector that deleted exon 3 of the murine *Aif* gene [Joza N. *et al.*, 2001; Vahsen N. *et al.*, 2004]. We cultured these lines routinely and harvested cells of different passage nº to assess the levels of AIF. The AIF-KO cell line, however, expressed some residual levels of AIF, shown both by WB, in whole-cell and mitochondria-enriched extracts, and by RT-PCR analysis. Fig.IV.20.A shows a representative RT-PCR with mRNA obtained of WT and AIF-KO cells, where cyclophilin A (*CYCA*) was used as a house-keeping control, whereas Fig.IV.20.B is a representative WB using whole-cell protein extracts. The bar chart presented in Fig.IV.20.C summarizes the data of AIF expression levels in whole-cell extracts of AIF1-10 and pU6-2 cell line and the ES cell lines, WT and AIF-KO, obtained in 4 independent WB experiments using cells of different passage numbers. In each separate experiment, the AIF expression level was normalized with the house-keeping gene β-actin (ACTB) expression. The AIF levels in the control cell lines, pU6-2 and WT, were considered as 100% AIF expression and then compared to AIF1-10 and AIF-KO expression, respectively. Of note, AIF expression in AIF1-10 was 10.81±2.73% compared to pU6-2 and AIF expression in AIF-KO was 6.86±3.75%, compared to ES WT line.

In summary, AIF-KO displays similar reduction of AIF protein expression compared to

AIF1-10 cell line.
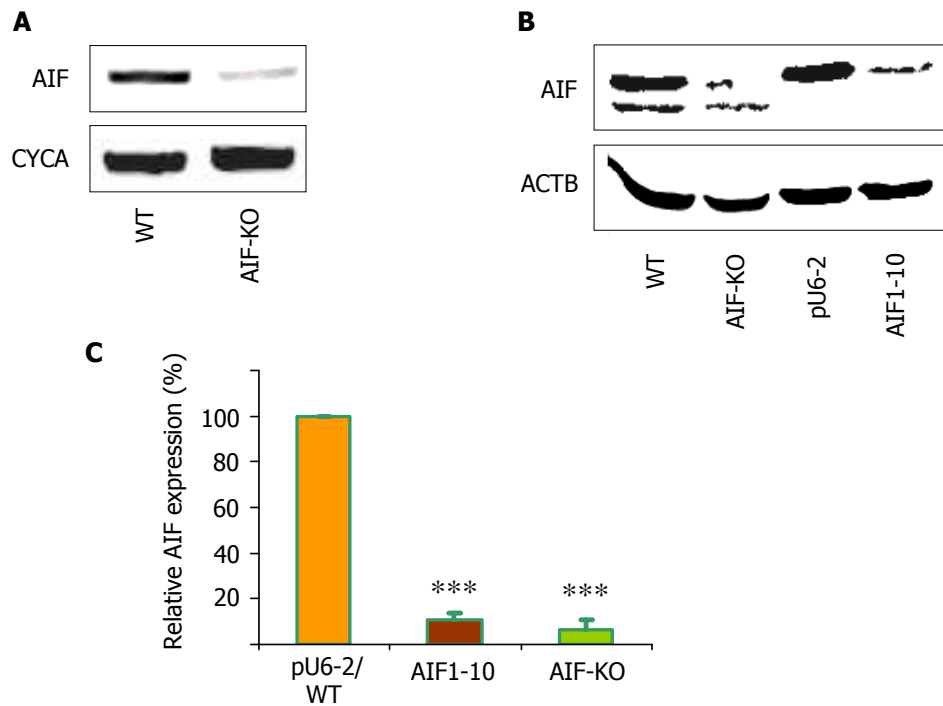
Figure IV.20. Analysis of AIF expression in mouse ES cell lines, AIF-KO and the control WT cell line. A. Representative RT-PCR result of AIF expression in AIF-KO and the WT cells. B. Representative WB result of AIF expression in ES cell lines versus Hep3B cell lines. C. Summary of the quantification of WB results showing relative AIF expression, mv± SEM, n=4, ***p<0.001.

Once we had quantified the expression levels of AIF in the mouse ES cell lines, we performed several experiments in order to characterize the phenotype. More specifically, we assessed the cellular proliferation of AIF-KO versus WT cells using the MTT assay and this was done in parallel with the cellular proliferation assessment of Hep3B cell lines, AIF1-10 and pU6-2. In both groups, cells were plated the day before the experiment in 96-well plates in complete culture medium and allowed to proliferate freely. The MTT assay was performed and absorbance recorded at three time points, as represented in the graphs in Fig.IV.21.A. The left panel describes the cellular proliferation in ES cells where AIF-KO cells (brown trace) display a significantly lower proliferation compared to the control cell line WT (orange trace). This reduction is slightly lower in comparison with the one presented by AIF1-10 cells (brown trace, right panel) versus their control cell line pU6-2 (orange trace, right panel). In detail, at day 3, AIF1-10 cell number was 73.24±4% of the control cell line pU6-2 mean value, whereas AIF-KO showed a lower reduction of the proliferation (80.71±3.65% of the control WT cell line mean value).

Next, we assessed the O_2 consumption in intact ES cells using Clark-type O_2-electrode. The protocol was the same as the one used in pU6-2 and siAIF cells measurements (see "IV.10. O_2 consumption measurement in intact cells"). As expected, we found that AIF-KO cells have a lower O_2 consumption rate, compared to the control WT cells, as shown in Fig.IV.21.B. The mean value of O_2 consumption in AIF-KO cells, of three separate experiments was 0.73 ± 0.09 nmolO_2/min/10^6cells, which compared to the rate of the control WT cells (1.02 ± 0.08 nmolO_2/min/10^6cells) results in some 28% reduction, similar to that displayed by the stable siAIF cells in Hep3B background used previously.
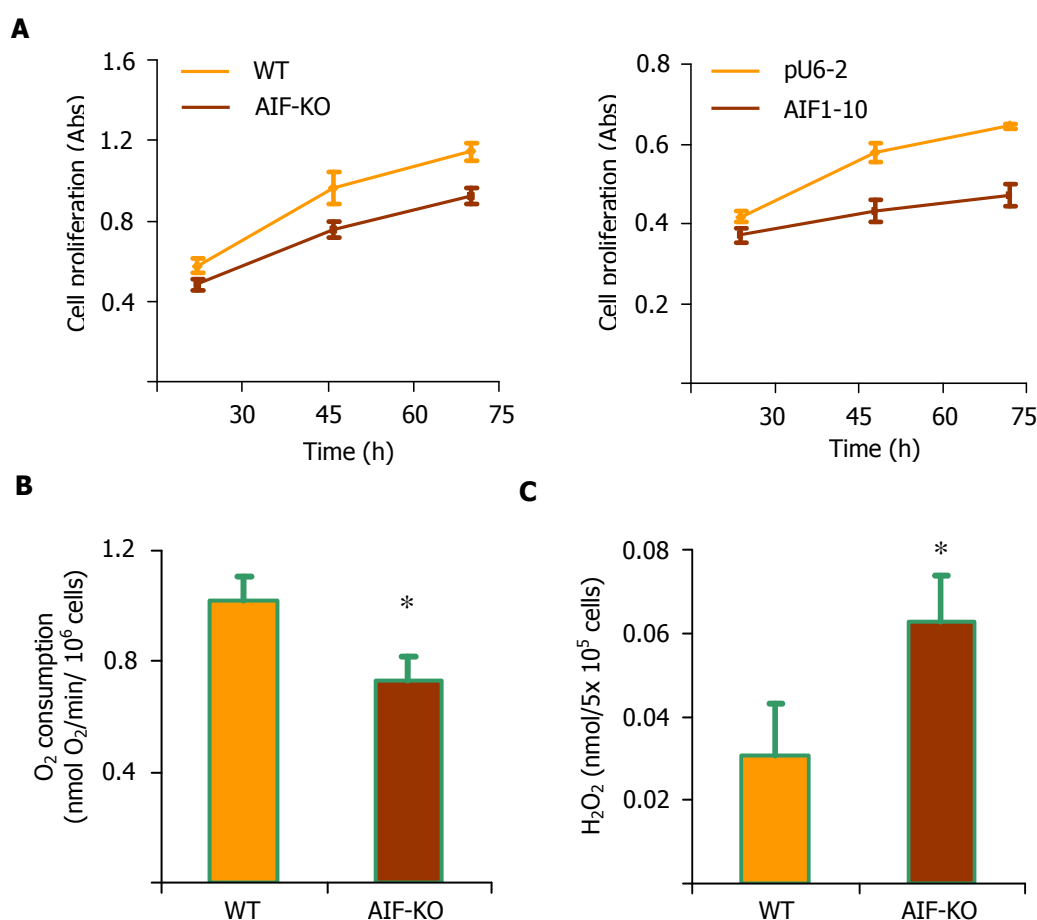
Figure IV.21. Analysis of the phenotypic characteristics of the mouse ES cell lines, AIF-KO and the control WT line. A. Cell proliferation of AIF-KO and WT cells (left panel), and AIF1-10 and pU6-2 cells (right panel), results represented as mv±SEM, n=6. B. O_2 consumption in AIF-KO and WT cells, results shown as mv±SEM, n=3, *p<0.05, analyzed by one-tailed student t-test. C. H_2O_2 levels in AIF-KO compared to control WT cell line, results are represented as mv±SEM, n=5, *p<0.05, analyzed by one-tailed student t-test.

Another parameter we considered important to analyze in the ES cell lines was the ROS level (Fig.IV.21.C). This was also performed in a very similar way as the

experiments carried out previously, with stable siAIF cells and controls (see chapter "IV.5.1. H_2O_2 measurement using the Amplex red kit"). Here, we observed higher levels of H_2O_2 in AIF-KO (0.063±0.009 nmolH_2O_2/5x10^{5}cells) versus WT cells (0.031±0.011 nmolH_2O_2/5x10^{5}cells), which is in accordance with the results shown previously, obtained with stable siAIF cells and controls in Hep3B background.

Taken together, these data suggest that the stable silencing of *AIF* in Hep3B cells leads to a general and not an isolated phenotype, as it can be observed in other cellular models where AIF expression has been nearly abolished, such as a specific AIF-KO ES cell line.

IV.16. Analysis of the relationship between Trx and AIF

IV.16.1. Basal Trx1 and Trx2 expression in siAIF cells

Silencing of *AIF* in our cellular model is accompanied by a significant increase in the ROS levels as shown in previous chapters. In order to broaden the knowledge of the mechanism of this increase, we decided to study the expression of several redox-active proteins and redox-sensitive transcription factors, some of which were shown to be modified (see chapters IV.6, IV.8 and IV.9). Knowing this, we also decided to analyze the expression of thioredoxins, a group of important redox-active enzymes involved in the cellular redox signaling and ROS scavenging. We assessed the steady-state levels of expression of both Trx1 (cytosolic form) and Trx2 (mitochondria-localized form) by performing WB analysis on whole-cell and mitochondria-enriched protein extracts of stable siAIF cell line and controls. These studies suggested that Trx1 expression was not significantly modified in siAIF cells whilst Trx2 levels were largely diminished, as shown in Fig.IV.22.A and B. The panel A shows a representative WB performed on whole-cell extracts of pU6-2 and two siAIF cell lines: AIF1-10 and AIF2-4. Fig.IV.22.B summarizes the densitometry data of several separate WB experiments which suggest about 55% reduction of Trx2 expression in AIF1-10 cells and about 70% in AIF2-4 cells i.e. remaining 45% and 30% of the expression, respectively, compared to Trx2 expression in the control pU6-2 cell line, which was normalized to 100%. Importantly, reduction in the protein levels of Trx2 is a constant phenomenon, visible in both stable siAIF cell lines and using cell cultures with different passage numbers, and is not modified by their prolonged culturing.

Next, we aimed to study whether the decrease in Trx2 protein levels was a real consequence of *AIF* silencing and not an artifact resulting from prolonged culturing of the stable siAIF cells. To this end, we transfected t-25 flask cultures of Hep3B cells with pBS U6/PolIII/siAIF1 and pBS U6/PolIII/siGFP (control silencing cassette), and 72 h later looked at AIF and Trx2 protein levels in whole-cell extracts by standard WB. This experiment was performed three times, with a similar result. As shown in Fig.IV.22.C, transient silencing of *AIF* in Hep3B cells is accompanied by a reduction of Trx2 levels. Thus, we concluded that the decrease in Trx2 protein we observed in stable siAIF cell lines is not an artifact due to prolonged culturing of these cells.

To examine more closely the consequences of the decreased Trx2 expression in siAIF cells, we attempted to reverse this effect with antioxidant treatment of the cells in culture and thus determine whether the increased ROS levels in siAIF cells are related to the reduction of Trx2 expression. In more detail, we pretreated pU6-2 and AIF1-10 cells with 0.5 μM MitoQ or 2.5 mM NAC over 16 h and harvested the cells to obtain whole-cell protein extracts. Later, WB analysis was performed and Trx2 expression assessed. These experiments were carried out several times and the results suggested that neither MitoQ nor NAC treatment could restore the Trx2 expression levels in AIF1-10 cells (data not shown).

IV.16.2. Analysis of the redox state of Trx2

Having seen that Trx2 expression was significantly reduced in siAIF cells, we next wished to study its redox state. Using the specific thiol-binding compound AMS (see "III. Materials and methods", section "III.13.6. Analysis of the redox state of Trx2"), we were able to assess the *in vivo* redox state of Trx2. These experiments revealed that Trx2 present in AIF1-10 cells and theTrx2 expressed in the control pU6-2 cells were in the same redox state (seen as an absence of size shift in the Trx2 specific band on the WB). This assay was performed three times and a representative result is shown in Fig.IV.22.D (lanes 1 and 2 show pU6-2 and AIF1-10 protein samples without treatment with AMS, whereas lanes 3 and 4 show AMS-treated extracts). As a control condition we used H_2O_2 treatment, a stimulus known to modify the redox state of redox-active proteins, such as Trx2. For this, t-25 flasks of pU6-2 cells were treated with 1 mM H_2O_2 in HBSS for 30 min. Then, the cells were harvested and processed for Trx2 redox state analysis. As shown in Fig.IV.22.E, treatment of pU6-2 cells with H_2O_2

provoked oxidation of Trx2, seen as a shift in the molecular size of the Trx2 band in the WB (lane 3 and 4). This experiment was repeated three times with a similar result.
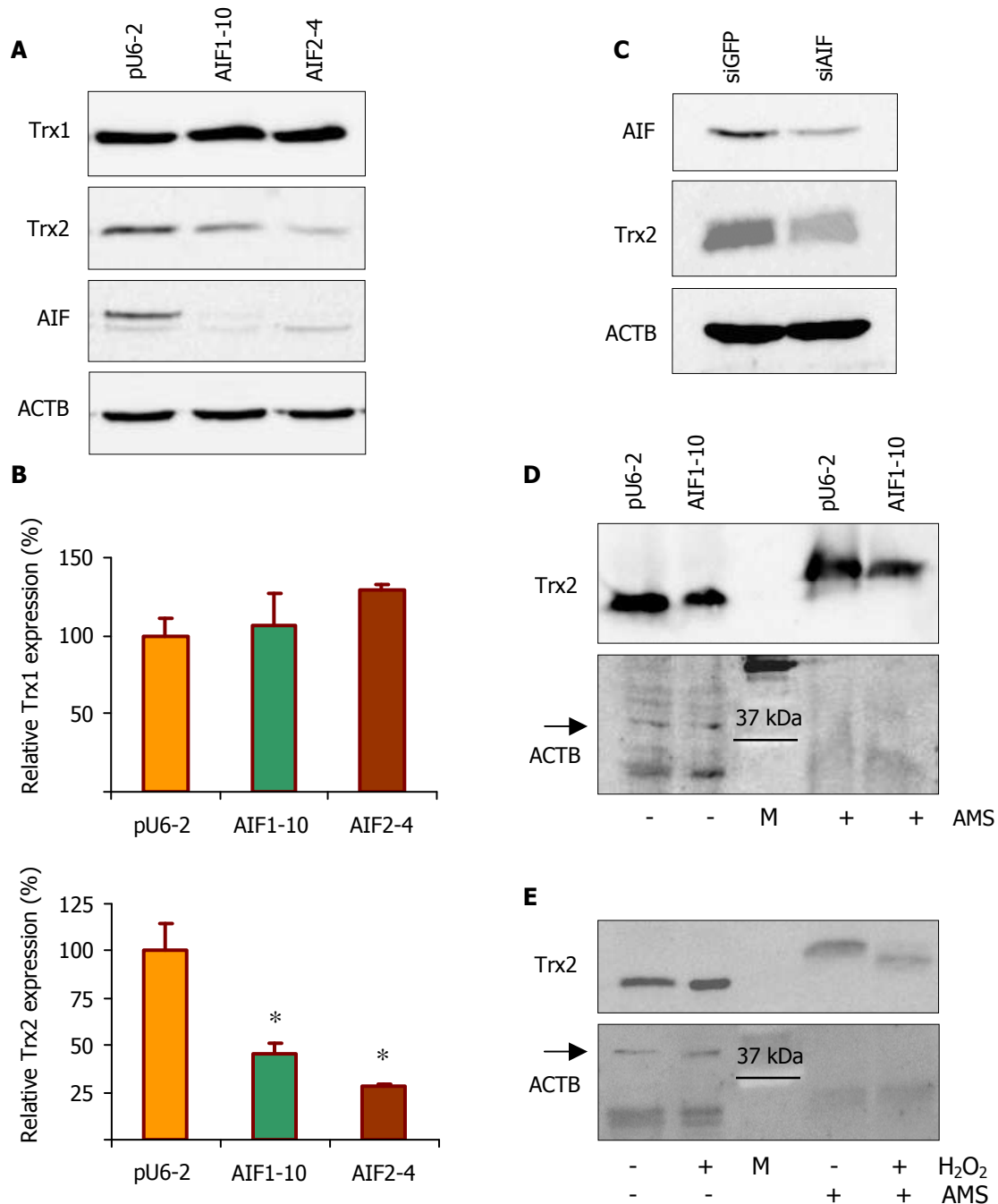
Figure IV.22. Trx expression analysis in siAIF cells and the control pU6-2 cell line. A. Representative WB showing Trx1 and Trx2 expression in siAIF cells and control pU6-2 cells. B. Quantification of WB results for Trx1 expression in pU6-2 (n=5), AIF1-10 (n=4) and AIF2-4 (n=2) results shown as mv±SEM, p>0.05; and Trx2 expression in pU6-2 (n=6), AIF1-10 (n=4) and AIF1-10 (n=2), results shown as mv±SEM, *p<0.05. C. Representative WB showing that transient *AIF* silencing in Hep3B cells also leads to decrease in Trx2 expression. D. Analysis of the *in vivo* redox state of Trx2 in pU6-2 and AIF1-10 cells-a representative WB. E. Analysis of the *in vivo* redox state of Trx2 in pU6-2 cells after H$_2$O$_2$ treatment-a representative WB.

IV.16.3. Trx1 and Trx2 overexpression experiments

In order to further examine the relationship between thioredoxins and AIF we decided to overexpress Trx1 and Trx2 in our cellular model. For this, we generated several vectors, as described in detail in chapter "III.3.2. Protein overexpression plasmids". We made a single construct to overexpress Trx1, called pcDNA3/Trx1 which contained full length, wild type Trx1 cDNA whereas four Trx2-expressing vectors were generated, namely pcDNA/Trx2 expressing the entire WT human Trx2, pcDNA/Trx2-F expressing a Flag-tagged human Trx2, as well as pcDNA3/Trx2Δ, expressing a truncated form of Trx2 which lacks the putative MLS (aa 1-60) and pcDNA3/Trx2Δ-F, the truncated form of Trx2 tagged with Flag (a C-terminal 11 aa tag). These four constructs are schematically depicted in Fig.IV.23.C.

Prior to the experiments of Trx2 overexpression in siAIF cells and controls, we aimed to assess the amount and localization of the overexpressed AIF in our cellular model. This was of particular importance, as we wanted to ensure that the overexpressed Trx2 was truly targeted to the mitochondrion and could thus have a more physiological effect. While Trx2 was expected to accumulate in the mitochondrion after transfection of the cells with the corresponding plasmid, the deleted form of Trx2, Trx2Δ was not expected to be directed to the mitochondria and would accumulate in the cytosol as a result of the absence of the MLS.

To address the question of the localization of the overexpressed Trx2, we developed 2 different experimental approaches. In the fist approach, t-25 flasks of Hep3B cells were transiently transfected with pcDNA3/Trx2-F and pcDNA3/Trx2Δ-F as described in chapter "III.2.3. Transfection experiments". Then, 72 h after the transfection, the cells were harvested and mitochondria-enriched protein extracts obtained. Next, we performed WB analysis, which showed that the bulk of the overexpressed Trx2 was localized in the mitochondrial fraction as opposed to Trx2Δ. The overexpressed proteins were tagged with Flag and thus membranes were probed with anti-Flag antibody, in order to distinguish between the endogenous and the overexpressed Trx2. Tubulin and Porin were analyzed as house-keeping genes to verify protein loading and the purity of the cytosolic and mitochondria-enriched fractions. This experiment was performed twice with the same result. A representative WB is shown in Fig.IV.23.A.

In the second approach, the overexpressed Trx2 was labeled by immunofluorescence and visualized by confocal microscopy. For these analyses, we employed 24-well plates of HeLa cell cultures, which were transiently transfected with pcDNA3/Trx2-F and pcDNA3/Trx2Δ-F. Later, 27 h after the transfection the cells were fixed on the coverslip glasses and incubated with anti-Flag antibody followed by incubation with secondary FITC-conjugated antibody. In order to visualize mitochondria, we used the fluorochrome Mitotracker Red. As expected, in the HeLa cells transfected with pcDNA3/Trx2-F, the red fluorescence of Mitotracker Red co-localized with Flag (fluorescence in green), indicating that Trx2 was targeted to the mitochondria (Fig. IV.23.B). This co-localization was not visible in the HeLa cells transfected with pcDNA3/Trx2Δ-F, suggesting that Trx2Δ-F was not in the mitochondria but distributed in the cytosolic compartment. This experiment was performed twice with a very similar result.

Having shown the mitochondrial localization of overexpressed Trx2, next we wanted to study if Trx2 and Trx1 overexpression could reverse some of the parameters altered in siAIF cells. More in detail, we aimed to analyze the expression of Complex I 39 and 20 kDa subunits, which, as described in previous chapters, is diminished in siAIF cells. Also, we aimed to look at the normoxic HIF-1α expression levels, which, we showed, are increased in siAIF cells. To this end, t-25 flasks of AIF1-10 and pU6-2 cells were transfected with pcDNA3/Trx1, pcDNA3/Trx2 and control pcDNA3 empty vector. Then, 72 h later, the cells were harvested and whole-cell or mitochondria enriched protein extracts were obtained. Standard WB analyses were performed to examine Complex I subunits and HIF-1α expression. Also, the levels of Trx1, Trx2 and house-keeping protein β-actin were assessed. As shown in Fig.IV.24.A, Complex I subunits expression levels, in whole-cell protein extracts, were not reversed after transient Trx1 or Trx2 overexpression in AIF1-10 cells. These experiments were performed several times (not less than four) and similar results were obtained.

However, when we examined normoxic HIF-1α stabilization in whole-cell protein extracts of AIF1-10 cells by WB, interestingly we observed that it was partially restored to control levels after both Trx1 and Trx2 overexpression. Of note, Trx2 overexpression was much more effective and could almost completely reverse the normoxic HIF-1α phenotype in AIF1-10 cells. This result was recorded in three independent experiments and representative WB images are shown in Fig.IV.24.A. We also

overexpressed the deleted MLS-lacking form of Trx2, Trx2Δ, but this, neither could restore Complex I subunits or HIF-1α expression to the wild type levels detected by WB in whole-cell extracts (results not shown).
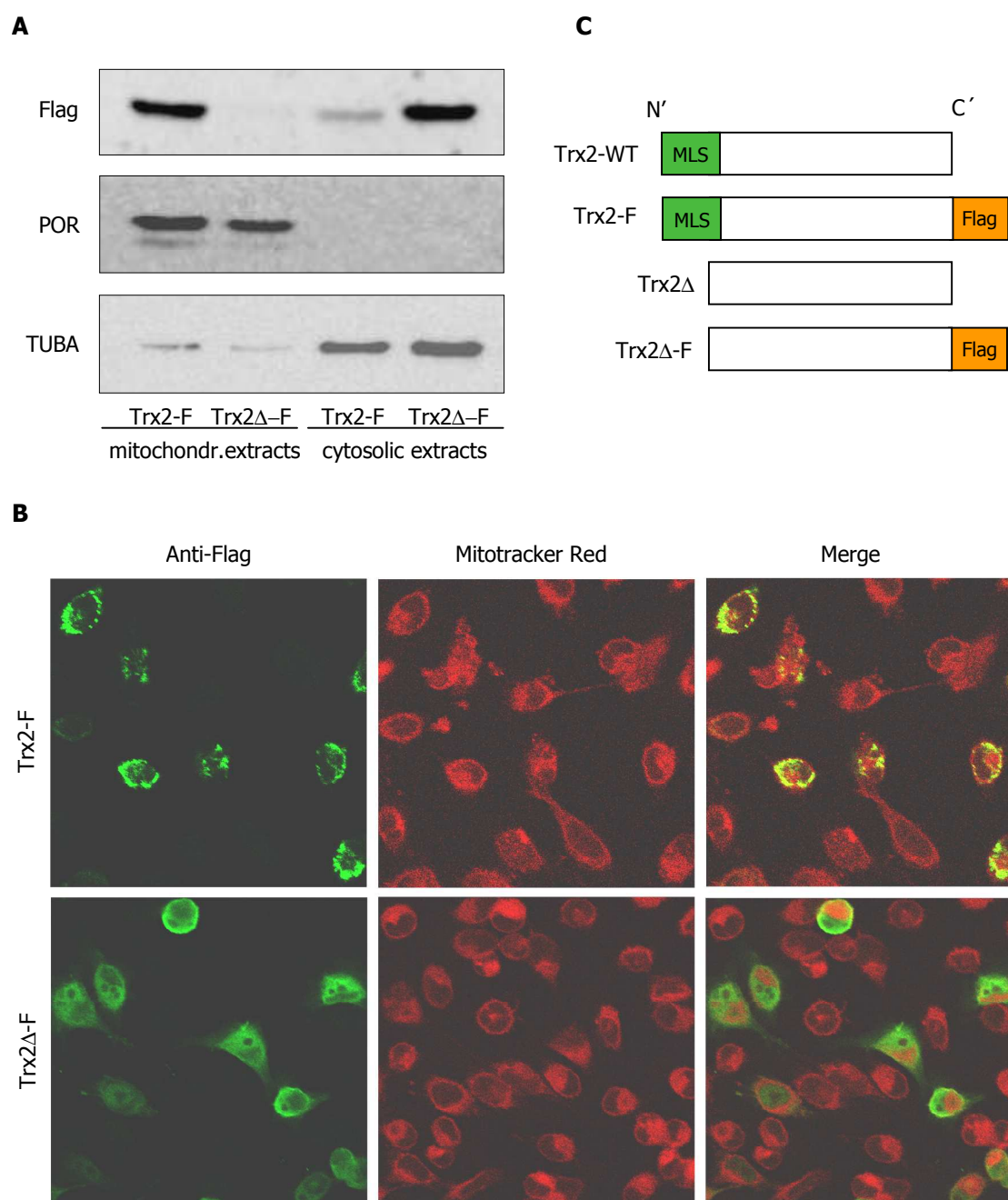
Figure IV.23. Overexpressed Trx2 but not Trx2Δ is targeted to mitochondria. A. Representative WB showing Trx2 expression in the mitochondria-enriched and cytosolic protein fractions of Hep3B cells were Trx2-F and Trx2Δ-F have been transiently overexpressed. B. Representative confocal immunofluorescence microscopy images of HeLa cells, transfected with pcDNA3/Trx2-F and pcDNA3/Trx2Δ-F, marked with Mitotracker Red and Flag fluorescence. C. Schematic representation of Trx2-WT (contains MLS, aa 1-60), the truncated form Trx2Δ which lacks the MLS and the corresponding Flag-tagged proteins (Trx2-F and Trx2Δ-F), not to scale.

We also wanted to see if Trx2 overexpression in AIF1-10 cells could reverse the respiration defect these cells present (see chapter "IV.10. O_2 consumption measurement in intact cells"). For this, t-75 flasks of pU6-2 and AIF1-10 cultures were transfected with pcDNA3 empty vector or pcDNA3/Trx2, using LipofectAMINE^{TM} 2000 as described previously. Then, 72 h after the transfection, the cells were detached using Trypsin-EDTA and counted with a hemacytometer. Immediately, 2-3 million cells were suspended in HBSS and taken to the O_2 chamber in the previously calibrated Clark-type oxygen electrode and O_2 consumption was recorded. Another portion of the cellular suspension was immediately centrifuged and the cellular pellet frozen for WB. This analysis was later carried out in order to assess the Trx2 expression levels at the time point when O_2 consumption was monitored and verify the efficacy of the Trx2 overexpression.

The graph represented in Fig.IV.24.B summarizes the data obtained in four independent experiments, suggesting that Trx2 overexpression does not modify basal O_2 consumption in the control pU6-2 cells (2.42±0.280 nmolO_2/min/10^{6}cells in Trx2-overexpressed pU6-2 cells versus 2.40±0.121 nmolO_2/min/10^{6}cells recorded in empty vector-transfected pU6-2 cells), whereas it can recover the respiration defect present in AIF1-10 cells (1.53±0.101 nmolO_2/min/10^{6}cells in Trx2-overexpressed AIF1-10 cells versus 1.86±0.223 nmolO_2/min/10^{6}cells recorded in empty vector-transfected pU6-2 cells).

However, the recovery we registered was only partial and not statistically significant when all the data together were analyzed with the t-test. Although the levels of overexpressed Trx2 seemed quite high in these experiments, as analyzed by WB in whole-cell and mitochondria-enriched protein extracts (a representative result of a WB using whole-cell protein extracts is shown in Fig.IV.24.C), we believe that it might have been not enough to fully reverse the respiration phenotype in siAIF cells. Alternatively, Trx2 expression and rescue of the respiration are independent.

In summary, both Trx1 and Trx2 overexpression can restore the normal normoxic expression levels of HIF-1α in siAIF cells but neither of these redox-active proteins is able to recover Complex I subunits expression. Also Trx2 overexpression can partially reverse the O_2 consumption defect of siAIF cells detected in intact-cell respiration experiments.
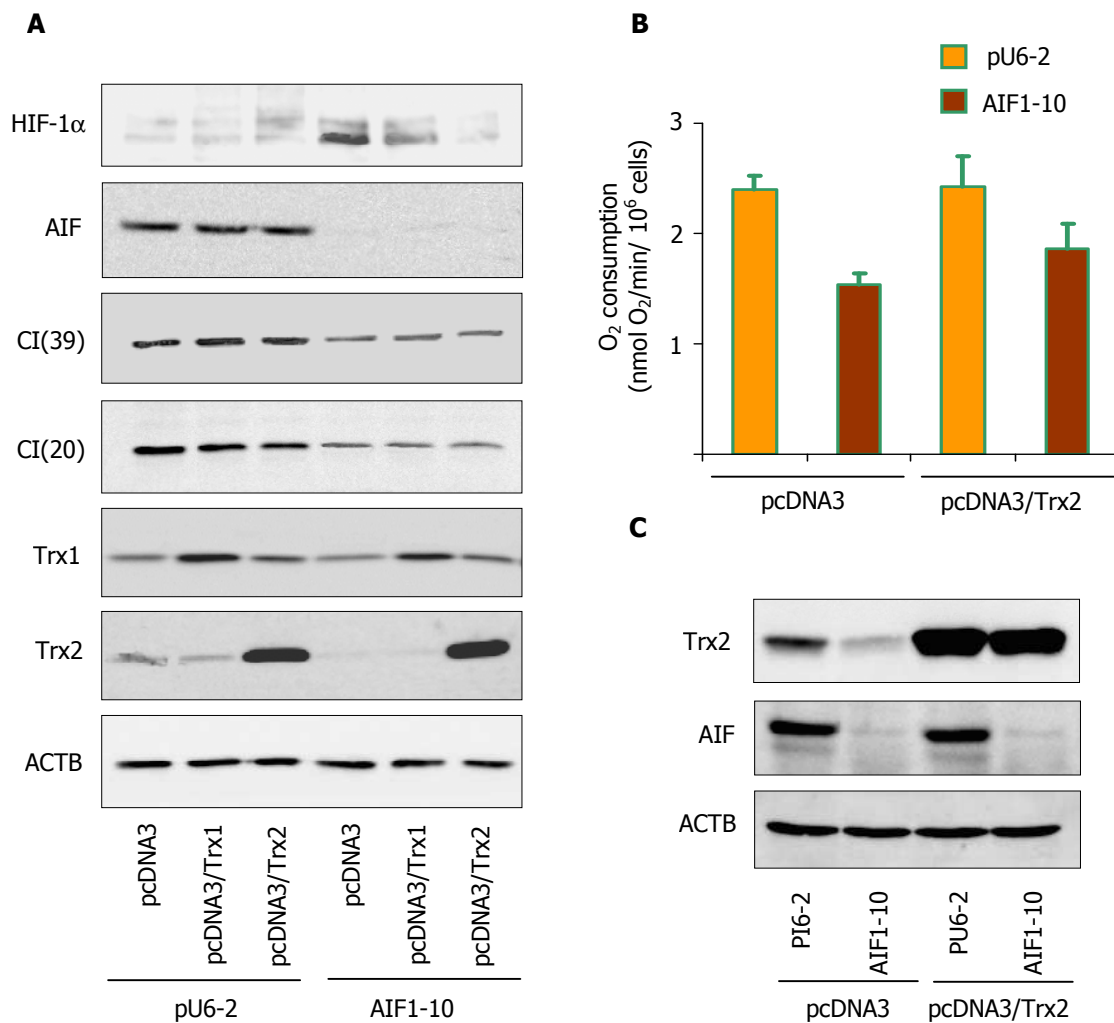
Figure IV.24. Trx overexpression in AIF1-10 and the control pU6-2 cells. A. Representative WB result of Trx1 and Trx2 overexpression in pU6-2 and AIF1-10 cells, protein levels of HIF-1α, AIF, CI(39), CI(20), Trx1, Trx2 and the house-keeping ACTB are shown. B. O$_2$ consumption in intact pU6-2 and AIF1-10 cells after Trx2 overexpression, results shown as mv±SEM, n=4, p>0.05. C. Representative WB images showing Trx2 overexpression in pU6-2 and AIF1-10 cells (O$_2$ consumption experiment).

IV.16.4. Transient silencing of *TRX2*

To further investigate the relationship between the Trx2 expression decrease in our stable siAIF cells and the phenotype these cells display, we decided to transiently silence *TRX2* and analyze the expression of specific proteins. To achieve this, we transfected t-25 flasks cultures of Hep3B cells with pBS U6/PolIII/siTrx2-cassete A, pBS U6/PolIII/siTrx2-cassete B, and pBS U6/PolIII/siGFP (control silencing cassette). Then, 72 h later, we harvested the cells and obtained whole-cell protein extracts. Standard WB protocol was employed to look at the expression of several proteins of interest:

AIF, CI(39) and CI(20). We also verified Trx2 levels and used β-actin expression as a house-keeping control. As shown in Fig.IV.25.A, transient silencing of *TRX2* in Hep3B cells using both siTrx2-cassete A and cassette B resulted in large reduction of Trx2 protein expression. This, however, does not alter AIF or Complex I subunits levels, at least in our model. The experiment was repeated three times with a similar result.

IV.16.5. Co-immunoprecipitation of AIF and Trx2

Having shown that both stable and transient AIF silencing leads to significant and constant decrease in Trx2 protein expression in our cellular model, we hypothesized that these two proteins may be in a close contact in the mitochondria. One way of addressing this question was to perform co-immunoprecipitation studies and analyze whether AIF and Trx2 could co-immunoprecipitate. To this end, pU6-2 and AIF1-10 cell cultures, grown under standard culturing conditions, were collected and whole-cell extracts obtained. A small portion of these extracts was not processed for immunoprecipitation and was kept as a control loading on the WB. Then, whole-cell protein extracts on pU6-2 and AIF1-10 cells were applied on an agarose resin, conjugated to anti-AIF antibody to immunoprecipitate AIF (for details, see chapter "III.13.4. Immunoprecipitation and co-immunoprecipitation"). Later, WB analysis was carried out to look at immunoprecipitated AIF and co-immunoprecipitated Trx2. On the same Western blot, we applied whole-cell extracts of pU6-2 and AIF1-10 as a control. As represented in Fig.IV.25.B, AIF was successfully immunoprecipitated, the band corresponding with AIF is clearly visible in the immunoprecipitated samples, however a large higher-molecular band is also visible in these samples, probably arising from the heavy chain of the   anti-AIF Ig. Of note, we could not observe any co-immunoprecipitated Trx2. This experiment was performed several times (at least four), with similar results.

In order to overcome the detection limits of this technique, we additionally increased the amount of resin used, or the amount of total protein in the whole-cell extract which was incubated with the resin, but none of these protocol modifications enabled us to visualize any Trx2 band on the WB after co-immmunoprecipitation.

Thus, in conclusion, in our hands and with our immunoprecipitation approach, AIF and Trx2 can not co-immunoprecipitate.
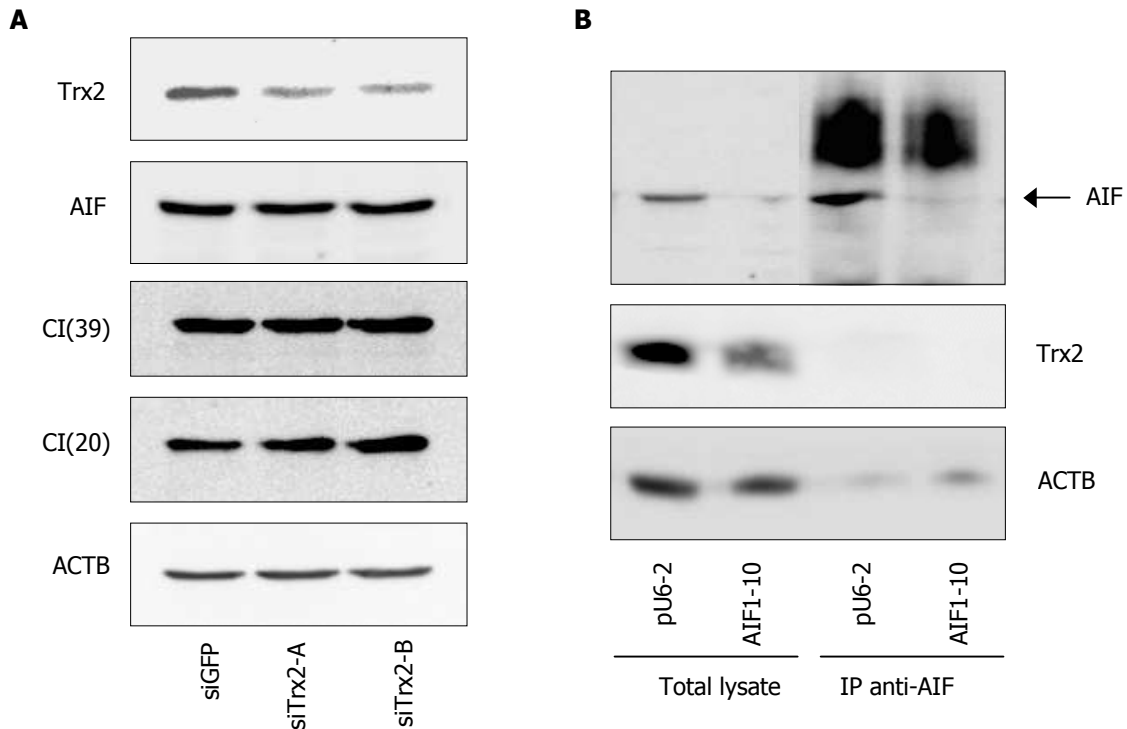
Figure IV.25. Analysis of the relationship between AIF and Trx2 in our cellular model. A. Representative WB showing Trx2, AIF, CI(39) and CI(20) expression in Trx2-silenced Hep3B cells. B. Representative WB of immunoprecipitated AIF showing an absence of co-immunoprecipitated Trx2.

IV.16.6. Proteomic studies on AIF

To further study the role of AIF in the mitochondria, we analyzed the proteins to which AIF may bind or closely interact with. Also, it was of a particular interest for us to find out whether Trx2 is one of these putative AIF partners. To study these protein-AIF interactions, we developed pull-down experiments coupled to mass spectrometry (MS) for direct protein identification. We employed AIF as bait in immunoprecipitation assays, using pU6-2 and AIF1-10 cell extracts, being AIF1-10 the most adequate, internal control. The proteins detected by mass spectrometry analysis were the same for pU6-2 immunoprecipitated sample and the negative internal control sample, AIF1-10. These proteins include: Ig kappa chain V-II region 26-10 (KV2A7_MOUSE), Ig gamma-2B chain C region, membrane-bound form (GCBM_MOUSE), Thioredoxin-dependent peroxide reductase, mitochondrial precursor (PRDX3_HUMAN), Tubulin alpha-ubiquitous chain (TBAK_HUMAN) and Tubulin beta-5 chain (TBB5_HUMAN). The fact that these proteins were detected in both pU6-2 and AIF1-10 suggests that these are not specific for AIF. Moreover, surprisingly we were not able to detect AIF in the pU6-2 sample, meaning that possibly there was not enough starting protein material or

the conditions of the immunoprecipitation have to be improved.

As indicated in Materials and Methods, Chapter "III.13.5. Proteomic studies", a small portion of the immunoprecipitated protein extracts were checked for the presence of AIF by WB, revealing that AIF had been successfully immunoprecipitated (result not shown). However, it must be taken into account that WB is a signal-amplification technique, whereas MS is a direct technique requiring a minimal amount of protein for positive detection. Furthermore, binding partners of interest probably are low abundance proteins. Thus, small amounts of protein partners, binding specifically to the AIF bait, could be masked by the more abundant, non-specific binders to both the antibody and the solid support employed in the pull-down experiment.

In summary, these preliminary proteomic results were attained with a single experiment, and are therefore not conclusive. It would be necessary to repeat this proteomic study using an improved protocol to draw conclusions about AIF protein interactions and binding.

DISCUSSION

"If you are going to doubt something, doubt your limits"

Don Ward (1964-)

In the last few decades, there has been an increased interest in mitochondrial research, unequivocally proved by the large number of scientific publications, which deal with a number of different issues regarding mitochondria. The reasons for the large increase in the mitochondrial research field are many and are mainly due to several discoveries over the last couple of decades, some of which were real breakthroughs that revolutionized and accelerated mitochondrial research. Several of these important steps are listed:

- Mitochondria hold a central place in cellular metabolism and cellular signaling networks.
- Mitochondria are crucial players in PCD, an indispensable and universal biological phenomenon.
- Mitochondria are responsible for the so called "mitochondrial diseases". Mitochondrial cytopathies include more than 40 different identified disorders that have varying genetic features but all include failure in mitochondrial function. It is estimated that about one in every 5000 new born children develops a mitochondrial disease by the age of 10 years. Thus, there is a development of mitochondrial medicine- a new and rapidly growing medical sub-specialty.
- Mitochondria are involved in a wide range of clinically important conditions such as type 2 diabetes, atherosclerotic heart disease, stroke, cancer, aging and neurodegenerative disorders, including Parkinson's disease and Alzheimer's disease.

Taking into consideration the points listed above, it is easy to understand why studying the mitochondrial role of AIF seems promising. When this work was initiated, AIF had already been extensively studied as a mitochondrial protein involved in a variety of apoptotic events, some related to clinically-relevant conditions. However, the true physiological function of this protein in healthy, non-apoptotic cells was not known. Nevertheless, there was some challenging evidence in the literature suggesting that this physiological, mitochondrial role of AIF was related to the ROS metabolism and this seemed likely considering the fact that AIF is NADH-reductase. Armed with this knowledge, we decided to silence *AIF* in a cellular model and examine the cellular steady-state ROS levels. Notably, transient *AIF* silencing in two different human cell lines, Hep3B and HeLa, was accompanied by a significant increase in H_2O_2 levels. This effect was also observed when *AIF* was silenced in a prolonged, stable fashion in Hep3B

background and also in a mouse ES AIF-KO cell line. During the course of this work, several groups reported their data on ROS levels related to AIF, and surprisingly, AIF depletion in cells and animal models was shown to be correlated with both increased oxidative stress [Klein J.A. *et al.*, 2002; Joza N. *et al.*, 2005] and decreased levels of ROS [Urbano A. *et al.*, 2005] or even with no alterations in the redox state [Vahsen N. *et al.*, 2004]. The causes of these discrepancies may be various. These differences may reflect cell type and model-specificity and further arise from the different technical approaches used to detect and quantify ROS levels. In addition, many publications do not report direct measurements of ROS but rather assess ROS-related parameters and/or study the consequences of oxidative damage *in vitro* or *in vivo*.

After the increase in the ROS levels was determined in our experimental model, several questions emerged.

- Where do these ROS come from?
- Is this increase in ROS levels relevant?
- What are the biological consequences of this increase?

The fact that AIF is localized to the mitochondrion, and knowing that these organelles are the main site of intracellular ROS production, led us to hypothesize that the source of ROS generation after *AIF* silencing was the mitochondrion. Using rho⁰ cells, which lack functional mitochondrial ETC, we were able to show that this increase in ROS levels depends on the existence of a functional ETC as it does not occur in Hep3B rho⁰ cells. An alternative reading of this result could point to the mitochondrial ETC as the direct source of the ROS generated in siAIF cellular models. Due to the used methodological approach, we cannot distinguish between these two possibilities.

The ETC, particularly Complex I and III, is a notorious ROS-production site [Muller F.L. *et al.*, 2003; Adam-Vizi V. and Chinopoulos C., 2006] but there are several other mitochondrial enzymes known to produce ROS, such as: aconitase, alpha-ketoglutarate dehydrogenase (α-KGDH), monoamine oxidases (MAO), glycerol-3-phosphate dehydrogenase, dihydroorotate dehydrogenase and cytochrome b5 reductase (Fig.V.1), [for review see Andreyev A.Y. *et al.*, 2005]. Of a particular interest is the dihydrolipoyl dehydrogenase (Dld) component of α-KGDH which has been shown to have an important ROS-forming potential. Very intriguingly, a shift in the

intramitochondrial NADH/NAD$^+$ redox couple towards NADH has been suggested to cause ROS production by α-KGDH [Tretter L. and Adam-Vizi V., 2004; de Grey A.D., 2005]. Interestingly, α-KGDH is tightly bound on the IMM, on the matrix side [Maas E. and Bisswanger H., 1990], as represented in Fig.V.1. and even more intriguingly it has been shown to bind Complex I [Sumegi B. and Srere P.A., 1984]. ROS generation by this enzyme in relation to neurodegeneration has also been reported [Tretter L. and Adam-Vizi V., 2005].

Whether α-KGDH activity is altered in our siAIF cellular mode awaits future studies. To the best of our knowledge, there is no bibliographical evidence for any connection between AIF and this TCA enzyme. Also, Yulia Kushnareva and co-workers suggested that the reduction of the ROS-forming site in Complex I is regulated by the NAD$^+$/NADH ratio [Kushnareva Y. *et al.*, 2002]. Of note, the mitochondrial NAD pool is normally almost all in an oxidized state (i.e. NAD$^+$), but a deficient respiratory chain is predicted to cause it to become more reduced. Yet, we are unable to say whether silencing of *AIF* in our model leads to changes in the mitochondrial concentration of the NAD$^+$/NADH redox couple.

Mitochondrially-derived ROS are important for a multitude of cell redox-signaling processes and perturbations in mitochondrial ROS generation can, therefore, affect different life aspects such as cell cycle, cell proliferation and oxygen sensing. Various proteins (kinases, phosphatases and transcription factors) have been shown to be redox-sensitive. Thus, we were interested in studying the effects of the increased ROS levels in our cellular model and for this reason, we examined several redox-sensitive transcriptions factors, namely HIF-1α, NF-κB, and Nrf-2. While there were no visible changes in the protein levels of NF-κB, both HIF-1α and Nrf2 expression under basal conditions appeared to be increased. The normoxic stabilization of HIF-1α can have important physiological consequences. In tumours, rapid expansion of proliferating cells means that they can outgrow their vascular supply, resulting in impaired oxygen delivery and regions of tumour hypoxia. However, tumour cells often undergo genetic alterations which confers them resistance to these conditions. Of note, HIF1-α is highly expressed in a wide variety of cancers including colon, breast and prostate carcinomas [Zhong H. *et al.*, 1999].

Importantly, the normoxic HIF-1α stabilization in our stable siAIF cells can be reversed

by antioxidant treatments, using MitoQ and NAC, and also by overexpression of the redox-active protein thioredoxin. This finding points to the fact that the steady-state HIF-1α stabilization is a direct consequence of the increased ROS levels in these cells, which suggests that this ROS increase is relevant at the cellular level.

Another transcription factor which was up-regulated in siAIF cells is Nrf2. We showed that not only steady-state expression of Nrf2 is increased but also part of it is translocated to the nucleus. Also to establish a possible link between Nrf2 activation and ROS increase in our model, we tested whether exogenous addition of H_2O_2 in the control cells could lead to up-regulation of Nrf2. In a similar fashion as the stabilization of HIF-1α, H_2O_2 treatment of these cells resulted in increased steady-state levels of Nrf2 protein. In addition, we looked at the expression of several genes known to be transcriptional targets of Nrf2, such as *CAT* or *NQO1* but their expression was not altered. Thus, what the effects of Nrf2 increase in our model are, is not clear and awaits additional studies. In this context, it is important to stress that investigation of Nrf2 opens up new opportunities in understanding how antioxidant defense pathways work and may also serve as a possible target for designing novel therapies for treatment of diseases in which oxidative stress and toxicity are implicated. For example, Nrf2 has been shown to confer neuroprotection against mitochondrial damage induced by the mitochondrial complex II inhibitor 3-nitropropionic acid [Shih A.Y. *et al.*, 2005].

To our surprise, others redox-active enzymes such as SOD1 and SOD2 were not significantly altered in our siAIF cellular model. We detected just a slight decrease in SOD2 expression, both at mRNA and protein level, but whether this decrease was relevant was not studied further. Moreover, we did not register significant alterations in the overall cellular concentrations of GSH, suggesting that the ROS insult in siAIF cells is either not very strong or these cells have developed adaptive mechanisms to maintain the redox state of glutathione at physiological (WT) levels. The bibliographic evidence for GSH alterations in *AIF*-depleted models is ambiguous. Several studies have shown unchanged GSH levels, as in the case of wild type and mutant mouse hearts where *Aif* had been genetically removed [Joza N. *et al.*, 2005] or when GSH was assessed in *AIF*-deficient ES cells [Vahsen N. *et al.*, 2004]. On the contrary, when studying the regulation of cytoplasmic stress granules by AIF, Celine Candé and colleagues found that AIF-negative cells under stress conditions depleted non-oxidized

glutathione more rapidly than the cells expressing AIF [Candé C. *et al.*, 2004].

Furthermore, we aimed to study mitochondrial ETC assembly and function. We and others have shown that Complex I assembly is compromised in siAIF cells. In addition, we have shown that Complex I respiratory function is deficient in our model, measured as Complex I-dependent O_2 consumption in digitonin-permeabilized cells, resulting in an overall 30% reduction in intact cell respiration. This finding is important, knowing that deficiency of Complex I is the most common cause of disorders of the oxidative phosphorylation system in humans. Many neuropathies as well as cancer diseases present Complex I deficiencies, significantly correlated with the disease prognosis. The mechanism(s) by which AIF regulates mitochondrial respiration through Complex I remains to be determined. AIF is not an integral part of Complex I, rather it has been postulated that AIF holds some chaperone-like function regulating Complex I biogenesis and/or stability.

We aimed to study the link between Complex I defect and ROS, though it presented many difficulties. It is generally known that the inhibition of Complex I can lead to formation of ROS [Adams Jr J.D. *et al.*, 1993]. It has also been suggested that this incremented production of ROS could be due to shunting of electrons through Complex II, which may generate 5-7 times as many ROS as passing through Complex I (Dykens J.A., 1994). Clinically relevant is the fact that several examples of enhanced ROS production in genetic defects of Complex I are known in the literature, pointing to the fact that dysfunctional Complex I may subject cells to oxidative stress [Pitkanen S. and Robinson B.H., 1996; Robinson B.H., 1998]. In the same line, superoxide production was shown to be inversely related to Complex I activity in inherited Complex I deficiency [Verkaart S. *et al.*, 2007].

But can we be certain, at least theoretically, that Complex I is the origin of the increased ROS that we have detected in siAIF cells?

When studying ROS and Complex I, one faces the apparent paradox that damaged and non-functional Complex I produces ROS but also oxidative stress can damage Complex I and thus compromise its function. Often, these effects merge and cannot be discriminated. There is a wealth of bibliographical evidence showing that ROS can inhibit Complex I activity and this occurs even dose-dependently. *In vitro* studies on *in*

situ synaptic mitochondria have shown that 16-30% inhibition of Complex I is sufficient to stimulate ROS generation and lead to a collapse of $\Delta\psi_m$ in the presence of a concomitant oxidative stress [Chinopoulos C. and Adam-Vizi V., 2001]. Moreover, ROS insult can indirectly affect mitochondrial respiration. Treatment of isolated rat heart mitochondria with H_2O_2 was shown to result in a decline of state 3 NADH-linked respiration [Nulton-Persson A.C. and Szweda L.I., 2001]. These authors reported that exogenous addition of H_2O_2 to isolated mitochondria inactivated certain mitochondrial TCA enzymes (aconitase, α-KDGDH and SDH) without damaging ETC complexes.

How increased ROS are related to the defect of Complex I 39 and 20 kDa subunits expression in our cellular model remains elusive. All our attempts to reverse this defect with antioxidant treatments, using antioxidants (both a general and mitochondria-targeted antioxidant) and overexpressing Trx2 as an endogenous antioxidant, have failed. A similar result is described in the literature and it was obtained when CI expression was studied in AIF-deficient ES cells. In this scenario, Complex I levels could not be recovered by antioxidant treatment such as addition of tocopherol, decylubiquinone or GSH ester [Vahsen N. *et al.*, 2004]. Thus, we are unable to establish a direct link and claim that the decrease in Complex I expression is exclusively due to ROS increase. Alternative, indirect mechanisms can also account for the Complex I defect, resulting from *AIF* silencing. The redox activity of AIF might play a role in controlling the redox status of key components of Complex I, necessary for its correct maintenance and function. It is also plausible to suggest that AIF may participate in the redox modification of regulatory molecules, not themselves direct components of Complex I. In this respect, several groups have underlined the importance of native lipids for the stabilization and activation of Complex I within the IMM [Hirst J. *et al.*, 2003]. Tightly bound cardiolipin may be required for structural integrity of the complex and can even have a functional role. Notably, cardiolipin is a well-known target of oxidative stress damage. Knowing this, we may speculate that AIF is related to cardiolipin in a direct way or *via* the ROS insult produced when *AIF* is silenced.

In summary, additional functional studies on Complex I biogenesis and stability need to be undertaken in order to reveal the true mitochondrial role of AIF.

Remarkably, the respiration defect in siAIF cells can be reversed using antioxidant

treatment (NAC or MitoQ), or partially upon Trx2 overexpression. In view of this finding, we suggest that there is a direct link between the increased ROS production and loss of respiratory capacity in siAIF cellular model. This assumption has precedents in the literature, as it has been described in many pathophysiological models such as that of cardiac ischemia/reperfusion injury where there is a build-up of ROS which, in turn, can inactivate the mitochondrial ETC at Complex I and Complex III and thus lead to a decrease in oxygen consumption [Petrosillo G. *at al.*, 2003; Paradies G. *et al.*, 2004].
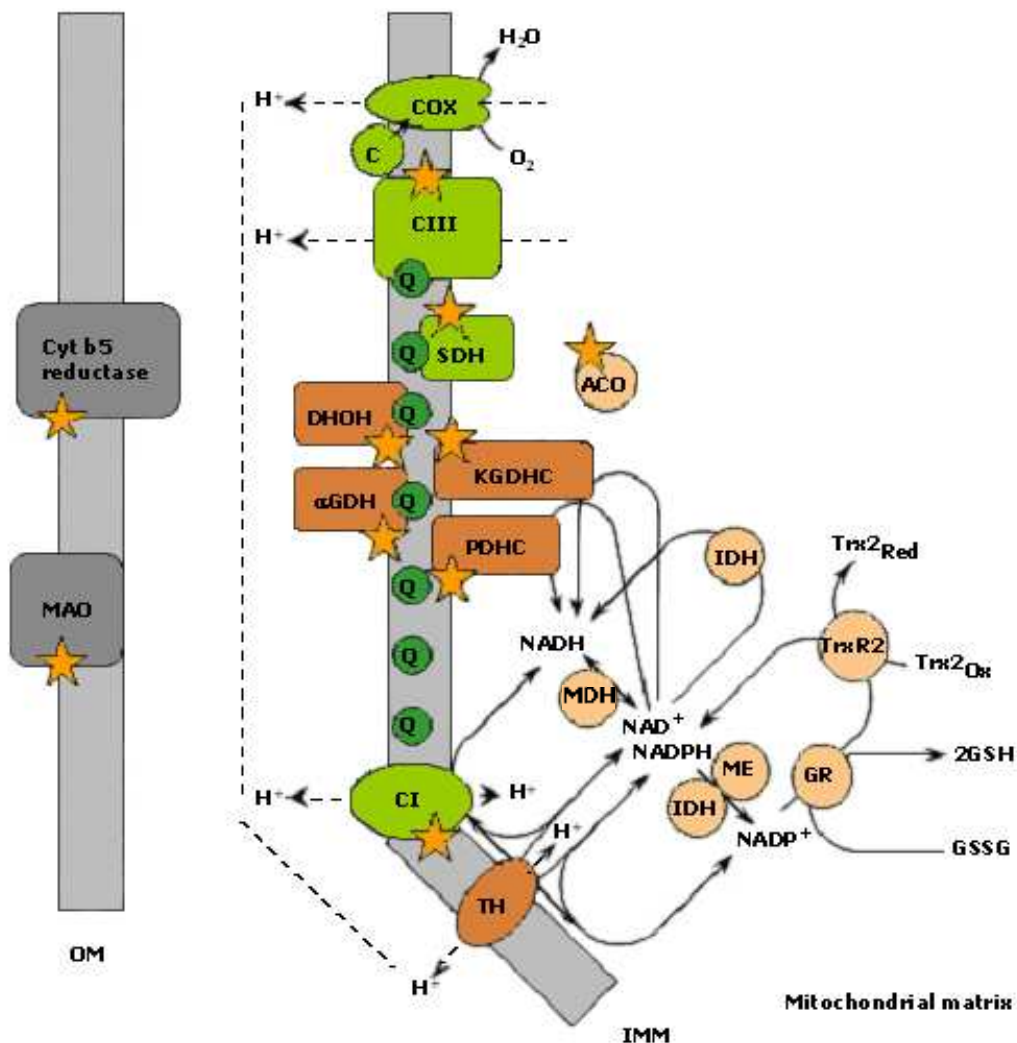
Figure V.1. Sources of ROS in the mitochondrion and connections with NAD/NADP metabolism. ROS-producing enzymes are marked with a star. Abbreviations: ACO (aconitase), COX (cytochrome *c* oxidase), c (cytochrome *c*), CI (Complex I), CIII (Complex III), PDHC (pyruvate dehydrogenase complex), SDH (succinate dehydrogenase), αGDH (α-glycerolphosphate dehydrogenase), MDH (malate dehydrogenase), IDH (isocitrate dehydrogenase), KGDHC (α-ketoglutarate dehydrogenase complex), MAO (monoamine oxidase), TH (transhydrogenase), GR (glutathione reductase), DHOH (dihydroorotate dehydrogenase), ME (malic enzyme) [modified from Andreyev A.Y. *et al.*, 2005].

Also, NAC treatment has been shown to improve the impaired OxPhos process in cybrids harboring a T8993G point mutation in mtDNA [Mattiazzi M. *et al.*, 2004]. This antioxidant has also been reported to protect against age-related inactivation of Complex I in mouse synaptic mitochondria [Banaclocha M.M. *et al.*, 1997].

Considering our results and the bibliographical evidence, we can suggest a dual mechanism for Complex I deficiency and ROS in our cellular model. We propose that AIF is necessary for Complex I assembly and this is prior to any ROS generation at the level of this complex. However, ROS coming from ETC and/or elsewhere contribute to the respiration defect as it can be improved using antioxidants. Thus, Complex I respiration deficiency can be due to both the lack of proper protein complex assembly and oxidative stress. The general model of AIF´s role in the mitochondrion is schematically represented in Fig.V.2.

As a further support for the proposed function of AIF as a redox modifier was the finding that AIF is up-regulated upon H_2O_2 treatment of cells and this increase occurs at a post-transcriptional level. To our knowledge this is the first time that the expression of AIF is shown to be up-regulated in cells by acute oxidative stress.

Moreover, the inhibition of Complex I has been shown to lead to loss of $\Delta\psi_m$ [Wu E.Y. *et al.*, 1990]. This is interesting as our siAIF cells display a significant decrease in $\Delta\psi_m$. It is important to stress that $\Delta\psi_m$ is a very important cellular parameter, often employed as an indicator of cellular viability. Disruption of $\Delta\psi_m$ can have many consequences as it is not only important for ATP generation but is also required for mitochondrial protein import and metabolite transport regulation. A severe drop in the $\Delta\psi_m$ targets cells for apoptosis or alternatively, necrosis. Interestingly, many studies have proven the correlation between ROS production and $\Delta\psi_m$. In this respect, increases in ROS can lead to $\Delta\psi_m$ reduction but also some articles provide evidence for the inverse phenomenon where changes in $\Delta\psi_m$ provoke ROS generation in the mitochondrion. Both increased and decreased $\Delta\psi_m$ have been shown to induce ROS formation or at least occur concomitantly, in different models.

The next question we addressed was, how does the respiration defect and the increase in ROS levels affect the overall metabolism of siAIF cells? For this, we assessed several parameters.
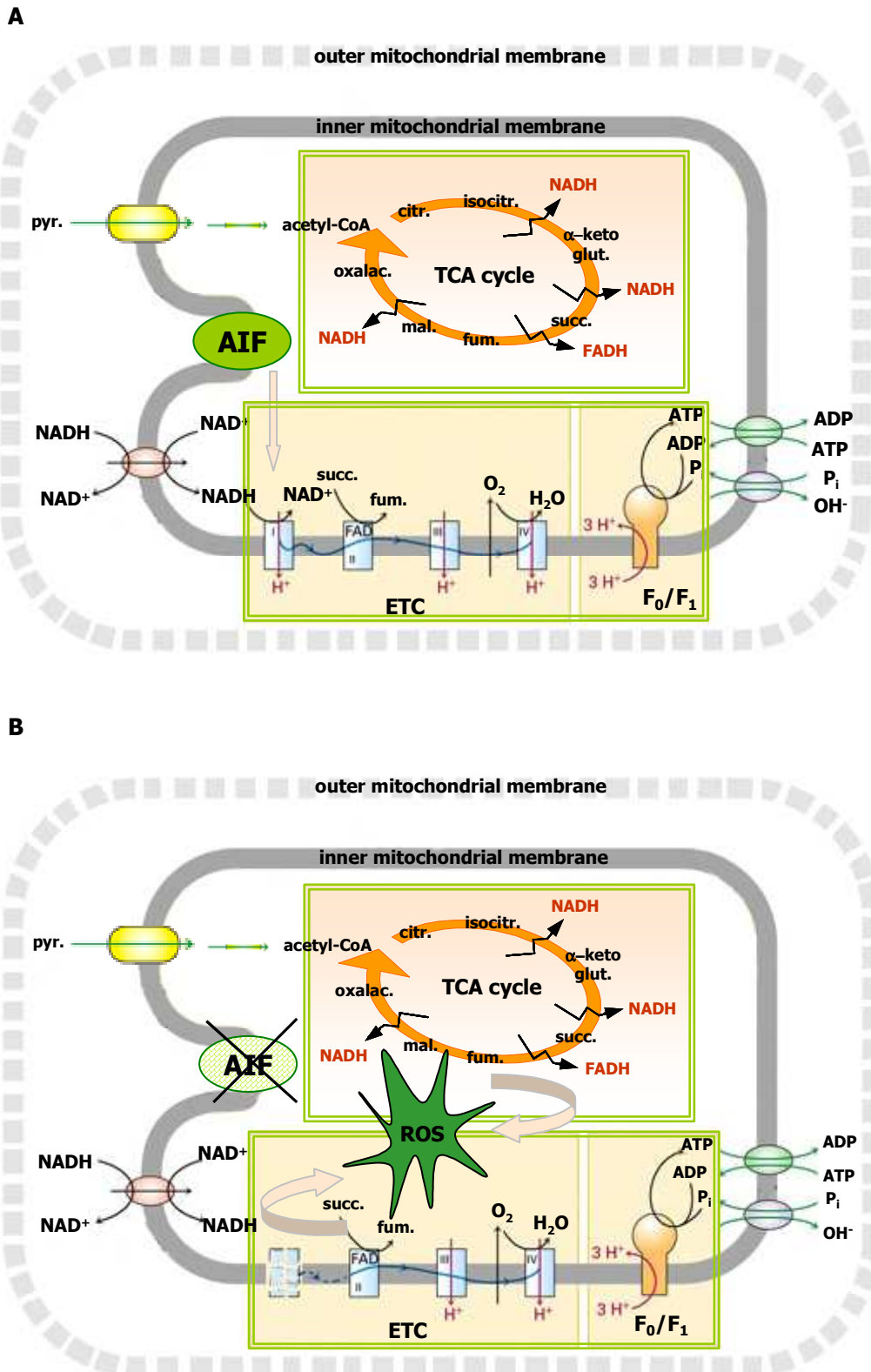
Figure V.2. Schematic model of the function of AIF in the mitochondrion. A. AIF is present in the mitochondrion, Complex I is assembled. B. AIF is absent, Complex I is misassembled, ROS production at ETC or other sources is increased. Abbreviations: pyr. (pyruvate), citr. (citrate), isocitr. (isocitrate), α-ketoglut. (α-ketoglutarate), succ. (succinate), fum. (fumarate), mal. (malate), oxalac. (oxalacetate).

Observed under ordinary light microscope and proliferating under normal cell culture conditions, siAIF cells and control cell lines show similar size, and morphology. Also, siAIF cells do not display any external signs of cell damage or death. However, siAIF cells proliferate at a significantly lower rate compared to wild type Hep3B cells and the control pU6-2 cell line, which proliferate at a very similar rate. Of note, the ATP levels of siAIF cells were very similar to that detected in control cells which led us to analyze the glycolytic capacity of these cells.

Expectedly, siAIF cells had a higher glycolytic capacity as they presented a higher glucose up-take and accumulated more lactate over a prolonged period of time in culture compared to control cell lines. We also observed that these cells manifested a lower capacity of growing on non-fermentable sugars such as galactose.

All these data suggest that the cellular metabolism in siAIF cells is switched towards glycolysis in order to cover the deficit of ATP generation by the OxPhos process. Very similar observations concerning the increased glucose dependency and lower proliferation rate were reported in AIF-deficient ES cells [Vahsen N. *et al.*, 2004]. The fact that siAIF cells have an increase in glycolysis and the fact that they proliferate slower (have lower energetic demands in this respect) explains why these cells can maintain normal (WT) ATP levels under basal conditions. Remarkably, different human tumour cells have been shown to display enhanced glycolysis dependency directly linked to the attenuated mitochondrial bioenergetic function, a phenomenon first described by Otto Warburg in 1920s.

It is noteworthy that antioxidant treatment of siAIF cells cannot restore normal proliferation in these cells. This can be interpreted in two ways. One possibility is that the biochemical changes siAIF cells undergo are deeper and more complicated than we expected, and thus cannot be overcome by elimination of the generated ROS or that the antioxidant treatment was not adequate, in terms of concentration and duration to restore the normal cellular metabolism and thus the proliferation rate.

Another observation that merits consideration in a metabolic context is the fact that siAIF cells present higher levels of the GAPDH transcript in comparison to their control counterparts. As GAPDH is a classic glycolytic enzyme this finding is in line with the results discussed in the previous paragraph. However, GAPDH has also been shown to

have other cellular functions [for review, see Chuang D.M. *et al.*, 2005]. Thus, it has been suggested that GAPDH acts as an intracellular messenger mediating apoptotic cell death, being this a part of a novel cellular death cascade. In addition, it has been proposed as a novel sensor of NO stress. Clinically, GAPDH regulation seems to be important for several pathological conditions such as diabetes and neurodegenerative disorders. Intriguingly, very recently Dongwon Baek and colleagues showed that GAPDH can suppress ROS generation in *Arabidopsis thaliana* and yeast models [Baek D. *et al.*, 2008]. Also, it is worth mentioning that GAPDH activity needs the presence of NAD^+ and the concentration ratio of $NAD^+/NADH$ can regulate its activity. If cytosolic NADH concentration is increased due to deficiencies in the mitochondrial OxPhos process, GAPDH activity can be diminished. We could speculate that a similar situation may be present in our cellular model where AIF has been depleted. Again, it would be essential to determine the relative $NAD^+/NADH$ concentration ratio in our cellular model, in the whole cell and the mitochondria specifically, in order to test this hypothesis. What are the consequences, other than promoting glycolysis, of the increase of GAPDH expression in siAIF cells is not known and needs additional investigation.

Aiming to further study the consequences of *AIF* silencing at the mitochondrial level, we found that Trx2 levels were significantly decreased in our siAIF cells without affecting the redox state of the Trx2 protein. The fact that silencing of *AIF* and Trx2 reduction in our model are truly related was confirmed by performing transient silencing experiments, which had the same outcome. The thioredoxins and related enzymes (such as thioredoxin reductases) are ubiquitous redox proteins whose tissue distribution, genetics and reaction mechanism have been widely studied. However, little is known about the mitochondrial isoforms of these proteins. Of note, there is now mounting evidence that Trx1 and Trx2 are quite different in terms of activity and regulation. Namely, Trx1 and Trx2 display quite different aa sequence in the protein interaction domain, conferring them different specificity and also Trx2 seems to be more resistant to oxidation, as suggested by the lack of a few structural (non-catalytic) Cys residues, which are present in other mammalian thioredoxins [Spyrou G. *et al.*, 1997]. Intriguingly, unlike Trx1, Trx2 is highly expressed in heart and skeletal muscle [Spyrou G. *et al.*, 1997], suggesting a specific protective and/or regulatory role of Trx2 in these metabolically active tissues. Also, Trx2 is highly expressed in the neurons of several brain regions, particularly in those with a prominent free radical production and

thus may provide important neuronal defense against ROS and redox-related damage. In this direction, it is tempting to speculate that Trx2 may play a role in neurodegenerative diseases such as PD.

The mitochondrial Trx system seems to be essential for mammalian embryonic development as the disruption of *Trx2* gene in the mouse results in massive apoptosis during early embryogenesis and embryonic lethality [Nonn L. *et al.*, 2003]. However, overexpression of Trx2 or TrxR2, or both, does not necessarily improve cell survival or resistance to ROS-promoting factors [Patenaude A. *et al.*, 2004], indicating that unidentified factors control their ROS-protecting role in the mitochondria. Remarkably, Trx2 has been suggested to interact with the mitochondrial respiratory chain complexes regulating $\Delta\psi_m$, which accounts for its role as an anti-apoptotic mitochondrial protein. All of the above points to the suggestion that the mitochondrial function of Trx2 obviously goes beyond its specific function as a mitochondrial-ROS defence player.

The similarity between AIF as an oxidoreductase enzyme and the thioredoxin system, consisting of Trx, TrxR and NADPH, as a powerful protein-disulfide antioxidant, has already been suggested in the literature [van Empel V.P.M. *et al.*, 2005].

Taking into consideration that AIF depletion in our model leads to a clear reduction in Trx2 expression, we speculated that these proteins may be in a rather direct contact. However, our attempts to establish a possible link between AIF and Trx2, using co-immunoprecipitation and proteomic approach did not succeed. Yet, we believe that in order to discard any direct correlation between AIF and Trx2 in our hands, the techniques we employed should be improved. Furthermore, additional studies with different approaches in this respect are needed as **the lack of evidence is not necessarily evidence of the lack.**

CONCLUSIONS

"It is never too late to be what you might have been"

George Eliot (1819-1880)

1. We have designed efficient siRNA cassettes which abolished the expression of the *AIF* gene in a cellular model.

2. Stable siAIF KD cell lines have been successfully generated in a human hepatoma cell line, Hep3B.

3. Characterization of these cell lines revealed that:

    *   Silencing of *AIF* in a cellular model leads to a significant increase in ROS levels and these ROS are of mitochondrial origin.

    *   The increase of ROS in siAIF cells is relevant as two redox-sensitive transcription factors, HIF-1 and Nrf2, are up-regulated.

    *   Silencing of AIF is accompanied by Complex I deficiency resulting in compromised oxygen consumption. The defect in mitochondrial respiration can be recovered with antioxidant treatments but the same treatments cannot restore normal Complex I protein expression.

    *   siAIF cells display a higher glycolytic capacity and lower proliferation rate presumably comprising adaptive metabolic mechanisms.

    *   *AIF* silencing is followed by a significant decrease in Trx2 expression levels.

4. The results obtained in this work suggest that AIF holds an integral mitochondrial function, as a redox modifier and a chaperone like-molecule, involved in maintenance of the redox balance in the mitochondrion and necessary for Complex I assembly.

VII. FUTURE PERSPECTIVES

"Science is always wrong, it never solves a problem without creating ten more"

George Bernard Shaw (1856-1950)

The concept of oxidative stress is currently suffering from excessive popularity, caused, in most cases, by scientists who try to "sell" the idea that oxidative stress is involved in almost all pathological conditions and/or try to "sell" antioxidant molecules as life prolongers or healing molecules for many diseases. On the other hand, studying the differences between oxidative stress conditions and redox regulation/signaling is also an interesting challenge. The fact that AIF is involved in the mitochondrial ROS metabolism makes it a very promising target for future investigations both in physiological (redox signaling) and pathological (oxidative stress) conditions.

Future studies should also focus on AIF-interacting molecules in the mitochondria, specifically binding proteins which could reveal more details about the true mitochondrial role of AIF.

Moreover, it would be of a particular interest to establish models for AIF involvement in neurodegenerative disorders and possibly other mitochondria-associated diseases.

VIII. REFERENCES

"The fuel on which science runs is ignorance"

Matt Ridley (1958-)

Adam-Vizi V, Chinopoulos C: Bioenergetics and the formation of mitochondrial reactive oxygen species. Trends Pharmacol Sci. 2006; 27(12): 639-645.

Adams JD Jr, Klaidman LK, Leung AC: MPP$^+$ and MPDP$^+$ induced oxygen radical formation with mitochondrial enzymes. *Free Rad Biol Med.* 1993;15(2): 181-186.

Almeida S, Brett A, Gois IN, Oliveira CR, Rego AC: Caspase-dependent and – independent cell death induced by 3-nitropropionic acid in rat cortical neurons. *J Cell Biochem*. 2006; 98: 93-101.

Andreyev AY, **Kushnareva YE**, **Starkov AA**: Mitochondrial metabolism of reactive oxygen species. *Biochemistry (Mosc).* 2005; 70(2): 200-214.

Arany Z, Huang LE, Eckner R, Bhattacharya S, Jiang C, Goldberg MA, Bunn HF, Livingston DM: An essential role for p300/CBP in the cellular response to hypoxia. *Proc Natl Acad Sci U S A.* 1996; 93(23): 12969-12973.

Arcari P, Masullo L, Masullo M, Catanzano F, Bocchini V: A NAD(P)H oxidase isolated from the archaeon Sulfolobus solfataricus is not homologous with another NADH oxidase present in the same microorganism. Biochemical characterization of the enzyme and cloning of the encoding gene. *J Biol Chem.* 2000; 275(2): 895-900.

Arner ES, Zhong L, Holmgren A: Preparation and assay of mammalian thioredoxin and thioredoxin reductase. *Methods Enzymol.* 1999; 300: 226-239.

Arner ES, Holmgren A: Physiological functions of thioredoxin and thioredoxin reductase. *Eur J Biochem.* 2000; 267: 6102-6109.

Arnoult D, **Tatischeff I**, **Estaquier J**, **Girard M**, **Sureau F**, **Tissier JP**, **Grodet A**,**Dellinger M**, **Traincard F**, **Kahn A**, **Ameisen JC**, **Petit PX**: On the evolutionary conservation of the cell death pathway: mitochondrial release of an apoptosis-inducing factor during Dictyostelium discoideum cell death. *Mol Biol Cell.* 2001; 12(10): 3016-30.

Aw TY: Intracellular compartmentation of organelles and gradients of low molecular weight species. *Int Rev Cytol.* 2000; 192: 223-253.

Babcock DF, Herrington J, Goodwin PC, Park YB, Hille B.: Mitochondrial participation in the intracellular Ca^{2+} network. *J Cell Biol*. 1997; 136: 833-844.

Baek D, Jin Y, Jeong JC, Lee HJ, Moon H, Lee J, Shin D, Kang CH, Kim DH, Nam J, Lee SY, Yun DJ: Suppression of reactive oxygen species by glyceraldehyde-3-phosphate dehydrogenase. *Phytochemistry.* 2008; 69(2): 333-338.

Baeuerle PA: The inducible transcription activator NF-kappa B: regulation by distinct protein subunits*. Biochim Biophys Acta.* 1991; 1072(1): 63-80.

Balaban RS, Nemoto S, Finkel T: Mitochondria, oxidants and aging. *Cell*. 2005; 120: 483-495.

Banaclocha MM, Hernández AI, Martínez N, Ferrándiz ML: N-acetylcysteine protects against age-related increase in oxidized proteins in mouse synaptic mitochondria. *Brain Res.* 1997; 762(1-2): 256-258.

Barber BR: Two new mutations. *Mouse News Lett*. 1971; 45: 34-35.

Bárdos JI, Ashcroft M: Hypoxia-inducible factor-1 and oncogenic signalling. *Bioessays.* 2004; 26(3): 262-269.

Barhan D, Trinder P: An improved colour reagent for the determination of blood glucose by the oxidase system. *Analyst*. 1972; 97: 142.

Barrientos A: In vivo and in organello assessment of OXPHOS activities. *Methods.* 2002; 26(4): 307-316.

Beal MF: Aging, energy and oxidative stress in neurodegenerative diseases. *Annals of Neurol.* 1995; 38, 357-366.

BelAiba RS, Djordjevic T, Bonello S, Flugel D, Hess J, Kietzmann T, Gorlach A: Redox-sensitive regulation of the HIF pathway under non-hypoxic conditions in pulmonary artery smooth muscle cells. *Biol Chem.* 2004; 385: 249–257.

Bereiter-Hahn J, Voth M: Dynamics of mitochondria in living cells: shape changes, dislocations, fusion, and fission of mitochondria. *Microsc Res Tech.* 1994; 27: 198-219.

Bossy-Wetzel E, Newmeyer DD, Green DR: Mitochondrial cytochrome c release in apoptosis occurs upstream of DEVD-specific caspase activation and independently of mitochondrial transmembrane depolarization. *EMBO J.* 1998; 17(1): 37-49.

Boveris A, Cadenas E: Mitochondrial production of superoxide anions and its relationship to the antimycin insensitive respiration. *FEBS Lett.* 1975; 54: 311-314.

Boveris A, Cadenas E: Cellular sources and steady-state levels of reactive oxygen species. In: L.B. Clerch, D.J. Massaro (eds.). Oxygen, Gene Expression and Cellular Function. Marcel Dekker, New York, 1997; 1-25.

Bradham CA, Qian T, Streetz K, Trautwein C, Brenner DA, Lemasters JJ.: The mitochondrial permeability transition is required for tumor necrosis factor alpha-mediated apoptosis and cytochrome c release. *Mol Cell Biol.* 1998; 18(11): 6353-6364.

Brand MD, Affourtit C, Esteves TC, Green K, Lambert AJ, Miwa S, Pakay JL, Parker N: Mitochondrial superoxide: production, biological effects, and activation of uncoupling proteins. *Free Radic Biol Med.* 2004; 37(6): 755-767.

Braun JS, Novak R, Murray PJ, Eischen CM, Susin SA, Kroemer G, Halle A, Weber JR, Tuomanen EI, Cleveland JL: Apoptosis-inducing factor mediates microglial and neuronal apoptosis caused by pneumococcus. *J Infect Dis.* 2001; 184(10): 1300-1309.

Braun JS, Sublett JE, Freyer D, Mitchell TJ, Cleveland JL, Tuomanen EI, Weber JR: Pneumococcal pneumolysin and H(2)O(2) mediate brain cell apoptosis during meningitis. *J Clin Invest.* 2002; 109(1): 19-27.

Braun S, Hanselmann C, Gassmann MG, auf dem Keller U, Born-Berclaz C, Chan K, Kan YW, Werner S: Nrf2 transcription factor, a novel target of keratinocyte growth factor action which regulates gene expression and inflammation in the healing skin wound. *Mol Cell Biol.* 2002; 22(15): 5492-5505.

Bronson RT, Lane PW, Harris BS, Davisson MT: Harlequin (Hq) produces progressive cerebellar cortical atrophy. *Mouse Genome.* 1990; 87: 110.

Brookes PS, Levonen A., Shiva S, Sarti P, Darley-Usmar VM: Mitochondria: regulators of signal transduction by reactive oxygen and nitrogen species. *Free Radic Biol Med*. 2002; 33: 755-764.

Brown D, Yu BD, Joza N, Benit P, Meneses J, Firpo M, Rustin P, Penninger JM, Martin GR: Loss of Aif function causes cell death in the mouse embryo, but the temporal progression of patterning is normal. *Proc Natl Acad Sci U S A.* 2006; 103(26): 9918-9923.

Brunet CL, Gunby RH, Benson RS, Hickman JA, Watson AJ, Brady G: Commitment to cell death measured by loss of clonogenicity is separable from the appearance of apoptotic markers. *Cell Death Differ.* 1998; 5(1): 107-115.

Candé C, Vahsen N, Metivier D, Tourriere H, Chebli K, Garrido C, Tazi J, Kroemer G: Regulation of cytoplasmic stress granules by apoptosis-inducing factor. *J Cell Sci.* 2004; 117(Pt 19): 4461-4468.

Carter WO, Narayanan PK, Robinson JP: Intracellular hydrogen peroxide and superoxide anion detection in endothelial cells. *J Leukoc Biol.* 1994; 55(2): 253-258.

Cassarino DS, Bennett JP Jr: An evaluation of the role of mitochondria in neurodegenerative diseases: mitochondrial mutations and oxidative pathology, protective nuclear responses, and cell death in neurodegeneration. *Brain Res Brain Res Rev.* 1999; 29(1): 1-25.

Cecconi F, Alvarez-Bolado G, Meyer BI, Roth KA, Gruss P: Apaf1 (CED-4 homolog) regulates programmed cell death in mammalian development. *Cell.* 1998; 94(6): 727-737.

Chan K, Han XD, Kan YW: An important function of Nrf2 in combating oxidative stress: detoxification of acetaminophen. *Proc Natl Acad Sci U S A.* 2001; 98(8): 4611-4616.

Chance B, Sies H, Boveris A: Hydroperoxide metabolism in mammalian organs. *Physiol Rev.* 1979; 59: 527-605.

Chandel NS, McClintock DS, Feliciano CE, Wood TM, Melendez JA, Rodriguez AM, Schumacker PT: Reactive oxygen species generated at mitochondrial Complex III stabilize hypoxia-inducible factor-1a during hypoxia. *J Biol Chem.* 2000; 275(33): 25130-25138.

Chee JL, Guan XL, Lee JY, Dong B, Leong SM, Ong EH, Liou AK, Lim TM: Compensatory caspase activation in MPP+-induced cell death in dopaminergic neurons. *Cell Mol Life Sci.* 2005; 62(2): 227-238.

Chen Y, **Cai J**, **Murphy TJ**, **Jones DP**: Overexpressed human mitochondrial thioredoxin confers resistance to oxidant-induced apoptosis in human osteosarcoma cells. *J Biol Chem.* 2002; 277(36): 33242-3348.

Cheung EC, Joza N, Steenaart NA, McClellan KA, Neuspiel M, McNamara S, MacLaurin JG, Rippstein P, Park DS, Shore GC, McBride HM, Penninger JM, Slack RS: Dissociating the dual roles of apoptosis-inducing factor in maintaining mitochondrial structure and apoptosis. *EMBO J.* 2006; 25(17): 4061-4073.

Chinopoulos C, Adam-Vizi V: Mitochondria deficient in complex I activity are depolarized by hydrogen peroxide in nerve terminals: relevance to Parkinson's disease. *J Neurochem.* 2001; 76(1): 302-306.

Choi JH, Kim TN, Kim S, Baek SH, Kim JH, Lee SR, Kim JR: Overexpression of mitochondrial thioredoxin reductase and peroxiredoxin III in hepatocellular carcinomas. *Anticancer Res.* 2002; 22: 3331-3335.

Chuang DM, **Hough C**, **Senatorov VV**: Glyceraldehyde-3-phosphate dehydrogenase, apoptosis, and neurodegenerative diseases. *Annu Rev Pharmacol Toxicol.* 2005; 45: 269-290.

Clark LC, Wolf R, Granger D, Taylor Z: Continuous recording of blood oxygen tensions by polarography. *J Appl Physiol.* 1953; 6: 189-193.

Conrad M, Jakupoglu C, Moreno SG, Lippl S, Banjac A, Schneider M, Beck H, Hatzopoulos AK, Just U, Sinowatz F, Schmahl W, Chien KR, Wurst W, Bornkamm GW, Brielmeier M: Essential role for mitochondrial thioredoxin reductase in hematopoiesis, heart development, and heart function. *Mol Cell Biol.* 2004; 24(21): 9414-9423.

Coucouvanis E, Martin GR: Signals for death and survival: a two-step mechanism for cavitation in the vertebrate embryo. *Cell.* 1995; 83(2): 279-287.

Cregan SP, Fortin A, MacLaurin JG, Callaghan SM, Cecconi F, Yu SW, Dawson TM, Dawson VL, Park DS, Kroemer G, Slack RS: Apoptosis-inducing factor is involved in the regulation of caspase-independent neuronal cell death. *J Cell Biol.* 2002; 158(3): 507-517.

Damdimopoulos AE, Miranda-Vizuete A, Pelto-Huikko M, Gustafsson JA, Spyrou G: Human mitochondrial thioredoxin. Involvement in mitochondrial membrane potential and cell death. *J Biol Chem.* 2002; 277(36): 33249-33257.

A

Daugas E, Nochy D, Ravagnan L, Loeffler M, Susin SA, Zamzami N, Kroemer G: Apoptosis-inducing factor (AIF): a ubiquitous mitochondrial oxidoreductase involved in apoptosis. *FEBS Lett.* 2000; 476(3): 118-123.

B

Daugas E, Susin SA, Zamzami N, Ferri KF, Irinopoulou T, Larochette N, Prevost MC, Leber B, Andrews D, Penninger J, Kroemer G: Mitochondrio-nuclear translocation of AIF in apoptosis and necrosis. *FASEB J.* 2000; 14(5): 729-739.

Déas O, Dumont C, MacFarlane M, Rouleau M, Hebib C, Harper F, Hirsch F, Charpentier B, Cohen GM, Senik A: Caspase-independent cell death induced by anti-CD2 or staurosporine in activated human peripheral T lymphocytes. *J Immunol.* 1998; 161: 3375-3383.

De Grey AD: Reactive oxygen species production in the mitochondrial matrix: implications for the mechanism of mitochondrial mutation accumulation. *Rejuvenation*

Res. 2005; 8(1): 13-17.

A

Delettre C, **Yuste VJ**, **Moubarak RS**, **Bras M**, **Lesbordes-Brion JC**, **Petres S**, **Bellalou J**, **Susin SA**: AIFsh, a novel apoptosis-inducing factor (AIF) pro-apoptotic isoform with potential pathological relevance in human cancer. *J Biol Chem.* 2006; 281(10): 6413-6427.

B

Delettre C, **Yuste VJ**, **Moubarak RS**, **Bras M**, **Robert N**, **Susin SA:** Identification and characterization of AIFsh2, a mitochondrial apoptosis-inducing factor (AIF) isoform with NADH oxidase activity. *J Biol Chem.* 2006; 281(27): 18507-18518.

Desagher S, Osen-Sand A, Nichols A, Eskes R, Montessuit S, Lauper S, Maundrell K, Antonsson B, Martinou JC: Bid-induced conformational change of Bax is responsible for mitochondrial cytochrome c release during apoptosis. *J Cell Biol.* 1999; 144(5): 891-901.

Dong Z, Saikumar P, Griess GA, Weinberg JM, Venkatachalam MA: Intracellular Ca2+ thresholds that determine survival or death of energy-deprived cells. *Am J Pathol.* 1998; 152(1): 231-240.

Du C, Fang M, Li Y, Li L, Wang X: Smac, a mitochondrial protein that promotes cytochrome c-dependent caspase activation by eliminating IAP inhibition. *Cell.* 2000; 102(1): 33-42.

Dumont C, Durrbach A, Bidere N, Rouleau M, Kroemer G, Bernard G, Hirsch F, Charpentier B, Susin SA, Senik A: Caspase-independent commitment phase to apoptosis in activated blood T lymphocytes: reversibility at low apoptotic insult. *Blood.* 2000; 96(3): 1030-1038.

Dykens J A: Isolated cerebral and cerebellar mitochondria produce free radicals when exposed to elevated Ca^{2+} and Na^{2+}: implications for neurodegeneration. *J. Neurochem.* 1994; 63(2): 584-591.

Eguchi Y, Shimizu S, Tsujimoto Y: Intracellular ATP levels determine cell death fate by apoptosis or necrosis. *Cancer Res.* 1997; 57(10): 1835-1840.

Ernst MK, Dunn LL, Rice NR: The PEST-like sequence of I kappa B alpha is responsible for inhibition of DNA binding but not for cytoplasmic retention of c-Rel or RelA homodimers. *Mol Cell Biol.* 1995; 15(2): 872-882.

A

Ferri KF, Jacotot E, Blanco J, Este JA, Zamzami N, Susin SA, Xie Z, Brothers G, Reed JC, Penninger JM, Kroemer G: Apoptosis control in syncytia induced by the HIV type 1-envelope glycoprotein complex: role of mitochondria and caspases. *J Exp Med.* 2000; 192(8): 1081-1092.

B

Ferri KF, Jacotot E, Leduc P, Geuskens M, Ingber DE, Kroemer G: Apoptosis of syncytia induced by the HIV-1-envelope glycoprotein complex: influence of cell shape and size. *Exp Cell Res.* 2000; 261(1): 119-126.

C

Ferri KF, Jacotot E, Blanco J, Este JA, Kroemer G: Mitochondrial control of cell death induced by HIV-1-encoded proteins. *Ann N Y Acad Sci*. 2000; 926: 149-164.

Fire A, Xu S, Montgomery MK, Kostas SA, Driver SE, Mello CC: Potent and specific genetic interference by double-stranded RNA in Caenorhabditis elegans. *Nature.* 1998; 391(6669): 806-811.

Fonfria E, Dare E, Benelli M, Sunol C, Ceccatelli S: Translocation of apoptosis-inducing factor in cerebellar granule cells exposed to neurotoxic agents inducing oxidative stress. *Eur J Neurosci.* 2002; 16(10): 2013-2016.

Forman HJ and **Boveris A**: Superoxide radical and hydrogen peroxide in mitochondria. 1982. In "Free Radicals in Biology. Vol V" (W.A. Pryor ed.) Academic Press, New York: 65-90.

Fridovich I: The biology of oxygen radicals. *Science.* 1978; 201: 875-880.

Fukami T, Nakasu S, Baba K, Nakajima M, Matsuda M: Hyperthermia induces translocation of apoptosis-inducing factor (AIF) and apoptosis in human glioma cell lines. *J Neurooncol.* 2004; 70(3): 319-331.

Genini D, Sheeter D, Rought S, Zaunders JJ, Susin SA, Kroemer G, Richman DD, Carson DA, Corbeil J, Leoni LM: HIV induces lymphocyte apoptosis by a p53-initiated, mitochondrial-mediated mechanism. *FASEB J.* 2001; 15(1): 5-6.

Genova ML, Ventura B, Giuliano G, Bovina C, Formiggini G, Parenti Castelli G, Lenaz G: The site of production of superoxide radical in mitochondrial Complex I is not a bound ubisemiquinone but presumably iron-sulfur cluster N2. *FEBS Lett.* 2001; 505(3): 364-368.

Goldstein JC, Waterhouse NJ, Juin P, Evan GI, Green DR: The coordinate release of cytochrome c during apoptosis is rapid, complete and kinetically invariant. *Nat Cell Biol.* 2000; 2(3): 156-162.

Grantz AA, Brummell DA, Bennett AB: Ascorbate free radical reductase mRNA levels are induced by wounding. *Plant Physiol.* 1995; 108(1): 411-418.

Green D, Kroemer G: The central executioners of apoptosis: caspases or mitochondria? *Trends Cell Biol.* 1998; 8(7): 267-271.

Grigorieff N: Three-dimensional structure of bovine NADH:ubiquinone oxidoreductase (complex I) at 22 A in ice. *J Mol Biol.* 1998; 277(5): 1033-1046.

Grilli M, Chiu JJ, Lenardo MJ: NF-kappa B and Rel: participants in a multiform transcriptional regulatory system. *Int Rev Cytol.* 1993; 143: 1-62.

Hakem R, Hakem A, Duncan GS, Henderson JT, Woo M, Soengas MS, Elia A, de la Pompa JL, Kagi D, Khoo W, Potter J, Yoshida R, Kaufman SA, Lowe SW, Penninger JM, Mak TW: Differential requirement for caspase 9 in apoptotic pathways in vivo. *Cell.* 1998; 94(3): 339-352.

Halvey PJ, **Watson WH**, **Hansen JM**, **Go YM**, **Samali A**, **Jones DP**:

Compartmental oxidation of thiol-disulphide redox couples during epidermal growth factor signalling. *Biochem J.* 2005; 386(Pt 2): 215-219.

Han D, Antunes F, Canali R, Rettori D, Cadenas E: Voltage-dependent anion channels control the release of the superoxide anion from mitochondria to cytosol. *J Biol Chem.* 2003; 278: 5557-5563.

Harman D: Aging: A theory based on free radical and radiation chemistry. *J Gerontol.* 1956; 11: 298-300.

Hirsch T, Marchetti P, Susin SA, Dallaporta B, Zamzami N, Marzo I, Geuskens M, Kroemer G.: The apoptosis-necrosis paradox. Apoptogenic proteases activated after mitochondrial permeability transition determine the mode of cell death. *Oncogene.* 1997; 15(13): 1573-1581.

Hirst J, Carroll J, Fearnley IM, Shannon RJ, Walker JE: The nuclear encoded subunits of complex I from bovine heart mitochondria. *Biochim Biophys Acta.* 2003; 1604(3): 135-150.

Hisatomi T, Sakamoto T, Murata T, Yamanaka I, Oshima Y, Hata Y, Ishibashi T, Inomata H, Susin SA, Kroemer G: Relocalization of apoptosis-inducing factor in photoreceptor apoptosis induced by retinal detachment in vivo. *Am J Pathol.* 2001; 158(4): 1271-1278.

Hisatomi T, Sakamoto T, Goto Y, Yamanaka I, Oshima Y, Hata Y, Ishibashi T, Inomata H, Susin SA, Kroemer G: Critical role of photoreceptor apoptosis in functional damage after retinal detachment. *Curr Eye Res.* 2002; 24(3): 161-172.

Hofhaus G, Shakeley RM, Attardi G: Use of polarography to detect respiration defects in cell cultures *Methods Enzymol.* 1996; 264: 476–483.

Hoshino T, Nakamura H, Okamoto M, Kato S, Araya S, Nomiyama K, Oizumi K, Young HA, Aizawa H, Yodoi J: Redox-active protein thioredoxin prevents proinflammatory cytokine- or bleomycin-induced lung injury. *Am J Respir Crit Care Med.* 2003; 168(9): 1075-1083.

Hotta M, Tashiro F, Ikegami H, Niwa H, Ogihara T, Yodoi J, Miyazaki J: Pancreatic beta cell-specific expression of thioredoxin, an antioxidative and antiapoptotic protein, prevents autoimmune and streptozotocin-induced diabetes. *J Exp Med.* 1998; 188(8): 1445-1451.

Jacobson MD, Weil M, Raff MC: Programmed cell death in animal development. *Cell.* 1997; 88(3): 347-354.

Jacotot E, Ravagnan L, Loeffler M, Ferri KF, Vieira HL, Zamzami N, Costantini P, Druillennec S, Hoebeke J, Briand JP, Irinopoulou T, Daugas E, Susin SA, Cointe D, Xie ZH, Reed JC, Roques BP, Kroemer G: The HIV-1 viral protein R induces apoptosis via a direct effect on the mitochondrial permeability transition pore. *J Exp Med.* 2000; 191(1): 33-46.

Jaiswal AK: Regulation of genes encoding NAD(P)H:quinone oxidoreductases. *Free Rad Biol Med.* 2000; 29(3-4): 254-262.

Jarasch ED, Grund C, Bruder G, Heid HW, Keenan TW, Franke WW: Localization of xanthine oxidase in mammary-gland epithelium and capillary endothelium. *Cell.* 1981; 25(1): 67-82.

Jellinger KA: Post mortem studies in Parkinson's disease--is it possible to detect brain areas for specific symptoms? *J Neural Transm Suppl.* 1999; 56: 1-29.

Jezek P, Hlavata L: Mitochondria in homeostasis of reactive oxygen species in cell, tissues and organism. *Int J Biochem Cell Biol.* 2005; 37: 2478-2503.

Jimenez A, Hernandez JA, Pastori G, del Rio LA, Sevilla F: Role of the ascorbate-glutathione cycle of mitochondria and peroxisomes in the senescence of pea leaves *Plant Physiol.* 1998; 118(4): 1327-1335.

Joza N, Susin SA, Daugas E, Stanford WL, Cho SK, Li CY, Sasaki T, Elia AJ, Cheng HY, Ravagnan L, Ferri KF, Zamzami N, Wakeham A, Hakem R, Yoshida H, Kong YY, Mak TW, Zuniga-Pflucker JC, Kroemer G, Penninger JM: Essential role of the mitochondrial apoptosis-inducing factor in programmed cell death. *Nature.*

2001; 410(6828): 549-554.

Joza N, **Oudit GY**, **Brown D**, **Bénit P**, **Kassiri Z**, **Vahsen N**, **Benoit L**, **Patel MM**, **Nowikovsky K**, **Vassault A**, **Backx PH**, **Wada T**, **Kroemer G**, **Rustin P**, **Penninger JM:** Muscle-specific loss of apoptosis-inducing factor leads to mitochondrial dysfunction, skeletal muscle atrophy, and dilated cardiomyopathy. *Mol Cell Biol.* 2005; 25(23): 10261-10272.

Kang SW, Chae HZ, Seo MS, Kim K, Baines IC, Rhee SG: Mammalian peroxiredoxin isoforms can reduce hydrogen peroxide generated in response to growth factors and tumor necrosis factor-alpha. *J Biol Chem.* 1998; 273: 6297-6302.

Keeney PM, Xie J, Capaldi RA, Bennett JP Jr: Parkinson's disease brain mitochondrial complex I has oxidatively damaged subunits and is functionally impaired and misassembled. *J Neurosci.* 2006; 26(19): 5256-5264.

Kim MR, Chang HS, Kim BH, Kim S, Baek SH, Kim JH, Lee SR, Kim JR: Involvements of mitochondrial thioredoxin reductase (TrxR2) in cell proliferation. *Biochem Biophys Res Commun.* 2003; 304: 119-124.

Klein JA, Longo-Guess CM, Rossmann MP, Seburn KL, Hurd RE, Frankel WN, Bronson RT, Ackerman SL: The harlequin mouse mutation downregulates apoptosis-inducing factor. *Nature.* 2002; 419(6905): 367-374.

Klein JA, Ackerman SL: Oxidative stress, cell cycle and neurodegeneration. *J Clin Invest.* 2003; 111: 785-793.

Kobayashi T, **Kishigami S**, **Sone M**, **Inokuchi H**, **Mogi T**, **Ito K**: Respiratory chain is required to maintain oxidized states of the DsbA-DsbB disulfide bond formation system in aerobically growing Escherichia coli cells. *Proc Natl Acad Sci U S A.* 1997; 94(22): 11857-11862.

Krajewski S, Krajewska M, Ellerby LM, Welsh K, Xie Z, Deveraux QL, Salvesen GS, Bredesen DE, Rosenthal RE, Fiskum G, Reed JC: Release of caspase-9 from mitochondria during neuronal apoptosis and cerebral ischemia. *Proc*

Natl Acad Sci U S A. 1999; 96(10): 5752-5757.

Krantic S, Mechawar N, Reix S, Quirion R: Apoptosis-inducing factor: A matter of neuron life and death. *Prog Neurobiol.* 2007; 81(3): 179-196.

Krishnamoorthy G, Hinkle PC: Studies on the electron transfer pathway, topography of iron-sulfur centers, and site of coupling in NADH-Q oxidoreductase. *J Biol Chem.* 1988; 263(33): 17566-17575.

Kroemer G, Reed JC: Mitochondrial control of cell death. *Nat Med.* 2000; 6(5): 513-519.

Kudin AP, **Bimpong-Buta NY**, **Vielhaber S**, **Elger CE**, **Kunz WS**: Characterization of superoxide-producing sites in isolated brain mitochondria. *J Biol Chem.* 2004; 279(6): 4127-4135.

Kushnareva Y, Murphy AN, Andreyev A: Complex I-mediated reactive oxygen species generation: modulation by cytochrome c and NAD(P)+ oxidation-reduction state. *Biochem J.* 2002; 368(Pt 2): 545-553.

Laemmli UK: Cleavage of structural proteins during the assembly of the head of bacteriophage T4. *Nature.* 1970; 227(5259): 680-685.

Lagarkova MA, Iarovaia OV, Razin SV: Large-scale fragmentation of mammalian DNA in the course of apoptosis proceeds via excision of chromosomal DNA loops and their oligomers. *J Biol Chem.* 1995; 270(35): 20239-20241.

Lassus P, Opitz-Araya X, Lazebnik Y: Requirement for caspase-2 in stress-induced apoptosis before mitochondrial permeabilization. *Science.* 2002; 297(5585): 1352-1354.

Lebovitz RM, **Zhang H**, **Vogel H**, **Cartwright J Jr**, **Dionne L**, **Lu N**, **Huang S**, **Matzuk MM:** Neurodegeneration, myocardial injury, and perinatal death in mitochondrial superoxide dismutase-deficient mice. *Proc Natl Acad Sci U S A.* 1996; 93(18): 9782-9787.

Leek RD, Stratford I, Harris AL: The role of hypoxia-inducible factor-1 in three-dimensional tumor growth, apoptosis, and regulation by the insulin-signaling pathway. *Cancer Res.* 2005; 65: 4147–4152.

Lehninger AL: The mitochondrion; molecular basis of structure and function. New York, W.A. Benjamin, 1964.

Leist M, Single B, Castoldi AF, Kuhnle S, Nicotera P: Intracellular adenosine triphosphate (ATP) concentration: a switch in the decision between apoptosis and necrosis. *J Exp Med.* 1997; 185(8): 1481-1486.

Li HY, Wu SY, Shi N: Transcription factor Nrf2 activation by deltamethrin in PC12 cells: Involvement of ROS. *Toxicol Lett.* 2007; 171(1-2): 87-98.

Li K, Li Y, Shelton JM, Richardson JA, Spencer E, Chen ZJ, Wang X, Williams RS: Cytochrome c deficiency causes embryonic lethality and attenuates stress-induced apoptosis. *Cell.* 2000; 101(4): 389-399.

Liou AK, Zhou Z, Pei W, Lim TM, Yin XM, Chen J: BimEL up-regulation potentiates AIF translocation and cell death in response to MPTP. *FASEB J.* 2005; 19(10): 1350-1352.

Liu X, Kim CN, Yang J, Jemmerson R, Wang X.: Induction of apoptotic program in cell-free extracts: requirement for dATP and cytochrome c. *Cell.* 1996; 86(1): 147-157.

Loeffler M, Kroemer G: The mitochondrion in cell death control: certainties and incognita. *Exp Cell Res.* 2000; 256(1): 19-26.

Loeffler M, Daugas E, Susin SA, Zamzami N, Metivier D, Nieminen AL, Brothers G, Penninger JM, Kroemer G: Dominant cell death induction by extramitochondrially targeted apoptosis-inducing factor. *FASEB J.* 2001; 15(3): 758-767.

Lorenzo HK, Susin SA, Penninger J, Kroemer G: Apoptosis inducing factor (AIF): a phylogenetically old, caspase-independent effector of cell death. *Cell Death Differ.*

1999; 6(6): 516-524.

Lorenzo HK, **Susin SA :** Mitochondrial effectors in caspase-independent cell death. *FEBS Lett.* 2004; 557(1-3): 14-20.

Loschen G, Flohe L, Chance B: Respiratory chain linked H(2)O(2) production in pigeon heart mitochondria. *FEBS Lett.* 1971; 18: 261-264.

Maas E, **Bisswanger H**: Localization of the alpha-oxoacid dehydrogenase multienzyme complexes within the mitochondrion. *FEBS Lett.* 1990; 277(1-2): 189-190.

Mancini M, Nicholson DW, Roy S, Thornberry NA, Peterson EP, Casciola-Rosen LA, Rosen A: The caspase-3 precursor has a cytosolic and mitochondrial distribution: implications for apoptotic signaling. *J Cell Biol.* 1998; 140(6): 1485-1495.

Mansfield KD, Guzy RD, Pan Y, Young RM, Cash TP, Schumacker PT, Simon MC: Mitochondrial dysfunction resulting from loss of cytochrome c impairs cellular oxygen sensing and hypoxic HIF-alpha activation. *Cell Metab.* 2005; 1(6): 393-399.

Marklund SL, Westman NG, Lundgren E, Roos G: Copper- and zinc-containing superoxide dismutase, manganese-containing superoxide dismutase, catalase, and glutathione peroxidase in normal and neoplastic human cell lines and normal human tissues. *Cancer Res*. 1982; 42(5): 1955-1961.

Marttila RJ, **Roytta M**, **Lorentz H**, **Rinne UK**: Oxygen toxicity protecting enzymes in the human brain. *J Neural Transm.* 1988; 74(2): 87-95.

Marzo I, Brenner C, Zamzami N, Jurgensmeier JM, Susin SA, Vieira HL, Prevost MC, Xie Z, Matsuyama S, Reed JC, Kroemer G: Bax and adenine nucleotide translocator cooperate in the mitochondrial control of apoptosis. *Science*. 1998; 281(5385): 2027-2031.

Massey V: Activation of molecular oxygen by flavins and flavoproteins. *J Biol Chem.* 1994; 269(36): 22459-22462.

Masutani H, Ueda S, Yodoi J: The thioredoxin system in retroviral infection and apoptosis. *Cell Death Differ.* 2005; 12 Suppl 1: 991-998.

Mate MJ, Ortiz-Lombardia M, Boitel B, Haouz A, Tello D, Susin SA, Penninger J, Kroemer G, Alzari PM: The crystal structure of the mouse apoptosis-inducing factor AIF. *Nat Struct Biol.* 2002; 9(6): 442-446.

Matsui M, Oshima M, Oshima H, Takaku K, Maruyama T, Yodoi J, Taketo MM: Early embryonic lethality caused by targeted disruption of the mouse thioredoxin gene. *Dev Biol.* 1996; 178(1): 179-185.

Mattiazzi M, Vijayvergiya C, Gajewski CD, DeVivo DC, Lenaz G, Wiedmann M, Manfredi G: The mtDNA T8993G (NARP) mutation results in an impairment of oxidative phosphorylation that can be improved by antioxidants. *Hum Mol Genet.* 2004; 13(8): 869-879.

McCarthy NJ, Whyte MK, Gilbert CS, Evan GI: Inhibition of Ced-3/ICE-related proteases does not prevent cell death induced by oncogenes, DNA damage, or the Bcl-2 homologue Bak. *J Cell Biol.* 1997; 136(1): 215-227.

Minamikawa T, Williams DA, Bowser DN, Nagley P: Mitochondrial permeability transition and swelling can occur reversibly without inducing cell death in intact human cells. *Exp Cell Res.* 1999; 246: 26-37.

Miramar MD, Costantini P, Ravagnan L, Saraiva LM, Haouzi D, Brothers G, Penninger JM, Peleato ML, Kroemer G, Susin SA: NADH oxidase activity of mitochondrial apoptosis-inducing factor. *J Biol Chem.* 2001; 276(19): 16391-16398.

Mitchell P, Moyle J: Stoichiometry of proton translocation through the respiratory chain and adenosine triphosphatase systems of rat liver mitochondria. *Nature.* 1965; 208: 147-151.

Mitsui A, Hamuro J, Nakamura H, Kondo N, Hirabayashi Y, Ishizaki-Koizumi S, Hirakawa T, Inoue T, Yodoi J: Overexpression of human thioredoxin in transgenic mice controls oxidative stress and life span. *Antioxid Redox Signal.* 2002;

4(4): 693-696.

Mohanty JG, Jaffe JS, Schulman ES, Raible DG: A highly sensitive fluorescent micro-assay of H_2O_2 release from activated human leukocytes using a dihydroxyphenoxazine derivative. *J Immunol Methods*. 1997; 202: 133-141.

Moi P, Chan K, Asunis I, Cao A, Kan YW: Isolation of NF-E2-related factor 2 (Nrf2), a NF-E2-like basic leucine zipper transcriptional activator that binds to the tandem NF-E2/AP1 repeat of the beta-globin locus control region. *Proc Natl Acad Sci U S A.* 1994; 91(21): 9926-9930.

Mosmann T: Rapid Colorimetric Assay for Cellular Growth and Survival: Application to Proliferation and Cytotoxicity Assays. *J Immunol Methods.* 1983; 65: 55-63.

Muller FL, Roberts AG, Bowman MK, Kramer DM: Architecture of the Qo site of the cytochrome bc_1 complex probed by superoxide production. *Biochemistry*. 2003; 42: 6493-6499.

Nguyen T, Sherratt PJ, Huang HC, Yang CS, Pickett CB: Increased protein stability as a mechanism that enhances Nrf2-mediated transcriptional activation of the antioxidant response element. Degradation of Nrf2 by the 26 S proteasome. *J Biol Chem.* 2003; 278(7): 4536-4541.

Nicholls DG, Locke RM: Thermogenic mechanisms in brown fat. *Physiol Rev.* 1984; 64: 1-64.

Nieminen AL, Byrne AM, Herman B, Lemasters JJ: Mitochondrial permeability transition in hepatocytes induced by t-BuOOH: NAD(P)H and reactive oxygen species. *Am J Physiol.* 1997; 272(4 Pt 1): C1286-1294.

Nohl H, **Gille L**, **Staniek K**: Intracellular generation of reactive oxygen species by mitochondria. *Biochem Pharmacol.* 2005; 69(5): 719-723.

Nonn L, Williams RR, Erickson RP, Powis G: The absence of mitochondrial thioredoxin 2 causes massive apoptosis, exencephaly, and early embryonic lethality in

homozygous mice. *Mol Cell Biol.* 2003; 23(3): 916-922.

Nordberg J, Arnér ES: Reactive oxygen species, antioxidants, and the mammalian thioredoxin system. *Free Radic Biol Med.* 2001; 31: 1287-1312.

Nulton-Persson AC, Szweda LI: Modulation of mitochondrial function by hydrogen peroxide. *J Biol Chem.* 2001; 276(26): 23357-23361.

Ohiro Y, Garkavtsev I, Kobayashi S, Sreekumar KR, Nantz R, Higashikubo BT, Duffy SL, Higashikubo R, Usheva A, Gius D, Kley N, Horikoshi N: A novel p53-inducible apoptogenic gene, PRG3, encodes a homologue of the apoptosis-inducing factor (AIF). *FEBS Lett.* 2002; 524(1-3): 163-171.

Okouchi M, **Ekshyyan O**, **Maracine M**, **Aw TY**: Neuronal apoptosis in neurodegeneration. *Antioxid Redox Signal.* 2007; 9(8): 1059-1096.

Otera H, Ohsakaya S, Nagaura Z-I, Ishihara N, Mihara K: Export of mitochondrial AIF in response to proapoptotic stimuli depends on processing at the intermembrane space. *EMBO J.* 2005; 14: 1375-1386.

Pani G, Bedogni B, Colavitti R, Anzevino R, Borrello S, Galeotti T: Cell compartmentalization in redox signaling. *IUBMB Life.* 2001, 52: 7-16.

Paradies G, Petrosillo G, Pistolese M, Di Venosa N, Federici A, Ruggiero FM: Decrease in mitochondrial Complex I activity in Ischemic/Reperfused Rat Heart. Involvement of reactive oxygen species and cardiolipin. *Circ Res.* 2004; 94(1): 53-59.

Pastorino JG, Chen ST, Tafani M, Snyder JW, Farber JL: The overexpression of Bax produces cell death upon induction of the mitochondrial permeability transition. *J Biol Chem.* 1998, 273(13): 7770-7775.

Patenaude A, Ven Murthy MR, Mirault ME: Mitochondrial thioredoxin system: effects of TrxR2 overexpression on redox balance, cell growth, and apoptosis. *J Biol Chem.* 2004; 279(26): 27302-27314.

Petit PX, Goubern M, Diolez P, Susin SA, Zamzami N, Kroemer G: Disruption of the outer mitochondrial membrane as a result of large amplitude swelling: the impact of irreversible permeability transition. *FEBS Lett.* 1998; 426(1): 111-116.

Petrosillo G, Ruggiero FM, Di Venosa N, Paradies G: Decreased Complex III activity in mitochondria isolated from rat heart subjected to ischemia and reperfusion: role of reactive oxygen species and cardiolipin. *FASEB J.* 2003; 17(6): 714-716.

Pi J, Qu W, Reece JM, Kumagai Y, Waalkes MP: Transcription factor Nrf2 activation by inorganic arsenic in cultured keratinocytes: involvement of hydrogen peroxide. *Exp Cell Res.* 2003; 290(2): 234-245.

Piette J, **Piret B**, **Bonizzi G**, **Schoonbroodt S**, **Merville MP**, **Legrand-Poels S**, **Bours V:** Multiple redox regulation in NF-kappaB transcription factor activation. *Biol Chem.* 1997; 378(11): 1237-1245.

Pitkanen S, Robinson BH: Mitochondrial complex I deficiency leads to increased production of superoxide radicals and induction of superoxide dismutase. *J Clin Invest.* 1996; 98(2): 345-351.

Powis G, **Montfort WR**: Properties and biological activities of thioredoxins. *Annu Rev Pharmacol Toxicol.* 2001; 41: 261-295.

Quignon F, De Bels, F, Koken M, Feunteun J, Ameisen J C, de The H: PML induces a novel caspase-independent death process. *Nat. Genet.* 1998; 20: 259-265.

Quillet-Mary A, **Jaffrezou JP**, **Mansat V**, **Bordier C**, **Naval J**, **Laurent G**: Implication of mitochondrial hydrogen peroxide generation in ceramide-induced apoptosis. *J Biol Chem.* 1997; 272(34): 21388-21395.

Ramos-Gomez M, Kwak MK, Dolan PM, Itoh K, Yamamoto M, Talalay P, Kensler TW: Sensitivity to carcinogenesis is increased and chemoprotective efficacy of enzyme inducers is lost in nrf2 transcription factor-deficient mice. *Proc Natl Acad Sci U S A.* 2001; 98(6): 3410-3415.

Ravagnan L, Gurbuxani S, Susin SA, Maisse C, Daugas E, Zamzami N, Mak T, Jaattela M, Penninger JM, Garrido C, Kroemer G: Heat-shock protein 70 antagonizes apoptosis-inducing factor. *Nat Cell Biol.* 2001; 3(9): 839-843.

Reaume AG, **Elliott JL**, **Hoffman EK**, **Kowall NW**, **Ferrante RJ**, **Siwek DF**, **Wilcox HM**, **Flood DG**, **Beal MF**, **Brown RH Jr**, **Scott RW**, **Snider WD**: Motor neurons in Cu/Zn superoxide dismutase-deficient mice develop normally but exhibit enhanced cell death after axonal injury. *Nat Genet.* 1996; 13(1): 43-47.

Reix S, Mechawar N, Susin SA, Quirion R, Krantic S: Expression of cortical and hippocampal apoptosis-inducing factor (AIF) in aging and Alzheimer's disease. *Neurobiol Aging.* 2007; 28(3): 351-356.

Rice G, Bump EA, Shrieve DC, Lee W, Kovacs M: Quantitative analysis of cellular glutathione by flow cytometry utilizing monochlorobimane: some applications to radiation and drug resistance in vitro and in vivo. *Cancer Res.* 1986; 46: 6105-6110.

Ritz D, **Beckwith J**: Roles of thiol-redox pathways in bacteria. *Annu Rev Microbiol.* 2001; 55: 21-48.

Robinson BH: Human Complex I deficiency: clinical spectrum and involvement of oxygen free radicals in the pathogenicity of the defect. *Biochym. Biophys. Acta.* 1998; 1364(2): 271-286.

Robinson KM, Lemire BD: A requirement for matrix processing peptidase but not for mitochondrial chaperonin in the covalent attachment of FAD to the yeast succinate dehydrogenase flavoprotein. *J Biol Chem.* 1996; 271(8): 4061-4067.

Rogers S, Wells R, Rechsteiner M: Amino acid sequences common to rapidly degraded proteins: the PEST hypothesis. *Science.* 1986; 234(4774): 364-368.

Rosenstock TR, **Carvalho AC**, **Jurkiewicz A**, **Frussa-Filho R**, **Smaili SS**: Mitochondrial calcium, oxidative stress and apoptosis in a neurodegenerative disease model induced by 3-nitropropionic acid. *J Neurochem.* 2004; 88(5): 1220-1228.

Rossmann MG, Liljas A, Branden CI, Benaszak LJ: Evolutionary and structural relationships among dehydrogenases.1975. In: Boyer, PD (ed), The Enzymes Vol.11, Oxidation-Reduction, Ch2, pp61-102, Academic Press, New York.

Rothe G, Valet G: Flow cytometric analysis of respiratory burst activity in phagocytes with hydroethidine and 2',7'-dichlorofluorescin. *J Leukoc Biol.* 1990; 47(5): 440-448.

Rozell B, Hansson HA, Luthman M, Holmgren A: Immunohistochemical localization of thioredoxin and thioredoxin reductase in adult rats. *Eur J Cell Biol.* 1985; 38(1): 79-86.

Rushmore TH, Morton MR, Pickett CB: The antioxidant responsive element. Activation by oxidative stress and identification of the DNA consensus sequence required for functional activity. *J Biol Chem.* 1991; 266(18): 11632-11639.

Rustin P, **von Kleist-Retzow JC**, **Vajo Z**, **Rotig A**, **Munnich A**: For debate: defective mitochondria, free radicals, cell death, aging-reality or myth-ochondria? *Mech Ageing Dev.* 2000; 114(3): 201-206.

Sahara S, Aoto M, Eguchi Y, Imamoto N, Yoneda Y, Tsujimoto Y: Acinus is a caspase-3-activated protein required for apoptotic chromatin condensation. *Nature.* 1999; 401(6749): 168-173.

Samejima K, Tone S, Kottke TJ, Enari M, Sakahira H, Cooke CA, Durrieu F, Martins LM, Nagata S, Kaufmann SH, Earnshaw WC: Transition from caspase-dependent to caspase-independent mechanisms at the onset of apoptotic execution. *J Cell Biol.* 1998; 143(1): 225-239.

Sauer H, Wartenberg M, Hescheler J: Reactive oxygen species as intracellular messengers during cell growth and differentiation. *Cell Physiol Biochem*. 2001; 11: 173-186.

Schägger H: Respiratory chain supercomplexes of mitochondria and bacteria. *Biochim Biophys Acta.* 2002; 1555(1-3): 154-159.

Schägger H, **de Coo R**, **Bauer MF**, **Hofmann S**, **Godinot C**, **Brandt U**: Significance of respirasomes for the assembly/stability of human respiratory chain complex I. *J Biol Chem.* 2004; 279(35): 36349-36353.

Schindler CK, Pearson EG, Bonner HP, So NK, Simon RP, Prehn JH, Henshall DC: Caspase-3 cleavage and nuclear localization of caspase-activated DNase in human temporal lobe epilepsy. *J Cereb Blood Flow Metab.* 2006; 26(4): 583-589.

Sebastiá J, Cristofol R, Martin M, Rodriguez-Farre E, Sanfeliu C: Evaluation of fluorescent dyes for measuring intracellular glutathione content in primary cultures of human neurons and neuroblastoma SH-SY5Y. *Cytometry A.* 2003; 51(1): 16-25.

Semenza GL, Wang GL: A nuclear factor induced by hypoxia via de novo protein synthesis binds to the human erythropoietin gene enhancer at a site required for transcriptional activation. *Mol Cell Biol.* 1992; 12(12): 5447-5454.

Severinghaus JW, Astrup PB: History of blood gas analysis. IV. Leland Clark's oxygen electrode. *J Clin Monit.* 1986; 2: 125-139.

Shigenaga MK, Hagen TM, Ames BN: Oxidative damage and mitochondrial decay in aging. *Proc Natl Acad Sci U S A.* 1994; 91: 10771-10778.

Shih AY, **Imbeault S**, **Barakauskas V**, **Erb H**, **Jiang L**, **Li P**, **Murphy TH**: Induction of the Nrf2-driven antioxidant response confers neuroprotection during mitochondrial stress in vivo. *J Biol Chem.* 2005; 280(24): 22925-22936.

Shimizu S, Narita M, Tsujimoto Y: Bcl-2 family proteins regulate the release of apoptogenic cytochrome c by the mitochondrial channel VDAC. *Nature.* 1999; 399(6735): 483-487.

Smith AG: Culture and differentiation of embryonic stem cells. *J Tiss Cult Meth.* 1991; 13: 89-94.

Spyrou G, **Enmark E**, **Miranda-Vizuete A**, **Gustafsson J:** Cloning and expression of a novel mammalian thioredoxin. *J Biol Chem.* 1997; 272(5): 2936-2941.

Starkov AA, Fiskum G, Chinopoulos C, Lorenzo BJ, Browne SE, Patel MS, Beal MF: Mitochondrial alpha-ketoglutarate dehydrogenase complex generates reactive oxygen species. *J Neurosci.* 2004; 24(36): 7779-7788.

Sui G, **Soohoo C**, **Affar el B**, **Gay F**, **Shi Y**, **Forrester WC**, **Shi Y**: A DNA vector-based RNAi technology to suppress gene expression in mammalian cells. *Proc Natl Acad Sci U S A.* 2002; 99(8): 5515-5520.

Sumegi B, Srere PA: Complex I binds several mitochondrial NAD-coupled dehydrogenases. *J Biol Chem.* 1984; 259(24): 15040-15045.

Sun XM, MacFarlane M, Zhuang J, Wolf BB, Green DR, Cohen GM: Distinct caspase cascades are initiated in receptor-mediated and chemical-induced apoptosis. *J Biol Chem.* 1999; 274(8): 5053-5060.

Susin SA, Zamzami N, Castedo M, Hirsch T, Marchetti P, Macho A, Daugas E, Geuskens M, Kroemer G: Bcl-2 inhibits the mitochondrial release of an apoptogenic protease. *J Exp Med.* 1996; 184(4): 1331-1341.

Susin SA, Zamzami N, Castedo M, Daugas E, Wang HG, Geley S, Fassy F, Reed JC, Kroemer G: The central executioner of apoptosis: multiple connections between protease activation and mitochondria in Fas/APO-1/CD95- and ceramide-induced apoptosis. *J Exp Med.* 1997; 186(1): 25-37.

A
Susin SA, Lorenzo HK, Zamzami N, Marzo I, Brenner C, Larochette N, Prevost MC, Alzari PM, Kroemer G: Mitochondrial release of caspase-2 and -9 during the apoptotic process. *J Exp Med.* 1999; 189(2): 381-394.

B
Susin SA, Lorenzo HK, Zamzami N, Marzo I, Snow BE, Brothers GM, Mangion J, Jacotot E, Costantini P, Loeffler M, Larochette N, Goodlett DR, Aebersold R, Siderovski DP, Penninger JM, Kroemer G: Molecular characterization of mitochondrial apoptosis-inducing factor. *Nature.* 1999; 397(6718): 441-446.

Susin SA, Daugas E, Ravagnan L, Samejima K, Zamzami N, Loeffler M, Costantini P, Ferri KF, Irinopoulou T, Prevost MC, Brothers G, Mak TW, Penninger J, Earnshaw WC, Kroemer G: Two distinct pathways leading to nuclear apoptosis. *J Exp Med.* 2000; 192(4): 571-580.

Swerdlow RH, Parks JK, Miller SW, Tuttle JB, Trimmer PA, Sheehan JP, Bennet Jr JP, Davis RE, Parker WD Jr: Origin and functional consequences of the complex I defect in Parkinson´s disease. *Annals Neurol.* 1996; 40: 663-671.

Szewczyk A, Wojtczak L: Mitochondria as a pharmacological target. *Pharmacol Rev.* 2002; 54: 101-127.

Taha TA, **Mullen TD**, **Obeid LM**: A house divided: ceramide, sphingosine, and sphingosine-1-phosphate in programmed cell death. *Biochim Biophys Acta.* 2006; 1758(12): 2027-2036.

Takagi Y, Mitsui A, Nishiyama A, Nozaki K, Sono H, Gon Y, Hashimoto N, Yodoi J: Overexpression of thioredoxin in transgenic mice attenuates focal ischemic brain damage. *Proc Natl Acad Sci U S A.* 1999; 96(7): 4131-4136.

Tanaka T, Hosoi F, Yamaguchi-Iwai Y, Nakamura H, Masutani H, Ueda S, Nishiyama A, Takeda S, Wada H, Spyrou G, Yodoi J: Thioredoxin-2 (TRX-2) is an essential gene regulating mitochondria-dependent apoptosis. *EMBO J.* 2002; 21(7): 1695-1703.

Tarpey MM, Wink DA, Grisham MB: Methods for detection of reactive metabolites of oxygen and nitrogen: in vitro and in vivo considerations. *Am J Physiol Regul Integr Comp Physiol.* 2004; 286: R431-444.

Thompson CB: Apoptosis in the pathogenesis and treatment of disease. *Science.* 1995; 267(5203): 1456-1462.

Toomey D, Mayhew SG: Purification and characterisation of NADH oxidase from Thermus aquaticus YT-1 and evidence that it functions in a peroxide-reduction system. *Eur J Biochem.* 1998; 251(3): 935-945.

Trbovich AM, Hughes FM Jr, Perez GI, Kugu K, Tilly KI, Cidlowski JA, Tilly JL: High and low molecular weight DNA cleavage in ovarian granulosa cells: characterization and protease modulation in intact cells and in cell-free nuclear autodigestion assays. *Cell Death Differ.* 1998; 5(1): 38-49.

Tretter L, Adam-Vizi V: Generation of reactive oxygen species in the reaction catalyzed by alpha-ketoglutarate dehydrogenase. *J Neurosci.* 2004; 24(36): 7771-7778.

Tretter L, Adam-Vizi V: Alpha-ketoglutarate dehydrogenase: a target and generator of oxidative stress. *Philos Trans R Soc Lond B Biol Sci.* 2005; 360: 2335-2345.

Tyler DD: The mitochondrion in health and disease. VCH Publishers. 1992; London, 1-557.

Ueno M, Masutani H, Arai RJ, Yamauchi A, Hirota K, Sakai T, Inamoto T, Yamaoka Y, Yodoi J, Nikaido T: Thioredoxin-dependent redox regulation of p53-mediated p21 activation. *J Biol Chem.* 1999; 274(50): 35809-35815.

Urbano A, Lakshmanan U, Choo PH, Kwan JC, Ng PY, Guo K, Dhakshinamoorthy S, Porter A: AIF suppresses chemical stress-induced apoptosis and maintains the transformed state of tumor cells. *EMBO J.* 2005; 24: 2815-2826.

Vahsen N, Cande C, Briere JJ, Benit P, Joza N, Larochette N, Mastroberardino PG, Pequignot MO, Casares N, Lazar V, Feraud O, Debili N, Wissing S, Engelhardt S, Madeo F, Piacentini M, Penninger JM, Schagger H, Rustin P, Kroemer G: AIF deficiency compromises oxidative phosphorylation. *EMBO J.* 2004; 23(23): 4679-4689.

Vahsen N, Cande C, Dupaigne P, Giordanetto F, Kroemer RT, Herker E, Scholz S, Modjtahedi N, Madeo F, Le Cam E, Kroemer G: Physical interaction of apoptosis-inducing factor with DNA and RNA. *Oncogene.* 2006; 25(12): 1763-1774.

Vanacker H, Carver TL, Foyer CH.: Pathogen-induced changes in the antioxidant status of the apoplast in barley leaves. *Plant Physiol.* 1998; 117(3): 1103-1114.

Van Camp W, Capiau K, Van Montagu M, Inze D, Slooten L: Enhancement of oxidative stress tolerance in transgenic tobacco plants overproducing Fe-superoxide dismutase in chloroplasts. *Plant Physiol.* 1996; 112(4): 1703-1714.

van Empel VP, Bertrand AT, van der Nagel R, Kostin S, Doevendans PA, Crijns HJ, de Wit E, Sluiter W, Ackerman SL, De Windt LJ: Downregulation of apoptosis-inducing factor in harlequin mutant mice sensitizes the myocardium to oxidative stress-related cell death and pressure overload-induced decompensation. *Circ Res.* 2005; 96(12): e92-e101.

Vander Heiden MG, Thompson CB: Bcl-2 proteins: regulators of apoptosis or of mitochondrial homeostasis? *Nat Cell Biol.* 1999; 1(8): E209-216.

Vercammen D, Beyaert R, Denecker G, Goossens V, Van Loo G, Declercq W, Grooten J, Fiers W, Vandenabeele P: Inhibition of caspases increases the sensitivity of L929 cells to necrosis mediated by tumor necrosis factor. *J Exp Med.* 1998; 187(9): 1477-1485.

Verkaart S, Koopman WJ, van Emst-de Vries SE, Nijtmans LG, van den Heuvel LW, Smeitink JA, Willems PH: Superoxide production is inversely related to complex I activity in inherited complex I deficiency. *Biochim Biophys Acta.* 2007; 1772(3): 373-381.

Vieira HL, Kroemer G: Pathophysiology of mitochondrial cell death control. *Cell Mol Life Sci.* 1999; 56(11-12): 971-976.

Wang GL, Semenza GL: Purification and characterization of hypoxia-inducible factor 1. *J Biol Chem.* 1995; 270(3): 1230-1237.

Wu EY, Smith MT, Bellomo G, DiMonte D: Relationships between mitochondrial transmembrane potencial, ATP concentrations, and cytotoxicity in isolated rat hepatocytes. *Arch Biochem Biophys.* 1990; 282(2): 358-362.

Wu M, Xu LG, Li X, Zhai Z, Shu HB: AMID, an apoptosis-inducing factor-homologous mitochondrion-associated protein, induces caspase-independent

apoptosis. *J Biol Chem.* 2002; 277(28): 25617-25623.

Xiang J, Chao DT, Korsmeyer SJ: BAX-induced cell death may not require interleukin 1 beta-converting enzyme-like proteases. *Proc Natl Acad Sci U S A.* 1996; 93(25): 14559-14563.

Xie Q, Lin T, Zhang Y, Zheng J, Bonanno JA : Molecular cloning and characterization of a human AIF-like gene with ability to induce apoptosis. *J Biol Chem*. 2005; 280(20): 19673-19681.

Ye H, Cande C, Stephanou NC, Jiang S, Gurbuxani S, Larochette N, Daugas E, Garrido C, Kroemer G, Wu H: DNA binding is required for the apoptogenic action of apoptosis inducing factor. *Nat Struct Biol.* 2002; 9(9): 680-684.

Yim MB, Chock PB, Stadtman ER: Copper, zinc superoxide dismutase catalyzes hydroxyl radical production from hydrogen peroxide. *Proc Natl Acad Sci U S A.* 1990; 87: 5006-5010.

Yoshida H, Kong YY, Yoshida R, Elia AJ, Hakem A, Hakem R, Penninger JM, Mak TW: Apaf1 is required for mitochondrial pathways of apoptosis and brain development. *Cell.* 1998; 94(6): 739-750.

Yu JY, **DeRuiter SL**, **Turner DL**: RNA interference by expression of short interfering RNAs and hairpin RNAs in mammalian cells. *Proc Natl Acad Sci U S A.* 2002; 99(9): 6047-6052.

Zamzami N, Susin SA, Marchetti P, Hirsch T, Gomez-Monterrey I, Castedo M, Kroemer G: Mitochondrial control of nuclear apoptosis. *J Exp Med.* 1996; 183(4): 1533-1544.

Zamzami N, El Hamel C, Maisse C, Brenner C, Munoz-Pinedo C, Belzacq AS, Costantini P, Vieira H, Loeffler M, Molle G, Kroemer G: Bid acts on the permeability transition pore complex to induce apoptosis. *Oncogene.* 2000; 19(54): 6342-6350.

Zhang DD: Mechanistic studies of the Nrf2-Keap1 signaling pathway. _Drug Metab Rev._ 2006; 38: 769-789.

Zhang R, Al-Lamki R, Bai L, Streb JW, Miano JM, Bradley J, Min W: Thioredoxin-2 inhibits mitochondria-located ASK1-mediated apoptosis in a JNK-independent manner. _Circ Res._ 2004; 94(11): 1483-1491.

Zhang X, Chen J, Graham SH, Du L, Kochanek PM, Draviam R, Guo F, Nathaniel PD, Szabo C, Watkins SC and Clark RSB: Intranuclear localization of apoptosis-inducing factor (AIF) and large scale DNA fragmentation after traumatic brain injury in rats and in neuronal cultures exposed to peroxynitrite. _J Neurochem._ 2002; 82: 181-191.

Zhong H, De Marzo AM, Laughner E, Lim M, Hilton DA, Zagzag D, Buechler P, Isaacs WB, Semenza GL, Simons JW: Overexpression of hypoxia-inducible factor 1 alpha in common human cancers and their metastases. _Cancer Res._ 1999; 59(22): 5830-5835.

Zhu C, Qiu L, Wang X, Hallin U, Cande C, Kroemer G, Hagberg H and Blomgren K: Involvement of apoptosis-inducing factor in neuronal death after hypoxia-ischemia in the neonatal rat brain. _J Neurochem._ 2003; 86: 306-317.

Zoccarato F, Cavallini L, Alexandre A: Respiration-dependent removal of exogenous H_2O_2 in brain mitochondria: inhibition by Ca2+. _J Biol Chem_. 2004; 279: 4166-4174.

IX. RESUMEN

INTRODUCCIÓN

La Muerte Celular Programada (MCP) es un proceso natural, genéticamente regulado y altamente organizado, que forma parte del desarrollo y del control de la homeostasis en tejidos de organismos pluricelulares. Existen observaciones ocasionales al respecto desde mediados del siglo XIX, pero ha sido el análisis genético, realizado inicialmente en el nematodo *Caenorhabditis elegans*, el que ha permitido demostrar la existencia de programas genéticos de regulación de la muerte celular. La célula expresa los componentes moleculares que le van a permitir "suicidarse", dependiendo de un balance de señales procedentes de la misma célula (endógenas) y del medio ambiente celular (exógenas).

La caracterización del complejo mecanismo de la MCP está cambiando profundamente la comprensión de numerosas patologías humanas. Muchas enfermedades neurodegenerativas, el cáncer, diferentes tipos de esclerosis, los infartos cerebrales o las relacionadas con el envejecimiento, además de enfermedades autoinmunes e infecciones virales, están asociadas de alguna forma a la MCP. Algunos autores proponen que la mayoría de las enfermedades podrían tener un componente de pérdida del control de la MCP, lo que contribuiría a la patología. Es fácil, pues, entender que el estudio y la comprensión de los mecanismos moleculares de la muerte celular estén entre las prioridades de numerosos grupos de investigación en el ámbito de la biomedicina y la industria farmacéutica.

La apoptosis es una forma de MCP que se caracteriza por cambios morfológicos y bioquímicos en la célula, precisos y regulados, tales como: hinchamiento de la membrana celular, activación de las caspasas, reorganización del citoesqueleto, condensación y fragmentación de la cromatina y exposición de marcadores en la membrana celular, que actúan como señalizadores para la fagocitosis. Aunque durante mucho tiempo se consideraba que la mitocondria no formaba parte del proceso apoptótico, hoy en día está ampliamente reconocido que dicho orgánulo participa activamente en el suicidio celular. Entre los cambios que sufre la mitocondria en el proceso apoptótico se incluyen: la interrupción de la fosforilación oxidativa, la alteración en el potencial de membrana mitocondrial ($\Delta\psi_m$) y el equilibrio redox, la

permeabilización de la membrana mitocondrial y la liberación de proteínas proapoptóticas como algunas procaspasas, el cyt *c*, EndoG, Smac/Diablo y el **Factor Inductor de Apoptosis (AIF, "Apoptosis-Inducing Factor")**, este último objeto del presente estudio.

AIF fue descubierto en el año 1996 y posteriormente clonado en el 1999, por el grupo de Guido Kroemer (Centre Nacional de la Recherche Scientifique, Francia). Se trata de una flavoproteína ancestral, filogenéticamente bien conservada, presente tanto en el reino de Eucariota, como en Bacteria y Archaea. El AIF humano consta de 613 aminoácidos y muestra alta homología con el ortólogo de otras especies (92% con el AIF murino al nivel de toda la proteína y 95% al nivel del dominio C-terminal).

AIF se expresa durante todos los estadíos embrionarios y también en prácticamente todos los tejidos adultos. La proteína se sintetiza como un precursor de 67 kDa, organizado en tres dominios: la región N-terminal, residuos 1-100, que contiene una Señal para la Localización Mitocondrial (SLM), la región central de 27 aminoacidos ("spacer") y el dominio C-terminal que posee dos Señales para la Localización Nuclear (SLN). Una vez el precursor de AIF se encuentra en la mitocondria, el dominio N-terminal que lleva la SLM es recortado por parte de las proteasas mitocondriales. A continuación, se incorpora el grupo prostético FAD y de esta manera se obtiene la forma madura de AIF con un peso molecular de 57 kDa. Dentro de la mitocondria, AIF se localiza en el espacio intermembrana, posiblemente unido a la membrana interna, y forma parte de las proteínas denominadas poco abundantes (menos del 0,1% del total de las proteínas mitocondriales).

La conservación de los sitios de unión de NAD y FAD en AIF sugiere una actividad oxidoreductasa que además se ha comprobado *in vitro*. Como característica estructural importante de AIF destaca la presencia de una larga inserción en el dominio C-terminal que no presenta homología con otras proteínas. La delección de esta parte de AIF anula su actividad proapoptótica, de ahí que se crea que este dominio posee un papel fundamental en la muerte celular. También se ha descrito que el dominio C-terminal posee sitios de unión con chaperonas, con ADN y ARN; además hay evidencias de la presencia de un motivo PEST, involucrado en procesos de degradación proteica y característico de proteínas de rápida metabolización. Además, AIF posee 3 residuos de cisteina en su secuencia, aparentemente no involucrados en puentes disulfuro.

Distintos estímulos proapoptóticos provocan la translocación de AIF desde su localización fisiológica, en el espacio intermembrana, al citosol primero y posteriormente al núcleo, donde AIF induce la denominada "apoptosis nuclear", que se manifiesta como condensación de la cromatina y fragmentación de la misma en fragmentos de alto peso molecular, 50 kb. Aunque AIF no tiene actividad intrínseca de nucleasa, su carga neta positiva sugiere unión al ADN. La micro-inyección de AIF recombinante en células *in vitro* o la adición de AIF a núcleos aislados produce fenotipos apoptóticos como: condensación de la cromatina, disminución de $\Delta\psi_m$ y otros. Es importante resaltar que ninguno de estos efectos se puede inhibir con inhibidores de caspasas, lo que indica que AIF es un efector apoptótico que actúa independientemente de las caspasas.

Conviene añadir que AIF tiene un papel fundamental en el desarrollo embrionario temprano, ya que los embriones de ratón que carecen de *AIF* por completo ("Knock Out") no son viables.

En células no apoptóticas, como ya se ha expuesto, AIF se encuentra en el espacio intermembrana de la mitocondria, donde su función fisiológica se desconoce. Ensayos *in vitro* han mostrado que AIF posee actividad oxidoreductasa, aceptando electrones de NADH. Sin embargo, su actividad como NADH oxidasa *in vivo* no se ha estudiado, por lo que se desconoce el receptor al cual AIF le pasa electrones. También es importante añadir que la región redox-activa de AIF no es imprescindible para su función apoptótica.

Teniendo en cuenta el hecho de que AIF es una oxidoreductasa, en los últimos años se han llevado a cabo estudios que han tratado de esclarecer el papel de AIF como proteína participante en el equilibrio redox de la célula. En 2002, Jeffrey A. Klein y colaboradores publicaron un trabajo en la revista *Nature*, en el cual estudiaron detalladamente el mutante murino Arlequín (Hq) que exhibe un fenotipo caracterizado por degeneración progresiva de las neuronas del cerebelo y de la retina con el envejecimiento. Merece la pena mencionar también que muchas enfermedades neurodegenerativas humanas (Parkinson, Alzheimer, etc.) presentan un fenotipo similar. El mutante Arlequín posee una mutación en el gen de *Aif* que da a lugar a una disminución de los niveles de la proteína AIF de hasta un 80% en algunos órganos como el cerebro. Curiosamente, las células granuladas de este ratón, cultivadas *in*

vitro, muestran mayor susceptibilidad a la apoptosis inducida por peróxido en comparación con las mismas células parentales. La reintroducción de AIF en estas células hace que se recupere la resistencia a peróxido de hidrógeno. Con esta observación los autores dieron a conocer un nuevo papel de AIF, en la retirada o captación ("scavenger") de las Especies Reactivas de Oxígeno (EROs). No obstante, *in vitro*, AIF no sólo no se comporta como "scavenger" de las EROs, sino que las produce catalizando la transferencia de electrones de NADH a oxígeno molecular y generando radical superóxido, aunque esta situación no se podría extrapolar para las condiciones *in vivo* dado que se desconocen el donador y el aceptor de electrones.

También existen evidencias que le otorgan a AIF un papel protector de la integridad mitocondrial. Así, algunos trabajos defienden la participación de AIF en la cadena de transporte electrónico (CTE) en la mitocondria. Más en detalle, varias publicaciones en los últimos años han demostrado que AIF participa en el mantenimiento de la integridad del Complejo I de la CTE ya que la ausencia de AIF en varios modelos celulares está relacionada con deficiencias en este complejo, aunque el mecanismo de esta acción está por estudiar todavía. En este sentido, conviene añadir que muchas enfermedades mitocondriales se caracterizan con diferentes defectos a nivel del Complejo I, con consecuencias graves sobre el proceso de fosforilación oxidativa y el metabolismo de los EROs mitocondriales.

En resumen, el hecho de que AIF posea, aparte de su papel proapoptótico, otro papel participando en el equilibrio redox de la mitocondria, está claramente aceptado. Esto ha abierto nuevos horizontes en el entendimiento de los mecanismos de vida/muerte en los sistemas biológicos y ha convertido los estudios sobre AIF en un campo fascinante.

La intrigante "doble vida" de AIF aún tiene muchas incógnitas que tendrán que ser resueltas en futuros trabajos. Algunas de las preguntas que quedan por contestar para esclarecer la paradoja del comportamiento de "Dr. Jekyll and Mr.Hide" de AIF son las siguientes:

¿Cuál es el verdadero papel fisiológico de AIF?
¿Participa AIF en la captación y la retirada de las EROs o por el contrario, es un productor de las mismas?

OBJETIVO

El objetivo de este trabajo ha sido estudiar el papel fisiológico del AIF en la mitocondria, mediante el empleo de células genéticamente modificadas para perder la expresión del mismo.

METODOLOGÍA

Como modelo de trabajo se han usado células Hep3B (línea celular de hepatoma humano), empleando no obstante, en algunos estudios, la línea celular HeLa (carcinoma del cérvix de útero humano) o las líneas AIF-KO y el control CRE-AIF de células madre de ratón.

Para silenciar *AIF*, se ha usado la metodología de ARN de interferencia (ARNi), generando 3 cassettes de ARNi, dirigidas a tres regiones distintas del mRNA del AIF. Hicimos, primero, un estudio piloto para observar la expresión génica de las tres "splicing variants" de AIF en diferentes tejidos y poder ver si los cassettes (ARNi), diseñados los podían silenciar a los tres. En un primer lugar, los cassettes de ARNi se usaron para silenciar *AIF* de forma temporal, mediante transfección transitoria. Las células transfectadas de forma transitoria se usaron para comprobar la eficacia de los cassettes de interferencia y también para analizar los niveles de las EROs. Aparte de las células Hep3B, de esta manera hemos transfectado también la línea celular HeLa para analizar los niveles de las EROs. Una vez comprobada la eficacia de los cassettes de interferencia siAIF1, siAIF2 y siAIF3 en transfección transitoria, procedimos a la generación de las líneas de Hep3B con *AIF* silenciado de forma estable. Estas líneas son útiles porque ofrecen un silenciamiento duradero y constante a diferencia de las líneas donde *AIF* se ha silenciado de forma transitoria. Para la obtención de líneas estables de Hep3B, las células se cotransfectaron con el vector que contiene el cassette de interferencia y con otro plásmido, el pcDNA3.0, que expresa el marcador de resistencia a neomicina. Transfectando estos dos vectores en un alto ratio (5:1 o 10:1), uno puede seleccionar las células doble-transfectadas mediante su crecimiento en medio que contiene neomicina.

La misma técnica de ARNi se empleó también para silenciar *TRX2*, de forma transitoria, empleando dos cassettes de ARNi, Trx2-A y Trx2-B.

Para caracterizar las células carecientes de AIF utilizamos diferentes técnicas de biología molecular y bioquímica. Los niveles de las EROs se cuantificaron mediante una técnica de espectrofotometría utilizando "Amplex red kit" y también se usó la miscroscopía confocal. Esta última técnica también se empleó para determinar el potencial de membrana mitocondrial. La concentración de glutation reducido (GSH) se midió mediante fluorimetría y microscopia confocal. Los niveles de ATP se determinaron con un ensayo de bioluminiscencia, mientras que las concentraciones de lactato y glucosa en el medio se midieron mediante espectrometría. La expresión de muchas proteínas incluyendo AIF, los factores de transcripción HIF-1α, NF-κB y Nrf2, la survivina, Trx1 y Trx2, las subunidades de 39 y 20 kDa del Complejo I, la subunidad B del Complejo II y las subunidades 1 y 2 del Complejo IV de la CTE, se cuantificó mediante Western blot. También se realizaron PCRs genómicas y RT-PCRs semicuantitativas (para analizar la expresión génica de la Aldolasa A, GLUT1, AIF, GAPDH, KEAP1, NQO1 y las enzimas relacionadas con el estatus redox, SOD1, SOD2 y Catalasa), además de las RT-PCRs cuantitativas en tiempo real (para SOD1 y SOD2). La actividad transcripcional de HIF1 se analizó mediante "gene reporter assay", usando como "reporter gen" la luciferasa. Técnicas de biología molecular habituales se usaron para analizar la expresión génica de las tres "splicing variants" de AIF en diferentes tejidos y también para sobreexpresar tanto las proteínas Trx1 y Trx2 como generar Trx2 mutante, Trx2Δ (Trx2 con una delección en el N-terminal que elimina la secuencia SLM e impide que la proteína sea translocada a la mitocondria) y marcar estas proteínas con el epítopo Flag. La distribución de las Trx2 sobreexpresada en las células transfectadas se monitorizó utilizando técnicas de inmunofluorescencia y microscopía confocal. La posible relación entre AIF y Trx2 la abordamos con técnicas de coinmunoprecipitación y proteómica. El consumo de oxígeno en células intactas y células permeabilizadas con digitonina se realizó usando el electrodo de oxígeno, tipo Clark. La proliferación celular se determinó mediante el contaje de células en suspensión, con hemacitómetro, o usando el ensayo espectrofotométrico con MTT.

RESULTADOS Y DISCUSIÓN

Como se ha expuesto previamente, hoy en día existe mucha polémica respecto al papel que juega AIF en la generación/retirada de las EROs. Teniendo en cuenta dicha controversia en los trabajos existentes en la bibliografía, consideramos prioritaria la evaluación del estatus redox en las células carecientes de AIF. Para ello, silenciamos

AIF de forma transitoria en las células Hep3B y HeLa y detectamos los niveles de H_2O_2 usando el "Amplex red kit". En ambos casos se ha visto que los niveles de las EROs están aumentados significativamente, comprobando así que el aumento de las EROs no es específico para la línea celular Hep3B, sino que está ligado a la pérdida de AIF. Una vez visto que las células que poseen *AIF* silenciado muestran niveles aumentados de las EROs, lo siguiente era analizar de dónde proviene esta producción de EROs. Con el fin de corroborar si la generación de las EROs proviene de la mitocondria hicimos uso de células que carecen de mitocondrias funcionales, las denominadas células rhoº. Para obtener este fenotipo tratamos las células Hep3B con bromuro de etidio durante periodos largos, a dosis suficientes para anular la transcripción del ADN mitocondrial y no perjudicar el ADN nuclear. Ya que muchas de las subunidades de los complejos de la cadena de transporte electrónico en la mitocondria son codificadas por genes mitocondriales, una de las características de las células rhoº es la casi completa inhibición de la respiración celular. Una vez confirmada la presencia del fenotipo rhoº, procedimos a analizar los niveles de las EROs usando el "Amplex red kit". Transfectamos de forma transitoria las células Hep3B-rhoº, con el fin de silenciar *AIF* y cuantificamos los niveles de las EROs en estas células, comparándolos con las células rhoº de transfección control. Tal y como se esperaba, el silenciamiento de *AIF* en las células rhoº no conlleva un incremento de las EROs, sugiriendo que para la producción de EROs en nuestro modelo de *AIF* silenciado se precisa mitocondria funcional. Sin embargo, con este abordaje experimental no pudimos asegurar que las EROs aumentadas provienen de la CTE. Aunque las evidencias bibliográficas apuntan a la CTE como la principal fuente de EROs en la mitocondria, también existen algunos indicios de la presencia de otras enzimas generadoras de EROs, de las cuales algunas forman parte del ciclo de Krebs. La relación entre estas enzimas y AIF no se ha estudiado todavía. Tampoco sabemos si en nuestro modelo de *AIF* silenciado las actividades de estas enzimas se ven alteradas. La producción de EROs a nivel de la algunas enzimas del ciclo de Krebs puede estar relacionada con el ratio $NADH/NAD^+$, así que esto sería un punto añadido para futuros estudios del modelo celular de *AIF* silenciado.

Tras observar que el silenciamiento de *AIF* de forma transitoria produce un aumento significativo de las EROs, procedimos a su silenciamiento continuado, mediante transfección estable. De esta forma y seleccionando los clones resistentes a neomicina, obtuvimos 46 líneas de siAIF, 16 del cassette siAIF1, 14 del siAIF2 y 16 del siAIF3. A

continuación, realizamos análisis de Western blot y RT-PCRs para cuantificar los niveles de AIF y seleccionamos dos líneas, una de cada cassette, que presentaban mayor silenciamiento. Estas líneas, denominadas AIF-1-10 y AIF-2-4, son las líneas que se mantuvieron en cultivo durante periodos largos y se emplearon para la caracterización fenotípica mediante distintos ensayos de bioquímica y biología molecular. Como control, además de usar las células Hep3B de fenotipo salvaje, usamos la línea pU6-2, obtenida mediante transfección con el plásmido vacío.

A continuación, cuantificamos los niveles de las EROs intracelulares en las líneas siAIF mediante microscopía confocal. Usando distintos fluorocromos (HE y DCFH-DA), detectamos que tanto los niveles del superóxido como los de agua oxigenada y radical peroxilo, están aumentados respecto a la línea control, pU6-2. Curiosamente, detectamos también una reducción significativa en el potencial de la membrana mitocondrial, mientras que no había cambios en los niveles de glutation reducido.

La siguiente pregunta que nos hicimos era si este incremento de las EROs en nuestro modelo es relevante, desde el punto de vista fisiológico. Existen muchas evidencias de la conexión entre los niveles de las EROs y la cadena de transporte electrónico en la mitocondria tanto en condiciones fisiológicas como en patológicas. Sin embargo, revisando la bibliografía, no es fácil establecer las conexiones directas ya que parece que los efectos de las EROs sobre la CTE y viceversa forman una complicada red de causas y consecuencias. La CTE mitocondrial es el principal productor de EROs en la célula y sus defectos a menudo suponen un importante aumento de la generación de las EROs. Por otro lado, las EROs dañan la CTE provocando una disminución de la respiración mitocondrial. En vista de que las células siAIF muestran incrementados los niveles de las EROs, hemos considerado importante medir la respiración celular. Midiendo el consumo de oxígeno basal, observamos una inhibición significativa (de 35% aproximadamente) en las líneas siAIF, comparadas con las líneas control.

Por otra parte, quisimos ver si el defecto en la respiración celular se puede revertir usando antioxidantes. Para ello, empleamos dos antioxidantes, N-Acetil-Cisteína (NAC) y Mitoquinona (MitoQ). NAC es un antioxidante general que tiene distintos efectos en la célula, mientras que MitoQ es un antioxidante mitocondria-selectivo dado que por su alta carga positiva se acumula específicamente en la mitocondria. Después de haber tratado las células siAIF y las células control con los antioxidantes, medimos el

consumo de oxígeno y observamos que efectivamente el fenotipo de inhibición de la respiración mitocondrial en las líneas carecientes de AIF se puede revertir. Este efecto se ha podido comprobar tanto en el tratamiento con NAC como con MitoQ, no obstante ninguno de los dos tratamientos altera la respiración en la línea celular control. El consumo de oxígeno en células siAIF también se pudo recuperar sobreexpresando la proteína mitocondrial Trx2 que tiene papel protector en el metabolismo redox.

Obtenidos estos resultados, a continuación quisimos analizar la respiración de células permeabilizadas. Para permeabilizar las células se usa el detergente digitonina cuya alta afinidad para el colesterol permite permeabilizar sólo la membrana celular, mientras la membrana mitocondrial permanece intacta. La respiración basal de una célula permeabilizada es muy baja, ya que depende de los sustratos que se añaden de forma exógena. Con este procedimiento y usando la técnica de polarografía se puede detectar el consumo de oxígeno dependiente de cada complejo de CTE por separado. En condiciones normales, el Complejo I es el limitante de la CTE. También se conoce que este complejo es muy susceptible a alteraciones provocados por las EROs, curiosamente siendo él mismo el principal generador de superóxido en la CTE. Hay que añadir que en la literatura ya existen indicios que correlacionan el AIF con este complejo. Conociendo todo esto, decidimos analizar la respiración dependiente del Complejo I, empleando dos sustratos de este complejo, malato y glutamato, y su inhibidor específico, la rotenona. Observamos que en las líneas siAIF, la respiración dependiente de Complejo I se muestra significativamente inhibida, comparándola con la línea control, pU6-2. Sin embargo, la respiración dependiente del Complejo II, añadiendo succinato como sustrato, no se ve inhibida. Curiosamente, tras el pretratamiento de las células siAIF con MitoQ, la respiración dependiente del Complejo I está recuperada por completo. Concluyendo, se puede decir que el silenciamiento de *AIF* conlleva una disminución en la respiración mitocondrial que proviene del Complejo I y depende de los niveles de las EROs, puesto que se puede recuperar con pretratamiento antioxidativo.

Vista la implicación del Complejo I en el defecto de la OxPhos, procedimos a analizar la expresión de este macrocomplejo mediante WB. Estos estudios revelaron que la expresión de las subunidades de 39 y 20 kDa está significativamente reducida en las células siAIF y no se puede restaurar mediante tratamientos con los antioxidantes NAC y MitoQ, ni sobreexpresando las dos formas de tioredoxina, la citosólica, Trx1 o la

mitocondrial, Trx2. Por lo tanto, de qué forma está implicado el incremento de las EROs en la integridad del Complejo I se desconoce y requiere estudios adicionales. Es posible que el AIF posea un papel de chaperona, cuya presencia estabiliza el Complejo I. De otra manera, la falta de AIF puede resultar en un aumento de las EROs que dañan/inactivan otra(s) proteína(s) involucrada(s) en el mantenimiento del Complejo I. Cabe destacar también que la expresión de los otros complejos de la CTE en nuestro modelo de siAIF, analizada por WB, no se ve afectada, lo que apunta a un fenómeno exclusivo del Complejo I.

Para profundizar en los estudios sobre las consecuencias fisiológicas del incremento de las EROs, quisimos analizar algunos factores de transcripción, sensibles a los cambios redox, como Nrf2, HIF-1α y NF-κB. Mientras los niveles de expresión de NF-κB no se veían afectados por el silenciamiento de *AIF*, en el caso en HIF-1α y Nrf2 observamos una clara regulación a la alta. Es más, comprobamos también que el tratamiento de las células control con H_2O_2 exógena provoca un incremento en los niveles de HIF-1α y Nrf2. El papel directo de las EROs en la estabilización de HIF-1α en las células siAIF se pudo verificar mediante el tratamiento de las células con antioxidantes. La estabilización de HIF-1α en las líneas carecientes de AIF se puede revertir tras un tratamiento antioxidante, con NAC o MitoQ, o sobreexpresando Trx1 y Trx2. Además, la adición de H_2O_2 en las células control, provocó un aumento en los niveles de expresión de AIF, a nivel post-transcripcional. Todos estos resultados ponen de manifiesto el papel de AIF en el metabolismo redox celular.

A continuación procedimos a analizar la expresión de algunos genes diana de estos factores de transcripción y otros genes implicados en el mantenimiento del estatus redox celular. Mientras que en la expresión génica de la Aldolasa A, el transportador de Glucosa, Glut1, las enzimas redox, NQO1, Catalasa y SOD1, no hubo alteraciones visibles, sí detectamos una pequeña disminución en la expresión de SOD2 que no resultó ser estadísticamente significativa.

En vista de los resultados obtenidos de disminución en la fosfolorilación oxidativa, quisimos estudiar las consecuencias metabólicas de este fenómeno. Para ello analizamos varios parámetros que definen la capacidad de glucólisis de las células y el estado bioenergético de las mismas. Estos ensayos revelaron que los niveles de ATP en las células siAIF no eran diferentes de los niveles detectados en las líneas celulares

control; sin embargo, sí que se pudo detectar una mayor acumulación de lactato y un mayor consumo de glucosa. Además, las células siAIF muestran una tasa de proliferación basal inferior a la tasa detectada en las líneas control y tienen dificultad para proliferar en medio de cultivo que carece de glucosa y lleva galactosa en su lugar. También una de las enzimas principales en la ruta glucolítica, GAPDH, mostró una mayor expresión en comparación con la misma en las células control. Todo esto indica que el metabolismo glucolítico en las células siAIF está modulado a la alta. Es posible que esto junto con la disminución de la proliferación celular y por lo tanto también disminución de la demanda energética basal, sea un mecanismo de adaptación frente a la deficiencia en la respiración mitocondrial. Sin embargo, cabe mencionar que la enzima GAPDH posee otras funciones además de su papel en la glucólisis. Se ha visto que esta enzima esta involucrada en la regulación de procesos apoptóticos que puede ser de interés para futuros estudios.

Para profundizar en los estudios sobre el papel fisiológico de AIF, analizamos la expresión de las tioredoxinas, proteínas involucradas en el mantenimiento del equilibrio redox en la célula. Mientras que la expresión de la forma citosólica, Trx1, no se ve afectada, las células siAIF muestran una disminución significativa en la expresión de la tioredoxina mitocondrial, Trx2. Es importante mencionar que la Trx2 además de tener un papel antioxidativo en la mitocondria, parece poseer otras funciones. Por ejemplo, se ha visto que la Trx2 está implicada en la regulación de procesos apoptóticos en la mitocondria. Para analizar la posible relación entre el AIF y la tioredoxina, realizamos estudios de coinmunoprecipitación y un estudio preliminar de proteómica. Ninguno de estos ensayos pudo mostrar que entre el AIF y la Trx2 existe una relación directa aunque ambas técnicas en nuestras manos requieren ser mejoradas.

Obtenidos todos estos resultados, la hipótesis sobre el papel de AIF en nuestro modelo celular sería la siguiente: AIF está involucrado en el equilibrio redox de la mitocondria, ya que su silenciamiento provoca un aumento en los niveles de las EROs mitocondriales. Este aumento es relevante y tiene varias consecuencias bioquímicas, como la estabilización de algunos factores de transcripción, además de tener impacto sobre la CTE en la mitocondria. AIF está implicado en el mantenimiento de la integridad y/o la biogénesis del Complejo I. Cual es la fuente de las EROs incrementadas en la mitocondria y de qué manera están éstas implicadas en el defecto del Complejo I se desconoce y requiere de una investigación más exhaustiva.

CONCLUSIONES

1. Hemos diseñado cassettes de interferencia por RNA, eficaces en la inhibición de la expresión génica de AIF en un modelo celular.

2. Se ha logrado el establecimiento de líneas AIF KD estables usando células de Hep3B, línea celular de hepatoma humano.

3. La caracterización de estas líneas mostró que:

   • El silenciamiento de AIF en nuestro modelo celular conlleva a un incremento significativo en las EROs y éstas son de origen mitocondrial.

   • El incremento de las EROs es relevante puesto que dos factores de transcripción, sensibles al estatus redox, HIF-1 y Nrf2, se muestran activados.

   • El silenciamiento de AIF viene acompañado por una deficiencia en el Complejo I de la CTE, que resulta en una disminución en el consumo de oxígeno mitocondrial. Este defecto en la respiración mitocondrial puede ser revertido mediante tratamiento con antioxidantes, no siendo el caso cuando los mismos tratamientos se emplean para normalizar la expresión proteica de las subunidades del Complejo I.

   • Las células siAIF muestran una mayor capacidad glucolítica y una disminución en la tasa de proliferación celular, posiblemente como parte de un mecanismo metabólico de adaptación.

   • El silenciamiento de AIF viene acompañado por una disminución significativa en la expresión proteica de Trx2.

4. Los resultados obtenidos en esta Tesis Doctoral sugieren que AIF posee una función mitocondrial integradora, siendo involucrado en el mantenimiento del equilibrio redox celular y como chaperona molecular, participando en la biogénesis y el ensamblaje del Complejo I de la CTE en la mitocondria.